九州大学学術情報リポジトリ
Kyushu University Institutional Repository

Three-Dimensional Dynamics Model of Mooring Line for Coupled Motion Analysis of Floating Offshore Structure in Deep Water

ユダ, アプリ, ヘルマワン

https://doi.org/10.15017/2534442

出版情報：Kyushu University, 2019, 博士（工学）, 課程博士
バージョン：
権利関係：

Three-Dimensional Dynamics Model of Mooring Line for Coupled Motion Analysis of Floating Offshore Structure in Deep Water

July 2019

Yuda Apri Hermawan

Table of Content

Chapter 1 Introduction

1.1. General Overview

The demands of energy, especially for oil and natural gas, have increased rapidly in recent years. It is expected to continue to increase over the world because of population growth, industrial development, and growing economy. According to BP Energy Outlook 2019 shown in Fig. 1.1, the world consumption of oil and gas at 2040 account for almost 9 billion toe (tonne of oil equivalent), which means more than a half of energy consumptions in the world relies on oil and gas. This condition even happened during years and it is expected to rise continuously in the future due to the continuous national development of worldwide countries.

The rapid increase of energy demand in the future leads the gradual depletion of oil and gas resources in shallow offshore water as well as those in onshore. The expansion of oil and gas exploration is necessary to meet the demands of oil and gas in the world. As consequences, oil and gas exploration is gradually moving toward deep water area where is far from the land to compensate the growing demands. The offshore development for deep water operation is indispensable to sustain oil and gas exploitation in deep water area far from the land.

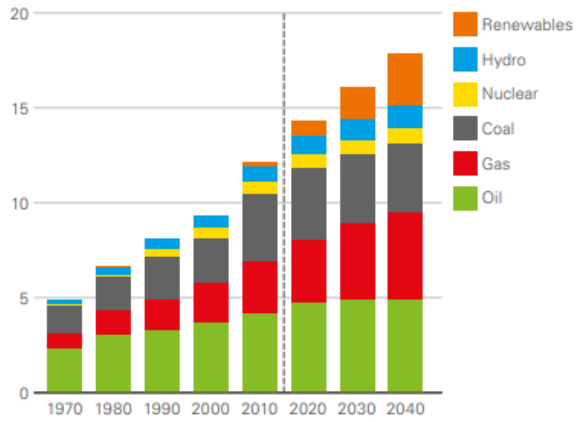

Fig. 1.1. World energy consumption (BP Energy Outlook,2019)

Nowadays, the number of offshore development for deep water operation is large and they have been evolved along with the increase of water depth. In Europe, the deep water offshore development can be found in the north of United Kingdom at where water depth is between 400-600 m and sea area with more than 1500 m depth exists in Ireland. The Gulf of Mexico (USA) and Brazil have many offshore development sites locating in the deep water of over 500 m while the deep water offshore areas also exist in West Africa, Nigeria, Gabon, Angola, and the Lower Congo Basin with 850-3000 m water depth. Deep water fields are

also discovered and most of them are being developed in Northwestern Australia (Jansz, Enfield, Laverda, Stybarrow, and Pluto) at 825-1325 m depth and sea areas over 400 m water depth exist in Southeastern Australia (Gippsland, Otway, and Great Australian Bight). Currently, the development of deep water offshore operation shifts to Asia, i.e. Eastern Asia (Caspian Sea, North Iran), India, South China Sea, and Southeast Asia. Especially in Indonesia, many deep water fields have been discovered. One of them has been operated (West Seno Field located at the sea area of about 1000 m depth) while the others are being developed. The deep water development is estimated to rise in the world and it is most likely located in area far from the land and severe sea conditions.

The massive oil and gas demand in the future tends to force the exploitation of oil and gas even at deep water, far from the land, and severe area. Oil and gas fields at such area is considered as the great challenge and attractive, however, they require a great attention. The oil and gas fields which are far from the land are not possible to access the onshore infrastructure or offshore pipelines while the deep water condition necessitates more consideration to ensure the safety of exploration and production processes. The severe sea condition makes the safety of exploration and production more susceptible. Moreover, the installation of offshore pipelines does not seem economical enough for such conditions.

With the growing demand of oil and gas, the engineering solutions, especially for offshore structure, have been proposed and continuously developed. The offshore structure generally can be classified into two groups i.e. bottom supported platform and floating offshore structure. The bottom supported platform encompasses Fixed Platform (FP), compliant tower, and Tension Leg Platform (TLP) whilst SPAR platform, semi-submersible, and ship-shaped structure (drillship, Floating Production, Storage and Offloading (FPSO), Floating Liquefied Natural Gas (FLNG), and Floating Storage Oil/Unit (FSO/FSU)) are classified as floating offshore structure. The classification of the offshore structure can be seen in Fig. 1.2.

Bottom supported platform is normally supported by a fixed jacket structure piled into the seabed (FP, compliant tower) or a tensioned vertical tether system connected to the seabed (TLP) by piled-foundation template. The bottom supported platform is economically feasible to be installed for 500 m to 1200 m water depth. It is installed as a fixed structure and cannot be moved to the other location. Unlike the bottom supported platform, the floating offshore structure can flexibly move since it is permanently moored by a flexible mooring system which allows the sufficient motions of the structure. It becomes more popular offshore structure because it is environmental friendly, faster construction, easiness in expansion and removal, cost efficiency, and less of ocean and marine habitats destructions

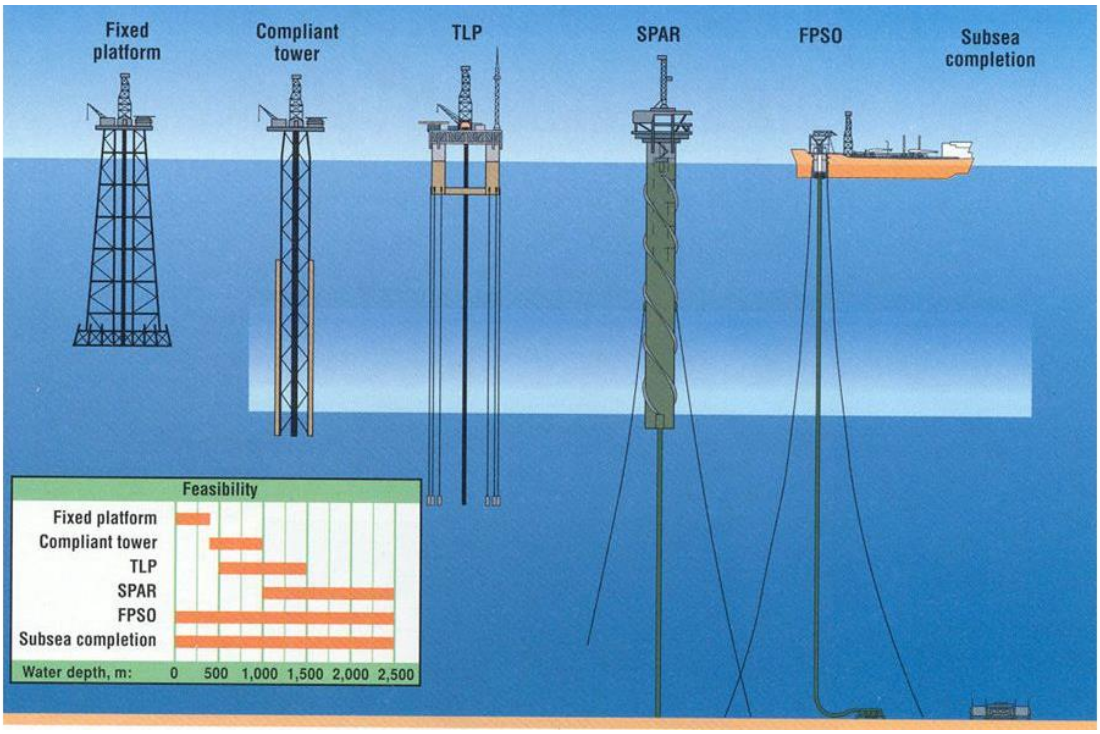

Fig. 1.2. Offshore structure (slideplayer.com)

(Wang et al., 2008). It can be used for 50-2500 m of offshore operations.

Talking over the floating offshore structures, one of the most important issue associated with them in recent decades is their mooring line system. Since a floating structure is connected to a flexible riser system which transports oil/gas from deep beneath of the seabed and cannot compensate the large motions of the floating structure, the mooring line system plays an important role to keep the structure in desired location and survive under severe sea condition. Safe mooring line system become vital for the floating offshore structure because the failure of riser system due to the collapse of the mooring line system can lead a fatal accident. The failure of mooring line may result a catastrophic consequences (Fontaine et al., 2013). Multi-impact problems including safety, technical aspect, environmental, marine pollution, and as well as cost can be induced by the failure of mooring line system.

Due to the importance of such mooring line system, the accurate prediction of mooring line behavior including its tension and motion is compulsory and it must be considered by incorporating the dynamic effects of mooring line. The dynamic effects of mooring line are becoming significant for deep water mooring along increase in the water depth. The calculation of mooring line motion become more complex since the modeling of mooring line dynamics is a challenging task in investigating moored floating offshore structure (Matha et al., 2011). The modeling of deep water mooring line dynamics is still an attractive

and topical research due to the complex problem of deep water mooring line, though the fundamental investigation has been established decades ago. An appropriate analysis method should be developed paying an attention for reflecting the condition properly.

On the other hand, recently, multi-component mooring line system consisting of various types of segment lines, clump weights and/or spring buoys, has been assessed as the proper solution for deep water mooring problem and severe sea conditions. The multi-component mooring line has superiority concerning the capability of station-keeping significantly comparing with the single-component mooring, even for deep water condition (Childers, 1974). This mooring line system began to be applied for deep water mooring system and it is continuously evolved until nowadays. However, as the increase of water depth, the dynamic effects of multi-component mooring lines are also becoming significant and important to predict the dynamic behavior of the mooring line, and it becomes more complex due to the variation of segment line properties. These dynamic effects are often neglected in multi-component line catenary method. Hence, an adequate numerical method which can delineate the complexities of the multi-component mooring line and provide accurate results is absolutely demanded.

Moreover, the consideration of possible environmental loads is considerably important against the dynamic motions of a floating offshore structure (Fontaine et al., 2013). The motions of the structures are sensitive to the direction of environmental loads (Lopez et al., 2017). The environmental loads with various directions including collinear and non-collinear conditions often occur in deep water and severe sea region. Non-collinear environmental condition may often cause larger response of the structures comparing with collinear conditions while the collinear condition may force the floating structure in large drifting motions. A combination of wind, wave, and current with different directions may be able to cause unpredicted response of the structures. The motion of the floating structure even vulnerable to the both in-line and in-between line conditions (Svalastog, 2017). Thus, environmental loads based on measured metocean data including collinear/non-collinear and in-line/in-between line conditions must be considered when performing motion analysis of a moored floating offshore structure.

1.2. Deep Water Mooring Line

Floating offshore structure concept is widely used for ocean oil and gas exploitation activities in deep water sea condition. The floating structure which is subjected to various environmental loads including wave, wind, and current is moored by an appropriate mooring line system to be kept in stationary position. This mooring line system mainly can be divided in two types, namely catenary and taut systems shown in Fig. 1.3.

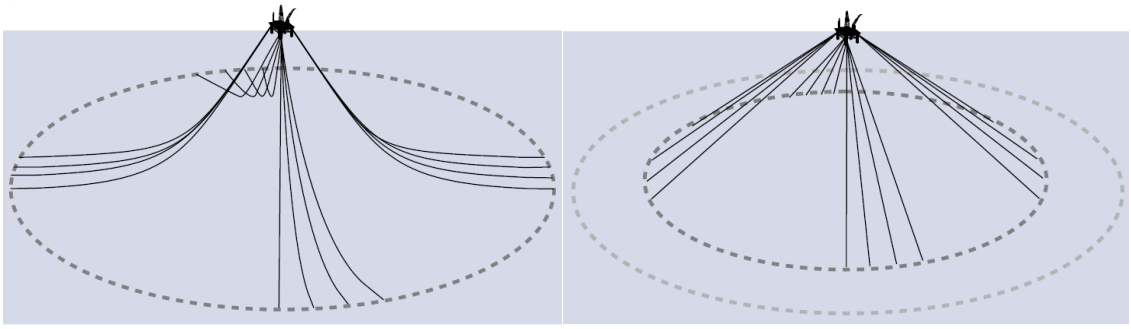

Fig. 1.3. Mooring type (Vryhof, 2010)

In catenary mooring system, the mooring line is calculated by using catenary geometric function in which the restoring force of mooring line is provided by the weight of the suspended mooring line part. The length of mooring line varies depending on the dynamic motion response of the floating structure. The mooring line should have a part with sufficient length to be laid on the seabed to prevent the mooring line being fully lifted up from the seabed. Fully suspended mooring line which causes vertical load at an anchor is strictly prohibited in this mooring system. On the contrary, the taut mooring system is installed with fully suspended mooring line in which the restoring force of the mooring line is provided by axial stretching and elasticity of the mooring line. It seems to be superior comparing with catenary system in deep water activities (Shanying, 2013), however, the taut mooring causes a trench which can degrade the capacity of anchor and thereby, the mooring line replacement is necessary during service life which means it is costly (Bhattacharjee, 2014).

There are various types of mooring line configuration system used for deep water operation. It includes of single point mooring (SPM), turret system, and spread mooring systems, with the most of them consist of multi-leg mooring lines. The types of mooring line configuration including the number, type, arrangement, and spacing of the mooring line depends on the type and severity of the environmental loads. Generally, the multi-leg mooring lines arrange several groups of mooring lines. Each group usually consists of three to five mooring lines.

Typically, the mooring line is designed to keep the floating offshore structure within a particular allowable horizontal offset in order to ensure the safety of continuous production operation process. Ba (2011) reported that the limit during production operation is normally held up to 5-6 % of water depth, however, 2-3 % of water depth is mostly applied in actual condition. This limit is constrained by the limitation of subsea equipment. Despite that, 10-20 % of water depth is often used for floating structure operated in water depth less than 400 m likely with implemented in Indonesia. Otherwise, Childers (1973) noted that the limit of horizontal offset was usually designed within 8-10 % of water depth.

The study of deep water mooring line including its dynamics basically has been carried out decades ago, however, it still being evolved up to present days since the complexity and challenge of deep water mooring line are continuously developed. As the part of a floating structure, a mooring line is generally treated as a cable rod structure and hence the theoretical background of mooring line calculation adopts the inherent characteristic of a slender rod structure. Several numerical mooring line models have been generated based on slender rod theory to express the mooring line behavior. The dynamic analysis of slender rods with inextensible elastic rod is presented in Garrett (1982) while Tjavaras (1996) was then examined the dynamic response of highly extensible cable based on Lagrangian formulation. The modelling of mooring line as a slender rod also studied by Mavrakos et al. (1996) to introduce the dynamics of mooring line for deep water applications. Recently, the rod theory was adopted to develop mooring line dynamics model based on finite difference and finite element (FE) model as carried out by Katifeoglou and Chatjigeorgiou (2012) and Palm et al. (2013).

The development of mooring line dynamics model is progressing lively to reach more accurate results, time efficiency, and lower cost in calculation. It continues to be expanded to more versatility model but still able to accommodate the nonlinearities of the mooring line and certainly has an accurate result. Together with two previous model, lumped mass model has been developed for expressing mooring line dynamics and it was considered as more advantageous model. Straightforwardness mathematical model, less amount of calculation time and versatility are inherent to this model (Huang, 1994). In addition, since mooring line system is disturbed by external disturbance coming in a three-dimensional direction, the mooring line dynamics model should be modelled in three-dimensional manner. This work has been pioneered by Nakajima et al. (1982) and Huang (1994) for lumped mass and finite difference models respectively.

Moreover, most recent application of deep water mooring line incorporates the use of multi-component mooring line system to outcome the technical problem of deep water mooring line. This application also needs a proper model to predict mooring line behavior either in static and dynamic conditions. Several techniques and methods have been presented over the years, however the methods which involve the overall complexity of multi-component mooring line is limited.

Furthermore, deep water mooring line analysis coupled with a floating offshore structure must be carried out by using an appropriate approach since improper analysis approach may inflict the lack of accuracy. Generally, there are several prevailing analysis approaches for conducting mooring line analysis: static, quasi-static, time domain, quasi-dynamic, and

coupled dynamic approach. In static and quasi-static approaches, the dynamic effects of mooring lines which are important to predict line tension precisely are completely neglected. Meanwhile, quasi-dynamic analysis and time domain approaches are frequently conducted through uncoupled motion model which solves the motions of floating body and mooring lines separately to simplify complex interaction between them. The line dynamics is accomplished by imposing fairlead motion to the line motion. Calculation time can be reduced by using the calculation method while obtained results may become approximate solutions. Moreover, accurate estimation of floating structure's response which changes depending on mooring line shape and tension is very important concerning the safety and reliability of mooring lines itself.

1.3. Literature Review

In recent decades, deep water and severe sea conditions are substantial issue for oil and gas exploitation activities. It is challenging to operate a floating offshore structure under complex environmental loads arisen in deep water and severe sea conditions. The operations need to be paid attention conscientiously, especially focusing on mooring, because an adequate mooring line system is necessary to keep the floating structure surviving under the complex environmental conditions. The mooring line system is becoming more intricate and needs to be designed in a complex manner (Ansari, 1999).

A mooring line can be considered as a flexible slender structure which is subjected to surface water waves, current, internal forces, and other external disturbance such as the motions of floating structure induced by wave, wind, and current. Since the mooring line is designed based on the loads acting on the mooring line during its lifetime and it strongly affects to the operational safety, an accurate prediction of mooring line motion is obviously important. To predict the motion of mooring line precisely, the dynamics effect of mooring line must be incorporated (Hall and Goupee, 2015).

The modeling of the dynamic behavior of a mooring line is challenging task even for single-component mooring line. It needs laborious efforts since the analysis of mooring line dynamics is literally arduous due to the nonlinearities of a mooring line motions (Lo, 1982). Plenty of dynamics models have been arisen for investigating mooring line dynamics. These models can be categorized into a finite difference model (Huang, 1994), a finite element (FE) model (Roussel, 1976), a lumped mass model (Walton and Polachek, 1960), a nonlinear boundary-value problem method (Chiou, 1990), and a multi-body dynamics model (Kreuzer and Wilke, 2003). The finite difference, FE, and lumped mass models are popularly used to address the problems of mooring line dynamics.

In the finite difference model, the governing equation of mooring line is discretized in both space and time, performing time-space calculation simultaneously while the lumped-mass model discretizes the governing equations in space only and integrating to time-step calculation (Hall and Goupee, 2015). Otherwise, the FE model uses the fundamental of FE method to bring the developed governing equations of mooring line into numerical model since the analytical solution is difficult to be implemented due to the highly nonlinearity of the equations (Tahar and Kim, 2008).

A finite difference model based on Lagrangian formulation for cable dynamics was presented by Tjavaras (1996). It was applied for modeling the dynamics of risers (Katifeoglou and Chatjigeorgiou, 2012) and considering the presence of current (Chen et al., 2018). Moreover, a FE model has been presented by Garret (1982) and exerted with/without taking bending and torsional stiffnesses into account (Bucham et al., 2004; and Aamo and Fossen, 2000). The model was extended by various manners i.e. mixed FE model (Montano et al., 2007), high order FE model (Escalante et al., 2011) and discontinuous Galerkin method (Palm et al., 2013). It was also applied for a multi-component mooring line to investigate the feasibility of polyester mooring line (Tahar and Kim, 2008). A FE model was also used for developing FE analysis tool called *Code_Aster* to establish the dynamic simulation of a mooring line (Antonutti, et al., 2018). However, both models were commonly developed based on slender rod model. It has versatility and can tackle various boundary conditions in discretization of a mooring line (Xiong, 2016), but more complex mathematical model is required when considering mooring line (Chai and Varyani, 2006). On the other hand, the FE model has pertinence feature in predicting mooring line dynamics, however the computations become slower, time consuming and costly (Hall and Goupee, 2015).

Comparing with the above models, the lumped mass model is assessed as more efficient for calculating mooring line dynamics with good accuracy. The discretization in the lumped mass model makes the model to resemble the FE model (Azcona et al., 2017) and exhibits features which are identical to a straight-line element FE model (Lee and Tu, 2018). The lumped mass model can characterize the necessary features of mooring line dynamics and evade unnecessary features in the FE model which may increase computation time (Hall and Goupee, 2015). The discretization has intelligible simplicity and obvious physical meaning for every part of mathematical formulations, providing the efficiency in numerical calculations (Xiong et al., 2016). However, the lumped mass model needs to be improved to achieve more accurate prediction results for multi-component mooring line.

Studies using the lumped mass model were firstly started by Walton and Polachek, (1960). The study introduced the lumped mass model for a single-component mooring line

through two-dimensional discretization. The model was further extended by Nakajima et al. (1982), taking the elasticity of a mooring line into account. Nakajima et al. (1983) expanded the model to three-dimensional model and verified with experimental results. The results were good though the model was only applied for a single-component line. The other studies related to the lumped mass model can be observed in (Chai et al., 2002b; Low and Langley, 2006 and Xiong et al., 2016). Moreover, the validations of the lumped mass model were carried out through model test data (Hall and Goupee, 2015) and a FE based dynamic code (Azcona et al., 2017). Both validations indicate the satisfaction of the model in the prediction of dynamic mooring line.

In fact, many studies concerning to dynamic mooring line models have been published. However, it is considered that the studies of mooring line dynamics model in three-dimensional manner need to be developed further for the sake of getting more precise simulation results. The three-dimensional mooring line has not been tackled comprehensively while the mooring line essentially moves and is disturbed by external loads in three-dimensional space. A three-dimensional mooring line model proposed by Huang (1994) solely provided the mooring line only while time-based dynamic tensions which were important to capture the behavior of mooring line dynamics were not provided in Chai et al. (2002a, 2002b). Three-dimensional mooring line calculation part is also not clearly mentioned in detail though Low and Langley (2006) succeed to perform an analysis of moored deep water floating structure.

Furthermore, to cope with the complexity of deep water mooring problems, a multi-component mooring line system consisting of various segment lines, clump weights, and buoy is considered as the most apropos mooring line system applied for the deep water and severe sea conditions. It has superiority comparing with single-component mooring line system (Childers, 1974). Mooring line tension and the length of catenary line can be reduced by varying the composition of mooring line segments as well as attaching clump weights/buoys. The cost of a mooring line can also be decreased through the appropriate arrangement of the line segments. Recently, the multi-component mooring line is widely used for deep water offshore structure (Ba, 2011; Vazquez-Hernandez et al., 2011; Qiao et al., 2013 and Xie et al., 2015) and it is proven that the mooring line system can withstand external forces under severe sea conditions (Ha, 2011). The multi-component mooring line is also used and expanded into a new mooring system which is called hybrid mooring line system (Ji et al., 2011; Yuan et al., 2014 and Xu et al., 2018) to reduce vertical anchoring force in taut mooring. The yaw motion of a ship-type floating offshore structure with the mooring line system in deep water (Sanchez-Mondragon et al., 2018) and the dynamic

response of a semi-submersible platform with the mooring line system (Ghafari and Dardel, 2018) were evaluated. Experimental works related to the mooring line system can be found in (Zhao et al., 2013 and Lopez et al., 2017).

The applications of the multi-component mooring line for deep water conditions are expected to be escalated owing to the increase of operations in deep water conditions. The inclusion of the dynamic effects of a mooring line into motion analysis is strongly essential for deep water mooring, because these effects become significantly concomitant with the increase of water depth. It must be considered in the prediction of mooring performance when investigating the responses of a floating offshore structure (Ansari, 1991).

Further, though many studies of mooring line dynamics have been published, the studies focused on the modeling of the dynamics of a multi-component mooring line were limited. A model of a multi-component mooring line was solely presented in static manner (Ansari, 1980) while the inclusion of dynamic effects was firstly proposed in Nakajima et al. (1982) by two-dimensional lumped mass model. The dynamic manners of a multi-component mooring line could be expressed well in both studies, but calculated results were only provided for identical segment lines. Moreover, an extended model presented in (Van den Boom, 1985 and Chai et al., 2002b) could figure the dynamic behavior of a multi-component mooring line with various segment types, however the portion of a multi-component line in the proposed algorithm was not explained clearly. Furthermore, Khan and Ansari (1986) provided formulae and succeeded to demonstrate the dynamic behavior of a multi-component mooring line combining with the motion of a moored offshore vessel (Ansari, 1991). Unfortunately, it was restricted for inextensible mooring line since the influence of line elasticity was not performed.

In addition, to predict the performance of a mooring line incorporating with the motion of a floating offshore structure, quasi-static (Masciola et al., 2013; Chai et al., 2002a and Figueirodo and Brojo, 2017) and quasi-dynamic (Bureau Veritas, 1998, 2004) approaches are frequently used. Both approaches were developed based on the catenary solutions (Bauduin and Naciri, 2000) and thereby the dynamic effects of a mooring line were literally excluded (Johanning et al., 2005, 2007 and Ha, 2011). Accordingly, the quasi-static approach is considered to be inadequate method to apply for deep water conditions (Mavrakros et al., 1996). Meanwhile, the mooring line tension and the motion of a floating structure were calculated separately in the quasi-dynamic approach for the sake of computation time and simplification of complex interaction between them. This may lead to the depreciation of calculation accuracy.

Coupled dynamics approach is assessed to be the most rigorous method to carry out the dynamic analysis of the motion of a floating offshore structure. Both dynamic effects of a mooring line and a floating structure are simultaneously obtained by using the approach. The basic theoretical study of the approach was presented by Ormberg et al. (1998) while its application discussing mooring line dynamics can be found in (Heurtier et al., 2001; Garret, 2005 and Low and Langley, 2006, 2008). Recently, this approach was often used to address the hydrodynamic problems in offshore fields (Ji et al., 2016; Jacob et al., 2012a, 2012b and Zhao et al., 2018).

1.4. Objectives

Based on the aforementioned premises, this study intends to develop a numerical model for conducting coupled analysis of a deep water floating offshore structure incorporating with three-dimensional dynamics of a mooring line. Wave, wind, and current loads are also taken into account in the numerical model. A dynamics model of a three-dimensional multi-component mooring line is also evolved to comply with the necessity of the multi-component mooring line for deep water operation. The dynamics model is further used to study the necessities of three-dimensional treatment in calculating the motions of a mooring line. The calculated results are compared with results based on two-dimensional model to investigate the effect of three-dimensional motions. Furthermore, to ensure the ability of the developed model for realistic operation, the coupled motions analysis of a ship-type floating offshore structure under the combination of environmental conditions is conducted. The motions of the floating structure and the tension of its mooring line are investigated.

In this study, three-dimensional lumped mass model for a single-component mooring line (Nakajima et al.,1983) is improved by integrating interaction between the mooring line and the seabed and considering anchor force and its motion at first. The model is then coupled with the equations of motion built up by combining MMG model with conventional floating motion equations. Furthermore, the model is extended to be applied for a multi-component mooring line to develop dynamics model for a multi-component mooring line. By using the developed model, it is expected that the motions of multi-component mooring line can be reproduced allowing the individual motion of connection point between each segment. Moreover, to investigate the effectiveness of the model, numerical simulations of dynamic motions are performed for both single- and multi-component mooring lines.

The aim of this study is to develop a three-dimensional dynamics model of a mooring line which is applicable for multi-component mooring line system for conducting the coupled analysis of deep water floating offshore structure and mooring lines. This study takes into account the influence of wave, wind, and current loads and involves overall

inherent characteristics of the mooring line. The analysis of a moored deep water floating structure under the combination of environmental loads is also conducted.

The objectives of this study include;

a. to develop an adequate numerical model taking into account the simultaneous interaction between a floating offshore structure and its mooring line considering three-dimensional mooring line dynamics,
b. to develop three-dimensional dynamics model of a multi-component mooring line to be coupled with a floating offshore structure including interaction between a mooring line and the seabed and anchor motion,
c. to conduct numerical simulations of a floating offshore structure moored with various mooring configuration systems under various environmental conditions by applying the extended three-dimensional dynamics model,
d. to simulate the coupled motions of multi-component mooring lines and a floating offshore structure under various environmental condition by applying the developed three-dimensional dynamics model.

In this study, a ship-type structure is used as the considered floating offshore structure since such structure is frequently used in deep water purpose and more sensitive to the directions of environmental loads. This study will contribute not only in developing mooring line model but also to the development of deep water operation.

1.5. Thesis Layout

This thesis consists of six chapters where Chapter 1 introduces a general overview of this study including a brief review of deep water operation, offshore structure and deep water mooring line system. A literature review is presented associated with mooring line dynamics, multi-component mooring line, and mooring line analysis approach. The objectives and expected outcome of this research as well as a brief layout of this thesis are also presented.

Chapter 2 describes numerical model used for introducing simultaneous motion between a ship-type floating offshore structure and mooring line considering wave, wind, and current loads. In this chapter the method used for obtaining wave forces is described and the hydrodynamic coefficients used in simultaneous motion equations combining mathematical maneoeuvring model based on the Manoeuvring Modeling Group (MMG) and conventional floating body motion equations are presented.

A three-dimensional dynamics model for calculating mooring line is presented in Chapter 3 involving line-seabed interaction and dragging anchor motion. The governing equation of three-dimensional dynamics model for mooring line and its solution are explained in this chapter. Numerical simulations associated with the coupling of this mooring

line model and a ship-type structure are carried out. The simulations involve single line, double line, and multi-leg mooring systems including turret and spread mooring which are performed under various environmental conditions for each system.

Furthermore, to outcome the problem of multi-component mooring line dynamics, three-dimensional dynamics model of a multi-component mooring line is developed and presented in Chapter 4. The verification of the developed model either for the mooring line itself and its coupling with a ship-type structure are provided. Comparison against two-dimensional model results are also presented.

Moreover, to verify the developed multi-component mooring line dynamics model to be applied in realistic operation, the coupling of the developed model with a ship-type structure under realistic operation is simulated and reported in Chapter 5. The characteristics of mooring line, mooring line configuration, and environmental data are considered based on measured metocean data. The various cases including collinear/non-collinear and in-line/in-between line conditions are accounted to the simulations. Finally, the conclusion of this research and recommendation for future work are drawn in Chapter 6.

Chapter 2 Motion Equations for Moored Floating Offshore Structure

2.1. Introduction

A floating offshore structure moored in open sea is subjected to environmental loads and restoring force generated by its mooring line tension. The environmental loads are induced by current, wind, and wave which are normally coming from various and probably in different directions. These loads force the floating structure to move in six degrees of freedom and thereby the floating offshore structure must be considered to have six degrees of freedom (6 DOF) motion. The 6 DOF motion generates the displacements of the floating structure from her desired position, and those may cause the dropping of operation efficiency up to the collapsing of subsea equipment.

On the other hand, since the floating structure is moored by a set of mooring line(s), the inclusion of mooring line tension must be taken into account when calculating the 6 DOF motion of the moored floating structure. The relation between the motions of the floating structure and its mooring lines is very tight and interdependent each other. The motions of the floating structure are influenced by the mooring lines motions and vice versa. Hence, this complex condition requires a proper simultaneous 6 DOF motion equations. Generally speaking, when considering the motion of a moored floating offshore structure under environmental loads, it is necessary to provide simultaneous 6 DOF motion equations including wave, wind, current, and mooring line tension loads.

In this chapter, the numerical model used for considering external disturbances comprising of wave, wind, current, and mooring line tension in 6 DOF motion equations is provided. The coordinate system used for the 6 DOF motion equations is presented in Section 2.2 while the method used for calculating floating body motions in waves is provided in Section 2.3. The verification of the method can be observed in Section 2.4. Section 2.5 presents the mathematical model involving the presence of wind, current, tension and wave drifting forces. The mathematical model is presented based on Manoeuvring Modeling Group (MMG) model to introduce the coupled-motion effect between the floating structure and the mooring lines simultaneously. The simultaneous 6 DOF motion equations of a floating offshore structure comprising of wave, wind, current, and mooring line tension is introduced in Section 2.6 while time domain simulation model based on those 6 DOF motion equations is provided in Section 2.7. Finally, the discussion of the presented simultaneous 6 DOF motion is summarized in Section 2.8.

2.2. Coordinate System

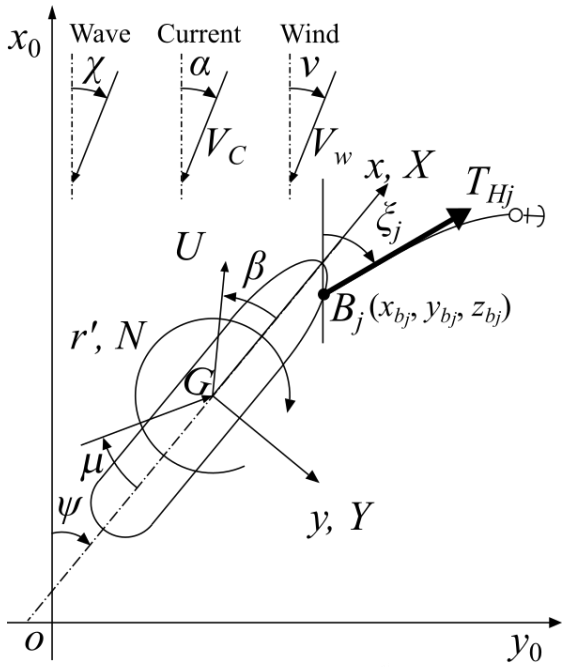

Fig. 2.1. Global coordinate system

Six degrees of freedom (6 DOF) motion of a ship-type floating offshore structure refer to global coordinate system illustrated in Fig. 2.1. $o - x_0y_0z_0$ is an earth-fixed coordinate system with the origin of z_0-axis on the water surface while $G - xyz$ is a body-fixed coordinate system with the origin at the center of gravity G of the floating structure. Let X, Y, and N are external forces acting on the floating body in x and y directions and moment around z-axis passing the center of gravity G respectively. Wind speed and

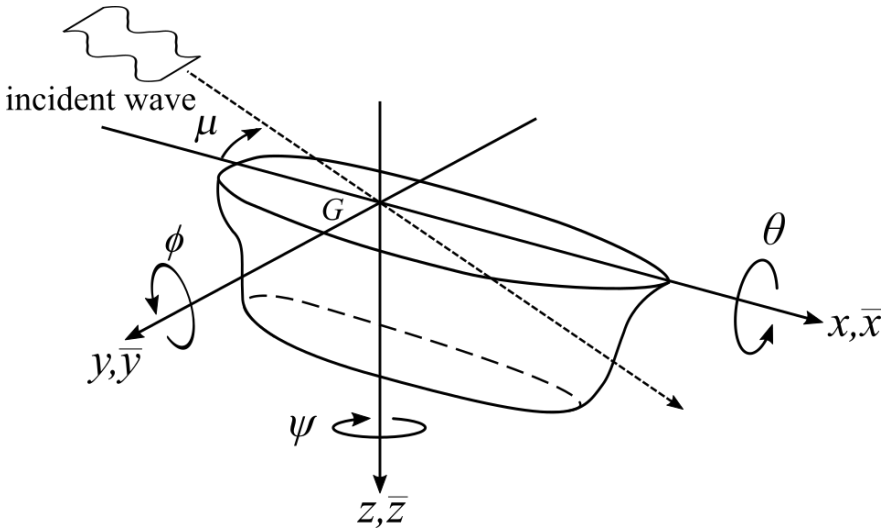

Fig. 2.2. Body-fixed coordinate system for 6 DOF motion

current velocity are denoted as V_w and V_C while wave, wind, and current directions are indicated as χ, α, and ν. Wave direction relative to the floating structure is denoted as μ.

In Fig. 2.1, $B_j(x_{b_j}, y_{b_j}, z_{b_j})$ indicates the position of the attached point of the j-th mooring line in the body-fixed coordinate system and ξ_j is an angle between the j-th mooring line measured from x_0-axis. The speed of the floating structure and its component in x and y directions are denoted as U, u, and v respectively. Drift angle, heading angle, and yaw rate are indicated by β, ψ, and r respectively. The 6 DOF motion associated with the floating structure is described based on the body-fixed coordinate system and they are denoted as $d_m(\bar{x}, \bar{y}, \bar{z}, \theta, \phi, \psi)$ as shown in Fig. 2.2. $\bar{x}$, $\bar{y}$, $\bar{z}$, θ, ϕ, and ψ respectively represent surge, sway, heave, roll, pitch, and yaw motions. In this study, it is assumed that the floating offshore structure does not have forward speed and stay at stationary position in ideal incompressible fluid. Forces acting on the floating structure comprise of wave exciting forces (E_3, E_5, E_4), wave drifting forces (Y_D, N_D), hull forces including current effects (X_H, Y_H, N_H), wind forces (X_W, Y_W, N_W), and tension forces (X_T, Y_T, N_T) caused by mooring lines.

2.3. Calculation of Floating Body Motions in Waves

In order to investigate the motion of floating offshore structure subjected to waves, the basic theory of floating body dynamics in waves must be considered. Since the floating body in waves can be regarded as a free floating body induced by wave forces coming from various directions, 6 DOF motion is inherent to the floating body. This 6 DOF motion can be introduced by considering radiation and diffraction wave forces acting on the floating body.

Forces acting on a floating body in waves can be divided into the following components,

- Force acting to Floating body in waves
  - Radiation Force
    - Added Mass Force
    - Wave Damping Force
  - Wave Exciting Force
    - Froude – Krylov Force
    - Wave Diffraction Force
  - Hydrostatic Restoring Force
  - Viscous Damping Force
  - Wave Drifting Force
  - Others

Radiation force is hydrodynamic force acting on the floating body induced by waves generated by the motion of the floating body while wave exciting force is the hydrodynamic force caused by the incident waves acting on the floating body. Hydrostatic restoring force

is force which forces the floating body to its equilibrium position when the floating body is disturbed by the external disturbances. Viscous damping force is force caused by the viscosity of fluid and it normally has a very small value comparing with the other forces and it is usually neglected. Furthermore, apart from the component which oscillate with the same period of waves (1st order), such as radiation force and wave exciting force, there is a wave force component that acts constantly when averaged over time (2nd order). This steady force is called wave drifting force and it affects to the floating body motions especially for the floating body without forward speed (stationary). Moreover, the other forces acting on the floating body can be caused by swell waves, current, slowly-varying drift force, etc.

2.3.1. Method for Calculating Hydrodynamic Forces Acting on Floating Body in Waves

To calculate hydrodynamic forces acting on the floating body in waves, linear potential theory may be applied to estimate radiation force and wave forces. In addition, considering the fact that the floating body used in this study is ship-type in which it means that the hull is a slender body, thus, the strip method can be used. The strip method is a method to obtain the hydrodynamic forces acting on the floating body by integrating pressure on hull surface along the longitudinal direction. It considers the hull as a slender body and the hull is divided into two-dimensional cross sections. The pressure on the hull surface is obtained by integrating the pressure acting on the cross sections obtained by determining two-dimensional velocity potential which represents flow field around the cross sections. Though the strip method is a calculation method ignoring three-dimensional shape effect, it is known that it can estimate the hydrodynamic forces with sufficient accuracy (Watanabe et al., 1994).

There are two strip methods called as OSM (Ordinary Strip Method) and NSM (New Strip Method). OSM is a method for estimating the hydrodynamic forces by mapping the Lewis form, which is a virtual shape similar to the cross section of a hull, to a circle by means of conformal mapping. Since it is easy to calculate and can give a result with reasonable accuracy, it is widely used (Watanabe et al., 1994). On the other hand, NSM addresses the boundary conditions of an object faithfully to the hull cross-sectional shape by distributing singular points in the cross section of the hull and calculate the hydrodynamic forces in consideration of the inclusion of forward speed. Even so, NSM is also applicable to the floating body in waves without forward speed. In this study, the hydrodynamic forces acting on the floating body in waves is obtained by using NSM (Kashiwagi and Iwashita, 2012) to estimate added mass coefficients, wave damping coefficients, wave exciting forces, and wave drifting forces in frequency domain to be used for time domain calculation.

2.3.2. Six Degrees of Freedom of Floating Body Motions

By using coordinate system shown in Fig. 2.2, the 6 DOF motion of a floating body in waves for each motion mode $x_j(j = 1\sim6)$ can be expressed as follows,

$$\left.\begin{aligned} x_1(t) &= \mathrm{Re}\left[X_1 e^{i\omega t}\right] = \bar{x}(t) = \mathrm{Re}\left[X e^{i\omega t}\right], \\ x_2(t) &= \mathrm{Re}\left[X_2 e^{i\omega t}\right] = \bar{y}(t) = \mathrm{Re}\left[Y e^{i\omega t}\right], \\ x_3(t) &= \mathrm{Re}\left[X_3 e^{i\omega t}\right] = \bar{z}(t) = \mathrm{Re}\left[Z e^{i\omega t}\right], \\ x_4(t) &= \mathrm{Re}\left[X_4 e^{i\omega t}\right] = \theta(t) = \mathrm{Re}\left[\Theta e^{i\omega t}\right], \\ x_5(t) &= \mathrm{Re}\left[X_5 e^{i\omega t}\right] = \phi(t) = \mathrm{Re}\left[\Xi e^{i\omega t}\right], \\ x_6(t) &= \mathrm{Re}\left[X_6 e^{i\omega t}\right] = \psi(t) = \mathrm{Re}\left[\Psi e^{i\omega t}\right]. \end{aligned}\right\} \tag{2.1}$$

Here, $X_j(j = 1\sim6)$ and X, Y, Z, Θ, Ξ, Ψ are complex motion amplitude of each motion mode while ω is wave circular frequency.

Since the shape of floating offshore structure especially for ship-type normally can be regarded as symmetrical for central longitudinal section and the whole of 6 DOF motion are not coupled simultaneously at the same time, the 6 DOF motion can be divided into two groups. The first group consists of surge, heave, and pitch $(j = 1, 3, 5)$ called longitudinal motion and the other is lateral motion consisting of sway, roll, and yaw $(j = 2, 4, 6)$. Since both motion groups are not coupled, the coupling between the two groups is neglected in the following floating body motion equations. The 6 DOF motion equations is described as follows.

Considering the motion of floating body in waves, the following equation can be introduced.

$$\sum_{j=1}^{6} M_{ij}\ddot{x}_{ij} = F_i(t) \qquad (i = 1\sim6). \tag{2.2}$$

In this equation, subscript i is the direction of wave forces, j is the direction of floating body motions while M_{ij} represents a mass matrix which is expressed by the following equation,

$$M_{ij} = \begin{bmatrix} m & 0 & 0 & 0 & 0 & 0 \\ 0 & m & 0 & 0 & 0 & 0 \\ 0 & 0 & m & 0 & 0 & 0 \\ 0 & 0 & 0 & I_{xx} & 0 & 0 \\ 0 & 0 & 0 & 0 & I_{yy} & 0 \\ 0 & 0 & 0 & 0 & 0 & I_{zz} \end{bmatrix}, \tag{2.3}$$

where m is floating body mass and I_{xx}, I_{yy}, and I_{zz} represent the moments of inertia around x-, y-, and z-axis respectively. The force acting on the floating body in waves $F_i(t)$ can be expressed as follows,

$$F_i(t) = F_i^R(t) + F_i^S(t) + F_i^W(t) \qquad (i = 1\sim6), \tag{2.4}$$

in which $F_i^R(t)$ is wave radiation force, $F_i^S(t)$ hydrostatic restoring force, and $F_i^W(t)$ wave excitation force.

- Wave radiation force

  Wave radiation force consists of added mass force which is proportional to the magnitude of motion acceleration and wave damping force that is proportional to the motion velocity. Hence, the wave radiation force $F_i^R(t)$ can be expressed by the following equation consisting of added mass coefficient A_{ij} and wave damping force coefficient B_{ij},

$$F_i^R(t) = -\sum_{j=1}^{6}\left\{A_{ij}\ddot{x}_j(t)\right\} + B_{ij}\dot{x}_j(t) \qquad (i = 1\sim6). \tag{2.5}$$

  The added mass and wave damping coefficients for 6 DOF motion can be expressed by the following matrix,

$$A_{ij} = \begin{bmatrix} A_{11} & 0 & A_{13} & 0 & A_{15} & 0 \\ 0 & A_{22} & 0 & A_{24} & 0 & A_{26} \\ A_{31} & 0 & A_{33} & 0 & A_{35} & 0 \\ 0 & A_{42} & 0 & A_{44} & 0 & A_{46} \\ A_{51} & 0 & A_{53} & 0 & A_{55} & 0 \\ 0 & A_{62} & 0 & A_{64} & 0 & A_{66} \end{bmatrix}, \tag{2.6}$$

$$B_{ij} = \begin{bmatrix} B_{11} & 0 & B_{13} & 0 & B_{15} & 0 \\ 0 & B_{22} & 0 & B_{24} & 0 & B_{26} \\ B_{31} & 0 & B_{33} & 0 & B_{35} & 0 \\ 0 & B_{42} & 0 & B_{44} & 0 & B_{46} \\ B_{51} & 0 & B_{53} & 0 & B_{55} & 0 \\ 0 & B_{62} & 0 & B_{64} & 0 & B_{66} \end{bmatrix}. \tag{2.7}$$

- Hydrostatic restoring force

  Only heave, roll, and pitch modes have this force, and thereby the hydrostatic restoring forces can be expressed as follows using restoring force coefficient C_{ij},

$$F_i^S(t) = -\sum_{j=3}^{5} C_{ij}x_j(t) \qquad (i = 3\sim5). \tag{2.8}$$

  The restoring force coefficients for 6 DOF motion can be expressed as follows,

$$C_{ij} = \begin{bmatrix} 0 & 0 & 0 & 0 & 0 & 0 \\ 0 & 0 & 0 & 0 & 0 & 0 \\ 0 & 0 & C_{33} & 0 & C_{35} & 0 \\ 0 & 0 & 0 & C_{44} & 0 & 0 \\ 0 & 0 & C_{53} & 0 & C_{55} & 0 \\ 0 & 0 & 0 & 0 & 0 & 0 \end{bmatrix}. \tag{2.9}$$

- Wave exciting force

  This force can be classified into two wave force components i.e. Froude Krylov force and wave diffraction force. Froude Krylov force is wave force related to the incident waves in which this force is obtained by integrating the fluid pressure when incident waves aren't disturbed by the presence of the floating body. On the other hand, wave diffraction force is wave force caused by the scattering waves due to the presence of the floating body. This force is obtained by integrating the fluctuating pressure in the scattered waves disturbed by the floating body. If circular frequency of incident waves is denoted as ω_0, the wave exciting force can be expressed as,

$$F_i^W(t) = \mathrm{Re}\left[E_i e^{i\omega_0 t}\right] \qquad (i = 1\sim6), \tag{2.10}$$

  in which E_i represent the complex amplitude of wave exciting force.

By substituting forces acting on the floating body described above into Eq. (2.2), the following equation is obtained,

$$\sum_{j=1}^{6}\left\{\left(M_{ij}+A_{ij}\right)\ddot{x}_j(t)+B_{ij}\dot{x}_j(t)+C_{ij}x_j(t)\right\} = F_i^W(t) \qquad (i = 1\sim6). \tag{2.11}$$

Eq. (2.11) can be expressed as follows if the coupled motion equations are rewritten for each direction of the motions.

- <u>Longitudinal motion</u>

$$\left.\begin{aligned}
&\text{surge: j} = 1\\
&\quad (M+A_{11})\ddot{x}(t)+B_{11}\dot{x}(t)+A_{13}\ddot{z}(t)+B_{13}\dot{z}(t)\\
&\qquad +A_{15}\ddot{\phi}(t)+B_{15}\dot{\phi}(t) = \mathrm{Re}\left[E_1 e^{i\omega_0 t}\right],\\
&\text{heave: j} = 3\\
&\quad A_{31}\ddot{x}(t)+B_{31}\dot{x}(t)+(M+A_{33})\ddot{z}(t)+B_{33}\dot{z}(t)+C_{33}z(t)\\
&\qquad +A_{35}\ddot{\phi}(t)+B_{35}\dot{\phi}(t)+C_{35}\phi(t) = \mathrm{Re}\left[E_3 e^{i\omega_0 t}\right],\\
&\text{pitch: j} = 5\\
&\quad A_{51}\ddot{x}(t)+B_{51}\dot{x}(t)+A_{53}\ddot{z}(t)+B_{53}\dot{z}(t)+C_{53}z(t)\\
&\qquad +\left(I_{yy}+A_{55}\right)\ddot{\phi}(t)+B_{55}\dot{\phi}(t)+C_{55}\phi(t) = \mathrm{Re}\left[E_5 e^{i\omega_0 t}\right].
\end{aligned}\right\} \tag{2.12}$$

- Lateral motion

$$\left.\begin{aligned}
&\text{sway: j} = 2\\
&(M + A_{22})\ddot{y}(t) + B_{22}\dot{y}(t) + A_{24}\ddot{\theta}(t) + B_{24}\dot{\theta}(t)\\
&\qquad + A_{26}\ddot{\psi}(t) + B_{26}\dot{\psi}(t) = \mathrm{Re}\left[E_2 e^{i\omega_0 t}\right],\\
&\text{roll: j} = 4\\
&A_{42}\ddot{y}(t) + B_{42}\dot{y}(t) + (I_{xx} + A_{44})\ddot{\theta}(t) + B_{44}\dot{\theta}(t) + C_{44}\theta(t)\\
&\qquad + A_{46}\ddot{\psi}(t) + B_{46}\dot{\psi}(t) = \mathrm{Re}\left[E_4 e^{i\omega_0 t}\right],\\
&\text{yaw: j} = 6\\
&A_{62}\ddot{y}(t) + B_{62}\dot{y}(t) + A_{64}\ddot{\theta}(t) + B_{64}\dot{\theta}(t)\\
&\qquad + (I_{zz} + A_{66})\ddot{\psi}(t) + B_{66}\dot{\psi}(t) = \mathrm{Re}\left[E_6 e^{i\omega_0 t}\right].
\end{aligned}\right\} \quad (2.13)$$

2.3.3. Linear Potential Theory for Floating Body in Waves

By using the strip method, hydrodynamic forces acting on a hull as a three-dimensional object are obtained by integrating two-dimensional hydrodynamic forces acting on the cross section of the hull along ship length. Therefore, the linear potential theory in two-dimensional plane is firstly considered.

In order to calculate the hydrodynamic force acting on the floating body induced by waves, a velocity potential $\Phi(x)$ can be introduced by assuming the fluid is inviscid, incompressible, and irrotational. Here, $x = (y, z)$ is the position of singular point in two-dimensional hull cross section. This velocity potential should satisfy the Laplace equation

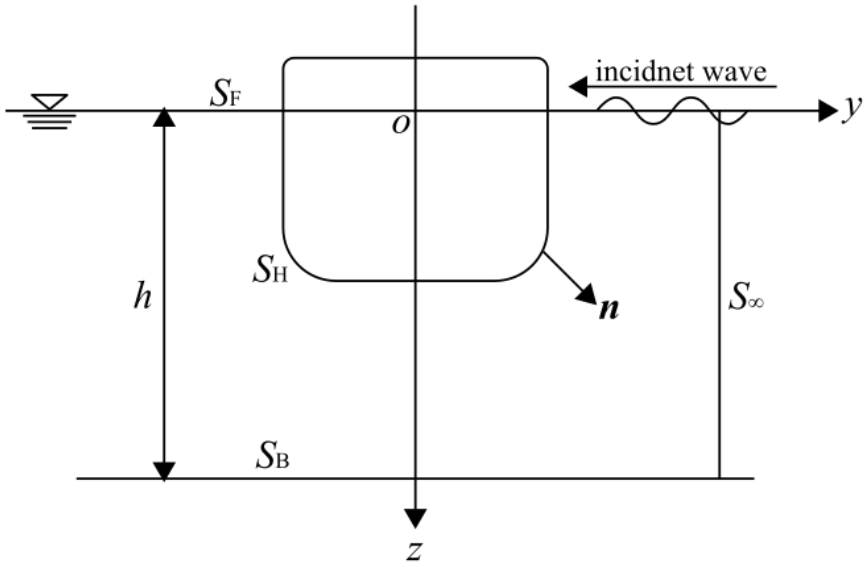

Fig. 2.3. Two-dimensional coordinate system

$[L]$ by continuity equation in the fluid. Based on free surface wave theory, it also should satisfy free surface condition on $S_F[F]$, water bottom condition on $S_B[B]$, body surface condition on $S_H[H]$ while the problem in time domain must be satisfied to the initial condition $[I]$. These boundary conditions are shown in Fig. 2.3. Therefore, the following conditions can be introduced,

$$[L] \qquad \frac{\partial^2\Phi}{\partial y^2}+\frac{\partial^2\Phi}{\partial z^2}=0 \qquad \text{for } h \geq z \geq 0, \tag{2.14}$$

$$[F] \qquad \frac{\partial^2\Phi}{\partial t^2}+g\frac{\partial^2\Phi}{\partial z}=0 \qquad \text{on } z=0, \tag{2.15}$$

$$[B] \qquad \frac{\partial\Phi}{\partial z}=0 \qquad \text{on } z=h, \tag{2.16}$$

$$[H] \qquad \frac{\partial\Phi}{\partial n}=V\cdot n \qquad \text{on } S_H, \tag{2.17}$$

$$[I] \qquad \frac{\partial\Phi}{\partial t}=0, \quad \Phi=0 \qquad \text{at } t=0. \tag{2.18}$$

V, n are velocity vector and normal vector at hull surface respectively while h is water depth.

Consider incident waves coming from the positive direction of y-axis in two-dimensional coordinate system shown in Fig. 2.3. The flow field around the body is considered to periodically oscillate at the same circular frequency of incident waves ω_0. The velocity potential representing the flow field around the hull can be expressed as follows by using complex velocity potential $\phi(x)$.

$$\Phi(x,t)=\mathrm{Re}\left[\phi(x)e^{i\omega_0 t}\right]. \tag{2.19}$$

Substituting Eq. (2.19) into Eq. (2.15) and eliminating time term, the free surface condition $[F]$ for the complex velocity potential $\phi(x)$ becomes as follows,

$$\frac{\partial\phi}{\partial z}-k_0\phi=0. \tag{2.20}$$

Here, k_0 is wave number of the incident waves at infinite water depth.

Next, consider the body surface condition shown in Eq. (2.17). The velocity component V_j in j direction ($j=2$: sway, $j=3$: heave, $j=4$: roll) can be expressed as,

$$\mathrm{V}_j=\dot{x}_j(t), \tag{2.21}$$

$$\mathrm{V}_j=\mathrm{Re}\left[i\omega_0 X_j e^{i\omega_0 t}\right]. \tag{2.22}$$

$x_j(t)$ $\left(=\mathrm{Re}\left[i\omega_0 X_j e^{i\omega_0 t}\right]\right)$ is j-mode motion displacement of the floating body and X_j is the complex amplitude of floating body motions. Substituting Eq. (2.17) into Eq. (2.22) and excluding time term $i\omega_0 t$, the following expression can be gained,

$$\frac{\partial \Phi}{\partial n} = \sum_{j=2}^{4} i\omega_0 X_j n_j, \tag{2.23}$$

$$n = (n_y, n_z) = (n_2, n_3), \quad n_4 = (x \times n)_1 = yn_z - zn_y. \tag{2.24}$$

Since Eq. (2.23) is a superposition of each oscillation mode, it is convenient to consider the velocity potential as the sum of the velocity potential of each oscillation mode. However, the velocity potential must include the velocity potential of incident waves $\phi_0(x)$. In order to satisfy the Eq. (2.23), a new velocity potential $\phi_D(x)$ that cancels the normal velocity due to the incident waves is introduced. Then, the velocity potential can be expressed as,

$$\phi(x) = \frac{ig\zeta_a}{\omega_0}\{\phi_0(x) + \phi_D(x)\} + \sum_{j=2}^{4} i\omega_0 X_j \phi_j(x). \tag{2.25}$$

If the following equations are satisfied, Eq. (2.23) is satisfied.

$$\frac{\partial(\phi_0+\phi_D)}{\partial n} = 0, \tag{2.26}$$

$$\frac{\partial \phi_j}{\partial n} = n_j \qquad (j = 2\sim4). \tag{2.27}$$

$\phi_D(x)$ in Eq. (2.25) represents a diffraction potential due to scattering waves caused by the presence of floating body. Also, $\phi_j(x)$ $(j = 2\sim4)$ represents the radiation potential due to j-mode oscillation of the floating body.

Finally, consider the initial condition $[I]$. When incident waves act on the floating body, the disturbance of the fluid gradually develops as an initial value problem, but after a sufficient time, periodic oscillation of circular frequency ω_0 is same as circular frequency of the incident waves. Assuming that the current time is $t = 0$, the initial condition of Eq. (2.18) can be regarded as the condition at $t = -\infty$. Therefore, boundary condition to be replaced with the initial condition is required. The boundary condition is given as wave radiation condition $[R]$. The radiation condition represents that disturbances waves propagate outwards from the floating body. It can be expressed by the following equation,

$$[R] \qquad \phi_j \sim e^{\pm ik_0 y} \qquad \text{as } y \to \pm\infty. \tag{2.28}$$

2.3.4. Two-dimensional Boundary Element Method

The boundary conditions in the frequency domain which must be satisfied by the complex velocity potential $\phi_j(j = 2\sim4, D)$ are summarized as follows,

$$[L] \qquad \frac{\partial^2 \Phi_j}{\partial y^2} + \frac{\partial^2 \Phi_j}{\partial z^2} = 0 \qquad \text{for } h \geq z \geq 0, \tag{2.29}$$

$$[F] \qquad \frac{\partial \Phi_j}{\partial z} - k_0 \phi_j = 0 \qquad \text{on } z = 0, \tag{2.30}$$

$$[B] \qquad \frac{\partial \Phi_j}{\partial z} = 0 \qquad \text{on } z = h, \tag{2.31}$$

$$[H] \qquad \begin{cases} \frac{\partial \phi_j}{\partial n} = n_j \ \ (j = 2 \sim 4) \\ \frac{\partial (\phi_0 + \phi_D)}{\partial n} = 0 \end{cases} \qquad \text{on } S_H, \tag{2.32}$$

$$[R] \qquad \phi_j \sim e^{\pm i k_0 y} \qquad \text{as } y \to \pm \infty. \tag{2.33}$$

There are several solution methods which can be used for obtaining the velocity potential ϕ_j satisfying the boundary condition above. As instance, frequently used methods are as follows,

- Boundary Element Method (Closed-Fit method)
  - Direct method
  - Indirect method (singularity distribution method)
- Conformal mapping method (Ursell-Tasai method)
- Domain decomposition method

Boundary Element Method is widely used to obtain the velocity potential on the body surface since the method is robust. Boundary Element Method (BEM) is also called as Boundary Integral Equation Method (BIEM) or free-surface Green function method since it solves the velocity potential ϕ_j by constructing the integral equation using Laplace equation and Green function satisfying free surface condition. It is also called as Closed-Fit method since the singular point can be distributed accurately close to the hull cross section and the boundary value problem is introduced in that cross section (Watanabe et al., 1994). In indirect method, the velocity potential is obtained by making singularity distributions on the hull surface. The radiation potentials induced by those singularity distributions can be obtained while the wave forces are obtained by using Kochin function (Watanabe et al., 1994 and Maeda, 1959). Otherwise, the direct method is a direct solution method calculating velocity potential by using integral equation derived from Green's formula.

Conformal mapping method, so-called Ursell-Tasai method, calculates the velocity potential on body surface based on the flow field around a cylinder shape transformed from the realistic hull shape. In this method, the circle shape is transformed by mapping the realistic shape of hull cross section (Lewis form) conformal to unit circle used in Ursell's method (Journee and Massie, 2001) while Tasai method is established to solve flow field around the Lewis form. On the other hand, the domain decomposition method called as an eigen-function expansion method is often used to calculate a flow field around a two-dimensional rectangular floating body and a three-dimensional vertical column floating body at finite water depth.

In fact, there are various methods to determine the velocity potential ϕ_j, but the application of the methods for a ship-type hull introduced in domain composition method couldn't be found while the Ursell-Tasai method uses the Lewis form for introducing bow and stern part. The Ursell-Tasai method seems not to be capable since the Lewis form is difficult to express a narrow shape which usually appears in the bow and stern parts of the ship-type hull. Moreover, because the indirect method must take two calculation steps i.e. calculating the strength of source points from the integral equation and integrating it around the cross section of the hull, the direct method of boundary element method is used in this study.

Considering a fluid region V and a surface region S surrounding it, Gauss's divergence theorem becomes,

$$\iint_V \left[\phi_j \nabla^2 G - G\nabla^2 \phi_j\right] dV = -\int_S \left[\phi_j \frac{\partial G}{\partial n} - G\frac{\partial \phi_j}{\partial n}\right] d\ell. \tag{2.34}$$

Here, G is Green function. It satisfies $\nabla\phi \to 0$ and $\nabla G \to 0$ at infinity S_∞. Also, the Laplace equation at fluid region V is,

$$\left.\begin{aligned} \nabla^2 \phi_j(Q) &= 0, \\ \nabla^2 G(P;Q) &= \delta(y-\eta)\delta(z-\zeta). \end{aligned}\right\} \tag{2.35}$$

$P(x, y)$ is an arbitrary point (field point) in the fluid, and $Q(\eta, \zeta)$ is the coordinates of the source point. Therefore, the following equation can be obtained by substituting the Eq. (2.35) into the Eq. (2.34).

$$C_P \phi_j(P) = \iint_S \left\{\frac{\partial \phi_j(Q)}{\partial n_Q} G(Q;P) - \phi_j(Q)\frac{\partial G(Q;P)}{\partial n_Q}\right\} dS(Q). \tag{2.36}$$

The boundary surface S can be expressed as $S = S_H + S_F + S_\infty + S_B$. C_P is the amount of net flux from point source, in which $C_P = 1$ when the field point P is in the fluid and $C_P = 1/2$ when the field point P is on a body surface. Moreover, since $G(P;Q)$ satisfies same conditions as the boundary conditions $([F], [B], [R])$ which are satisfied by $\phi_j(Q)$, the integrand on the right-hand side of Eq. (2.36) on the boundary surfaces automatically becomes zero. Therefore, only the integral on the floating body surface S_H remains. Assuming that field point P is on the floating body surface, a boundary integral equation can be obtained with $C_P = 1/2$ as follows,

$$\frac{1}{2}\phi_j(P) = \iint_S \left\{\frac{\partial \phi_j(Q)}{\partial n_Q} G(Q;P) - \phi_j(Q)\frac{\partial G(Q;P)}{\partial n_Q}\right\} dS(Q), \tag{2.37}$$

in which, G can be expressed as follows,

$$G(y,z;\eta,\zeta) = \frac{1}{2\pi}\log\frac{r}{r_1} + G_F(y-\eta,\ z-\zeta), \tag{2.38}$$

where,

$$\left.\begin{matrix} r \\ r_1 \end{matrix}\right\} = \sqrt{(y-\eta)^2 + (z \mp \zeta)^2}, \tag{2.39}$$

$$\left.\begin{aligned} G_F(y-\eta, z-\zeta) &= -\frac{1}{\pi}\lim_{\mu\to 0}\int_0^\infty \frac{e^{k(z+\zeta)}\cos k(y-\eta)}{k-(K-i\mu)}dk, \\ &= -\frac{1}{\pi}PV\int_0^\infty \frac{e^{k(z+\zeta)}\cos k(y-\eta)}{k-K}dk + ie^{K(z+\zeta)}\cos K(y-\eta), \\ &= -\frac{1}{\pi}\int_0^\infty \frac{k\cos k(z+\zeta)+K\sin k(z+\zeta)}{k^2+K^2}e^{-k|y-\eta|}dk + ie^{K(z+\zeta)-iK|y-\eta|}. \end{aligned}\right\} \tag{2.40}$$

Here, K represents the wave number of incident wave at infinite water depth ($K = k_0$) while k is the wave number of arbitrary wave. PV denotes principal value integral.

To solve the boundary integral equation shown in Eq. (2.36), a numerical solution method based on the zero-order element collocation method (Kinoshita, 2003) is used. This numerical solution has accommodated an approach for eliminating irregular frequencies that often appear in calculating the velocity potential by using boundary integral equation. Modified Haraguchi-Ohmatsu's method is used to get rid of those irregular frequencies (Haraguchi and Ohmatsu, 1983) in this method.

2.3.5. Boundary Value Problem in New Strip Method (NSM)

By assuming the fluid is inviscid, incompressible, and irrotational, a velocity potential can be introduced. It is defined through considering incident waves in term of its direction and amplitude. When the direction of the incident waves relative to the floating structure is denoted as μ (i.e., following sea is represented as $\mu = 0^\circ$ as shown in Fig. 2.2) and the amplitude of the waves is assumed as ζ_a, velocity potential Φ_0 representing incident waves in infinite water depth can be expressed by the following equation,

$$\Phi_0(x,t) = \mathrm{Re}\left[\frac{ig\zeta_a}{\omega_0}\phi_0(x)e^{i\omega_0 t}\right], \tag{2.41}$$

where,

$$\phi_0(x) = e^{-k_0 z - ik_0(x\cos\mu + y\sin\mu)}. \tag{2.42}$$

Here, g, ω_0, and k_0 represent the gravitational acceleration, circular frequency of the incident waves, and wave number of the incident waves, respectively. The relationship among g, ω_0, and k_0 can be expressed $k_0 = \omega_0^2/g$. Due to the effect of forward speed,

the circular frequency of incident waves can be replaced by ω_e called encounter wave circular frequency which is different from the circular frequency of the incident waves. By considering the forward speed U, an encounter wave circular frequency ω_e is indicated as follows,

$$\omega_e = \omega_0 - k_0 U \cos\mu\,. \tag{2.43}$$

First, let us consider the condition of the hull surface when the forward speed is zero. Considering same as the two-dimensional problem, Eq. (2.17) can be expressed as,

$$\left.\begin{aligned} \frac{\partial\phi}{\partial n} &= \sum_{j=1}^{6} i\omega_e X_j n_j\,, \\ (n_1, n_2, n_3) = n, \quad & (n_1, n_2, n_3) = x \times n, \end{aligned}\right\} \tag{2.44}$$

in which n_j represents normal vector in j-direction. Here, because the length of hull L is relatively longer comparing with hull breadth B and draft d, the following relation holds in for the normal vector component on the body surface except for the bow and stern ends.

$$n_1 \ll n_2, n_3. \tag{2.45}$$

Therefore, if the x-direction component is omitted as a higher order term, Eq. (2.44) becomes,

$$\frac{\partial\phi}{\partial n} = i\omega_e\{X_2 n_y + X_3 n_z + X_4(yn_z - zn_y) + X_5(-xn_z) + X_6(xn_y)\}. \tag{2.46}$$

By considering the forward speed, Eq. (2.46) becomes,

$$\frac{\partial\phi}{\partial n} = i\omega_e\left[X_2 n_y + X_3 n_z + X_4(yn_z - zn_y) + X_5\left\{-\left(x - \frac{U}{i\omega_e}\right)n_z\right\} + X_6\left\{\left(x - \frac{U}{i\omega_e}\right)n_y\right\}\right]. \tag{2.47}$$

The disturbance velocity potential $\phi(x)$ can be obtained by adding velocity potential for the incident waves ϕ_0, radiation potential $\phi_j (j = 1 \sim 6)$, and diffraction potential ϕ_D as follows,

$$\phi(x) = \frac{g\zeta_a}{i\omega_e}\{\phi_0(x) + \phi_D(x)\} + \sum_{j=2}^{6} i\omega_e X_j \phi_j(x)\,. \tag{2.48}$$

Since normal vector in $j = 1$ direction is very small comparing with those in other two directions as expressed by Eq. (2.45), the velocity potential in the direction is omitted in Eq. (2.48). X_j represents a complex motion amplitude of the floating body in j-direction. If the following conditions are satisfied, Eq. (2.44) is also satisfied as the sum of them.

$$\frac{\partial}{\partial n}(\phi_0 + \phi_D) = 0, \tag{2.49}$$

$$\frac{\partial \phi_j}{\partial n} = n_j \quad (j = 2, 3, 4), \tag{2.50}$$

$$\left.\begin{aligned} \frac{\partial \phi_5}{\partial n} &= -\left(x - \frac{U}{i\omega_e}\right) n_3, \\ \frac{\partial \phi_6}{\partial n} &= \left(x - \frac{U}{i\omega_e}\right) n_2. \end{aligned}\right\} \tag{2.51}$$

The radiation potential $\phi_j (j = 5, 6)$ can be expressed by the following equations using ϕ_3 and ϕ_2 satisfying Eq. (2.50) since $x - \frac{U}{i\omega_e}$ is constant in y and z directions.

$$\left.\begin{aligned} \phi_5 &= -\left(x - \frac{U}{i\omega_e}\right) \phi_3, \\ \phi_6 &= \left(x - \frac{U}{i\omega_e}\right) \phi_2. \end{aligned}\right\} \tag{2.52}$$

Therefore, if the two-dimensional problem is solved, ϕ_5 and ϕ_6 can also be determined. In addition, ϕ_1 can be obtained by the same method as two-dimensional problem, and the radiation potential ϕ_1 satisfies the following equation,

$$\frac{\partial \phi_1}{\partial n} = n_1. \tag{2.53}$$

Moreover, $\phi_D(x)$ in Eq. (2.48) represents the diffraction velocity potential due to the floating body scattering the incident waves. Since the diffraction potential ϕ_D satisfies the Eq. (2.49), it can be approximated as follows,

$$\left.\begin{aligned} \frac{\partial \phi_D}{\partial n} &= -\frac{\partial \phi_0}{\partial n} \\ &\simeq -\left(\frac{\partial \phi_0}{\partial y} n_y + \frac{\partial \phi_0}{\partial z} n_z\right) \\ &= k_0 \phi_0 \left(i \sin\mu \, n_y - n_z\right) \\ &= k_0 e^{k_0 z - i k_0 y \sin\mu} \left(i \sin\mu \, n_y - n_z\right). \end{aligned}\right\} \tag{2.54}$$

From Eq. (2.54), ϕ_D can be expressed as follows using the radiation potentials ϕ_3 and ϕ_D, hence, the diffraction potential ϕ_D can be written in the following formula.

$$\phi_D = k_0 e^{-k_0 z - i k_0 x \cos\mu} (i\phi_2 \sin\mu + \phi_3). \tag{2.55}$$

Thus, it is possible to obtain from the radiation potential without directly solving the diffraction problem.

Finally, the expression of the boundary conditions for velocity potential ϕ_j (j = 1~6) in the frequency domain which should be satisfied are summarized as follows,

$$[L] \quad \frac{\partial^2 \Phi_j}{\partial y^2} + \frac{\partial^2 \Phi_j}{\partial z^2} = 0 \quad \text{for } h \geq z \geq 0, \tag{2.56}$$

$$[F] \quad \frac{\partial \Phi_j}{\partial z} - k_0 \phi_j = 0 \quad \text{on } z = 0, \tag{2.57}$$

$$[B] \quad \frac{\partial \Phi_j}{\partial z} = 0 \quad \text{on } z = h, \tag{2.58}$$

$$[H] \quad \begin{cases} \frac{\partial \phi_j}{\partial n} = n_j \qquad (j = 1 \sim 4) \\ \phi_5 = -\left(x - \frac{U}{i\omega_e}\right)\phi_3 \\ \phi_6 = \left(x - \frac{U}{i\omega_e}\right)\phi_2 \end{cases} \quad \text{on } S_H, \tag{2.59}$$

$$[R] \quad \phi_j \sim e^{\pm iky} \quad \text{as } y \to \pm\infty. \tag{2.60}$$

Calculating the radiation potentials which satisfy the above boundary conditions using the boundary integral method in Eq. (2.36), the velocity potential for each cross section can be obtained.

2.3.6. Hydrodynamic Forces Calculation

Considering the linear term of pressure given by Bernoulli's pressure equation and taking out only the term that oscillates periodically at the encounter circular frequency ω_e, the pressure of the fluid can be expressed as,

$$P(x;t) = Re\left[\{p_D(x) + p_R(x) + p_S(x)\}e^{i\omega_e t}\right], \tag{2.61}$$

where,

$$p_D(x) = \rho g \zeta_a \{\phi_0(x) + \phi_D(x)\}, \tag{2.62}$$

$$p_R(x) = \rho i \omega_e \sum_{j=1}^{6} i\omega_e X_j \phi_j(x), \tag{2.63}$$

$$p_S(x) = \rho g (X_3 + yX_4 - xX_5), \tag{2.64}$$

$p_D(x)$ and $p_R(x)$ are fluctuating pressure in diffraction and radiation problems respectively, and $p_S(x)$ is fluctuating component of hydrostatic pressure based on motion displacement.

The radiation force acting on the body in i-direction is expressed as follows,

$$F_i = -\int_L dx \int_C P_R(x) n_i d\ell = \rho (i\omega_e)^2 \sum_{j=2}^{4} X_j \int_L dx \int_C \phi_j n_i d\ell \equiv \sum_{j=2}^{4} f_{ij}, \tag{2.65}$$

in which ρ is water density. C and L represent the shape of a hull section and ship length respectively. Since an imaginary part exists in the Green Function related to progressive wave on the water surface, the radiation potential ϕ_j is typically given as a complex number. Thus, assuming that $\phi_j = \phi_{js} + i\phi_{jc}$, the radiation force f_{ij} that works in the i-direction due to the j-mode oscillation is derived as,

$$
\begin{aligned}
f_{ij} &= \rho(i\omega_e)^2 X_j \int_L dx \int_C \{\phi_{js} + i\phi_{jc}\} n_i d\ell\,, \\
&= -(i\omega_e)^2 X_j \left[-\rho \int_L dx \int_C \phi_{js} n_i d\ell\right] - i\omega_e X_j \left[-\rho \int_L dx \int_C \phi_{jc} n_i d\ell\right].
\end{aligned} \tag{2.66}
$$

According to Eq. (2.66), it can be noted that $(i\omega_e)^2 X_j$ and $i\omega_e X_j$ represent acceleration and velocity respectively and thus an added mass coefficient A_{ij} and a damping coefficient B_{ij} can be written as,

$$
\left.
\begin{aligned}
A_{ij} &= -\rho \int_L dx \int_C \phi_{js} n_i d\ell\,, \\
B_{ij} &= -\rho \int_L dx \int_C \phi_{jc} n_i d\ell\,.
\end{aligned}
\right\} \tag{2.67}
$$

The force component f_{ij} can be written as the transfer function T_{ij} respected to the motion $X_j\left(f_{ij} = T_{ij} X_j\right)$. By substituting Eq. (2.66) to Eq. (2.65), the following equations are established.

$$
\left.
\begin{aligned}
F_{ij} &= -\sum_{j=1}^{6} \left[(i\omega_e)^2 A_{ij} + i\omega_e B_{ij}\right] X_j = \sum_{j=1}^{6} T_{ij} X_i\,, \\
T_{ij} &= (i\omega_e)^2 \left\{A_{ij} + \frac{1}{i\omega_e} B_{ij}\right\} = -(i\omega_e)^2 \{-\rho \int_L dx \int_C \phi_j n_i d\ell\}, \\
Z_{ij} &= A_{ij} + \frac{1}{i\omega_e} B_{ij}.
\end{aligned}
\right\} \tag{2.68}
$$

Here, the radiation forces also can be expressed as Z_{ij}.

Furthermore, wave force in diffraction problem E_j consists of two components i.e. Froude Krylov force E_j^{FK} contributed by ϕ_0 due to incident waves and diffraction force E_j^D contributed by ϕ_D due to waves scattering by the floating body. Those component wave forces can be written as follows,

$$
E_j = E_j^{FK} + E_j^D, \tag{2.69}
$$

where,

$$
\left.
\begin{aligned}
E_j^{FK} &= \rho g \zeta_a \int_L dx \int_C \phi_0(x) n_j d\ell \\
&= -\rho g \zeta_a \int_L e^{-ik_0 x \cos\mu} \left\{\int_C k_0 e^{-ik_0 z - ik_0 x \cos\mu} n_j d\ell\right\} dx,
\end{aligned}
\right\} \tag{2.70}
$$

$$
\left.
\begin{aligned}
E_j^D &= \rho g \zeta_a \int_L dx \int_C \phi_D(x) n_j d\ell \\
&= -\rho g \zeta_a \int_L k_0 e^{-ik_0 z - ik_0 x \cos\mu} \left\{\int_C (i \sin\mu\, \phi_2 - \phi_3) n_j ds\right\} d\ell.
\end{aligned}
\right\} \tag{2.71}
$$

Thus, the diffraction force for each motion direction can be summarized,

$$
E_j^D = \begin{cases}
-\rho g \zeta_a \int_L k_0 e^{-ik_0 z - ik_0 x \cos\mu} \left\{-\int_C \phi_3 n_j d\ell\right\} dx & (j = 1, 3, 5), \\
i\rho g \zeta_a \sin\mu \int_L k_0 e^{-ik_0 z - ik_0 x \cos\mu} \left\{-\int_C \phi_2 n_j d\ell\right\} dx & (j = 2, 4, 6).
\end{cases} \tag{2.72}
$$

2.3.7. Hydrodynamic Forces Acting on Center of Gravity

The hydrodynamic forces described above are respected to the midship of hull. Since the equations of motions must be considered to the center of gravity G, the transformation of each hydrodynamic force to around the center of gravity G is necessary. By assuming the position of the center of gravity G from midship are denoted as x_G in x-axis direction and and z_G in z-axis direction respectively, the normal vector n^G and the complex velocity potential ϕ_j^G at the center of gravity G can be expressed by the following equations,

$$\left.\begin{aligned} n_1^G &= n_1, \\ n_2^G &= n_2, \\ n_3^G &= n_3, \\ n_4^G &= yn_z - (z - z_G)n_y = n_4 + z_G n_2, \\ n_5^G &= -(x - x_G)n_z = n_5 + x_G n_3, \\ n_6^G &= (x - x_G)n_y = n_6 - x_G n_2, \end{aligned}\right\} \tag{2.73}$$

$$\left.\begin{aligned} \phi_1^G &= \phi_1, \\ \phi_2^G &= \phi_2, \\ \phi_3^G &= \phi_3, \\ \phi_4^G &= \phi_4 + z_G\phi_2, \\ \phi_5^G &= \phi_5 + x_G\phi_3, \\ \phi_6^G &= \phi_6 - x_G\phi_2. \end{aligned}\right\} \tag{2.74}$$

Therefore, radiation force Z_{ij}^G, wave exciting force E_i^G, and hydrostatic restoring force C_{ij}^G acting on the center of gravity G similarly can be expressed by the following equation,

- Longitudinal motion

$$\left.\begin{aligned} Z_{11}^G &= Z_{11}, \\ Z_{13}^G &= Z_{13}, \\ Z_{31}^G &= Z_{31}, \\ Z_{15}^G &= Z_{15} + x_G Z_{13}, \\ Z_{51}^G &= Z_{51} + x_G Z_{31}, \\ Z_{33}^G &= Z_{33}, \\ Z_{35}^G &= Z_{35} + x_G Z_{33}, \\ Z_{53}^G &= Z_{53} + x_G Z_{33}, \\ Z_{55}^G &= Z_{55} + x_G(Z_{35} + Z_{53}) + x_G^2 Z_{33}, \end{aligned}\right\} \tag{2.75}$$

$$\left.\begin{aligned} C_{33}^G &= C_{33}, \\ C_{35}^G &= C_{35} + x_G, \\ C_{53}^G &= C_{53} + x_G, \\ C_{55}^G &= C_{55} + x_G + \ x_G(C_{35} + C_{53}) + x_G^2, \end{aligned}\right\} \tag{2.76}$$

$$\left.\begin{aligned} E_1^G &= E_1, \\ E_3^G &= E_3, \\ E_5^G &= E_5 + x_G E_3, \end{aligned}\right\} \tag{2.77}$$

- Lateral motion

$$\left.\begin{aligned} Z_{22}^G &= Z_{22}, \\ Z_{24}^G &= Z_{24} + z_G Z_{22}, \\ Z_{26}^G &= Z_{26} - x_G Z_{22}, \\ Z_{42}^G &= Z_{42} + \ z_G Z_{22}, \\ Z_{62}^G &= Z_{62} - \ x_G Z_{22}, \\ Z_{44}^G &= Z_{44} + x_G(Z_{24} + Z_{42}) + z_G^2 Z_{22}, \\ Z_{46}^G &= Z_{46} + \ z_G Z_{26} + x_G(Z_{42} + z_G Z_{22}), \\ Z_{64}^G &= Z_{64} - \ x_G Z_{24} + z_G(Z_{62} - x_G Z_{22}), \\ Z_{66}^G &= Z_{66} - \ x_G(Z_{26} + Z_{62}) - x_G^2 Z_{22}, \end{aligned}\right\} \tag{2.78}$$

$$C_{44}^G = C_{44}, \tag{2.79}$$

$$\left.\begin{aligned} E_2^G &= E_2, \\ E_4^G &= E_4 + z_G E_2, \\ E_6^G &= E_6 + x_G E_2. \end{aligned}\right\} \tag{2.80}$$

2.3.8. Non-dimensional Motion Equations

By using the coefficients at the center of gravity described above, the motion equation for longitudinal motion is given as follow,

$$\left.\begin{aligned} &\text{surge: j} = 1 \\ &\quad \left(M + A_{11}^G\right)\ddot{x}(t) + B_{11}^G\dot{x}(t) + A_{13}^G\ddot{z}(t) + B_{13}^G\dot{z}(t) \\ &\qquad + A_{15}^G\ddot{\phi}(t) + B_{15}^G\dot{\phi}(t) = E_1^G e^{i\omega_e t}, \\ &\text{heave: j} = 3 \\ &\quad A_{31}^G\ddot{x}(t) + B_{31}^G\dot{x}(t) + \left(M + A_{33}^G\right)\ddot{z}(t) + B_{33}^G\dot{z}(t) + C_{33}^G z(t) \\ &\qquad + A_{35}^G\ddot{\phi}(t) + B_{35}^G\dot{\phi}(t) + C_{35}^G\phi(t) = E_3^G e^{i\omega_e t}, \\ &\text{pitch: j} = 5 \\ &\quad A_{51}^G\ddot{x}(t) + B_{51}^G\dot{x}(t) + A_{53}^G\ddot{z}(t) + B_{53}^G\dot{z}(t) + C_{53}^G z(t) \\ &\qquad + \left(I_{yy} + A_{55}^G\right)\ddot{\phi}(t) + B_{55}^G\dot{\phi}(t) + C_{55}^G\phi(t) = E_5^G e^{i\omega_e t}. \end{aligned}\right\} \tag{2.81}$$

Similarly, the motion equation for lateral motion is given as follow,

$$\left.\begin{aligned}
&\text{sway: j} = 2\\
&\quad \left(M + A_{22}^{G}\right)\ddot{y}(t) + B_{22}^{G}\dot{y}(t) + A_{24}^{G}\ddot{\theta}(t) + B_{24}^{G}\dot{\theta}(t)\\
&\qquad\qquad + A_{26}^{G}\ddot{\psi}(t) + B_{26}^{G}\dot{\psi}(t) = E_{2}^{G}e^{i\omega_e t},\\
&\text{roll: j} = 4\\
&\quad A_{42}^{G}\ddot{y}(t) + B_{42}^{G}\dot{y}(t) + \left(I_{xx} + A_{44}^{G}\right)\ddot{\theta}(t) + B_{44}^{G}\dot{\theta}(t) + C_{44}^{G}\theta(t)\\
&\qquad\qquad + A_{46}^{G}\ddot{\psi}(t) + B_{46}^{G}\dot{\psi}(t) = E_{4}^{G}e^{i\omega_e t},\\
&\text{yaw: j} = 6\\
&\quad A_{62}^{G}\ddot{y}(t) + B_{62}^{G}\dot{y}(t) + A_{64}^{G}\ddot{\theta}(t) + B_{64}^{G}\dot{\theta}(t)\\
&\qquad\qquad + \left(I_{zz} + A_{66}^{G}\right)\ddot{\psi}(t) + B_{66}^{G}\dot{\psi}(t) = E_{6}^{G}e^{i\omega_e t}.
\end{aligned}\right\} \quad (2.82)$$

By dividing both sides of Eq. (2.81) by $\rho\nabla$ for $(j = 1, 2)$ and $\rho\nabla\frac{L}{2}$ for $(j = 5)$, the following equations can be obtained,

$$\left.\begin{aligned}
&\text{surge: j} = 1\\
&\quad \left(1.0 + \frac{A_{11}^{G}}{\rho\nabla}\right)\ddot{x}(t) + \frac{B_{11}^{G}}{\rho\nabla}\dot{x}(t) + \frac{A_{13}^{G}}{\rho\nabla}\ddot{z}(t) + \frac{B_{13}^{G}}{\rho\nabla}\dot{z}(t)\\
&\qquad + \frac{A_{15}^{G}}{\rho\nabla\frac{L}{2}}\frac{L}{2}\ddot{\phi}(t) + \frac{B_{15}^{G}}{\rho\nabla\frac{L}{2}}\frac{L}{2}\dot{\phi}(t) = \frac{g\zeta_a A_w}{\nabla}\frac{E_1^G}{\rho g\zeta_a A_w}e^{i\omega_e t},\\
&\text{heave: j} = 3\\
&\quad \frac{A_{31}^{G}}{\rho\nabla}\ddot{x}(t) + \frac{B_{31}^{G}}{\rho\nabla}\dot{x}(t) + \left(1.0 + \frac{A_{33}^{G}}{\rho\nabla}\right)\ddot{z}(t) + \frac{B_{33}^{G}}{\rho\nabla}\dot{z}(t) + \frac{gA_w}{\nabla}\frac{C_{33}^{G}}{\rho gA_w}z(t)\\
&\qquad + \frac{A_{35}^{G}}{\rho\nabla\frac{L}{2}}\frac{L}{2}\ddot{\phi}(t) + \frac{B_{35}^{G}}{\rho\nabla\frac{L}{2}}\frac{L}{2}\dot{\phi}(t) + \frac{gA_w}{\nabla}\frac{C_{35}^{G}}{\rho gA_w\frac{L}{2}}\frac{L}{2}\phi(t) = \frac{g\zeta_a A_w}{\nabla}\frac{E_3^G}{\rho g\zeta_a A_w}e^{i\omega_e t},\\
&\text{pitch: j} = 5\\
&\quad \frac{A_{51}^{G}}{\rho\nabla\frac{L}{2}}\ddot{x}(t) + \frac{B_{51}^{G}}{\rho\nabla\frac{L}{2}}\dot{x}(t) + \frac{A_{53}^{G}}{\rho\nabla\frac{L}{2}}\ddot{z}(t) + \frac{B_{53}^{G}}{\rho\nabla\frac{L}{2}}\dot{z}(t) + \frac{gA_w}{\nabla}\frac{C_{53}^{G}}{\rho gA_w\frac{L}{2}}z(t)\\
&+ \left(\frac{I_{yy}}{\rho\nabla\left(\frac{L}{2}\right)^2} + \frac{A_{55}^{G}}{\rho\nabla\left(\frac{L}{2}\right)^2}\right)\frac{L}{2}\ddot{\phi}(t) + \frac{B_{55}^{G}}{\rho\nabla\left(\frac{L}{2}\right)^2}\frac{L}{2}\dot{\phi}(t) + \frac{gA_w}{\nabla}\frac{C_{55}^{G}}{\rho\nabla A_w\left(\frac{L}{2}\right)^2}\frac{L}{2}\phi(t) = \frac{g\zeta_a A_w}{\nabla}\frac{E_5^G}{\rho g\zeta_a A_w\frac{L}{2}}\frac{L}{2}e^{i\omega_e t}.
\end{aligned}\right\} \quad (2.83)$$

Thus, the equation of longitudinal motion expressed in non-dimensional is as follows,

$$\left.\begin{aligned}
&\text{surge: j} = 1\\
&\quad \left(1.0 + A_{11}^{G}{}'\right)\ddot{x}(t) + B_{11}^{G}{}'\dot{x}(t) + A_{13}^{G}{}'\ddot{z}(t) + B_{13}^{G}{}'\dot{z}(t)\\
&\qquad + A_{15}^{G}{}'\frac{L}{2}\ddot{\phi}(t) + B_{15}^{G}\frac{L}{2}\dot{\phi}(t) = \frac{g\zeta_a A_w}{\nabla}E_1^{G}{}'e^{i\omega_e t},\\
&\text{heave: j} = 3\\
&\quad A_{31}^{G}{}'\ddot{x}(t) + B_{31}^{G}{}'\dot{x}(t) + \left(1.0 + A_{33}^{G}{}'\right)\ddot{z}(t) + B_{33}^{G}{}'\dot{z}(t)\\
&\qquad + \frac{gA_w}{\nabla}C_{33}^{G}{}'z(t) + A_{35}^{G}{}'\frac{L}{2}\ddot{\phi}(t) + B_{35}^{G}{}'\frac{L}{2}\dot{\phi}(t) + \frac{gA_w}{\nabla}\frac{L}{2}C_{35}^{G}{}'\phi(t) = \frac{g\zeta_a A_w}{\nabla}E_3^{G}{}'e^{i\omega_e t},\\
&\text{pitch: j} = 5\\
&\quad A_{51}^{G}{}'\ddot{x}(t) + B_{51}^{G}{}'\dot{x}(t) + A_{53}^{G}{}'\ddot{z}(t) + B_{53}^{G}{}'\dot{z}(t) + \frac{gA_w}{\nabla}C_{53}^{G}{}'z(t)\\
&\qquad + \left(I_{yy}{}' + A_{55}^{G}{}'\right)\frac{L}{2}\ddot{\phi}(t) + B_{55}^{G}{}'\frac{L}{2}\dot{\phi}(t) + \frac{gA_w}{\nabla}\frac{L}{2}C_{55}^{G}\phi(t) = \frac{g\zeta_a A_w}{\nabla}E_5^{G}{}'e^{i\omega_e t}.
\end{aligned}\right\} \quad (2.84)$$

Similarly, dividing both side of Eq. (2.82) by $\rho\nabla$ for $(j = 2,4)$ and $\rho\nabla\frac{B}{2}$ for $(j = 6)$, the following equations can be obtained,

$$\left.\begin{aligned}
&\text{sway: j} = 2\\
&\left(1.0 + \frac{A_{22}^G}{\rho\nabla}\right)\ddot{y}(t) + \frac{B_{22}^G}{\rho\nabla}\dot{y}(t) + \frac{A_{24}^G}{\rho\nabla\frac{B}{2}}\frac{B}{2}\ddot{\theta}(t) + \frac{B_{24}^G}{\rho\nabla\frac{B}{2}}\frac{B}{2}\dot{\theta}(t)\\
&\qquad + \frac{A_{26}^G}{\rho\nabla\frac{L}{2}}\frac{L}{2}\ddot{\psi}(t) + \frac{B_{26}^G}{\rho\nabla\frac{L}{2}}\frac{L}{2}\dot{\psi}(t) = \frac{g\zeta_a A_w}{\nabla}\frac{E_2^G}{\rho g\zeta_a A_w}e^{i\omega_e t},\\
&\text{roll: j} = 4\\
&\frac{A_{42}^G}{\rho\nabla\frac{B}{2}}\ddot{y}(t) + \frac{B_{42}^G}{\rho\nabla\frac{B}{2}}\dot{y}(t) + \left(\frac{I_{xx}}{\rho\nabla\left(\frac{B}{2}\right)^2} + \frac{A_{44}^G}{\rho\nabla\left(\frac{B}{2}\right)^2}\right)\frac{B}{2}\ddot{\theta}(t) + \frac{B_{44}^G}{\rho\nabla\left(\frac{B}{2}\right)^2}\frac{B}{2}\dot{\theta}(t)\\
&\qquad + \frac{gA_w}{\nabla}\frac{C_{44}^G}{\rho gA_w\left(\frac{B}{2}\right)^2}\frac{B}{2}\theta(t) \quad + \frac{A_{46}^G}{\rho\nabla\frac{L}{2}\frac{B}{2}}\frac{L}{2}\ddot{\psi}(t) + \frac{B_{46}^G}{\rho\nabla\frac{L}{2}\frac{B}{2}}\frac{L}{2}\dot{\psi}(t) = \frac{g\zeta_a A_w}{\nabla}\frac{E_4^G}{\rho g\zeta_a A_w}e^{i\omega_e t},\\
&\text{yaw: j} = 6\\
&\frac{A_{62}^G}{\rho\nabla\frac{L}{2}}\ddot{y}(t) + \frac{B_{62}^G}{\rho\nabla\frac{L}{2}}\dot{y}(t) + \frac{A_{64}^G}{\rho\nabla\frac{L}{2}\frac{B}{2}}\frac{B}{2}\ddot{\theta}(t) + \frac{B_{64}^G}{\rho\nabla\frac{L}{2}\frac{B}{2}}\frac{B}{2}\dot{\theta}(t)\\
&\qquad + \left(\frac{I_{zz}}{\rho g\left(\frac{L}{2}\right)^2} + \frac{A_{66}^G}{\rho g\left(\frac{L}{2}\right)^2}\right)\frac{L}{2}\ddot{\psi}(t) + \frac{B_{66}^G}{\rho g\left(\frac{L}{2}\right)^2}\frac{L}{2}\dot{\psi}(t) = \frac{g\zeta_a A_w}{\nabla}\frac{E_6^G}{\rho g\zeta_a A_w\frac{L}{2}}e^{i\omega_e t}.
\end{aligned}\right\} \quad (2.85)$$

Thus, the equation of lateral motion expressed in non-dimensional is as follows,

$$\left.\begin{aligned}
&\text{sway: j} = 2\\
&\left(1.0 + A_{22}^{G\prime}\right)\ddot{y}(t) + B_{22}^{G\prime}\dot{y}(t) + A_{24}^{G\prime}\frac{B}{2}\ddot{\theta}(t) + B_{24}^{G\prime}\frac{B}{2}\dot{\theta}(t)\\
&\qquad + A_{26}^{G\prime}\frac{L}{2}\ddot{\psi}(t) + B_{26}^{G\prime}\frac{L}{2}\dot{\psi}(t) = \frac{g\zeta_a A_w}{\nabla}E_2^{G\prime}e^{i\omega_e t},\\
&\text{roll: j} = 4\\
&A_{42}^{G\prime}\ddot{y}(t) + B_{42}^{G\prime}\dot{y}(t) + \left(I_{xx}{}' + A_{44}^{G\prime}\right)\frac{B}{2}\ddot{\theta}(t) + B_{44}^{G\prime}\frac{B}{2}\dot{\theta}(t)\\
&\qquad + \frac{gA_w}{\nabla}C_{44}^{G\prime}\frac{B}{2}\theta(t) \quad + A_{46}^{G\prime}\frac{L}{2}\ddot{\psi}(t) + B_{46}^{G\prime}\frac{L}{2}\dot{\psi}(t) = \frac{g\zeta_a A_w}{\nabla}E_4^{G\prime}e^{i\omega_e t},\\
&\text{yaw: j} = 6\\
&A_{62}^{G\prime}\ddot{y}(t) + B_{62}^{G\prime}\dot{y}(t) + A_{64}^{G\prime}\frac{B}{2}\ddot{\theta}(t) + B_{64}^{G\prime}\frac{B}{2}\dot{\theta}(t)\\
&\qquad + \left(I_{zz}{}' + A_{66}^{G\prime}\right)\frac{L}{2}\ddot{\psi}(t) + B_{66}^{G}\frac{L}{2}\dot{\psi}(t) = \frac{g\zeta_a A_w}{\nabla}E_6^{G\prime}e^{i\omega_e t}.
\end{aligned}\right\} \quad (2.86)$$

Here, non-dimensionalization of the coefficients of motion equations are defined as follows,

$$M = \rho\nabla, \quad M' = \frac{M}{\rho\nabla} = 1.0, \quad (2.87)$$

$$\left.\begin{aligned}
I_{xx} &= \frac{W}{g}\kappa_{xx}^2, \qquad I'_{xx} = \frac{I_{xx}}{\rho\nabla\left(\frac{B}{2}\right)^2},\\
I_{yy} &= \frac{W}{g}\kappa_{yy}^2, \qquad I'_{yy} = \frac{I_{yy}}{\rho\nabla\left(\frac{L}{2}\right)^2},\\
I_{zz} &= \frac{W}{g}\kappa_{zz}^2, \qquad I'_{zz} = \frac{I_{zz}}{\rho\nabla\left(\frac{L}{2}\right)^2},
\end{aligned}\right\} \quad (2.88)$$

$$\left.\begin{aligned} C_{33} &= \rho g A_w, & C'_{33} &= \frac{C_{33}}{\rho g A_w}, \\ C_{35} &= C_{53} = -\rho g \int_{S_w} x dx dy, & C'_{35} &= C'_{53} = \frac{C_{35}}{\rho g A_w \frac{L}{2}}, \\ C_{55} &= W\overline{GM}_L, & C'_{55} &= \frac{C_{55}}{\rho \nabla A_w \left(\frac{L}{2}\right)^2}, \\ C_{44} &= W\overline{GM}, & C'_{44} &= \frac{C_{44}}{\rho \nabla A_w \left(\frac{B}{2}\right)^2}, \end{aligned}\right\} \tag{2.89}$$

$$Z'_{ij} = \frac{Z_{ij}}{\rho \nabla \epsilon_i \epsilon_j} = \frac{A_{ij}}{\rho \nabla \epsilon_i \epsilon_j} - i \frac{B_{ij}}{\rho \nabla \omega_e \epsilon_i \epsilon_j}, \tag{2.90}$$

$$E'_i = \frac{E_i}{\rho g \zeta_a A_w \epsilon_i}, \tag{2.91}$$

$$\epsilon_i = \begin{cases} 1 & (i = 1 \sim 3), \\ \frac{B}{2} & (i = 4), \\ \frac{L}{2} & (i = 5, 6). \end{cases} \tag{2.92}$$

M, W and ∇ are mass, weight and volume displacement of the floating body while κ_{xx}, κ_{yy}, and κ_{zz} are radius of gyration around x, y, and z axes respectively. A_w is water plane area while S_w represents the shape of water plane area. $\overline{GM}_L$ and $\overline{GM}$ are longitudinal and transverse metacentric height measured from G respectively.

2.4. Verification of Floating Body Motions Calculations

To verify the capability of the calculation method for obtaining hydrodynamic forces acting on the hull in waves by New Strip Method described in the previous section, numerical simulations were conducted to be compared with experimental results. Hydrodynamic forces in waves acting on the SR108 container ship and her motions are calculated and compared with the results from model experiments (Takahashi, 1987). The principle dimensions of SR108 container ship can be seen in Table 2.1 while the heave and pitch motions for both numerical calculation and model experiment are shown in Fig. 2.4. In this calculation, the ship is assumed to have forward speed ($F_n = 0.25$) and the investigated incident wave

Table 2.1. Principle Dimensions of SR108

Notation	Value
Length	175.000 m
Breath	25.375 m
Draft	9.5025 m
C_b	0.576

angles are taken every 30° from 0° to 180°.

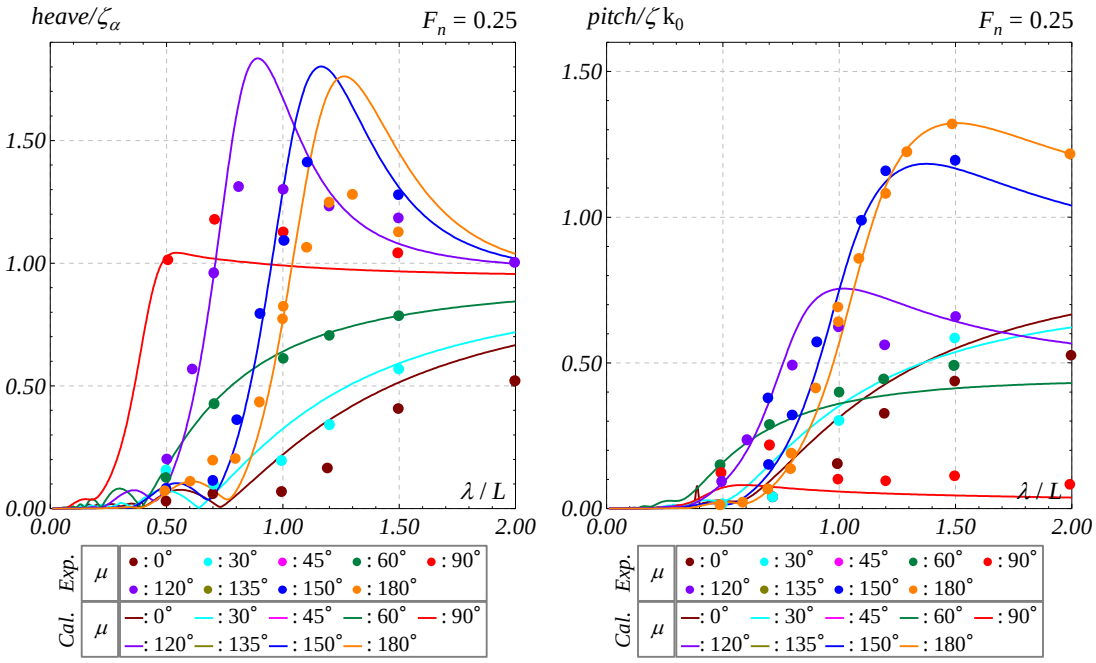

Fig. 2.4. Comparison result for SR108 (heave and pitch motions)

According to Fig. 2.4, the calculation results for both heave and pitch motions of SR108 show a good agreement though there are slight differences. For heave motion in Fig. 2.4, the differences between the calculation results and the experimental results occurs at $\lambda/L = 1.0$ at $\mu = 0°,\ 30°, \text{and}\ 60°$. Similar differences also appear in the calculation results for modified wigley hull based on the NSM and the Enhanced Unified Theory performed by Kashiwagi et al. (2000). The reason of this differences is the NSM and the Enhanced Unified Theory are linear theories. They can estimate the hydrodynamic forces around three-dimensional hull accurately in the range of small amplitude motion. However, as reported by Takaishi and Kuroi (1997), since nonlinearity becomes larger in large amplitude motion, the nonlinearity appears at the resonance point of motion, thereby those linear theories cannot solve the resonance motion exactly. Even so, since the calculation results generally have sufficient accuracy for both motions, the calculation method by NSM can be considered to be sufficient to calculate the hydrodynamic forces and the motions of a floating structure in waves.

For further verification, same kind of calculations also has been made for ESSO OSAKA with zero forward speed as the target vessel used in this research (It will be explained in detail in the next chapter). The principle dimensions of ESSO OSAKA are provided in Table 2.2 while the motions results are shown in Fig. 2.5.

Table 2.2. Principle Dimensions of ESSO OSAKA

Notation	Value
Length	325.000 m
Breath	53.000 m
Draft	22.05 m
C_b	0.810

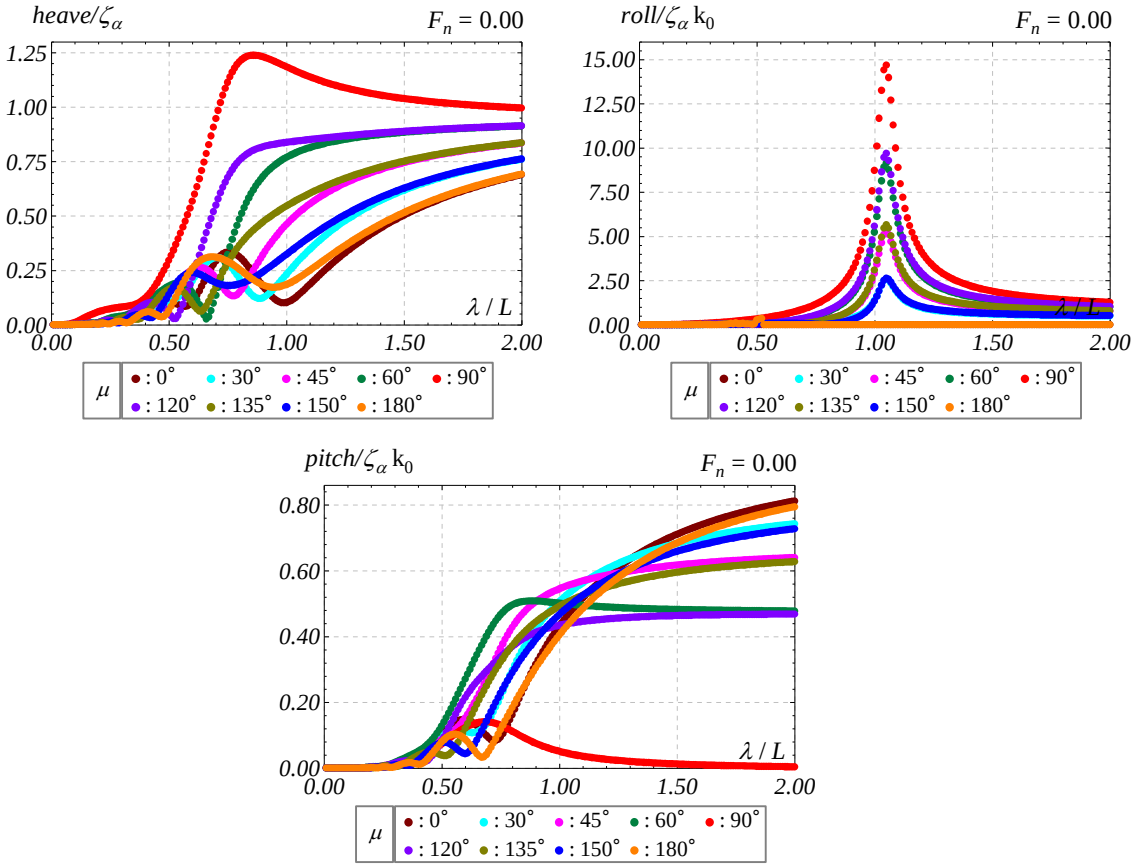

Fig. 2.5. Calculation results for ESSO OSAKA (heave, pitch, roll)

2.5. Mathematical Model for External Forces

If a floating offshore structure is treated to be kept in a stationary position by a mooring system, it is important to specify the motion of the floating structure and its displacement especially in horizontal plane. The displacement of the floating structure in horizontal plane is mainly affected by horizontal plane motions such as surge, sway, and yaw when the floating structure is moored by mooring system. On the other hand, though vertical motions such as heave, pitch, and roll do not affect the horizontal displacement so much, these

motions are also necessary to be investigated to ensure the safety operation of the floating structure. Moreover, external disturbances such as wave, wind, and current as well as mooring line tension which act on the floating offshore structure must be considered properly. Therefore, the mathematical model to represent the horizontal motion and the vertical motion of the floating structure must be introduced. The mathematical model should take the external disturbances into account including mooring line tension.

In this study, a combination of mathematical model based on Manoeuvring Modeling Group (MMG) and conventional floating body motion equations are used to perform the simultaneous analysis of coupled-motions between the floating structure and mooring lines. Three-dimensional lumped mass method is used to calculate the dynamics of mooring lines including the effects of hydrodynamic forces and their elasticity. The calculated mooring line motion is combined with the floating body motion in the horizontal plane calculated by using MMG model to introduce the coupled-motion effect between the floating body and the mooring lines simultaneously. The external forces comprising wave, wind, and current forces are included into the mathematical model.

The mathematical model based on MMG model used in this study is explained as follows. By using the coordinate system shown in Fig. 2.1, the following relation is established.

$$\left.\begin{aligned} m\ddot{x}_0 &= X_0, \\ m\ddot{y}_0 &= Y_0, \\ I_{zz}\ddot{\psi} &= N, \end{aligned}\right\} \tag{2.93}$$

m and I_{zz} are the mass and the moment of inertia of the floating structure. X_0 and Y_0 are axial components of force acting on the floating body in the earth-fixed coordinate system. The axial component X_0 and Y_0 can be transformed to the axial component in the body-fixed coordinate system by the following equations,

$$\left.\begin{aligned} X &= X_0 \cos\psi + Y_0 \sin\psi, \\ Y &= Y_0 \cos\psi - X_0 \sin\psi. \end{aligned}\right\} \tag{2.94}$$

Substituting Eq. (2.93) into Eq. (2.94) gives following equations,

$$\left.\begin{aligned} X &= m(\ddot{x}_0 \cos\psi + \ddot{y}_0 \sin\psi), \\ Y &= m(\ddot{y}_0 \cos\psi - \ddot{x}_0 \sin\psi). \end{aligned}\right\} \tag{2.95}$$

The velocity component $\dot{x}_0$, $\dot{y}_0$ in the inertial system is expressed by the following equation using velocity component u, v in the x- and y-axis directions of the body-fixed coordinate system.

$$\left.\begin{aligned}\dot{x}_0 &= u\cos\psi - v\sin\psi,\\ \dot{y}_0 &= v\cos\psi + u\sin\psi.\end{aligned}\right\} \tag{2.96}$$

By differentiating Eq. (2.96), the following equations for acceleration component in the x- and y-axis directions can be obtained.

$$\left.\begin{aligned}\ddot{x}_0 &= \dot{u}\cos\psi - u\dot{\psi}\sin\psi - \dot{v}\sin\psi - v\dot{\psi}\cos\psi,\\ \ddot{y}_0 &= \dot{v}\cos\psi - v\dot{\psi}\sin\psi + \dot{u}\sin\psi + u\dot{\psi}\cos\psi.\end{aligned}\right\} \tag{2.97}$$

Substituting Eq. (2.97) into Eq. (2.95), the equations of motion respect to the body-fixed coordinate system are given as,

$$\left.\begin{aligned}m(\dot{u} - v\dot{\psi}) &= X,\\ m(\dot{v} + u\dot{\psi}) &= Y,\\ I_{zz}\ddot{\psi} &= N.\end{aligned}\right\} \tag{2.98}$$

Further, taken into account the effect of added mass due to the movement of the body in viscous fluid, Eq. (2.98) becomes,

$$\left.\begin{aligned}(m + m_x)\dot{u} - (m + m_y)vr &= X,\\ (m + m_y)\dot{v} + (m + m_x)ur &= Y,\\ (I_{zz} + i_{zz})\dot{r} &= N,\end{aligned}\right\} \tag{2.99}$$

where,

m,m_x,m_y : hull mass, added mass component in x- and y-axis directions,

I_{zz}, i_{zz} : moment and added moment of inertia around z-axis,

u, v : velocity component in x- and y-axis directions,

r : yaw rate.

Here, considering the effect of current, relative velocity components u^* and v^* acting on the center of gravity of the hull need to be established. The relative velocity components u^* and v^* can be expressed as follows by involving the ship speed U, drift angle β, and heading angle ψ.

$$\left.\begin{aligned}u^* &= U\cos\beta + V_C\cos(\psi - \alpha),\\ v^* &= -U\sin\beta - V_C\sin(\psi - \alpha).\end{aligned}\right\} \tag{2.100}$$

in which, V_C and α are the velocity and direction of current respect to the earth-fixed coordinate system respectively. Then, Eq. (2.99) can be rewritten by considering the effect of the relative velocity components u^* and v^* as follows,

$$\left.\begin{aligned}(m+m_x)\dot{u}^* - (m+m_y)v^*r &= X,\\ (m+m_y)\dot{v}^* + (m+m_x)u^*r &= Y,\\ (I_{zz}+i_{zz})\dot{r} &= N.\end{aligned}\right\} \tag{2.101}$$

Finally, substituting Eq. (2.101) into Eq. (2.100), the equations of motion in horizontal plane are expressed by the following equations.

$$\left.\begin{aligned}(m+m_x)\dot{u} - (m+m_y)vr - (m_x-m_y)V_c r\sin(\psi-\alpha) &= X,\\ (m+m_y)\dot{v} + (m+m_x)ur - (m_y-m_x)V_c r\cos(\psi-\alpha) &= Y,\\ (I_{zz}+i_{zz})\dot{r} &= N.\end{aligned}\right\} \tag{2.102}$$

The external forces X, Y, and moment N are expressed by the following equations based on the MMG model report's idea (Ogawa et al., 1997).

$$\left.\begin{aligned}X &= X_H + X_W + X_T,\\ Y &= Y_H + Y_W + Y_T + Y_D,\\ N &= N_H + N_W + N_T + N_D.\end{aligned}\right\} \tag{2.103}$$

Here, subscripts H, W, T and D respectively indicate hydrodynamic forces, wind forces, mooring line tension forces and wave drift forces acting on the hull. In this study, propeller thrust and rudder forces are not considered. Furthermore, wave drift force in x-axis direction is not considered since that force tends to be small comparing with the other forces.

2.5.1. Hydrodynamic Forces

Hydrodynamic forces acting on the hull are expressed as follows, according to Yasukawa and Yoshimura (2015),

$$\left.\begin{aligned}X_H, Y_H &= \frac{1}{2}\rho L d U^{*2} \times X'_H, Y'_H,\\ N_H &= \frac{1}{2}\rho L^2 d U^{*2} \times N'_H.\end{aligned}\right\} \tag{2.104}$$

in which ρ is water density while L and d are the length and draught of the floating structure respectively. U^* represents relative speed over current, X'_H and Y'_H are non-dimensional hydrodynamic forces in x- and y-directions and N'_H is non-dimensional yaw moment.

(1) Non-dimensional Longitudinal Hydrodynamic Force X'_H

In this study, non-dimensional longitudinal hydrodynamic force X'_H is calculated based on the following model proposed by Kijima et al. (1990),

$$X'_H = X'_{uu}\cos\beta^*|\cos\beta^*| + X'_{\beta r} r'\sin\beta^*, \tag{2.105}$$

r' represents non-dimensional yaw rate ($= rL/U$) and β^* is relative drift angle considering

current velocity. X'_{uu} is non-dimensional resistance in forward straight motion and $X'_{\beta r}$ represents the variation of longitudinal force due to drift and yaw motions. Since the non-dimensional value of yaw rate r' is small for vessel without forward speed (stationary vessel) (Ahn, 2003), Eq. (2.105) can be expressed by the following equation neglecting the term of r'.

$$X'_H = X'_{uu} \cos\beta^* |\cos\beta^*|. \tag{2.106}$$

(2) Non-dimensional Latera Hydrodynamic Force Y'_H and Moments N'_H

When a ship runs with forward speed, drift angle is relatively small and dominant force component acting on a ship hull is lift forces. However, at the case of low speed motion, especially for the vessel speeds close to 0, the lateral motion of the vessel becomes relatively larger so that drift angle has relatively large value. Occasionally, the value of non-dimensional yaw rate becomes large. In consequences, drift and yaw motions become to have dominant effect on hydrodynamic forces acting on the hull. It means that the main component of hydrodynamic forces shifts from lift force to cross flow drag force. Because the moored floating structure tends to move with low speed, hydrodynamic forces for large drift angle should be taken into consideration.

Therefore, calculation of Y'_H and N'_H is classified into two conditions according to the magnitude of drift angle, i.e. for the condition with small drift angle $(\beta \leq 30°)$ and the condition with large drift angle $(\beta > 30°)$. It should be noted that drift angle β is replaced with relative drift angle β^* when the influences of current is considered.

a. Small drift angle $(\beta^* \leq 30°)$

In this study, Y'_H and N'_H for the condition with small relative drift angle $(\beta^* \leq 30°)$ are calculated by the following mathematical models presented by Kijima et al. (1990).

$$\left.\begin{aligned} Y'_H &= Y'_\beta\beta^* + Y'_r r' + Y'_{\beta\beta}\beta^*|\beta^*| + Y'_{rr} r'|r'| + \left(Y'_{\beta\beta r}\beta^* + Y'_{\beta rr} r'\right)\beta^* r', \\ N'_H &= N'_\beta\beta^* + N'_r r' + N'_{\beta\beta}\beta^*|\beta^*| + N'_{rr} r'|r'| + +\left(N'_{\beta\beta r}\beta^* + N'_{\beta rr} r'\right)\beta^* r'. \end{aligned}\right\} \tag{2.107}$$

Here, Y'_β, Y'_r, and so on are hydrodynamic derivatives denoted as $Y'_\beta = \partial Y'_H/\partial\beta$, $Y'_r = \partial Y'_H/\partial r'$, and so on. These hydrodynamic derivatives were obtained by captive model tests.

b. Large drift angle $(\beta^* > 30°)$

Since the lateral motion of the floating structure in low speed motion becomes relatively larger comparing with running ship, a mathematical model presented by Muto et al. (2010) to consider the effect of large drift angle are adopted to calculate Y'_H and N'_H for large drift angle $(\beta^* > 30°)$. The lateral force and yaw moment are obtained by interpolating values given by the following formulae,

$$\left.\begin{aligned} Y_{H}{}'_{(r',\alpha)} &= A_{Y\alpha}r'^{2} + B_{Y\alpha}r' \ + C_{Y\alpha}, \\ N_{H}{}'_{(r',\alpha)} &= A_{N\alpha}r'^{2} + B_{N\alpha}r' + C_{N\alpha}, \end{aligned}\right\} \tag{2.108}$$

in which α indicates drift angles 45°, 90°, 135° and 180° at where inherent characteristics of lateral force and yaw moment are defined. $A_{Y\alpha}$, $B_{Y\alpha}$, $C_{Y\alpha}$ and $A_{N\alpha}$, $B_{N\alpha}$, $C_{N\alpha}$ are coefficients for Y'_H and N'_H. These coefficients are obtained by the following approximate formulae which consist of vessel's principal particulars,

$$\left.\begin{aligned} Y'_{H(r',45)} &= A_{Y45}r'^{2} + B_{Y45}r' + C_{Y45}, \\ A_{Y45} &= -0.251 \times \left(\frac{C_b^2 L}{B}\right)^2 + 1.533 \times \left(\frac{C_b^2 L}{B}\right) - 1.923, \\ B_{Y45} &= -4.828 \times \left(\frac{d}{B}\right)^2 + 6.147 \times \left(\frac{d}{B}\right) - 1.613, \\ C_{Y45} &= 0.297 \times \left(\frac{C_b^2 L}{B}\right)^2 - 2.102 \times \ \left(\frac{C_b^2 L}{B}\right) + 4.135, \end{aligned}\right\} \tag{2.109}$$

$$\left.\begin{aligned} N'_{H(r',45)} &= A_{N45}r'^{2} + B_{N45}, \\ A_{N45} &= -0.049 \times \left(\frac{C_b B}{d}\right)^2 + 0.301 \times \left(\frac{C_b B}{d}\right) - 1.556, \\ B_{N45} &= 0.812 \times 10^{-5} \times \left(\frac{(1-C_b)L^2}{d^2}\right)^2 - 0.001 \times \left(\frac{(1-C_b)L^2}{d^2}\right) + 0.131, \end{aligned}\right\} \tag{2.110}$$

$$\left.\begin{aligned} Y'_{H(r',90)} &= A_{Y90}r'^{2} + B_{Y90}r' + C_{Y90}, \\ A_{Y90} &= 0.068 \times \left(\frac{C_b^2 L}{B^2}\right)^2 - 3.853 \times \left(\frac{C_b^2 L}{B^2}\right) + 54.699, \\ B_{Y90} &= -591.264 \times \left(\frac{BC_b}{L}\right)^2 + 144.627 \times \left(\frac{BC_b}{L}\right) - 8.589, \\ C_{Y90} &= 25.572 \times \left(\frac{dC_b}{B}\right)^2 - 12.774 \times \ \left(\frac{dC_b}{B}\right) + 2.128, \end{aligned}\right\} \tag{2.111}$$

$$\left.\begin{aligned} N'_{H(r',90)} &= A_{N90}r'^{2} + B_{N90}r' + C_{N90}, \\ A_{N90} &= -0.003 \times \left(\frac{(1-C_b)L^2}{B^2}\right)^2 + 0.083 \times \left(\frac{(1-C_b)L^2}{B^2}\right) - 0.445, \\ B_{N90} &= 0.032 \times \left(\frac{dL}{B^2}\right)^2 - 0.187 \times \left(\frac{dL}{B^2}\right) + 0.195, \\ C_{N90} &= 0.043 \times \left(\frac{C_b B}{d}\right)^2 - 0.229 \times \ \left(\frac{C_b B}{d}\right) + 0.298, \end{aligned}\right\} \tag{2.112}$$

$$\left.\begin{aligned} Y'_{H(r',135)} &= A_{Y135}r'^{2} + B_{Y135}r' + C_{Y135}, \\ A_{Y135} &= -0.667 \times \left(\frac{C_b L}{B}\right)^2 + 7.117 \times \left(\frac{C_b L}{B}\right) - 18.303, \\ B_{Y135} &= -0.618 \times \left(\frac{C_b^2 L}{B}\right)^2 + 4.442 \times \left(\frac{C_b^2 L}{B}\right) - 7.946, \\ C_{Y135} &= 0.337 \times \left(\frac{C_b^2 L}{B}\right)^2 - 2.427 \times \ \left(\frac{C_b^2 L}{B}\right) + 4.769, \end{aligned}\right\} \tag{2.113}$$

$$\left.\begin{aligned} N'_{H(r',135)} &= A_{N135}r'^2 + B_{N135}r' + C_{N135}, \\ A_{N135} &= 4.936 \times \left(\frac{d}{B}\right)^2 - 3.020 \times \left(\frac{d}{B}\right) + 0.470, \\ B_{N135} &= -3.148 \times \left(\frac{B(1-C_b)^2}{d}\right)^2 + 1.353 \times \left(\frac{B(1-C_b)^2}{d}\right) - 0.206, \\ C_{N135} &= -427.089 \times \left(\frac{Bd^2}{L^3(1-C_b)}\right)^2 - 11.481 \times \left(\frac{Bd^2}{L^3(1-C_b)}\right) - 0.031, \end{aligned}\right\} \quad (2.114)$$

$$\left.\begin{aligned} Y'_{H(r',180)} &= A_{Y180}r'^2 + B_{Y180}r' + C_{Y180}, \\ A_{Y180} &= 57.749 \times \left(\frac{dC_b}{B}\right)^2 - 30.544 \times \left(\frac{dC_b}{B}\right) + 3.833, \\ B_{Y180} &= -2212.42 \times \left(\frac{B(1-C_b)}{L}\right)^2 + 175.133 \times \left(\frac{B(1-C_b)}{L}\right) - 3.150, \\ C_{Y180} &= 714.766 \times \left(\frac{C_b dL^2}{LB}\right)^2 - 22.156 \times \left(\frac{C_b dL^2}{LB}\right) + 0.1442, \end{aligned}\right\} \quad (2.115)$$

$$\left.\begin{aligned} N'_{H(r',180)} &= A_{N180}r'^2 + B_{N180}r' + C_{N180}, \\ A_{N180} &= -6.741 \times \left(\frac{B^2C_b}{Ld}\right)^2 + 5.899 \times \left(\frac{B^2C_b}{Ld}\right) - 1.159, \\ B_{N180} &= -7.3 \times 10^{-6} \times \left(\frac{(1-C_b)L^2}{d^2}\right)^2 + 0.002 \times \left(\frac{(1-C_b)L^2}{d^2}\right) - 0.182, \\ C_{N180} &= -0.001 \times \left(\frac{C_b^2 L}{d}\right)^2 + 0.022 \times \left(\frac{C_b^2 L}{d}\right) - 0.124, \end{aligned}\right\} \quad (2.116)$$

where,

$Y'_{H(r',45)}$: approximation of Y'_H at $\beta = 45°$,
$N'_{H(r',45)}$: approximation of N'_H at $\beta = 45°$,
$Y'_{H(r',90)}$: approximation of Y'_H at $\beta = 90°$,
$N'_{H(r',90)}$: approximation of N'_H at $\beta = 90°$,
$Y'_{H(r',135)}$: approximation of Y'_H at $\beta = 135°$,
$N'_{H(r',135)}$: approximation of N'_H at $\beta = 135°$,
$Y'_{H(r',180)}$: approximation of Y'_H at $\beta = 180°$,
$N'_{H(r',180)}$: approximation of N'_H at $\beta = 180°$.

2.5.2. Wind Forces

Wind forces acting on the floating structure are usually calculated by using empirical formulae involving the approximation of wind force coefficients. Only wind forces in the horizontal plane are considered since the wind force coming from the other directions are relatively small. Since the shape of the upper structure of the floating body above water surface is not simple, especially for ship-type floating structure, several methods have been existed for calculating wind forces acting on the floating structure. Approximate formulae for wind force coefficients based on experimental results are often used to predict those wind

forces and moment.

As the practical method, the methods to calculate wind forces and moment for ship are presented by Isherwood (1972) and Yamano and Saito (1997). They are linear multiple regression model based on experimental works. Another approximation method has been given by Yoneta (1992) by using coefficients obtained from the regression analysis of experimental results. OCIMF (1997) provides the wind load formulae by using coefficients obtained from experimental results of oil tanker while OCIMF (2010) presents wind force formulae only for longitudinal direction. In recent years, the shapes of ships are completely various, such as VLCC, PCC, FLNG, etc., and the shape of their upper-structure becomes complicated. Then, those estimation methods may lack reliability to estimate wind forces and moment acting on such vessels. Therefore, to minimize the lack of accuracy, approximate formulae for wind forces are proposed by Fujiwara et al. (1998) based on a wide range of experimental data consisting of various ship type such as VLCC, PCC, and LNG are used in this study.

(1) Approximation Formulae for Wind Forces and Moment

Assuming wind with wind speed V_W and wind direction ν coming to the hull in the earth-fixed coordinate system shown in Fig. 2.1, relative wind speed $\bar{V}$ and ν^* at the hull's center of gravity in the body-fixed coordinate system can be introduced in Fig. 2.6.

When a ship is traveling with forward speed U, drift angle β, and heading angle ψ, $\bar{V}_x$ and $\bar{V}_y$ which are x- and y-axis direction components of the relative wind velocity $\bar{V}$ at the midship of ship hull is expressed by the following equation.

$$\left.\begin{aligned} \bar{V}_x &= U\cos\beta - V_W\cos(\psi-\nu), \\ \bar{V}_y &= -U\sin\beta - V_W\sin(\psi-\nu). \end{aligned}\right\} \tag{2.117}$$

Thereby, the relative wind speed $\bar{V}$ and relative wind direction ν^* are expressed as follows,

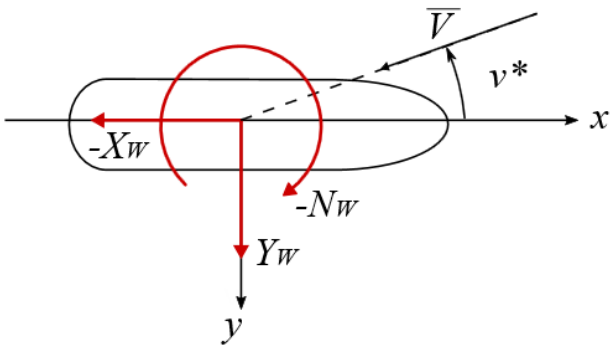

Fig. 2.6. Relative speed and relative wind directions

$$\left.\begin{aligned} \bar{V} &= \sqrt{\bar{V}_x^2 - \bar{V}_y^2}, \\ \nu^* &= \tan^{-1}\left(\frac{-\bar{V}_y}{\bar{V}_x}\right). \end{aligned}\right\} \tag{2.118}$$

When the wind force coefficients in longitudinal and lateral directions and wind moment coefficient are denoted as $C_X(\nu^*)$, $C_Y(\nu^*)$, and $C_N(\nu^*)$ respectively, the wind forces in longitudinal direction X_W and lateral direction Y_W as well as wind moment N_{W_M} around the midship of the vessel can be expressed as follows,

$$\left.\begin{aligned} X_W &= \frac{1}{2}\rho_A A_T \bar{V}^2 C_X(\nu^*), \\ Y_W &= \frac{1}{2}\rho_A A_L \bar{V}^2 C_Y(\nu^*), \\ N_{W_M} &= \frac{1}{2}\rho_A A_L L_{OA} \bar{V}^2 C_N(\nu^*). \end{aligned}\right\} \tag{2.119}$$

Here, ρ_A is density of the air. A_T and A_L are transverse and lateral projected areas respectively. The wind forces and moment coefficient $C_X(\nu^*)$, $C_Y(\nu^*)$, and $C_N(\nu^*)$ are obtained based on the formulae given by Fujiwara et al. (1998) as the function of relative wind direction ν^*. Since the acting forces are normally respected to the hull's center of gravity, the wind forces and moment can be calculated by using Eq. (2.119) with transforming N_{W_M} to hull's center of gravity by the following relation,

$$N_W = N_{W_M} - Y_W \cdot \overline{MG}. \tag{2.120}$$

(2) Approximation Formulae for Wind Forces and Moment Coefficients

The estimation equation given by Fujiwara et al. (1998) is also applicable to ships with complex upper structures. The wind forces and moment coefficients $C_X(\nu^*)$, $C_Y(\nu^*)$, and $C_N(\nu^*)$ are expressed as,

$$\left.\begin{aligned} C_X(\nu^*) &= X_0 + X_1 \cos\nu^* + X_3 \cos 3\nu^* + X_5 \cos 5\nu^*, \\ C_Y(\nu^*) &= Y_1 \sin\nu^* + Y_3 \sin 3\nu^* + Y_5 \sin 5\nu^*, \\ C_N(\nu^*) &= N_1 \sin\nu^* + N_2 \sin 2\nu^* + N_3 \sin 3\nu^*. \end{aligned}\right\} \tag{2.121}$$

Here, each coefficient X_0, X_{01}, etc. are expressed by the following equations.

$$
\left.
\begin{aligned}
X_0 &= x_{00} + x_{01}\frac{BH_{BR}}{A_T} + x_{02}\frac{C}{H_C} + x_{03}\frac{A_{OD}}{L_{OA}^2}, \\
X_1 &= x_{10} + x_{11}\frac{A_L}{L_{OA}B} + x_{12}\frac{LH_C}{A_L} + x_{13}\frac{L_{OA}H_{BR}}{A_L} + x_{14}\frac{A_{OD}}{A_L} \\
&\quad + x_{15}\frac{A_T}{L_{OA}B} + x_{16}\left(\frac{A_T}{L_{OA}^2}\right)^{-1} + x_{17}\left(\frac{H_C}{L_{OA}}\right)^{-1}, \\
X_3 &= x_{30} + x_{31}\left(\frac{L_{OA}H_{BR}}{A_L}\right)^{-1} + x_{32}\frac{A_L}{A_T} + x_{33}\frac{L_{OA}H_C}{A_L} + x_{34}\frac{A_{OD}}{A_L} \\
&\quad + x_{35}\frac{A_{OD}}{L_{OA}^2} + x_{36}\frac{C}{H_C} + x_{37}\frac{C_{BR}}{L_{OA}}, \\
X_5 &= x_{50} + x_{51}\left(\frac{A_{OD}}{A_L}\right)^{-1} + x_{52}\frac{C_{BR}}{L_{OA}} + x_{53}\frac{A_L}{L_{OA}B},
\end{aligned}
\right\} \tag{2.122}
$$

$$
\left.
\begin{aligned}
Y_1 &= y_{10} + y_{11}\frac{C_{BR}}{L_{OA}} + y_{12}\frac{C}{L_{OA}} + y_{13}\left(\frac{A_{OD}}{A_L}\right)^{-1} + y_{14}\frac{C}{H_C} + y_{15}\left(\frac{BH_{BR}}{A_T}\right)^{-1}, \\
Y_3 &= y_{30} + y_{31}\frac{A_L}{L_{OA}B} + y_{32}\frac{L_{OA}H_C}{A_L} + y_{33}\frac{C_{BR}}{L_{OA}} + y_{34}\left(\frac{H_{BR}}{B}\right)^{-1} \\
&\quad + y_{35}\frac{A_{OD}}{A_L} + y_{36}\left(\frac{BH_{BR}}{A_T}\right)^{-1}, \\
Y_5 &= y_{50} + y_{51}\left(\frac{A_L}{L_{OA}B}\right)^{-1} + y_{52}\left(\frac{H_{BR}}{L_{OA}}\right)^{-1} + y_{53}\frac{C_{BR}}{L_{OA}} + y_{54}\left(\frac{A_T}{B^2}\right)^{-1} \\
&\quad + y_{55}\frac{C}{L_{OA}} + y_{56}\frac{L_{OA}H_C}{A_L},
\end{aligned}
\right\} \tag{2.123}
$$

$$
\left.
\begin{aligned}
N_1 &= n_{10} + n_{11}\frac{C}{L_{OA}} + n_{12}\frac{L_{OA}H_C}{A_L} + n_{13}\left(\frac{A_L}{A_T}\right)^{-1} + n_{14}\frac{C}{H_C} \\
&\quad + n_{15}\frac{A_L}{LB} + n_{16}\frac{A_T}{L_{OA}^2} + n_{17}\left(\frac{A_T}{B^2}\right)^{-1} + n_{18}\frac{C_{BR}}{L_{OA}}, \\
N_2 &= n_{20} + n_{21}\frac{C_{BR}}{L_{OA}} + n_{22}\frac{C}{L_{OA}} + n_{23}\left(\frac{A_{OD}}{A_L}\right)^{-1} + n_{24}\frac{A_T}{B^2} \\
&\quad + n_{25}\left(\frac{H_{BR}}{L_{OA}}\right)^{-1} + n_{26}\left(\frac{BH_{BR}}{A_T}\right)^{-1} + n_{27}\frac{A_L}{L_{OA}B} + n_{28}\frac{A_L}{L_{OA}^2}, \\
N_3 &= n_{30} + n_{31}\frac{C_{BR}}{L_{OA}} + n_{32}\left(\frac{BH_{BR}}{A_T}\right)^{-1} + n_{33}\frac{A_L}{A_T},
\end{aligned}
\right\} \tag{2.124}
$$

where,

L_{OA} : length over all (m),

B : breadth (m),

A_T : transverse projected area (m^2),

A_L : lateral projected area (m^2),

A_{SS} : lateral projected area of superstructure (m^2),

A_{OD} : A_{SS} and lateral projected area of LNG tanks and container etc. on the deck,

C : distance from midship section to the center of A_L (m),

C_{BR} : distance from midship section to the center of A_{SS} (m),

H_{BR} : height of the top of superstructure (m),

H_C : height of the center of lateral projected area (m).

The meaning of each parameter is shown in Fig. 2.7. The figure shows the shape of the hull viewed from bow and starboard side direction respectively. Whilst the approximate value for each coefficient in Eq. (2.122) to Eq. (2.124) are provided in Table 2.3.

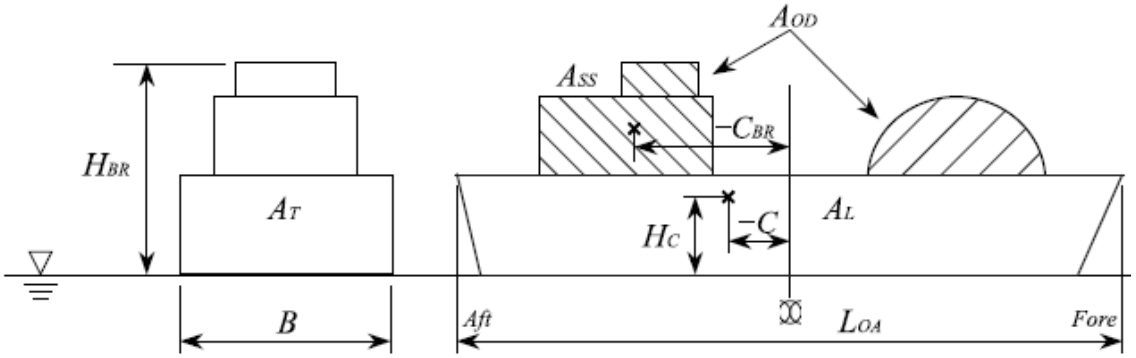

Fig. 2.7. Relative speed and relative wind directions

Table 2.3. Coefficient of independent variable for wave forces and moment coefficients

m =	0	1	2	3	4	5	6		
x_{0m}	-0.330	0.293	0.0193	0.683					
x_{1m}	-1.353	1.700	2.870	-0.463	-0.570	-0.570	-0.0123	0.0202	
x_{2m}	0.830	-0.413	-0.0827	-0.563	0.804	0.804	0.0401	-0.132	
x_{3m}	0.0372	-0.0075	-0.103	0.0921					
y_{1m}	0.684	0.717	-3.220	0.0281	0.0611	0.0661			
y_{2m}	-0.400	0.307	0.307	0.0519	0.0526	0.0526	0.0582		
y_{3m}	0.122	-0.166	-0.0054	-0.0481	-0.0136	-0.0136	-0.0297		
n_{1m}	0.299	1.710	0.183	-1.090	-0.0442	-0.0442	4.240	-0.0646	0.0306
n_{2m}	0.117	0.123	-0.323	0.0041	-0.166	-0.166	0.174	0.214	-1.060
n_{3m}	0.0230	-0.0385	-0.0339	0.0023					

2.5.3. Wave Drifting Forces

When incident waves act on a ship, besides unsteady force components caused by the first order wave force, the wave forces contain the second order steady force due to the various nonlinear effect of the waves. The forces are generally relatively small comparing with the first order force, and it can be neglected for a running ship, however this force needs to be considered for stationary vessel since it can cause large drift motions in horizontal plane. Wave drifting force in longitudinal direction acting on a ship with forward speed is called added resistance in which the magnitude of this force is also affected by the forward

speed. On the other hand, the lateral wave drifting force and moment are not affected by the forward speed. Since the influence of longitudinal wave drifting force for stationary vessel is relatively small comparing with the others, the wave drifting force for longitudinal direction can be neglected.

To obtain the wave drifting forces and moment acting on a ship, a theoretical method has been provided by Maruo (1960) excluding drifting moment and there were no computations presented. Manabe (1960) analyzed yaw moment for a drifting ship, but it neglected hydrodynamic restoring moment in order to favor the second-order inertial coupling effect of the ship. The method called Newman's method (Newman, 1967) existed to calculate drifting forces and moment by using the technique of linearized water wave problem applying the momentum relations to express the drifting forces and moment in terms of far-field disturbance (far-field method).

Kashiwagi and Ohkusu (1991) provided a new analysis method for investigating drifting forces and moment by using the principle of momentum conservation for a running ship expressing the velocity potential component in Fourier transform considering Green and Kochin functions. Other methods generated by taking the idea of unified theory (Newman and Sclavounos, 1980) were presented by Kashiwagi and Ohkusu (1993) which calculates the Kochin function by NSM and Kashiwagi (1995) for developing enhanced unified theory. Recently, the drifting forces and moment calculated by using a developing near-field method to be a new model called middle-field method i.e. Chen, 2004; 2005; 2006; and Chen and Rezende, 2009). This method is often used for three-dimensional panel method.

In this study, the method reported by Kashiwagi and Iwashita, 2012 for NSM is used for calculating wave drifting forces and moments. If there is no forward speed, exact calculations by the three-dimensional boundary element method are generally performed based on Maruo's drifting force theory and the theory of drifting moment by Newman. There is no need to solve high-order boundary value problems in this second-order steady-state hydrodynamic force calculation, and the forces and moment are estimated by integrating the linear velocity potential around the two-dimensional cross section obtained by the NSM over the body.

When the momentum conservation law is applied to the fluid region as shown in Fig. 2.3, the transverse wave drifting force F_d around the two-dimensional cross section can be expressed by the following equation.

$$F_d = -\overline{\int_{\infty}[pn_y + pn_y u_n]d\ell}, \tag{2.125}$$

Here, p is pressure, u_y and n_n are the y-direction and the normal direction components of the flow velocity, and those can be expressed by the following equations.

$$\left.\begin{aligned} p &= -\rho\left[\frac{\partial\Phi}{\partial t}+\frac{1}{2}\nabla\Phi\cdot\nabla\Phi\cdot \mathrm{gz}\right], \\ n_y u_n &= \frac{\partial\Phi}{\partial y}\ \ \frac{\partial\Phi}{\partial y}\ \ n. \end{aligned}\right\} \tag{2.126}$$

Substituting Eq. (2.126) to Eq. (2.125) where the integration is performed from the water bottom (z = -∞) to the water surface ($z = \zeta_{a\pm\infty}$), The higher order terms are neglected as minute quantities, and Eq. (2.125) can be modified as follows,

$$F_D = \frac{1}{2}\rho g\zeta_a^2|C_R|^2, \tag{2.127}$$

in which,

$$C_R = iH_7^+ - ik_0\sum_{j=2}^{4}\frac{X_j}{\zeta_a}H_j^+. \tag{2.128}$$

$H_j^+(j = 2\sim4, 7)$ is Kochin function expressed as follows,

$$\left.\begin{aligned} H_j^+ &= \int_{S_H}\left(\frac{\partial\phi_j}{\partial n}-\phi_j\frac{\partial}{\partial n}\right)e^{-k\xi+ik\eta}ds \qquad (j = 2,3,4), \\ H_7^+ &= \int_{S_H}\left(-(\phi_0+\phi_7)\frac{\partial}{\partial n}\right)e^{-k\xi+ik\eta}ds. \end{aligned}\right\} \tag{2.129}$$

Therefore, lateral force and yawing moment do to the wave drifting force are calculated by the following equations,

$$\left.\begin{aligned} Y_D &= \int_{S_H}F_D dx\ , \\ N_D &= \int_{S_H}(x-x_G)F_D dx. \end{aligned}\right\} \tag{2.130}$$

The non-dimensional wave drifting force can be introduced by the following relations.

$$Y_D' = \frac{Y_D}{\rho g\zeta_a^2 \mathrm{B}^2/L}, \tag{2.131}$$

$$N_D' = \frac{N_D}{\rho g\zeta_a^2 \mathrm{B}^2}. \tag{2.132}$$

2.5.4. Mooring Line Tension Forces

According to the coordinate system shown in Fig. 2.1, ξ_j is the angle between the x_0 axis of the earth-fixed coordinate system and the j-th mooring line while ψ is heading angle of the vessel. Assuming that the horizontal tension T_H of the j-th mooring line is known by the mooring line tension calculation method described in the next chapter, x-, y-axis components X_T, Y_T and the moment of mooring line N_T due to the horizontal mooring line tension T_H acting on the hull can be expressed by the following equation.

$$\left.\begin{aligned} X_T &= \sum_{j=1}^{N}\left\{T_{H\,j}\cos\left(\xi_j-\psi\right)\right\},\\ Y_T &= \sum_{j=1}^{N}\left\{T_{H\,j}\sin\left(\xi_j-\psi\right)\right\},\\ N_T &= \sum_{j=1}^{N}\left\{-T_{H\,j}\cos\left(\xi_j-\psi\right)y_{b\,j}+T_{H\,j}\sin\left(\xi_j-\psi\right)x_{b\,j}\right\}. \end{aligned}\right\} \tag{2.133}$$

Here, $x_{b\,j}$ and $y_{b\,j}$ are the position of the connection point of mooring line and the hull in the body-fixed coordinate system $G-xyz$ shown in Fig. 2.1 while N is the number of mooring line.

2.6. Simultaneous Motions Equations

The equations for simultaneous motion in time domain are given by the combinations of equations for manoeuvring motions in horizontal plane and equations for the vertical motions of a floating body. Substituting all the loads described in Section 2.5 in the horizontal plane motion written in Eq. (2.102), the following equations are established,

$$\left.\begin{aligned} (m+m_x)\dot{u}-(m+m_y)vr-(m_x-m_y)V_c r\sin(\psi-\alpha) &= X_H+X_W+X_T,\\ (m+m_y)\dot{v}+(m+m_x)ur-(m_y-m_x)V_c r\cos(\psi-\alpha) &= Y_H+Y_W+Y_T+Y_D,\\ (I_{zz}+i_{zz})\ \dot{r} &= N_H+N_W+N_T+N_D. \end{aligned}\right\} \tag{2.134}$$

On the other hand, by using the floating body motion equations described in Section 2.3 (Eq. (2.80), $j=3,5$; Eq. (2.81), $j=4$) the other three motion modes can be expressed by the following equation excluding three motion modes which have been expressed by MMG model in Eq. (2.133).

$$\left.\begin{aligned} \left(M+A_{33}^{G}\right)\ddot{z}(t)+B_{33}^{G}\dot{z}(t)+C_{33}^{G}z(t)+A_{35}^{G}\ddot{\phi}(t)+B_{35}^{G}\dot{\phi}(t)+C_{35}^{G}\phi(t) &= E_3^G e^{i\omega t},\\ A_{53}^{G}\ddot{z}(t)+B_{53}^{G}\dot{z}(t)+C_{53}^{G}z(t)+\left(I_{yy}+A_{55}^{G}\right)\ddot{\phi}(t)+B_{55}^{G}\dot{\phi}(t)+C_{55}^{G}\phi(t) &= E_5^G e^{i\omega t},\\ \left(I_{xx}+A_{44}^{G}\right)\ddot{\theta}(t)+B_{44}^{G}\dot{\theta}(t)+C_{44}^{G}\theta(t) &= E_4^G e^{i\omega t}. \end{aligned}\right\} \tag{2.135}$$

Here, C is the restoring force coefficient of the floating structure while a superscript G indicates that the force components acting on the center of gravity G. Since it is considered that the effect of wave forces for the horizontal drift motions of a floating structure is small comparing with the other forces and the coupling between horizontal and vertical motions can be assumed to be small, the wave forces in horizontal plane motion and the coupling between horizontal motion expressed by Eq. (2.134) and vertical motion expressed by Eq. (2.135) was neglected. Finally, by solving these equations simultaneously in time domain as well as calculating dynamic mooring line motions, the dynamic motions of the floating structure and the mooring lines can be reproduced.

2.7. Time Domain Simulations

Time domain simulations are established by solving Eq. (2.134) and Eq. (2.135) simultaneously. The following relation can be obtained from Eq. (2.134) for calculating u, v, and r.

$$\frac{du}{dt} = \frac{(m+m_y)vr+(m_x+m_y)V_C r\sin(\psi-\alpha)}{m+m_x} + \frac{X}{m+m_x}, \tag{2.136}$$

$$\frac{dv}{dt} = \frac{-(m+m_x)ur+(m_y-m_x)V_C r\cos(\psi-\alpha)}{m+m_y} + \frac{Y}{m+m_y}, \tag{2.137}$$

$$\frac{dr}{dt} = \frac{N}{I_{zz}+i_{zz}}. \tag{2.138}$$

The following relations is established between heading angle ψ and yaw rate r,

$$\frac{d\psi}{dt} = r, \tag{2.139}$$

Here, assuming that the coordinate of the center of gravity of the vessel G is (x_0, y_0) in the earth-fixed coordinate system, the following relation can be expressed,

$$\left.\begin{aligned}\frac{dx_0}{dt} &= U\cos(\psi-\beta),\\ \frac{dy_0}{dt} &= U\sin(\psi-\beta).\end{aligned}\right\} \tag{2.140}$$

Meanwhile, heave, pitch, and roll can be expressed by Eq. (2.140) applying non-dimensional wave forces in Section 2.3.9. The following equations are established by considering (Eq. (2.83), $j = 3{,}5$; Eq. (2.85), $j = 4$) excluding three motion modes which have been expressed in Eq. (2.138) and Eq. (2.139).

$$\left.\begin{aligned}&\text{heave: j} = 3\\ &\quad \left(1.0 + A_{33}^{G\prime}\right)\ddot{z}(t) + B_{33}^{G\prime}\dot{z}(t) + \frac{gA_w}{\nabla}C_{33}^{G\prime}z(t)\\ &\qquad\qquad + A_{35}^{G\prime}\frac{L}{2}\ddot{\phi}(t) + B_{35}^{G\prime}\frac{L}{2}\dot{\phi}(t) + \frac{gA_w}{\nabla}\frac{L}{2}C_{35}^{G\prime}\phi(t) = \frac{g\zeta_a A_w}{\nabla}E_3^{G\prime}e^{i\omega_e t},\\ &\text{pitch: j} = 5\\ &\quad A_{53}^{G\prime}\ddot{z}(t) + B_{53}^{G\prime}\dot{z}(t) + \frac{gA_w}{\nabla}C_{53}^{G\prime}z(t)\\ &\qquad + \left(I_{yy}{}' + A_{55}^{G\prime}\right)\frac{L}{2}\ddot{\phi}(t) + B_{55}^{G\prime}\frac{L}{2}\dot{\phi}(t) + \frac{gA_w}{\nabla}\frac{L}{2}C_{55}^{G}\phi(t) = \frac{g\zeta_a A_w}{\nabla}E_5^{G\prime}e^{i\omega_e t},\\ &\text{roll: j} = 4\\ &\quad \left(I_{xx}{}' + A_{44}^{G\prime}\right)\frac{B}{2}\ddot{\theta}(t) + B_{44}^{G\prime}\frac{B}{2}\dot{\theta}(t) + \frac{gA_w}{\nabla}C_{44}^{G\prime}\frac{B}{2}\theta(t)\\ &\qquad\qquad + A_{46}^{G\prime}\frac{L}{2}\ddot{\psi}(t) + B_{46}^{G\prime}\frac{L}{2}\dot{\psi}(t) = \frac{g\zeta_a A_w}{\nabla}E_4^{G\prime}e^{i\omega_e t}.\end{aligned}\right\} \tag{2.141}$$

Since the hydrodynamic forces induced by incoming waves become complex and time consuming when calculating time domain simulation, a dataset of wave forces acting on center of gravity including non-dimensional added mass force coefficient $A_{ij}^{G\prime}$ wave

damping force coefficient $B_{ij}^{G\prime}$, wave exciting force $E_i^{G\prime}$, wave drifting force $Y_D^{G\prime}$ and wave drifting moment $N_D^{G\prime}$ in frequency domain are obtained to be used in the time domain simulations. The wave forces dataset are calculated for stationary vessel $(F_n = 0)$ under various range for the conditions of wave length and direction shown in Table 2.4. The magnitude of wave force for the wave length and direction which are not included in Table 2.4 are linearly interpolated according to the relative incident angle and wavelength

Table 2.4. Frequency domain wave range dataset

Notation	lower	upper	step
$\lambda/_L$	0.01	2.00	0.01
μ	0	3	1

for each time step and then used in the time domain simulations. Non-dimensional wave forces can be converted to dimensional values by Eqs. (2.90)-(2.91) and Eqs. (2.131)-(2.132). Moreover, the added mass used in Eqs. (2.136)-(2.137) are obtained by using Motora's chart (Motora, 1959a-1959c, 1960a-1960b).

2.8. Concluding Remarks

According to the coupled-motion equations presented in this chapter, the following conclusions can be summarized,

- The method to calculate the motion of floating body in waves has been presented. The New Strip Method (NSM) is used for estimating the hydrodynamic forces acting on the hull by obtaining velocity potential using Boundary Element Method (BEM).
- The comparison of the calculation results based on the method against experimental results has been also presented. The comparison results show a good agreement between both numerical and experimental results.
- The simultaneous motion equations established by the combination of horizontal plane motion based on MMG model and vertical motion based on conventional floating body motions were also presented. The mathematical model of the simultaneous motion can cover external disturbance including wave (1st and 2nd order forces), wind, and current. Both 1st and 2nd order wave forces applied to the simultaneous equations (time domain simulations) can be taken from the dataset of wave forces in frequency domain obtained by NSM.
- The restoring forces generated by dynamic mooring line tension also can be introduced in the simultaneous motion equations. By using those simultaneous motion equations,

coupling between the mooring line motions and 6 DOF motion of the floating body can be introduced.

Therefore, based on the abovementioned reasons, the derived simultaneous motion equations including the effect of external disturbances can be used to investigate the motions of a floating offshore structure moored in waves especially for deep water conditions.

Chapter 3 Three-Dimensional Dynamics Model of Mooring Line for Coupled Motion Analysis of Floating Offshore Structure

3.1. Introduction

Since the number of floating offshore structure operated in deep water area far from the land and in severe environmental conditions increases, mooring line system belongs to a floating structure needs to be paid attention elaborately. The problems related to mooring lines increase concomitant with the deep water and severe environmental conditions because the dynamic effects of mooring lines motions are becoming significant with the increase of the water depth. Consequently, accurate prediction of mooring line tension is extremely required to guarantee the work safety and survivability of the floating structure. The design of mooring line system must comply with all requirements related to the environmental conditions in deep water fields. Therefore, an appropriate analysis method should be developed paying an attention reflecting the condition properly.

Several methods have been existed for analyzing such mooring line system. Most of them use catenary method to introduce the effects of mooring lines. Samadi and Hassanabad (2017) used the principle of catenary equation to investigate the hydrodynamic response of a truss spar floating platform. Catenary theory using quasi-static analysis method is adopted by Figueirodo and Brojo (2017) to propose a parametric study in order to investigate mooring cost. Other related studies using catenary method are also conducted by Ganesan and Sen (2015), Yuan et al (2014) and Cerveira et al (2013).

To predict the performance of a mooring line coupled with a floating structure, a quasi-static approach is frequently used (Masciola et al., 2013a). The approach is even used for multi-component mooring line system (Chai et al., 2002a and Figueirodo and Brojo, 2017) and has been improved by considering seabed interactions (Jonkman, 2007) also by dealing with arbitrary multi-segment mooring line (Masciola et al., 2013b). The quasi-static approach is developed based on the catenary solutions and it provides mooring line shape and tension (Bauduin et al., 2000). This approach allows to obtain new static equilibrium conditions of mooring line for each updated position of top-end point (fairlead) in every time steps. However, it completely neglects the dynamic effects of mooring line ignoring motion dependency of mass, inertia effects, damping force, and fluid accelerations (current load) (Johanning et al., 2005). Moreover, this approach also requires the estimation of mooring line drag coefficient which can decrease the accuracy of mooring line calculations (Johanning et al., 2007). Though the quasi-static model is widely used for calculating the

mooring line tension, that model is considered to be inadequate to apply for deep water conditions (Mavrakros et al., 1996). The dynamic tension grows big in deep water mooring operation due to the first order motions of a floating offshore structure since the maximum dynamic tension stiffness moves to the range of wave frequency (Triantafyllou et al., 1985).

Another approach called quasi-dynamic approach then exists for taking dynamic effects of a floating offshore structure and a mooring line into account. The approach tries to bring up the nonlinearity of the mooring line through modelling it as a nonlinear spring. But, basically, only static spring reaction induces the motion of the floating offshore structure. The quasi-dynamic approach is considered to be preferred approach for offshore mooring applications and the detail of this approach is provided in (Bureau Veritas, 1998, 2004). However, because the mooring line tension is computed based on the static catenary response, the dynamic effects of mooring line are literally excluded (Ha, 2011). In addition, the mooring line tension and motion of a floating offshore structure are calculated separately for the sake of faster computation time and simplification of complex interaction between them. This may lead to the depreciation of calculation accuracy.

According to the above description, it can be said that the dynamic effects of mooring lines which are important to predict mooring line tension precisely are completely neglected in both static and quasi-static analysis methods. Meanwhile, quasi-dynamic analysis is frequently conducted through uncoupled motion model which solves the motions of a floating body and mooring lines separately to simplify complex interaction between them. In that approach, the mooring line dynamics is accomplished by imposing fairlead motion to mooring line motion. Calculation time can be reduced while obtained results may become approximate solutions. Moreover, accurate estimation of a moored floating structure's response which changes depending on mooring line characteristics is very important concerning the safety and reliability of the mooring lines. Thereby, the main idea of coupled dynamic approach must be taken when investigating the performance of a moored floating structure since that approach is assessed to be the most rigorous method and it has been widely used for analyzing the motion of a moored floating structure in recent years (Ji et al., 2016; Jacob et al., 2012a, 2012b and Zhao et al., 2018). In addition, since the mooring line actually moves in three-dimensional space, the dynamic motions of mooring line must be investigated by considering the three-dimensional dynamic behavior of the mooring line.

In this chapter, the three-dimensional dynamics model of a mooring line for coupled motion analysis of a floating offshore structure including its numerical simulations is provided. This chapter is started by three-dimensional dynamics model of a mooring line to introduce the behavior of mooring line dynamics presented in Section 3.2. The relation between a mooring line and a floating structure at the connection point of them is described

in Section 3.3 while the additional characteristics which are inherent with the mooring line such as anchor force and motion are presented in Section 3.4. Furthermore, numerical simulations involving various type of mooring line (single line, double lines, multi-leg turret mooring, and multi-leg spread mooring) are provided in Section 3.5 to verify the ability of the presented method. In the end of this chapter, the discussion of the proposed method is summarized in Section 3.6.

3.2. Dynamic Mooring Line Method

Many studies have been presented concerning to the dynamic effects of mooring lines. Finite difference and Finite Element (FE) methods which are widely used for calculating dynamic mooring line motion require more complex mathematical model and they are time consuming, and costly, especially for FE method. On the other hand, lumped mass method is considered as more efficient method since it resembles FE model, can pick up main necessary features only, and avoids unnecessary features in the FE model. It also has intelligible simplicity and obvious physical meaning in mathematical formulations as well as less in computation time. Moreover, the studies involving three-dimensional dynamic mooring line motion were merely a few whereas the mooring line moves and it is disturbed by external loads in three-dimensional space.

Conventionally, when calculating the tension of mooring line that moves due to the motion of its top point, the calculation of mooring line tension is often tackled statically without considering the motion of the mooring line. However, in fact, external forces act on the mooring line cause the motion of the mooring line in three-dimensional space. Hence, the calculation of mooring line tension must be handled by considering the dynamic motion of mooring line especially in three-dimensional motion. In addition, according to DNV 1996, dynamic mooring analysis is recommended for deep water more than 450 m or 200 m for F(P)SO. Further, DNV 2008 requires dynamic mooring analysis for FPSO operated in deep water more than 100 m.

To cope with the dynamic problems of mooring line, lumped mass method is used in this study for investigating the influence of hydrodynamic forces acting on the mooring line and the three-dimensional motion of the mooring line including its deformation due to the motion of a floating offshore structure. The lumped mass method is a mass point system model that divides a mooring line into several elements connected by a mass point. In this study, three-dimensional lumped mass method introduced by Nakajima et al. (1983) and Nakajima (1983) is used to investigate the dynamic motions of the mooring line. The detail of this calculation method is described below.

3.2.1. Three-Dimensional Lumped Mass Method

In this method, a mooring line is divided into a finite number of elements in which the mass and forces acting on the element concentrate to each mass point. Elastic deformation of the elements, line-seabed interaction and hydrodynamic drag force due to line motion are included in the calculation method.

The schematic diagram of the three-dimensional lumped mass method is shown in Fig. 3.1. A mooring line consists of $N-1$ mass points, approximating that they are connected by a mass-less linear spring between the mass points. It is assumed that the mass of an arbitrary mass point j is δ_j and tension forces acting on the mass point are T_j and T_{j-1} as shown in Fig. 3.1. The length including the elongation of each element is denoted as l_j. Node 1 is the anchor point, node $I-1$ is the end node laying on the seabed (touchdown point), node I the first hanging node and P the attached point of the mooring line on a floating structure. Meanwhile, χ is the line angle in line-fixed coordinate system with the origin at the anchor point and γ_j is the angle of line segment with the horizontal axis. In this calculation method, the masses of the first raised mass point which is dented as node I and the last mass point denoted as node N are considered 1.5 times than others.

In order to analyze the motion of mooring lines with original deformation, it is necessary to determine the initial state of the mooring line at first, including the position of each mass point and the tension between them. Now, by assuming that the mass of an arbitrary mass point j as δ_j and the tensions T_j and T_{j-1} act on the mass point as shown in Fig. 3.1, the vertical and horizontal equilibrium equations at the mass point j become as follows.

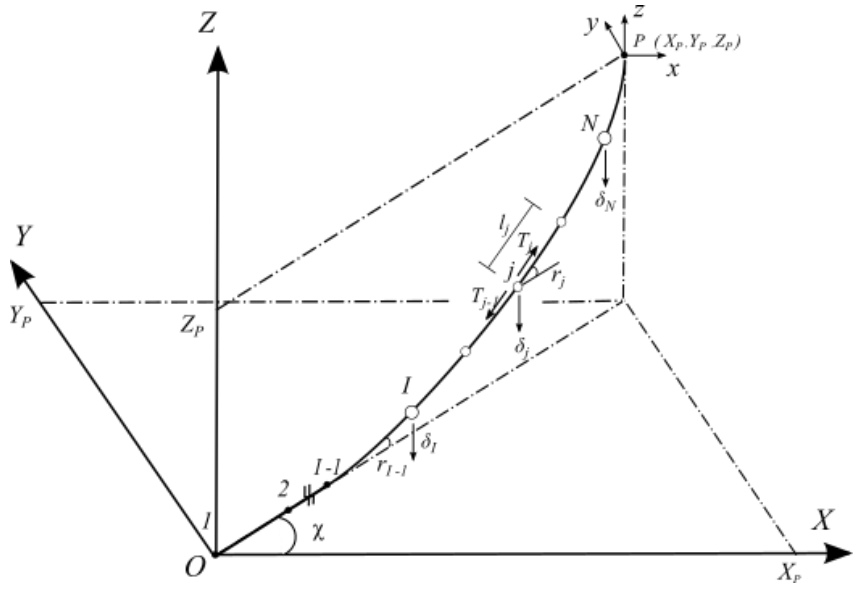

Fig. 3.1. Coordinate system of mooring line using 3D lumped mass method

$$\left.\begin{aligned} T_j \sin\gamma_j &= \textstyle\sum_{k=1}^{j} \delta_k\,, \\ T_j \cos\gamma_j &= T_1 \cos\gamma_1 \qquad (j = 1,2,\dots,N), \end{aligned}\right\} \tag{3.1}$$

in which, $\delta_1 = T_1 \sin\gamma_1$. Now, consider the position (x_P, y_P, z_P) of the point P at the upper end of the mooring line, the following equation is obtained as the boundary condition equation of initial state of mooring line equations.

$$\left.\begin{aligned} \sum_{j=1}^{N} l_j \sin\gamma_j &= z_P, \\ \sum_{j=1}^{N} l_j \cos\gamma_j &= \sqrt{x_P^2 + y_P^2}, \end{aligned}\right\} \tag{3.2}$$

Here, length of each element including the elongation l_j, can be given as follows taking into account the original length of the element $\bar{l}$, cross sectional area A, and Young's modulus E,

$$l_j = \bar{l}\left(1 + \frac{T_j}{E \cdot A}\right). \tag{3.3}$$

On the other hand, the position (x_j, y_j, z_j) of the mass point j can be calculated by the following equations.

$$\left.\begin{aligned} x_{j+1} &= \textstyle\sum_{k=1}^{j} l_k \cos\gamma_k \cos\chi\,, \\ y_{j+1} &= \textstyle\sum_{k=1}^{j} l_k \cos\gamma_k \sin\chi\,, \\ z_{j+1} &= \textstyle\sum_{k=1}^{j} l_k \sin\gamma_k\,, \\ &\qquad (j = 1,2,\dots,N-1), \end{aligned}\right\} \tag{3.4}$$

where $\chi = \tan^{-1}(x_P/y_P)$. Here, when the mooring line is equally divided, the masses of the first raised mass point $(j = I)$ and the last mass point $j = N$ are denoted as 1.5 times than others to match the whole mooring line as the described before.

3.2.2. Initial Static Condition of Mooring Line

The initial condition of a mooring line is obtained through the iterative calculation of the weight of each mass point as presented in Nakajima (1983). By combining Eq. (3.1) and Eq. (3.2), two equations for determining the initial static condition of the mooring line can be obtained, in which W_j is the weight of mass point j for $j = 1 \sim N+1$

$$W_1 = \frac{z_P/\bar{l} - \sum_{j=1}^{N}\left[\left\{T_j^{-1} + (A.E)^{-1}\right\}\sum_{k=2}^{j} W_k\right]}{\sum_{j=1}^{N} T_j^{-1} + N/(A.E)}, \tag{3.5}$$

where z_P is the vertical position of the attached point of the mooring line. Meanwhile, from Eq. (3.1) the following relation to calculate T_j is obtained,

$$T_j = \sqrt{T_1^2 - \mathrm{W}_1^2 + \left(\sum_{k=1}^{j} W_k\right)^2}. \tag{3.6}$$

According to Eq. (3.5) and Eq. (3.6), there are two unknowns, T_1 and W_1 which can be obtained by using Eq. (3.5) and Eq. (3.6) iteratively. The iterative calculation is repeated until the weight of the touchdown point node, W_{I-1} $(I > 2)$, becomes greater than 0. In the iteration, W_1 is treated as 0 if the calculated value of W_1 is less than 0. k indicates all mass points which are less than $j - 1$ $(k < j - 1)$ in which for k laying on seabed W_{k} and γ_{k} can be regarded as 0.

3.2.3. Forces Acting on Mooring Line

(1) Current Velocity

It is necessary to consider current velocity distribution in depth direction which affects to the mooring line motion. In this study, the magnitude of current velocity v_{cj} at z_j which is the vertical position of *j*-th mass point is approximated by the following equation.

$$v_{c\,j} = V_C \left(1 - \frac{z_j}{D_w}\right)^{\frac{1}{7}}. \tag{3.7}$$

Here, V_C is current velocity at water surface and D_w is water depth. The example of approximated vertical distribution of current velocity is shown in Fig. 3.2 for V_C = 1.0 m/s, 2.0 m/s, and 3.0 m/s with 500 m of water depth. Further, referring to the local mooring line coordinate system as shown in Fig. 3.1, axial components of current velocities denoted as $v_{x\,j}, v_{y\,j}$, and $v_{z\,j}$ can be written as,

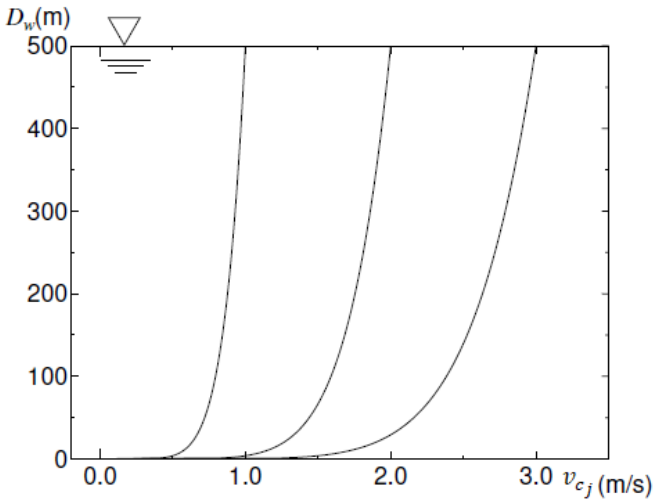

Fig. 3.2. Current velocity distribution in depth direction

$$\left.\begin{aligned} v_{x_j} &= v_{c_j}\cos\alpha_c, \\ v_{y_j} &= v_{c_j}\sin\alpha_c, \\ v_{z_j} &= 0. \end{aligned}\right\} \tag{3.8}$$

α_c, is the current direction referred to the x-axis of local mooring line coordinate system.

(2) Hydrodynamic Force

Based on Nakajima et al. (1983), hydrodynamic forces acting on each mass point are expressed by the following equations,

$$\left.\begin{aligned} f_{dx_j} &= -\left(\sin\bar{\beta}_j\cdot\cos\bar{\theta}_j\cdot\cos\phi_j+\sin\bar{\theta}_j\cdot\sin\phi_j\right)f_{dn_j}+\left(\cos\bar{\beta}_j\cdot\cos\bar{\theta}_j\right)f_{dt_j}, \\ f_{dy_j} &= \left(\cos\bar{\beta}_j\cdot\cos\phi_j\right)f_{dn_j}+\left(\sin\bar{\beta}_j\right)f_{dt_j}, \\ f_{dz_j} &= -\left(\sin\bar{\beta}_j\cdot\cos\bar{\theta}_j\cdot\cos\phi_j-\cos\bar{\theta}_j\cdot\sin\phi_j\right)f_{dn_j}+\left(\cos\bar{\beta}_j\cdot\cos\bar{\theta}_j\right)f_{dt_j}, \end{aligned}\right\} \tag{3.9}$$

while hydrodynamic drag forces in normal and tangential directions are calculated by,

$$\left.\begin{aligned} f_{dn_j} &= -\tfrac{1}{2}\rho C_{dn}D_c\bar{l}\left|u_{n_j}\right|u_{n_j}, \\ f_{dt_j} &= -\tfrac{1}{2}\rho C_{dt}D_c\bar{l}\left|u_{t_j}\right|u_{t_j}, \end{aligned}\right\} \tag{3.10}$$

where,

$$\left.\begin{aligned} u_{t_j} &= u_{\xi_j}, \\ u_{n_j} &= \sqrt{u_{v_j}^2+u_{\eta_j}^2}, \\ \phi_j &= \tan^{-1}\left(\frac{u_{\eta_j}}{u_{v_j}}\right). \end{aligned}\right\} \tag{3.11}$$

In which, u_{ξ_j}, u_{v_j}, and u_{η_j} are obtained by the following matrix,

$$\begin{bmatrix} u_{\xi_j} \\ u_{v_j} \\ u_{\eta_j} \end{bmatrix} = \begin{bmatrix} \cos\bar{\beta}_j\cos\bar{\theta}_j & \sin\bar{\beta}_j & \sin\bar{\theta}_j\cos\bar{\beta}_j \\ -\sin\bar{\beta}_j\cos\bar{\theta}_j & \cos\bar{\beta}_j & -\sin\bar{\beta}_j\sin\bar{\theta}_j \\ -\sin\bar{\theta}_j & 0 & -\cos\bar{\theta}_j \end{bmatrix} \times \begin{bmatrix} \dot{x}_j - v_{x_j} \\ \dot{y}_j - v_{y_j} \\ \dot{z}_j - v_{z_j} \end{bmatrix}. \tag{3.12}$$

Here, $\dot{x}_j, \dot{y}_j, \dot{z}_j$ and $v_{x_j}, v_{y_j}, v_{z_j}$ are the velocities of mass point and current respectively, while $\bar{\alpha}_{ij}, \bar{\beta}_{ij}, \bar{\theta}_{ij}$ are the average angle of mass point referred to three axes of local mooring line coordinate system. Meanwhile, C_{dn} and C_{dt} are drag coefficient in normal and tangential directions respectively.

(3) Mooring Line-Seabed Interaction Force

Interaction forces (friction forces) f_{g_j} between a mooring line and the seabed caused by the existence of segment part laying on the seabed are given as follow,

$$\begin{bmatrix} f_{g_{x_j}} \\ f_{g_{y_j}} \\ f_{g_{z_j}} \end{bmatrix} = -w_c \lambda_c l_{laying} \begin{bmatrix} \dot{x}_j \\ \dot{y}_j \\ \dot{z}_j \end{bmatrix}, \tag{3.13}$$

in which, $\dot{z}_j$ is treated as zero for a segment laying on the seabed. λ_c and l_{laying} are the friction coefficient at the seabed and the length of the laying part of the segment. The friction coefficients due to soil type at the seabed are shown in Table 3.1.

Table 3.1. Friction coefficient on seabed based on soil type

Soil	λ_a	λ_c
Sand	7.0	0.75
Mud	10.0	1.00

3.2.4. Three-Dimensional Motion Equations of Mooring Line

Coordinate system of the j-th mass point of the mooring line is shown in Fig. 3.4. Now, let us consider the case in which the mass point j moves arbitrarily. The external force applied to the mooring line should be concentrated on each mass point, and the element should be straight. In Fig. 3.4, three-dimensional motion equations of mass point j is given by the following equations.

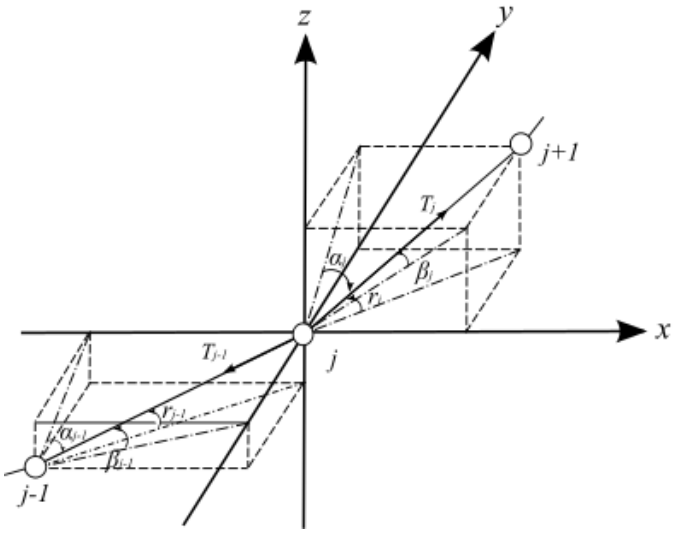

Fig. 3.4. Coordinate system of the j-th mass point of the mooring line

$$\begin{bmatrix} I_{1j} & I_{2j} & I_{3j} \\ J_{1j} & J_{2j} & J_{3j} \\ K_{1j} & K_{2j} & K_{3j} \end{bmatrix} \begin{bmatrix} \ddot{x}_j \\ \ddot{y}_j \\ \ddot{z}_j \end{bmatrix} = \begin{bmatrix} F_{xj} \\ F_{yj} \\ F_{zj} \end{bmatrix} \qquad (j = 2,3,\dots,N), \tag{3.14}$$

in which,

$$\left.\begin{aligned} F_{x_j} &= T_j \sin\alpha_j - T_{j-1}\sin\alpha_{j-1} + f_{dx_j}, \\ F_{y_j} &= T_j \sin\beta_j - T_{j-1}\sin\beta_{j-1} + f_{dy_j}, \\ F_{z_j} &= T_j \sin\gamma_j - T_{j-1}\sin\beta\gamma_{j-1} + f_{dz_j} - \delta_j, \end{aligned}\right\} \tag{3.15}$$

where,

$$\left.\begin{aligned} I_{1_j} &= M_j + A_{n_j}\cos^2\bar{\alpha}_j + A_{t_j}\sin^2\bar{\alpha}_j\,, \\ I_{2_j} &= \left(A_{t_j} - A_{n_j}\right)\sin\bar{\beta}_j \sin\bar{\alpha}_j \left(= J_{1_j}\right), \\ I_{3_j} &= \left(A_{t_j} - A_{n_j}\right)\sin\bar{\gamma}_j \sin\bar{\alpha}_j \left(= K_{1_j}\right), \\ J_{2_j} &= M_j + A_{n_j}\cos^2\bar{\beta}_j + A_{t_j}\sin^2\bar{\beta}_j\,, \\ J_{3_j} &= \left(A_{t_j} - A_{n_j}\right)\sin\bar{\beta}_j \sin\bar{\gamma}_j \left(= K_{2_j}\right), \\ K_{3_j} &= M_j + A_{n_j}\cos^2\bar{\gamma}_j + A_{t_j}\sin^2\bar{\gamma}_j\,. \end{aligned}\right\} \tag{3.16}$$

Here, I, J and K are component equations affected by mass points, M_j and added masses in normal and tangential directions of j-th mooring line element, A_{nj}, A_{tj}. $\ddot{x}_j$, $\ddot{y}_j$, $\ddot{z}_j$ and F_{xj}, F_{yj}, F_{zj} are the acceleration components and the external forces of mass points, respectively. On the other hand, f_{dx_j}, f_{dy_j}, and f_{dz_j} which are the components of drag force acting on the mooring line can be calculated by using f_{dn_j} and f_{dt_j} shown by Eq. (3.10) if they are unknown. Meanwhile, $\bar{\alpha}_j = (\alpha_j + \alpha_{j-1})/2$, $\bar{\beta}_j = (\beta_j + \beta_{j-1})/2$, $\bar{\gamma}_j = (\gamma_j + \gamma_{j-1})/2$, and $\bar{\theta}_j = (\theta_j + \theta_{j-1})/2$. α_j, β_j, γ_j, and $\bar{\theta}_j$ are three-dimensional mass point angle which can be determined as follows,

$$\left.\begin{aligned} \sin\alpha_j &= (x_{j+1} - x_j)/l_j, \\ \cos\alpha_j &= \sqrt{(z_{j+1} - z_j)^2 + (y_{j+1} - y_j)^2}/l_j, \\ \sin\beta_j &= (y_{j+1} - y_j)/l_j, \\ \cos\beta_j &= \sqrt{(x_{j+1} - x_j)^2 + (z_{j+1} - z_j)^2}/l_j, \\ \sin\gamma_j &= (z_{j+1} - z_j)/l_j, \\ \cos\gamma_j &= \sqrt{(x_{j+1} - x_j)^2 + (y_{j+1} - y_j)^2}/l_j, \\ \tan^{-1}\theta_j &= \frac{z_{j+1} - z_j}{x_{j+1} - x_j}, \end{aligned}\right\} \tag{3.17}$$

where,

$$l_j = \sqrt{\left(x_{j+1} - x_j\right)^2 + \left(y_{j+1} - y_j\right)^2 + \left(z_{j+1} - z_j\right)^2}. \tag{3.18}$$

3.2.5. Governing Equations and Solution Method of Mooring Line Motion Equations

The equations of motion of the j-th mass point of the mooring line are solved for acceleration $\ddot{x}_j, \ddot{y}_j, \ddot{z}_j$ as follows.

$$\left.\begin{aligned} \ddot{x}_j &= M_{1_j} F_{x_j} + M_{2_j} F_{y_j} + M_{3_j} F_{z_j}, \\ \ddot{y}_j &= N_{1_j} F_{x_j} + N_{2_j} F_{y_j} + N_{3_j} F_{z_j}, \\ \ddot{z}_j &= L_{1_j} F_{x_j} + L_{2_j} F_{y_j} + L_{3_j} F_{z_j}, \\ &\qquad (j = 2,3,\dots,N), \end{aligned}\right\} \tag{3.19}$$

in which,

$$\left.\begin{aligned} M_{1_j} &= \left(J_{2_j} K_{3_j} - K_{2_j} J_{3_j}\right)/\lambda, \\ M_{2_j} &= \left(K_{2_j} I_{3_j} - I_{2_j} K_{3_j}\right)/\lambda, \\ M_{3_j} &= \left(I_{2_j} J_{3_j} - J_{2_j} I_{3_j}\right)/\lambda, \\ N_{1_j} &= \left(K_{1_j} J_{3_j} - J_{1_j} K_{3_j}\right)/\lambda, \\ N_{2_j} &= \left(I_{1_j} K_{3_j} - K_{1_j} I_{3_j}\right)/\lambda, \\ N_{3_j} &= \left(J_{1_j} I_{3_j} - I_{1_j} J_{3_j}\right)/\lambda, \\ L_{1_j} &= \left(J_{1_j} K_{2_j} - K_{1_j} J_{2_j}\right)/\lambda, \\ L_{2_j} &= \left(K_{1_j} I_{2_j} - I_{1_j} K_{2_j}\right)/\lambda, \\ L_{3_j} &= \left(I_{1_j} J_{2_j} - J_{1_j} I_{2_j}\right)/\lambda, \end{aligned}\right\} \tag{3.20}$$

$$\lambda = I_{1_j}\left(J_{2_j} K_{3_j} - K_{2_j} J_{3_j}\right) - J_{1_j}\left(I_{2_j} K_{3_j} - K_{2_j} I_{3_j}\right) + K_{1_j}\left(I_{2_j} J_{3_j} - J_{2_j} I_{3_j}\right). \tag{3.21}$$

Eq. (3.19) then can be expressed as a function of mooring line tension T_j as follows,

$$\left.\begin{aligned} \ddot{x}_j &= \left(R_j T_j + P_j T_{j-1} + U_j\right)/\Delta t^2, \\ \ddot{y}_j &= \left(O_j T_j + H_j T_{j-1} + V_j\right)/\Delta t^2, \\ \ddot{z}_j &= \left(S_j T_j + Q_j T_{j-1} + W_j\right)/\Delta t^2, \\ &\qquad (j = 2,3,\dots,N), \end{aligned}\right\} \tag{3.22}$$

where,

$$\left.\begin{aligned}
R_j &= \left(M_{1_j}\sin\alpha_j + M_{2_j}\sin\beta_j + M_{3_j}\sin\gamma_j\right)\cdot \Delta t^2,\\
P_j &= \left(M_{1_j}\sin\alpha_{j-1} + M_{2_j}\sin\beta_{j-1} + M_{3_j}\sin\gamma_{j-1}\right)\cdot \Delta t^2,\\
O_j &= \left(N_{1_j}\sin\alpha_j + N_{2_j}\sin\beta_j + N_{3_j}\sin\gamma_j\right)\cdot \Delta t^2,\\
H_j &= \left(N_{1_j}\sin\alpha_{j-1} + N_{2_j}\sin\beta_{j-1} + N_{3_j}\sin\gamma_{j-1}\right)\cdot \Delta t^2,\\
S_j &= \left(L_{1_j}\sin\alpha_j + L_{2_j}\sin\beta_j + L_{3_j}\sin\gamma_j\right)\cdot \Delta t^2,\\
Q_j &= \left(L_{1_j}\sin\alpha_{j-1} + L_{2_j}\sin\beta_{j-1} + L_{3_j}\sin\gamma_{j-1}\right)\cdot \Delta t^2,\\
U_j &= \left[M_{1_j}f_{dx_j} + M_{2_j}f_{dy_j} + M_{3_j}\left(f_{dz_j} - \delta_j\right)\right]\cdot \Delta t^2,\\
V_j &= \left[N_{1_j}f_{dx_j} + N_{2_j}f_{dy_j} + N_{3_j}\left(f_{dz_j} - \delta_j\right)\right]\cdot \Delta t^2,\\
W_j &= \left[L_{1_j}f_{dx_j} + L_{2_j}f_{dy_j} + L_{3_j}\left(f_{dz_j} - \delta_j\right)\right]\cdot \Delta t^2.
\end{aligned}\right\} \tag{3.23}$$

Due to the effect of the interaction between the mooring line and the seabed, the coefficients U_j, V_j, and W_j can be rewritten as,

$$\left.\begin{aligned}
U_j &= \left[M_{1_j}\left(f_{dx_j} + f_{gx_j}\right) + M_{2_j}\left(f_{dy_j} + f_{gy_j}\right) + M_{3_j}\left(f_{dz_j} + f_{gz_j} - \delta_j\right)\right]\cdot \Delta t^2,\\
V_j &= \left[N_{1_j}\left(f_{dx_j} + f_{gx_j}\right) + N_{2_j}\left(f_{dy_j} + f_{gy_j}\right) + N_{3_j}\left(f_{dz_j} + f_{gz_j} - \delta_j\right)\right]\cdot \Delta t^2,\\
W_j &= \left[L_{1_j}\left(f_{dx_j} + f_{gx_j}\right) + L_{2_j}\left(f_{dy_j} + f_{gy_j}\right) + L_{3_j}\left(f_{dz_j} + f_{gz_j} - \delta_j\right)\right]\cdot \Delta t^2.
\end{aligned}\right\} \tag{3.24}$$

On the other hand, assuming that the mooring line does not extend, the constraint condition equation is given by the following equation,

$$\left(x_j - x_{j-1}\right)^2 + \left(y_j - y_{j-1}\right)^2 + \left(z_j - z_{j-1}\right)^2 = \bar{l}^2 \qquad (j = 2,3,\dots,N+1). \tag{3.25}$$

Here, $\bar{l}$ is the length of the mooring line element, but when considering the elongation of the mooring line, it becomes as follows,

$$\left(x_j - x_{j-1}\right)^2 + \left(y_j - y_{j-1}\right)^2 + \left(z_j - z_{j-1}\right)^2 = \bar{l}^2\left(1 + \frac{T_{j-1}}{A\cdot E}\right)^2 \quad (j = 2,3,\dots,N+1). \tag{3.26}$$

(1) Solution for non-elongated mooring line

In case when the elongation of the mooring line is not taken into consideration, the governing equations of mooring line motion can be generated from Eq. (3.22) and Eq. (3.23). The acceleration of mass point can be solved by using the difference formula given by Walton and Polachek (1960) to obtain the displacement of mooring line motion.

$$\left.\begin{aligned}
\ddot{s}_j^n &= \left(s_j^{n+1} - 2s_j^n + s_j^{n-1}\right)/\Delta t^2,\\
\dot{s}_j^n &= \left(s_j^{n+1} - s_j^{n-1}\right)/(2\Delta t).
\end{aligned}\right\} \tag{3.27}$$

Here, n indicates n-th time step and t is time. If time interval is denoted as Δt, $t = n \cdot \Delta t$. s_j means x_j, y_j, z_j while Eq. (3.22) and Eq. (3.27) are combined to obtain the following equations,

$$\left.\begin{aligned} x_j^{n+1} &= 2x_j^n - x_j^{n-1} + R_j^n \cdot T_j^n - P_j^n \cdot T_{j-1}^n + U_j^n, \\ y_j^{n+1} &= 2y_j^n - y_j^{n-1} + O_j^n \cdot T_j^n - H_j^n \cdot T_{j-1}^n + V_j^n, \\ z_j^{n+1} &= 2z_j^n - z_j^{n-1} + S_j^n \cdot T_j^n - Q_j^n \cdot T_{j-1}^n + W_j^n, \\ & \qquad (j = 2,3,\dots,N). \end{aligned}\right\} \tag{3.28}$$

According to Walton and Polachek (1960), let's consider Φ_j^{n+1} as shown in the following equation,

$$\begin{aligned} \Phi_j^{n+1} &= \frac{1}{2}\left[\left(x_j - x_{j-1}\right)^2 + \left(y_j - y_{j-1}\right)^2 + \left(z_j - z_{j-1}\right)^2 - l^2\right], \\ &= \Phi_j^{n+1}\left(T_{j-2}^n, T_{j-1}^n, T_j^n\right) \qquad (j = 2,3,\dots,N+1). \end{aligned} \tag{3.29}$$

According to the constraint condition, Eq. (3.29) must satisfy $\Phi_j^{n+1} = 0$. On the other hand, when the mooring line tension T_j^n is expressed by the summation of tentative mooring line tension $\tilde{T}_j^n$ and its correction amount ΔT_j^n as shown by Eq. (3.30), Eq. (3.31) can be obtained by performing Taylor expansion on Eq. (3.30),

$$T_j = \tilde{T}_j^n + \Delta T_j^n, \tag{3.30}$$

$$\begin{aligned} \Phi_j^{n+1} = \tilde{\Phi}_j^{n+1} &+ \frac{\partial \tilde{\Phi}_j^{n+1}}{\partial \tilde{T}_{j-2}^n} \cdot \Delta T_{j-2}^n + \frac{\partial \tilde{\Phi}_j^{n+1}}{\partial \tilde{T}_{j-1}^n} \cdot \Delta T_{j-1}^n \\ &+ \frac{\partial \tilde{\Phi}_j^{n+1}}{\partial \tilde{T}_j^n} \cdot \Delta T_j^n + (\text{Higher Order Term}), \end{aligned} \tag{3.31}$$

while "~" means the first approximate value of each component.

If the value of $\tilde{T}_j^n$ is sufficiently close to the value of tension T_j^n, the higher order terms in Eq. (3.31) can be omitted, and hence the following equation is derived.

$$\tilde{E}_j^{n+1} \cdot \Delta T_{j-2}^n - \tilde{F}_j^{n+1} \cdot \Delta T_{j-1}^n + \tilde{G}_j^{n+1} \cdot \Delta T_j^n = -\Phi_j^{n+1} \qquad (j = 2,3,\dots,N+1). \tag{3.32}$$

Eq. (3.32) can be rewritten as,

$$\begin{bmatrix} -\tilde{F}_2^{n+1} & \tilde{G}_2^{n+1} & 0 & 0 & \cdots & 0 & 0 & 0 \\ \tilde{E}_3^{n+1} & -\tilde{F}_3^{n+1} & \tilde{G}_3^{n+1} & 0 & \cdots & 0 & 0 & 0 \\ 0 & \tilde{E}_4^{n+1} & -\tilde{F}_4^{n+1} & \tilde{G}_4^{n+1} & \cdots & 0 & 0 & 0 \\ \vdots & \vdots & \vdots & \vdots & \ddots & \vdots & \vdots & \vdots \\ 0 & 0 & 0 & \cdots & \cdots & \tilde{G}_{N-1}^{n+1} & 0 & 0 \\ 0 & 0 & 0 & \cdots & \cdots & -\tilde{F}_N^{n+1} & \tilde{G}_N^{n+1} & 0 \\ 0 & 0 & 0 & \cdots & \cdots & \mathrm{E}_{N+1}^{n+1} & -\tilde{F}_{N+1}^{n+1} & \tilde{G}_{N+1}^{n+1} \end{bmatrix} \begin{bmatrix} \Delta T_1^n \\ \Delta T_2^n \\ \Delta T_3^n \\ \Delta T_4^n \\ \vdots \\ \Delta T_{N-2}^n \\ \Delta T_{N-1}^n \\ \Delta T_N^n \end{bmatrix} = \begin{bmatrix} -\tilde{\Phi}_2^{n+1} \\ -\tilde{\Phi}_3^{n+1} \\ -\tilde{\Phi}_4^{n+1} \\ -\tilde{\Phi}_5^{n+1} \\ \vdots \\ -\tilde{\Phi}_{N-1}^{n+1} \\ -\tilde{\Phi}_N^{n+1} \\ -\tilde{\Phi}_{N+1}^{n+1} \end{bmatrix}, \tag{3.33}$$

in which,

$$\tilde{\Phi}_j^{n+1} = \left[\left(\tilde{x}_j^{n+1} - \tilde{x}_{j-1}^{n+1}\right)^2 + \left(\tilde{y}_j^{n+1} - \tilde{y}_{j-1}^{n+1}\right)^2 + \left(\tilde{z}_j^{n+1} - \tilde{z}_{j-1}^{n+1}\right)^2 - \bar{l}^2\right]/2, \tag{3.34}$$

$$\left.\begin{aligned} \tilde{x}_j^{n+1} &= 2x_j^n - x_j^{n-1} + R_j^n \cdot \tilde{T}_j^n - P_j^n \cdot \tilde{T}_{j-1}^n + \tilde{U}_j^n, \\ \tilde{y}_j^{n+1} &= 2y_j^n - y_j^{n-1} + O_j^n \cdot \tilde{T}_j^n - H_j^n \cdot \tilde{T}_{j-1}^n + \tilde{V}_j^n, \\ \tilde{z}_j^{n+1} &= 2z_j^n - z_j^{n-1} + S_j^n \cdot \tilde{T}_j^n - Q_j^n \cdot \tilde{T}_{j-1}^n + \tilde{W}_j^n, \\ &\qquad (j = 2,3,\dots,N), \end{aligned}\right\} \tag{3.35}$$

where,

$$\left.\begin{aligned} \tilde{E}_j^{n+1} &= \frac{\partial \tilde{\Phi}_j^{n+1}}{\partial \tilde{T}_{j-2}^n} = P_{j-1}^n\left(\tilde{x}_j^{n+1} - \tilde{x}_{j-1}^{n+1}\right) + H_{j-1}^n\left(\tilde{y}_j^{n+1} - \tilde{y}_{j-1}^{n+1}\right) + Q_{j-1}^n\left(\tilde{z}_j^{n+1} - \tilde{z}_{j-1}^{n+1}\right), \\ F_j^{n+1} &= -\frac{\partial \tilde{\Phi}_j^{n+1}}{\partial \tilde{T}_{j-2}^n} = \left(P_j^n + R_{j-1}^n\right)\left(\tilde{x}_j^{n+1} - \tilde{x}_{j-1}^{n+1}\right) + \left(H_j^n + O_{j-1}^n\right)\left(\tilde{y}_j^{n+1} - \tilde{y}_{j-1}^{n+1}\right) \\ &\quad + \left(Q_j^n + S_{j-1}^n\right)\left(\tilde{z}_j^{n+1} - \tilde{z}_{j-1}^{n+1}\right), \\ \tilde{G}_j^{n+1} &= \frac{\partial \tilde{\Phi}_j^{n+1}}{\partial \tilde{T}_{j-2}^n} = R_j^n\left(\tilde{x}_j^{n+1} - \tilde{x}_{j-1}^{n+1}\right) + O_j^n\left(\tilde{y}_j^{n+1} - \tilde{y}_{j-1}^{n+1}\right) + S_j^n\left(\tilde{z}_j^{n+1} - \tilde{z}_{j-1}^{n+1}\right), \\ &\qquad (j = 2,3,\dots,N+1). \end{aligned}\right\} \tag{3.36}$$

By solving the Eq. (3.33) repeatedly until the value of ΔT_j converges to satisfy the constraint condition given in Eq. (3.34), the mooring line tension and its motion can be obtained.

(2) Solution for elongated mooring line

In case when the elongation of the mooring line is considered, the mooring line motion equation is solved by considering the following difference formulas using Houbolt method to correct the mass point displacements. According to the Houblt method, the acceleration and velocity of each mass point in *x*-direction are given as follows.

$$\left.\begin{aligned} \ddot{x}_j^n &= \left(2x_j^{n+1} - 5x_j^n + 4x_j^{n-1} - x_j^{n-2}\right)/\Delta t^2, \\ \dot{x}_j^n &= \left(11x_j^{n+1} - 18x_j^n + 9x_j^{n-1} - 2x_j^{n-2}\right)/6\Delta t^2, \end{aligned}\right\} \tag{3.36}$$

n indicate n-th time step, Δt is time interval and x represents the three dimensional directions (x, y and z) of mass points. This relation is also applied for the acceleration and velocity in y- and z-axis directions. The displacement of mass point can be obtained as follows using Eq. (3.22) and $\ddot{x}_j^n$ shown in Eq. (3.37).

$$\left.\begin{aligned} x_j^{n+1} &= \tfrac{5}{2}x_j^n - 2x_j^{n-1} + \tfrac{1}{2}x_j^{n-2} + \left(R_j^{n+1}\cdot T_j^{n+1} - P_j^{n+1}\cdot T_{j-1}^{n+1} + U_j^{n+1}\right)/2, \\ y_j^{n+1} &= \tfrac{5}{2}y_j^n - 2y_j^{n-1} + \tfrac{1}{2}y_j^{n-2} + \left(O_j^{n+1}\cdot T_j^{n+1} - H_j^{n+1}\cdot T_{j-1}^{n+1} + V_j^{n+1}\right)/2, \\ z_j^{n+1} &= \tfrac{5}{2}z_j^n - 2z_j^{n-1} + \tfrac{1}{2}z_j^{n-2} + \left(S_j^{n+1}\cdot T_j^{n+1} - Q_j^{n+1}\cdot T_{j-1}^{n+1} + W_j^{n+1}\right)/2, \\ & (j = 2,3,\dots,N+1). \end{aligned}\right\} \quad (3.38)$$

Similar to Eq. (3.29), the following equation for Ψ_j^{n+1} is obtained.

$$\begin{aligned} \tilde{\Psi}_j^{n+1} &= \left(\tilde{x}_j^{n+1} - \tilde{x}_{j-1}^{n+1}\right)^2 + \left(\tilde{y}_j^{n+1} - \tilde{y}_{j-1}^{n+1}\right)^2 + \left(\tilde{z}_j^{n+1} - \tilde{z}_{j-1}^{n+1}\right)^2 - \bar{l}^2\left(1 + \tilde{T}_{j-1}^{n+1}/E\cdot A\right)^2, \\ &= \Psi_j^{n+1}\left(\tilde{T}_{j-2}^{n+1}, \tilde{T}_{j-1}^{n+1}, \tilde{T}_j^{n+1}\right) \qquad (j = 2,3,\dots,N+1). \end{aligned} \quad (3.39)$$

Performing Taylor expansion on the Eq. (3.39) and assuming ΔT_j^{n+1} is small, the following equation is obtained,

$$\tilde{E}_j^{n+1}\cdot\Delta T_{j-2}^{n+1} - \tilde{F}_j^{n+1}\cdot\Delta T_{j-1}^{n+1} + \tilde{G}_j^{n+1}\cdot\Delta T_j^{n+1} = -\Psi_j^{n+1} \qquad (j = 2,3,\dots,N+1), \quad (3.40)$$

in which $T_j^{n+1} = \tilde{T}_j^{n+1} + \Delta T_j^{n+1}$.

$$\begin{bmatrix} -\tilde{F}_2^{n+1} & \tilde{G}_2^{n+1} & 0 & 0 & \cdots & 0 & 0 & 0 \\ \tilde{E}_3^{n+1} & -\tilde{F}_3^{n+1} & \tilde{G}_{i3}^{n+1} & 0 & \cdots & 0 & 0 & 0 \\ 0 & \tilde{E}_4^{n+1} & -\tilde{F}_4^{n+1} & \tilde{G}_4^{n+1} & \cdots & 0 & 0 & 0 \\ \vdots & \vdots & \vdots & \vdots & \ddots & \vdots & \vdots & \vdots \\ 0 & 0 & 0 & \cdots & \cdots & \tilde{G}_{N-1}^{n+1} & 0 & 0 \\ 0 & 0 & 0 & \cdots & \cdots & -\tilde{F}_N^{n+1} & \tilde{G}_N^{n+1} & 0 \\ 0 & 0 & 0 & \cdots & \cdots & \mathrm{E}_{N+1}^{n+1} & -\tilde{F}_{N+1}^{n+1} & \tilde{G}_{N+1}^{n+1} \end{bmatrix} \begin{bmatrix} \Delta T_1^{n+1} \\ \Delta T_2^{n+1} \\ \Delta T_3^{n+1} \\ \Delta T_4^{n+1} \\ \vdots \\ \Delta T_{N-2}^{n+1} \\ \Delta T_{N-1}^{n+1} \\ \Delta T_N^{n+1} \end{bmatrix} = \begin{bmatrix} -\tilde{\Psi}_2^{n+1} \\ -\tilde{\Psi}_3^{n+1} \\ -\tilde{\Psi}_4^{n+1} \\ -\tilde{\Psi}_5^{n+1} \\ \vdots \\ -\tilde{\Psi}_{N-1}^{n+1} \\ -\tilde{\Psi}_N^{n+1} \\ -\tilde{\Psi}_{N+1}^{n+1} \end{bmatrix}. \quad (3.41)$$

Here $\tilde{E}_j^{n+1}$ and $\tilde{G}_j^{n+1}$ are obtained from Eq. (3.36) by replacing P_j^n with $\tilde{P}_j^{n+1}$, Q_j^n with $\tilde{Q}_j^{n+1}$, R_j^n with $\tilde{R}_j^{n+1}$, S_j^n with $\tilde{S}_j^{n+1}$, O_j^n with $\tilde{O}_j^{n+1}$ and H_j^n with $\tilde{H}_j^{n+1}$ respectively, while $\tilde{F}_j^{n+1}$ should be modified considering the effect of the elongation as follows.

$$\left.\begin{aligned} \tilde{E}_j^{n+1} &= \frac{\partial\tilde{\Psi}_j^{n+1}}{\partial\tilde{T}_{j-2}^{n+1}} = P_{j-1}^{n+1}\left(\tilde{x}_j^{n+1} - \tilde{x}_{j-1}^{n+1}\right) + H_{j-1}^{n+1}\left(\tilde{y}_j^{n+1} - \tilde{y}_{j-1}^{n+1}\right) + Q_{j-1}^{n+1}\left(\tilde{z}_j^{n+1} - \tilde{z}_{j-1}^{n+1}\right), \\ F_j^{n+1} &= -\frac{\partial\tilde{\Psi}_j^{n+1}}{\partial\tilde{T}_{j-2}^{n+1}} = \left(P_j^{n+1} + R_{j-1}^{n+1}\right)\left(\tilde{x}_j^{n+1} - \tilde{x}_{j-1}^{n+1}\right) + \left(H_j^{n+1} + O_{j-1}^{n+1}\right)\left(\tilde{y}_j^{n+1} - \tilde{y}_{j-1}^{n+1}\right) \\ &\quad + \left(Q_j^{n+1} + S_{j-1}^{n+1}\right)\left(\tilde{z}_j^{n+1} - \tilde{z}_{j-1}^{n+1}\right)2\bar{l}^2\left(1 + T_{j-1}^{n+1}/E\cdot A\right)^2, \\ \tilde{G}_j^{n+1} &= \frac{\partial\tilde{\Psi}_j^{n+1}}{\partial\tilde{T}_{j-2}^{n+1}} = R_j^{n+1}\left(\tilde{x}_j^{n+1} - \tilde{x}_{j-1}^{n+1}\right) + O_j^{n+1}\left(\tilde{y}_j^{n+1} - \tilde{y}_{j-1}^{n+1}\right) + S_j^{n+1}\left(\tilde{z}_j^{n+1} - \tilde{z}_{j-1}^{n+1}\right), \\ & (j = 2,3,\dots,N+1). \end{aligned}\right\} \quad (3.42)$$

Also, $\widetilde{\Psi}_j^{n+1}$ in Eq. (3.39) can be expressed similar with Eq. (3.34) as the function of $\tilde{x}_j^{n+1}$, $\tilde{y}_j^{n+1}$, $\tilde{z}_j^{n+1}$, and $\tilde{T}_j^n$. Similar with Eq. (3.34) and Eq. (3.35), the following equations can be derived,

$$\widetilde{\Psi}_j^{n+1} = \left(\tilde{x}_j^{n+1} - \tilde{x}_{j-1}^{n+1}\right)^2 + \left(\tilde{y}_j^{n+1} - \tilde{y}_{j-1}^{n+1}\right)^2 + \left(\tilde{z}_j^{n+1} - \tilde{z}_{j-1}^{n+1}\right)^2 - \bar{l}^2\left(1 + \tilde{T}_{j-1}^{n+1}/E \cdot A\right)^2, \quad (3.43)$$

$$\left.\begin{aligned} \tilde{x}_j^{n+1} &= \tfrac{5}{2}x_j^n - 2x_j^{n-1} + \tfrac{1}{2}x_j^{n-2} + \left(R_j^{n+1} \cdot \tilde{T}_j^{n+1} - P_j^{n+1} \cdot \tilde{T}_{j-1}^{n+1} + \tilde{U}_j^{n+1}\right)/2, \\ \tilde{y}_j^{n+1} &= \tfrac{5}{2}y_j^n - 2y_j^{n-1} + \tfrac{1}{2}y_j^{n-2} + \left(O_j^{n+1} \cdot \tilde{T}_j^{n+1} - H_j^{n+1} \cdot \tilde{T}_{j-1}^{n+1} + \tilde{V}_j^{n+1}\right)/2, \\ \tilde{z}_j^{n+1} &= \tfrac{5}{2}z_j^n - 2z_j^{n-1} + \tfrac{1}{2}z_j^{n-2} + \left(S_j^{n+1} \cdot \tilde{T}_j^{n+1} - Q_j^{n+1} \cdot \tilde{T}_{j-1}^{n+1} + \tilde{W}_j^{n+1}\right)/2, \\ & (j = 2,3,\dots,N+1). \end{aligned}\right\} \quad (3.44)$$

Similarly, the mooring line tension and its motion for elongated mooring line can be obtained by solving Eq. (3.41) repeatedly until ΔT_j converges to satisfy the constraint condition given in Eq. (3.43). In this study, the method considering the elongation of mooring line is used.

3.3. Mooring Line Connection to Floating Structure

The motion of mooring line connection point at a floating structure is affected by the simultaneous motion of the floating structure. This simultaneous motion is generated by the coupled-motion between the floating structure and its mooring line. It forces the connection point and the floating structure concurrently.

The motion of a mooring line connection point can be described by considering line and body-fixed coordinate systems shown in Fig. 3.1 and Fig. 2.1 respectively. The top point P in Fig. 3.1 is assumed to be located at the connection point between the mooring line and floating structure (bellmouth) position $B_j(x_{b_j}, y_{b_j}, z_{b_j})$ of the floating structure figured in Fig. 2.1. The position of the bellmouth $B_{j_t}(x_{b_{j_t}}, y_{b_{j_t}}, z_{b_{t_j}})$ when the floating structure is disturbed by external forces can be given by the following expression using the displacements of the floating structure $d_m(\overline{x}, \bar{y}, \bar{z}, \theta, \phi, \psi)$,

$$\left.\begin{aligned} x_{b_{j_t}} &= \overline{OG}\sin\ \phi + x_{b_j}\cos\ \phi, \\ y_{b_{j_t}} &= \overline{OG}\cos\ \theta + y_{b_j}\sin\ \theta, \\ z_{b_{j_t}} &= z_{b_j} + \bar{z} + \left\{\overline{OG} - \left(\cos\theta + y_{b_j}\sin\ \theta\right)\cos\ \phi + x_{b_j}\sin\ \phi\right\}, \end{aligned}\right\} \quad (3.45)$$

where $\overline{OG}$ is the vertical distance between the center of gravity of the floating structure G and water surface. Thus, the positions of the connection point for each mooring line

$P_j(x_{P_j}, y_{P_j}, z_{P_j})$ in line coordinate system can be expressed as,

$$\left.\begin{aligned} x_{P_j} &= x_{P_{j_0}} - \Delta x_{b_j}, \\ y_{P_j} &= y_{P_{j_0}} - \Delta y_{b_j}, \\ z_{P_j} &= z_{P_{j_0}} - \Delta z_{b_j}, \end{aligned}\right\} \tag{3.46}$$

in which $P_{j_0}(x_{P_{j_0}}, y_{P_{j_0}}, z_{P_{j_0}})$ is the initial position of the each mooring line connection point P_j and ΔB_j is the each bellmouth displacement due to coupled dynamic motions which can be obtained as follows,

$$\left.\begin{aligned} \Delta x_{b_j} &= (x_G + x_{b_{j_t}} \cos\psi - y_{b_{j_t}} \sin\psi) - x_{b_j}, \\ \Delta y_{b_j} &= (y_G + x_{b_{j_t}} \sin\psi + y_{b_{j_t}} \cos\psi) - y_{b_j}, \\ \Delta z_{b_j} &= (z_G + z_{b_{j_t}}) - z_{b_j}, \end{aligned}\right\} \tag{3.47}$$

where $G(x_G, y_G, z_G)$ is the position of the center of gravity of the floating structure.

3.4. Anchoring Force and Motion

To provide the probability of the occurrence of dragging anchor, the following motion equation of an anchor given by Sasa and Incecik (2012) is used to express the anchor motion.

$$(M_A + m_A)\ddot{x}_A + D_A\dot{x}_A = T_L - P_A, \tag{3.48}$$

where M_A, m_A, and D_A are the mass of an anchor, the added mass of an anchor and frictional coefficient of an anchor in the soil, respectively. T_L is line tension acting on an anchor node and P_A is anchor force adopting the estimated formula given by Honda (1992),

$$P_A = w_a\lambda_a + w_c\lambda_c l_{laying}, \tag{3.49}$$

Here, λ_a is grip factor of an anchor, λ_c and l_{laying} are the friction resistance factor and laying part length of the mooring line. κ is the angle at the touchdown point. Since the anchor force changes due to the angle of touchdown point, the reduction factor $e^{-0.05\kappa}$ given by Inoue and Usui (1993) must be considered.

3.5. Numerical Simulation

3.5.1. Calculation Condition

In order to verify the capability of the proposed three-dimensional dynamics mooring line coupled with a floating offshore structure, analyses of coupled motions of the mooring lines and a ship-type floating offshore structure are conducted. In these analyses, the floating structure is moored by four various types of mooring configuration i.e. single mooring line (denoted as SL), double mooring lines (DL), multi-leg turret mooring (SP), and multi-leg

spread mooring (SM). The arrangement of mooring line is summarized in Table 3.2 while the schematic of those four mooring line configuration types are shown in Fig. 3.5.

Table 3.2. Mooring line arrangement for numerical simulation

Notation	I. Single Mooring Line	II. Double Mooring Lines	III. Multi-leg Turret Mooring	IV. Multi-leg Spread Mooring
Number of Line	1	2	6	6
Mooring line angle	0°	-30°, 30°	30°, 90°, 150°, 210°, 270°, 330°	30°, 90°, 150°, 210°, 270°, 330°
Connection point	single point	single point	single point	multi point

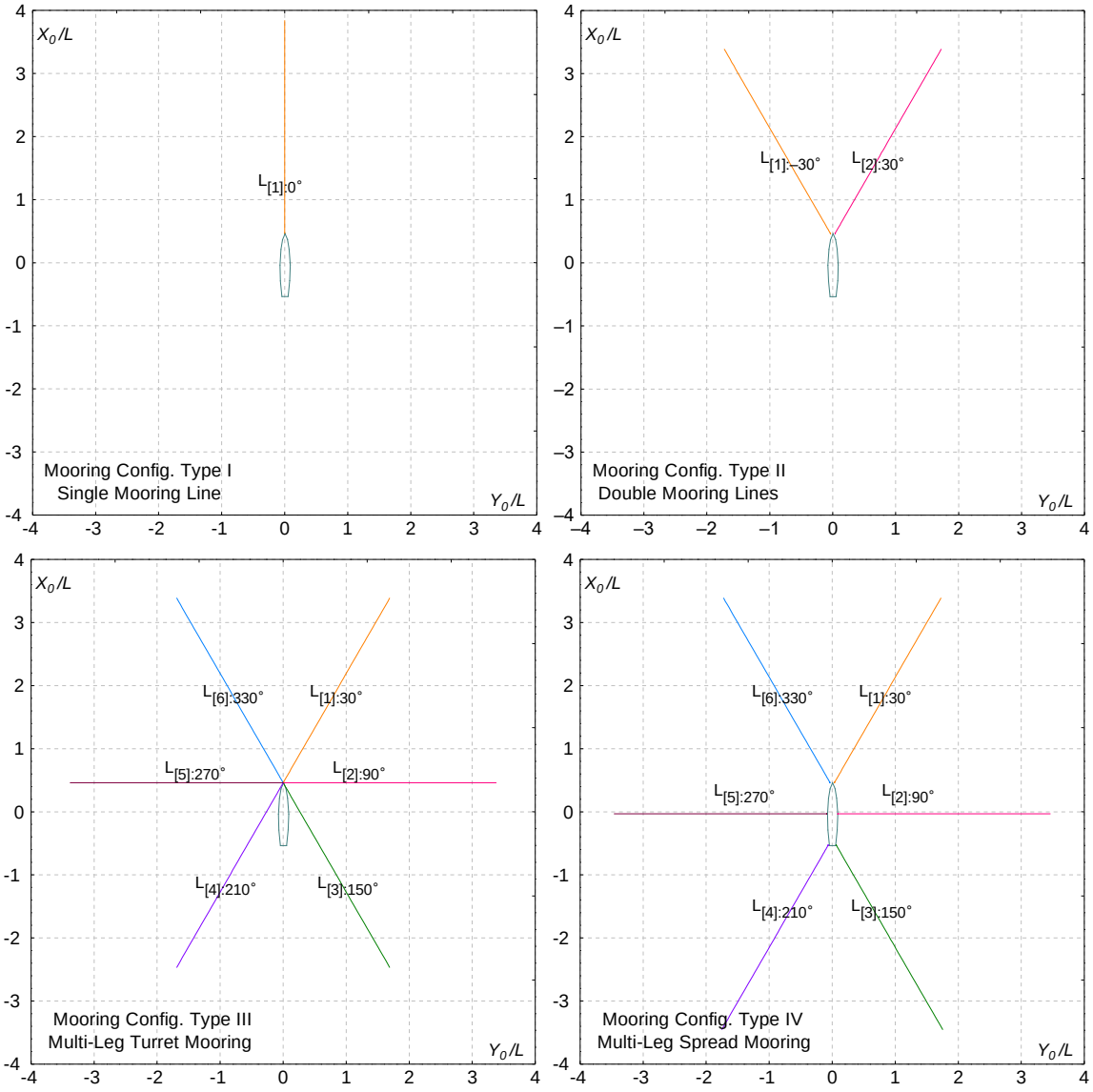

Fig. 3.5. Variation of mooring line configurations

In this numerical simulation, the floating structure is assumed to be moored with those various mooring configurations at the sea of 500 m depth in which the seabed condition is assumed as sand. As calculation condition to perform numerical simulations by applying the three-dimensional lumped mass method, the mooring line is divided into 80 elements while time increment Δt is equal to 0.01 second. The calculation time of numerical simulation is set about 17100 seconds (abt. 4.8 hours) with about 5500 seconds for pre-calculation time. The pre-calculation time is applied to avoid large transient motions or calculation errors due to sudden effect of disturbance forces acting on the floating structure. In this time, the magnitude of all external forces (wave, wind, and current) including their directions are increased gradually over that time. The value of drag forces and mooring line added mass coefficients are taken from Nakajima et al. (1993) $(C_{dn} = 2.18, C_{dt} = 0.17, C_{hn} = 1.98, C_{ht} = 0.20)$. Meanwhile, the initial tension (pre-tension) acting on the mooring line is taken as 0.25 kN.

At the beginning of the simulation, the center of gravity of the floating structure is placed at the origin of the earth-fixed coordinate system shown in Fig. 2.1 with the drift angle 0°. The initial shape of the mooring line is calculated by using static condition of lumped mass method referring the distance of the anchor determined by catenary analysis.

3.5.2. Floating Offshore Structure and Mooring Line Data

(1) Principle Dimension of Target Floating Offshore Structure and Mooring Line Properties

Target floating offshore structure used in these numerical simulations refer a VLCC (ESSO OSAKA) which is assumed to be as a ship-type floating offshore structure. The mooring line is a single component mooring line consisting of chain and an anchor. The height of bellmouth is assumed to be equal to draught while the coordinate position of

Table 3.3. Principle dimension of floating structure and mooring line properties

Floating Structure		Mooring Line	
L_{OA} (m)	343.00	Length (m)	1595.00
L_{PP} (m)	325.00	w_c (kg)	299.80
B (m)	53.00	D_c (m)	117.00
d (m)	22.05	E (kgf/m^2)	2.15×10^9
C_b	0.831	λ_c	0.75
KG	14.998	w_a(kg)	17250.00
$\overline{MG}$	10.3025	λ_a	7.00

bellmouth is depend on the mooring configuration (it will be explained in next subsection). The principal dimensions of the floating structure and mooring line as well as anchor characteristics are shown in Table 3.3.

(2) Projected Area for Wind Force Calculation

The shape of projected area for the target floating structure above water line is shown in Fig. 3.6. This figure shows front projection area's shape of the hull of the target floating structure seen from the bow direction and side projection area's shape seen from starboard direction. Based on those projected area, the characteristic parameter data required for calculating wind force is shown in Table 3.4. Also, the density of air ρ_a used for the calculation is taken as 0.1296 kgf·sec^2/m^4, which is measured at 5 ℃ of the air.

Fig. 3.6. Projected area of the target floating offshore structure (ESSO OSAKA)

Table 3.4. Characteristic parameter data for wind force calculation

Parameter	Value
A_T (m^2)	343.000
A_L (m^2)	2606.614
A_{OD} (m^2)	1450.550
C (m)	6.120
C_{BR} (m)	-107.020
H_{BR} (m)	37.600
H_C (m)	3.950

(3) Hydrodynamic Derivatives

Hydrodynamic derivatives used in these numerical simulations were obtained by captive model test carried out for VLCC model ship in the Seakeeping and Manoeuvring Basin at Department of Marine Systems Engineering, Faculty of Engineering, Kyushu University. Table 3.5 shows the values of the hydrodynamic derivatives used in these simulations.

Table 3.5. Hydrodynamic derivatives used for simulations

Derivative	Value	Derivative	Value
Y'_{β}	0.3439	N'_{β}	0.1342
Y'_{r}	-0.2339	N'_{r}	-0.0519
$Y'_{\beta\beta}$	0.0569	$N'_{\beta\beta}$	0.0120
Y'_{rr}	0.6056	N'_{rr}	-0.0206
$Y'_{\beta rr}$	0.4731	$N'_{\beta rr}$	-0.1561
$Y'_{\beta\beta r}$	0.1214	$N'_{\beta\beta r}$	-0.0695

3.5.3. Various Case of Simulations

To verify the capability of the proposed numerical model against to both various mooring line configurations system and various environmental conditions, numerical simulations are conducted. In these simulations, four types of mooring line configuration figured in Fig. 3.5 are subjected to various environmental conditions shown in Table 3.6.

In Table 3.5, H_W is wave height taken as equal to 2 m, V_C is current velocity, α is current direction, λ/L is wavelength-length ratio, and χ is wave direction. According to simulations have been done in advance, in these variation cases, the various environmental loads are arranged based on the difference of λ/L, the presence of wind force, and the direction of current relative to bow direction $(0°)$ under the various directions of wave and wind. Since the variation of environmental conditions shown in Table 3.5 are applied to every variation of mooring line configurations consists of 32 cases, totally 128 variation cases have been established. According to the simulations have been carried out, the results of several conditions are picked up and discussed representing the other several conditions which have the similar tendency of those results.

Table 3.6. Various environmental loads

Parameter	Value
H_w (m)	2.00
λ/L	0.50 , 1.00
χ $(deg.)$	30°, 60°
V_C (kn)	1.00
α $(deg.)$	0°, 30°
V_W (m/s)	0, 10
ν $(deg.)$	0°, 45°

3.5.4. Numerical Simulation Results

Motion analyses of the floating offshore structure are observed through the investigation of moored vessel motion components, i.e. vessel trajectory, mooring line motions, time histories of drift motion in horizontal plane and vertical motion which represent the behavior of the floating structure in given environmental conditions. Time histories of mooring line tension force including all environmental loads acting on the floating structure are also presented. Furthermore, to capture the simultaneous interactions between the floating structure and its mooring line, the motions of floating structure induced by mooring line and vice versa are investigated. In addition, the tension acting on the floating structure are evaluated reviewing how mooring line correlates with the motion of floating structure in 6 DOF motion.

As instance, the template of simulation results for all conditions can be seen in Fig. 3.7. Here, figure (a) shows the trajectory of the floating structure and her mooring line motion at interval of 100 seconds, figure (b) is the time histories of all forces acting on the floating structure, figure (c) presents the time histories of surge displacement, sway displacement and yaw motion respectively, and figure (d) shows heave, pitch and roll motions respectively. "SL" represents the type of mooring configuration (single line) while the number after "SL" is the given running case number for identification of the case.

(1) Single Mooring Line

In single mooring line system, the floating structure is moored by a mooring line deployed toward bow direction. The mooring line angle is 0° while the connection point of mooring line is located on the center line of the floating structure and 160 m forward from the midship. An anchor is attached on the bottom end of the mooring line. The results of this mooring configuration type can be observed in Fig. 3.7 to Fig. 3.18.

The simulation results of single mooring line for the case without the presence of wind force are shown in Fig. 3.7 to Fig.3.10. According to these results, when current comes from bow direction ($\alpha = 0°$) and wave comes from arbitrary direction as shown in Fig. 3.7 (SL-17) and Fig. 3.9 (SL-21), the floating structure only moves within small displacement. Since the current effect in longitudinal direction is small for the floating body without forward speed (or with low speed) and wave drifting force is also small comparing with other forces meanwhile the mooring line tension restrains the drifting motion of the floating structure, the floating structure only moves with small displacement. However, if the direction of wave relative to the heading of the floating structure increases close to beam sea condition, the vertical motion of the floating structure especially roll and heave increase while the horizontal drifting motion is almost same. This condition can be noticed by comparing

figures (d) in Fig. 3.7 (SL-17) and Fig. 3.9 (SL-21).

Meanwhile, when current direction isn't $0°$, the lateral force and moment acting on the floating structure increase and those become dominant loads acting on the floating structure. These loads force the floating structure to move in lateral direction. This condition can be recognized by comparing Fig. 3.8 (SL-18) and Fig. 3.7 (SL-17) as well as Fig. 3.10 (SL-22) and Fig. 3.9 (SL-21). Current angle used in Fig. 3.8 (SL-18) and Fig. 3.10 (SL-22) is $30°$. In addition, the increase of vertical motion due to the larger incident wave angle toward beam sea condition also occurs as shown in Fig. 3.10 (SL-22) (compare it with Fig. 3.8 (SL-22)). Moreover, since the heading of floating structure changes gradually following the direction of the dominant external force (current), in which the current direction is equal to the wave direction, the vertical motion of the floating structure decrease because the heading of floating structure tends to be same with the wave direction. By comparing Fig. 3.10 (SL-22) and Fig. 3.8 (SL-18), this relation can be observed. The effect of mooring line on restraining of the motion of the floating structure can be noticed in these cases (Fig. 3.8 and Fig. 3.10) in which the floating structure firstly moves toward her portside direction due to the lateral force and moment and then it moves back toward her starboard direction due to the restoring force generated by mooring line tension. This condition will occur repeatedly until the floating structure reaches her equilibrium conditions.

On the other hand, the effect of the presence of wind force is shown in Fig. 3.11 to Fig. 3.18. According to those figures, when current comes from $0°$ and wind also comes from $0°$ combined with wave coming from arbitrary direction, the heading of the floating structure is completely in $0°$ direction following the direction of current and wind because the dominant force acts in longitudinal direction. However, again, similar with Fig. 3.7 and Fig. 3.9. it can be noticed that the displacement of drifting motion in these cases is small while the vertical motion increases when the direction of waves relative to bow direction increases (Fig. 3.11 and Fig. 3.12). The presence of wind also increases the drift motion of the floating structure in longitudinal direction (comparing displacements in x_0 direction for Fig. 3.11 with that for Fig. 3.7 and Fig.3.12 with Fig. 3.9) and hence it increases the mooring line tension (see mooring line tension in x-direction shown in figure (b)).

Furthermore, the effect of mooring line tension on the motion of the floating structure combined with the various directions of external forces can be more clearly introduced in Fig. 3.13 to Fig. 3.18. In Fig. 3.13 and Fig. 3.14, in which wind and current come from the same direction $(\nu = \alpha = 30°)$ so that the floating structure moves toward lateral direction followed by the motion of the mooring lines. Since the mooring line restrains the floating structure, the distance between the floating structure and anchor point is almost constant during the simulation, though the floating structure moves far away toward lateral direction.

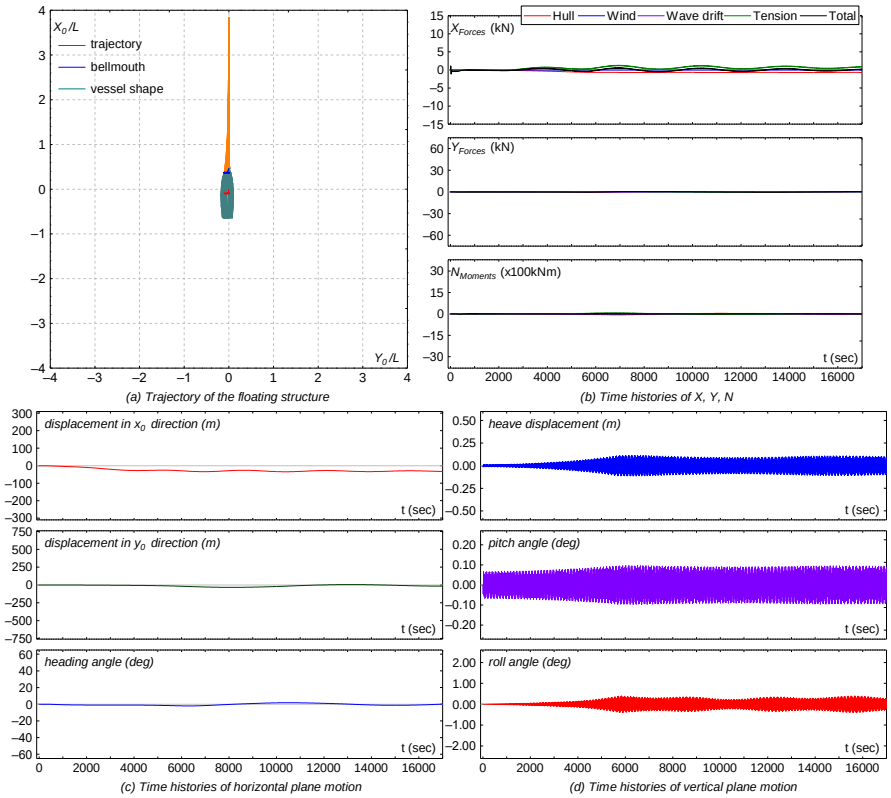

Fig. 3.7. $\lambda/L = 1.0$; $V_C = 1.0$ kn; $\alpha = 0°$; No wind; $\chi = 30°$ [SL-17]

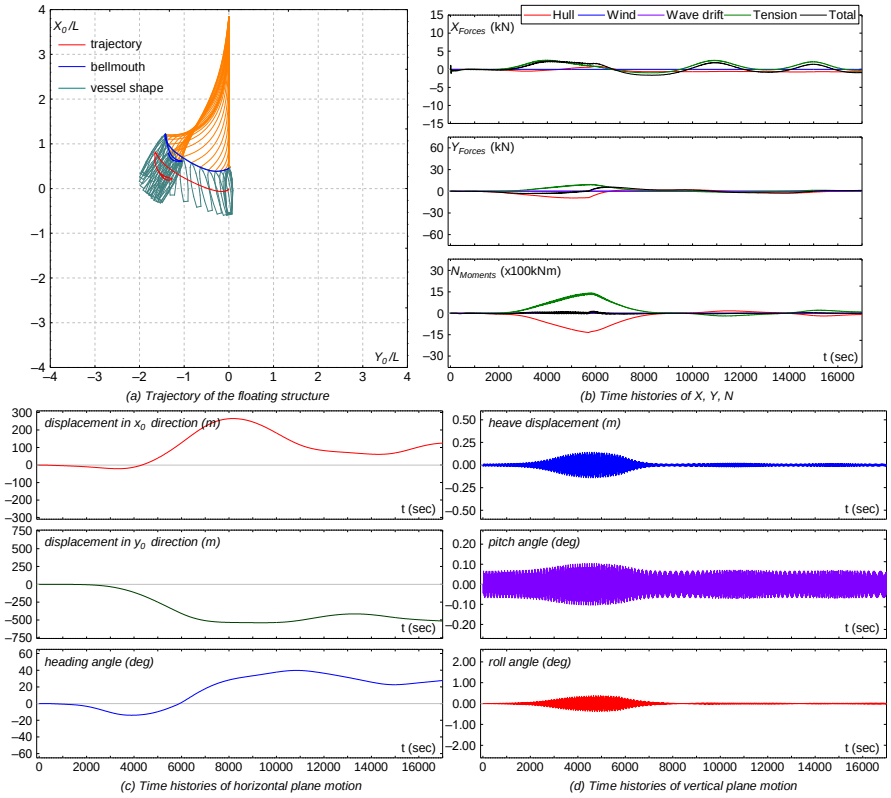

Fig. 3.8. $\lambda/L = 1.0$; $V_C = 1.0$ kn; $\alpha = 30°$; No wind; $\chi = 30°$ [SL-18]

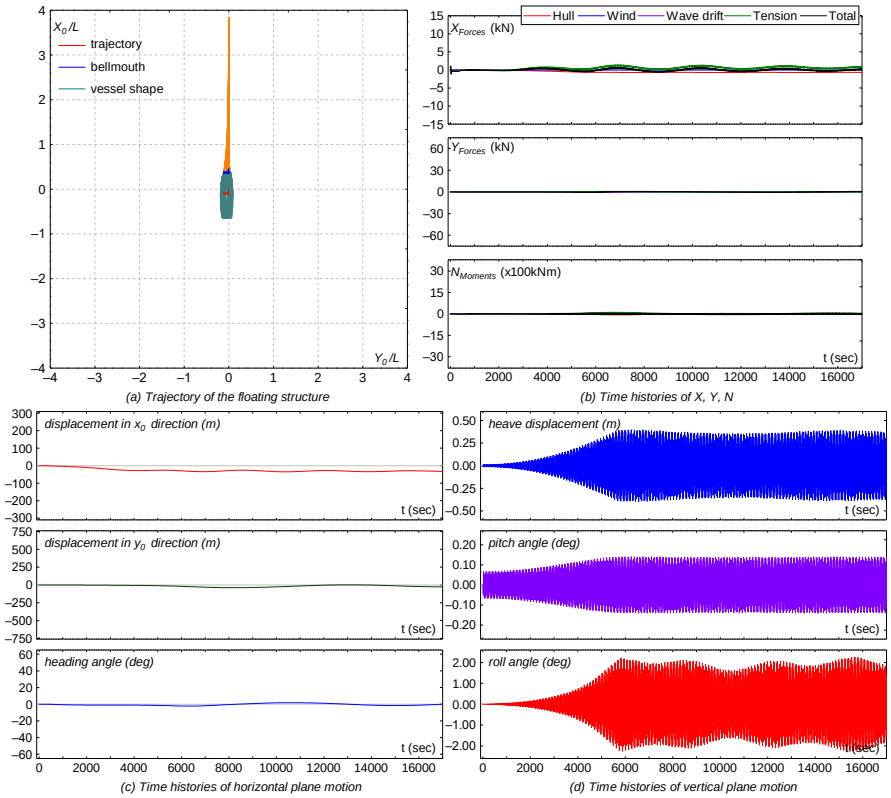

Fig. 3.9. $\lambda/L = 1.0$; $V_C = 1.0$ kn; $\alpha = 0°$; No wind; $\chi = 60°$ [SL-21]

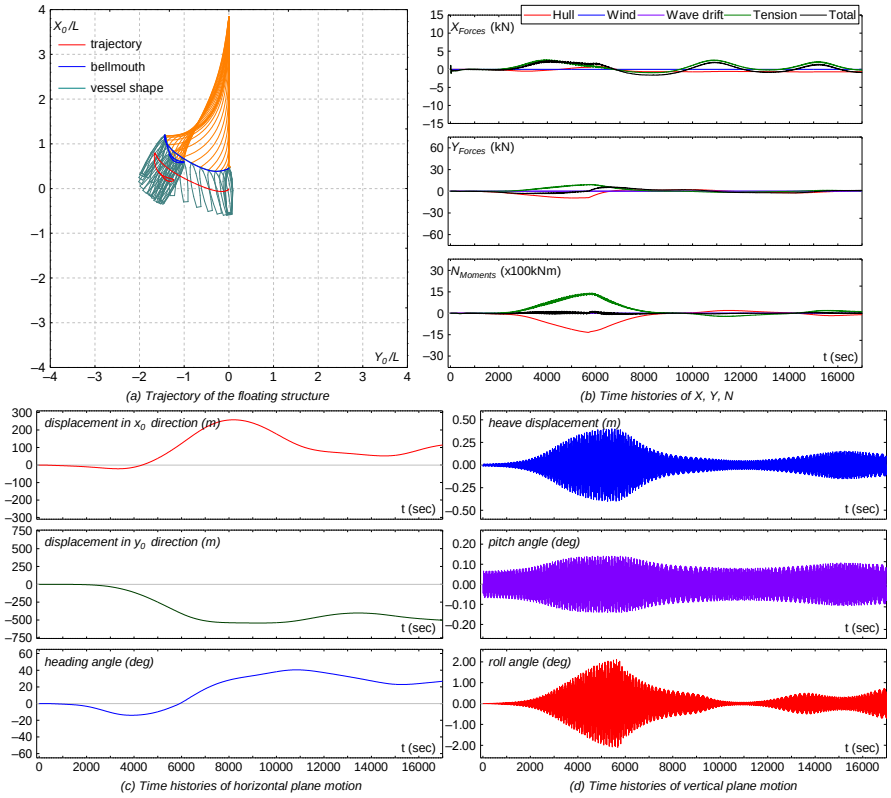

Fig. 3.10. $\lambda/L = 1.0$; $V_C = 1.0$ kn; $\alpha = 30°$; No wind; $\chi = 60°$ [SL-22]

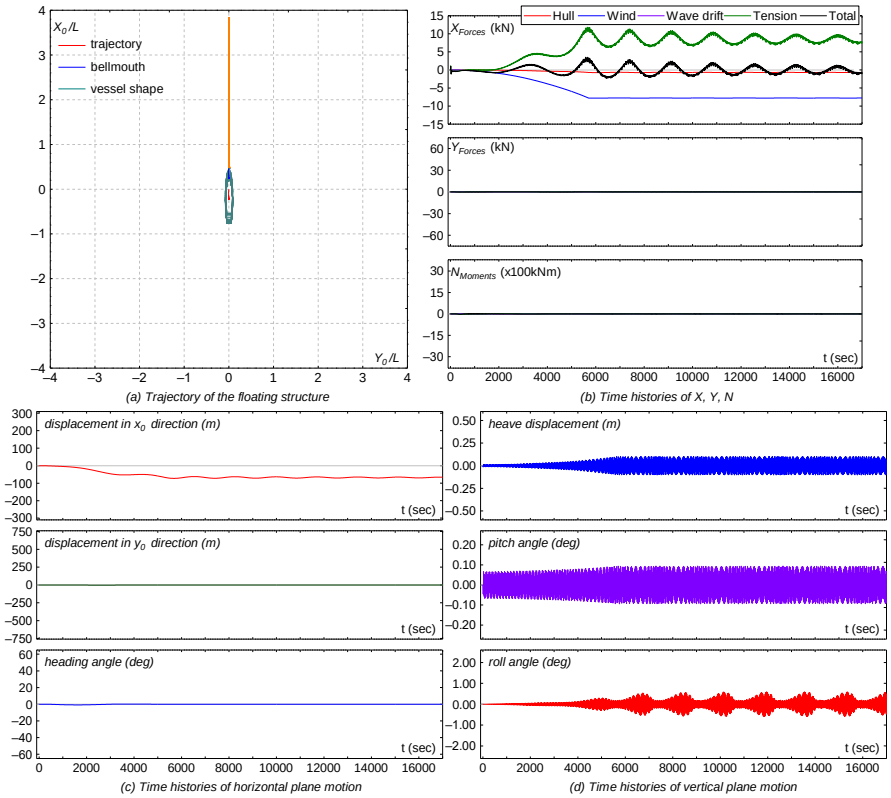

Fig. 3.11. $\lambda/L = 1.0$; $V_C = 1.0$ kn; $\alpha = 0°$; $V_W = 10$ m/s; $v = 0°$; $\chi = 30°$ [SL-25]

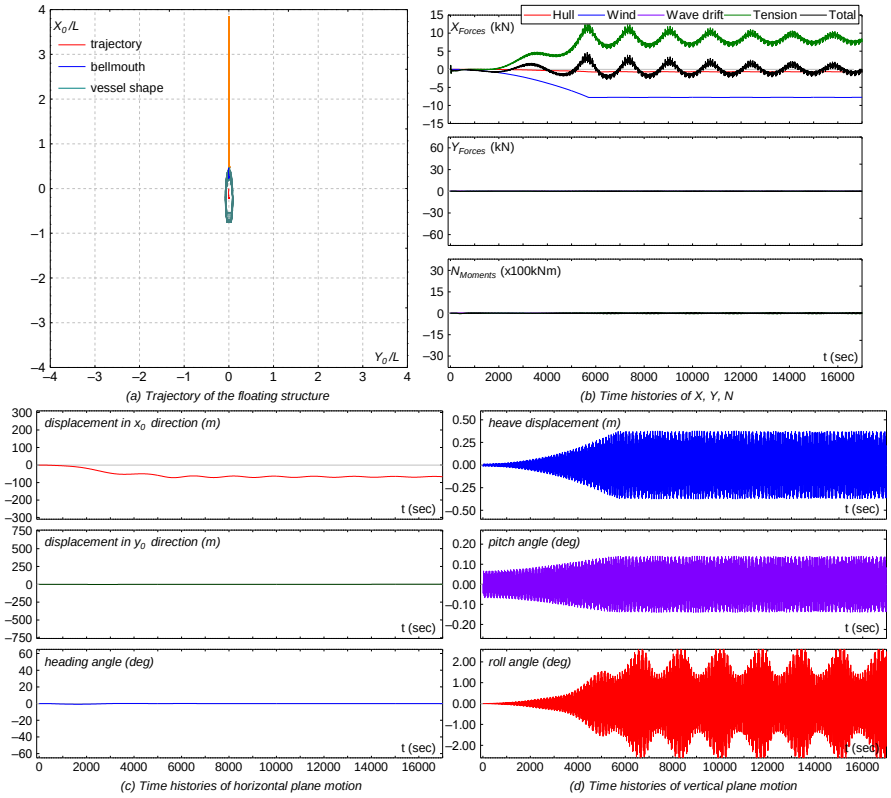

Fig. 3.12. $\lambda/L = 1.0$; $V_C = 1.0$ kn; $\alpha = 0°$; $V_W = 10$ m/s; $v = 0°$; $\chi = 60°$ [SL-29]

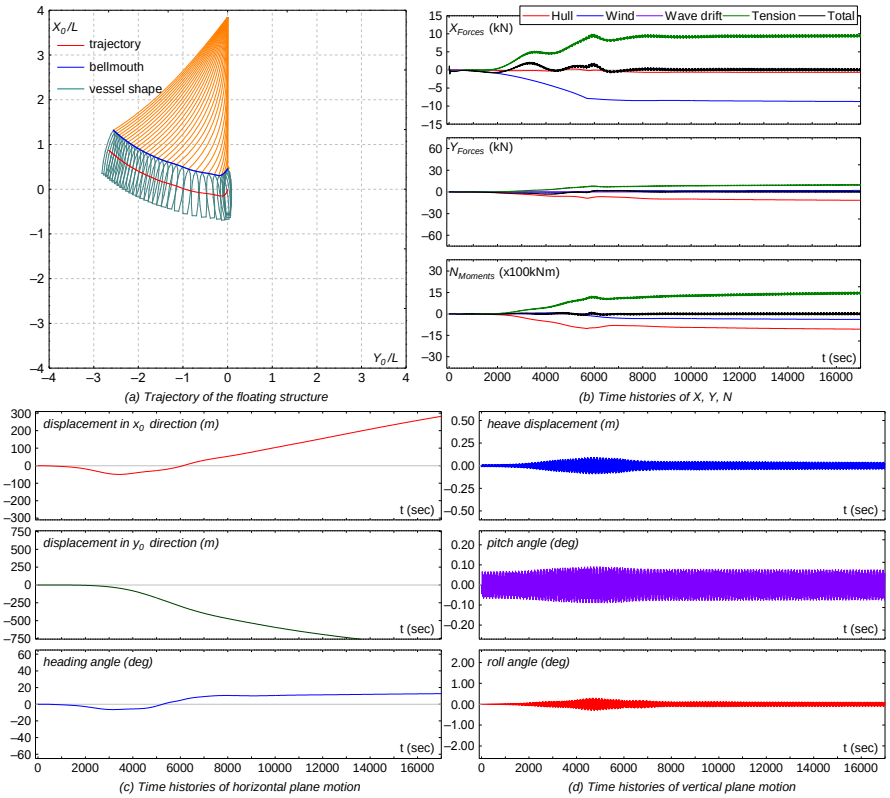

Fig. 3.13. $\lambda/L = 1.0;\ V_C = 1.0$ kn; $\alpha = 30°;\ V_W = 10$ m/s; $v = 0°;\ \chi = 30°$ [SL-26]

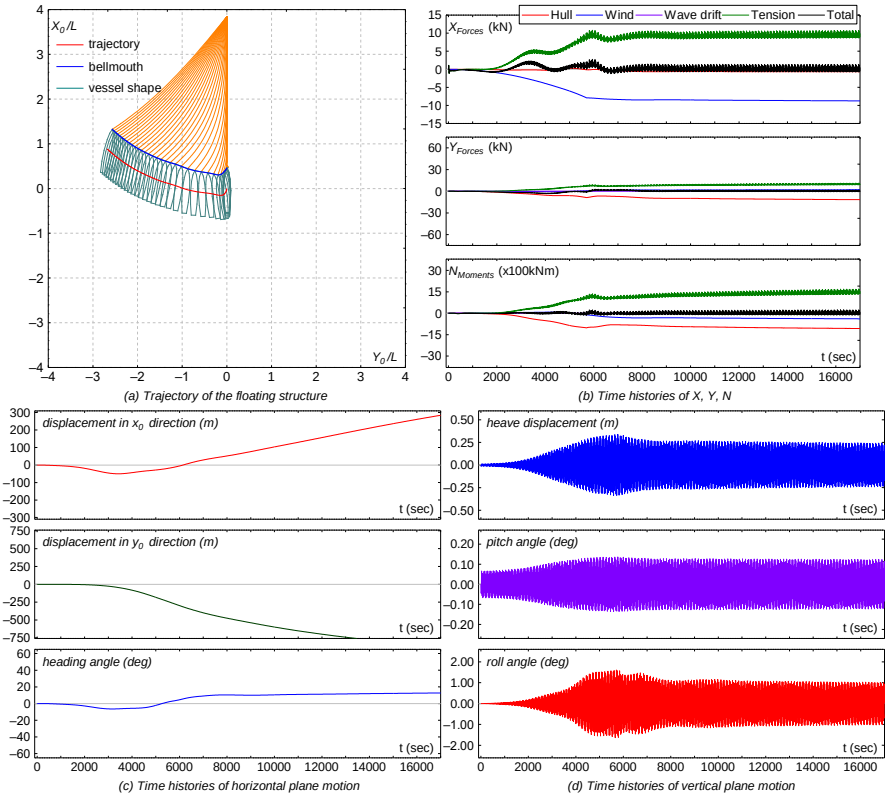

Fig. 3.14. $\lambda/L = 1.0;\ V_C = 1.0$ kn; $\alpha = 30°;\ V_W = 10$ m/s; $v = 0°;\ \chi = 60°$ [SL-30]

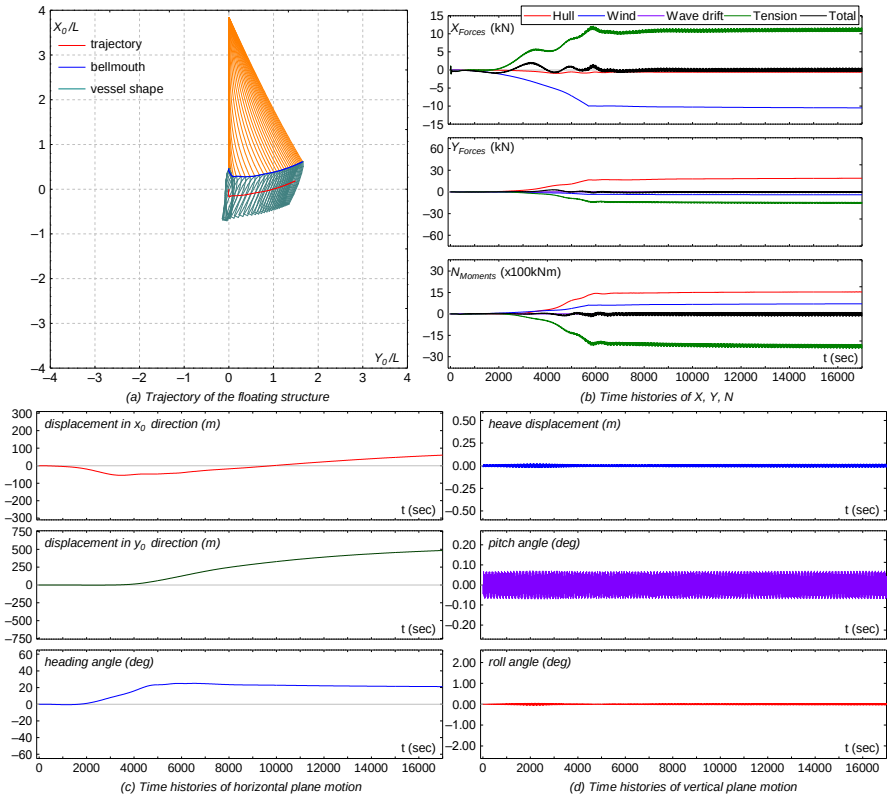

Fig. 3.15. $\lambda/L = 1.0;\ V_C = 1.0$ kn; $\alpha = 0°;\ V_W = 10$ m/s; $v = 45°;\ \chi = 30°$ [SL-27]

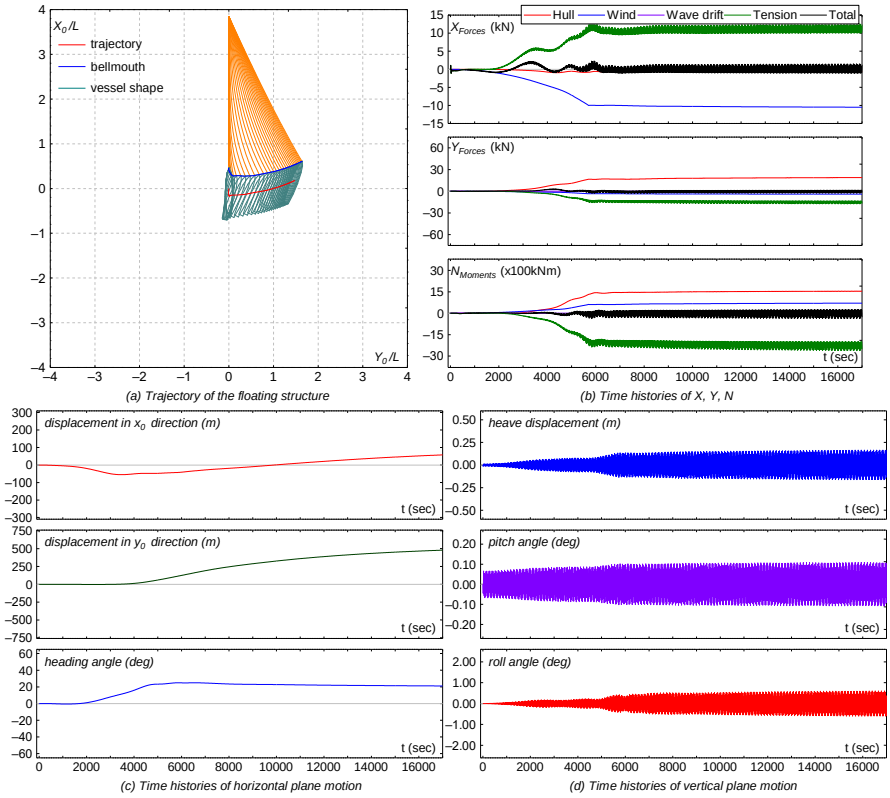

Fig. 3.16. $\lambda/L = 1.0;\ V_C = 1.0$ kn; $\alpha = 0°;\ V_W = 10$ m/s; $v = 45°;\ \chi = 60°$ [SL-31]

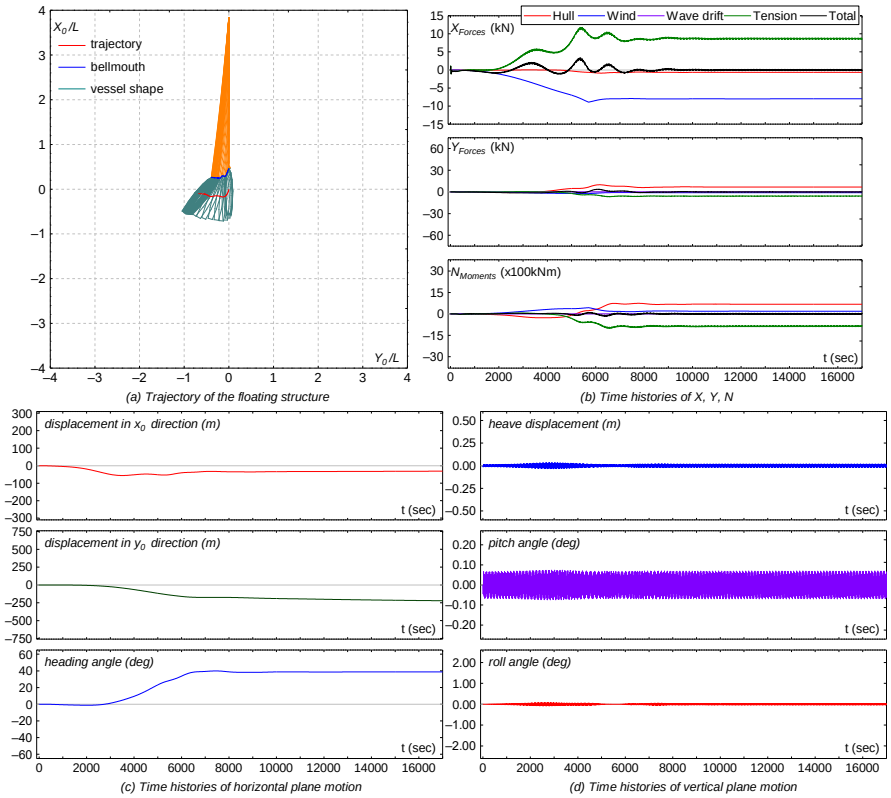

Fig. 3.17. $\lambda/L = 1.0$; $V_C = 1.0$ kn; $\alpha = 30°$; $V_W = 10$ m/s; $v = 45°$; $\chi = 30°$ [SL-28]

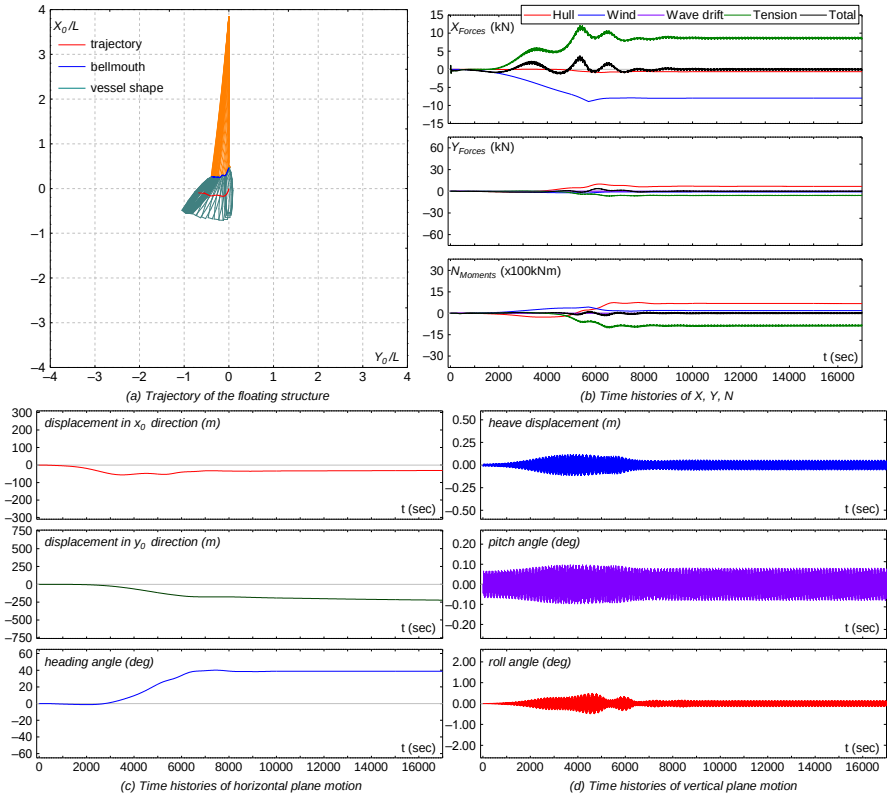

Fig. 3.18. $\lambda/L = 1.0$; $V_C = 1.0$ kn; $\alpha = 30°$; $V_W = 10$ m/s; $v = 45°$; $\chi = 60°$ [SL-32]

The contribution of the mooring line is also shown in non-uniform external force directions figured in Fig. 3.15 to Fig. 3.18. In addition, similar with the case in which there is no wind force, the increase of wave direction relative to the heading of the floating structure increases the vertical motion of the floating structure. It can be observed by comparing Fig. 3.13 with Fig. 3.14, Fig. 3.15 with Fig. 3.16, and Fig. 3.17 with Fig. 3.18.

(2) Double Mooring Lines

For double mooring lines system, the floating structure is moored by two mooring lines arranged symmetrically with an angle of 30-degrees against the floating structure's bow direction. The connection point of the mooring lines are located at $(x_{b_1}, y_{b_1}) = (160\ \text{m}, -11\ \text{m})$ and $(x_{b_2}, y_{b_2}) = (160\ \text{m}, 11\ \text{m})$. The results of this mooring configuration type can be observed in Fig. 3.19 to Fig. 3.30. The discussions of those results are explained as follows.

When current comes from bow directions and there is no wind at the same time, the floating structure seems move with very small displacement (it almost doesn't move) because there is two mooring lines which restrain the floating structure (Fig. 3.19 and Fig. 3.21). Meanwhile, similar with single line condition, if current comes from non-zero degree direction, the lateral force and moment increase and thereby the floating structure moves and rotates toward lateral direction (Fig. 3.20 and Fig. 3.22). However, because the number of mooring line withstood the floating structure increases, the displacement of the horizontal motion of the floating structure decreases comparing with that of single line mooring type (comparing Figs. 3.20 and 3.22 with Figs. 3.8 and 3.10 respectively). In these conditions, the coupled motion between double mooring lines can be recognized, because both lines move simultaneously following the motion of the floating structure. The effect of the larger incident angle of waves relative to bow direction is noticed in double mooring lines type comparing Figs. 3.21 and 3.22 with Figs. 3.19 and 3.20 respectively. It can be observed that the larger vertical motions occur concomitant with the larger incident angle of waves toward beam sea direction.

On the other hand, when current comes from 0°, the presence of wind coming from 0° enlarges the mooring line tension since the floating structure moves farther than the case without wind force. It can be observed by comparing Figs. 3.23 and Fig. 3.24.with Fig. 3.19 and Figs. 3.19 respectively. The presence of wind also increases the drift motion when the current force coming from non-zero direction. According to the simulated results for the case in which double mooring lines move with a floating structure, mooring line tension as well as their motions can be simulated well by the proposed dynamics model.

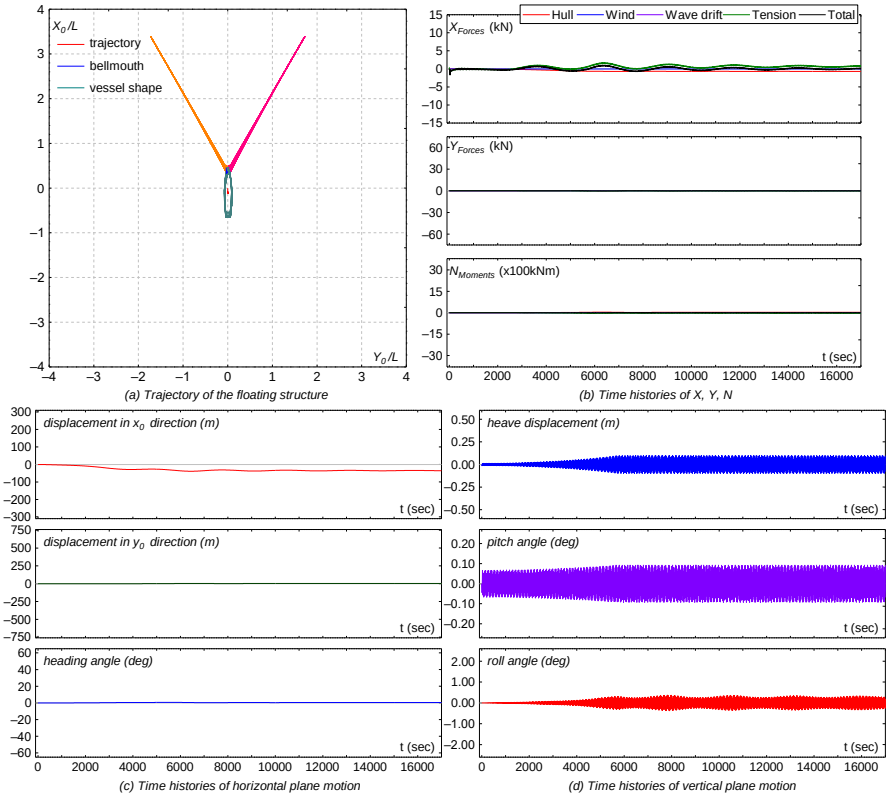

Fig. 3.19. $\lambda/L = 1.0$; $V_C = 1.0$ kn; $\alpha = 0°$; No wind; $\chi = 30°$ [DL-17]

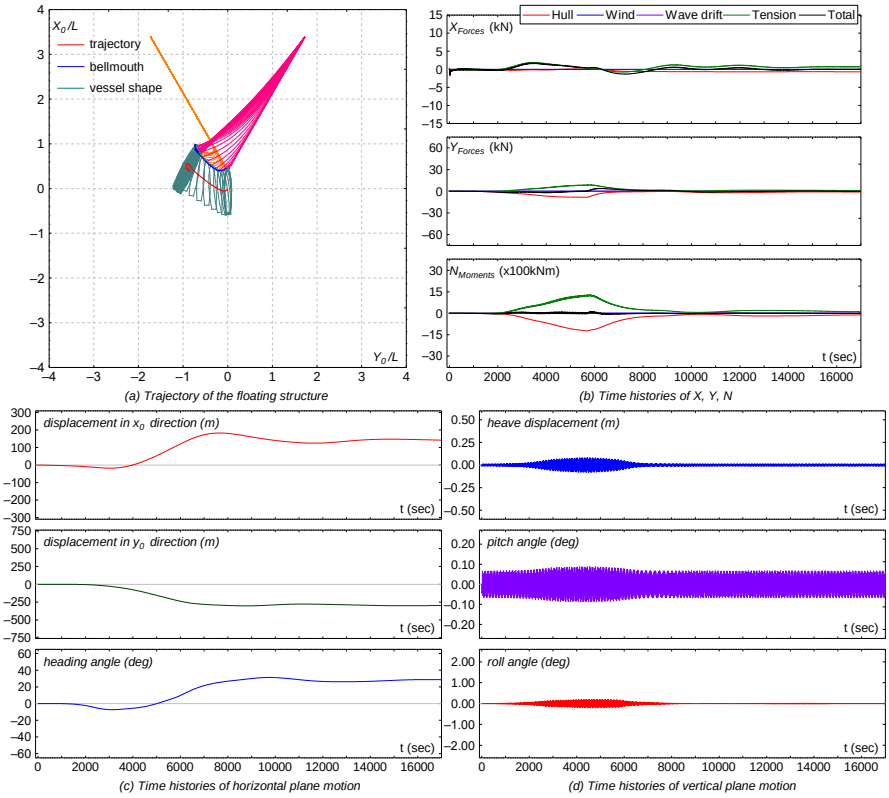

Fig. 3.20. $\lambda/L = 1.0$; $V_C = 1.0$ kn; $\alpha = 30°$; No wind; $\chi = 30°$ [DL-18]

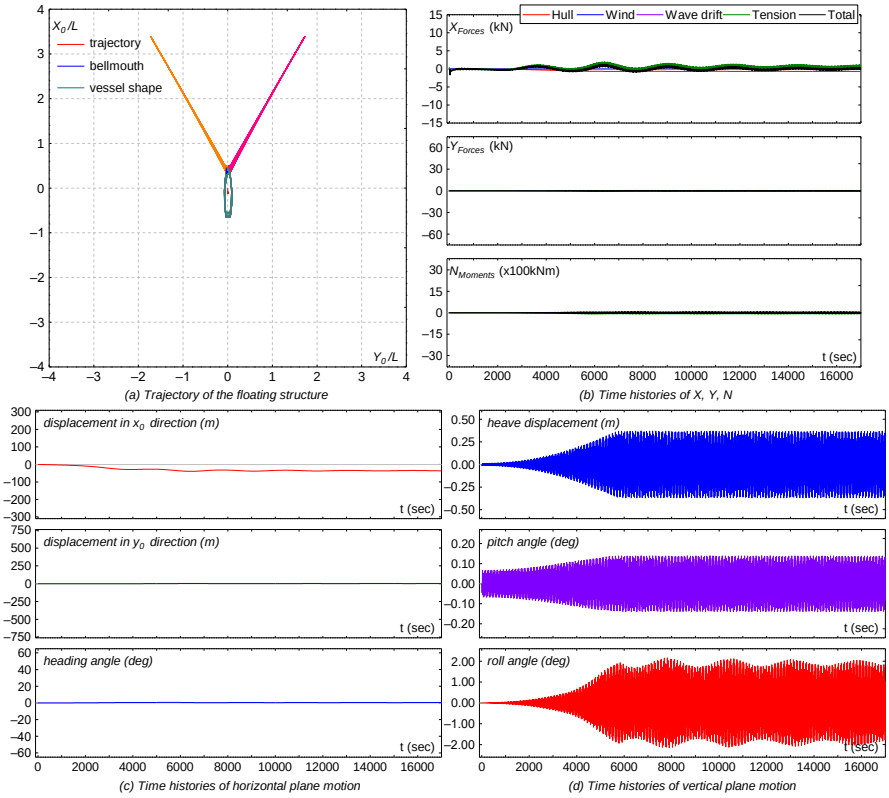

Fig. 3.21. $\lambda/L = 1.0$; $V_C = 1.0$ kn; $\alpha = 0°$; No wind; $\chi = 60°$ [DL-21]

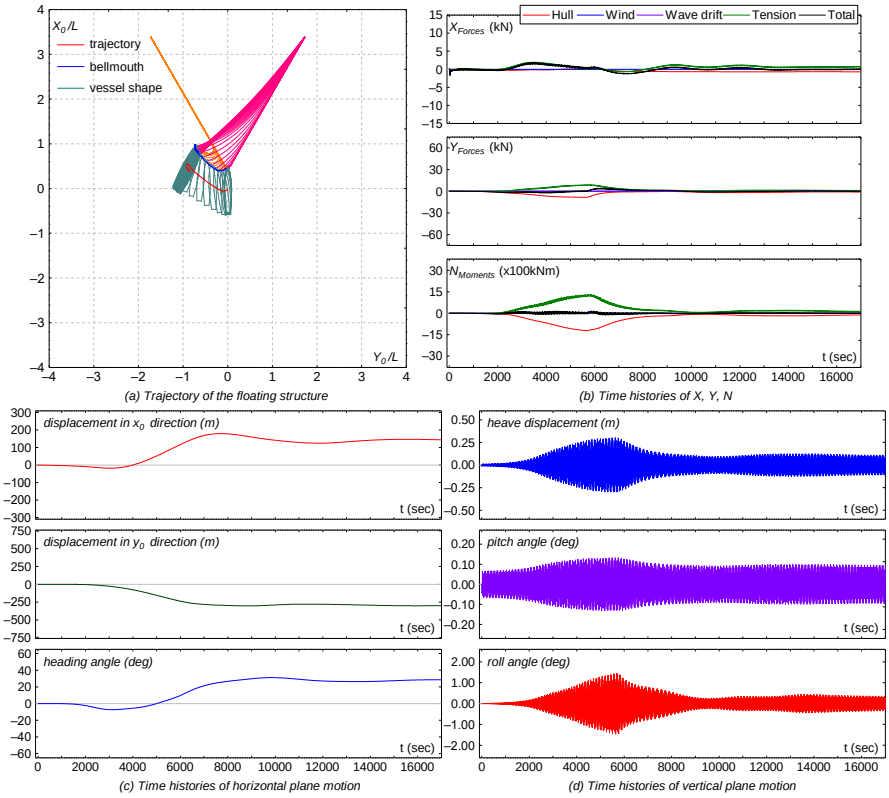

Fig. 3.22. $\lambda/L = 1.0$; $V_C = 1.0$ kn; $\alpha = 30°$; No wind; $\chi = 60°$ [DL-22]

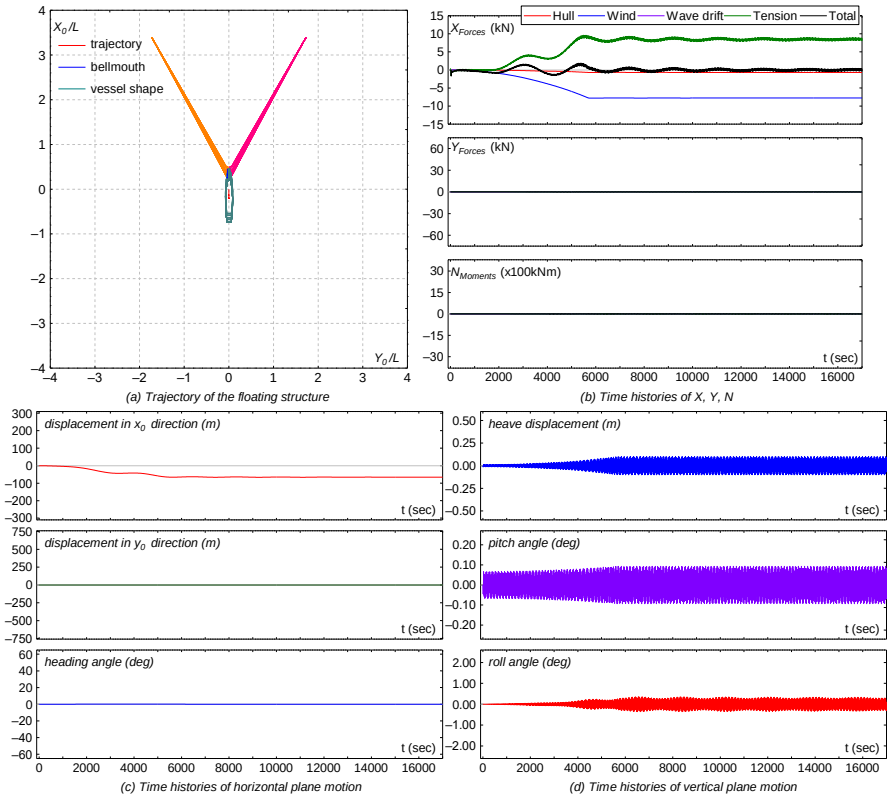

Fig. 3.23. $\lambda/L = 1.0;\ V_C = 1.0$ kn; $\alpha = 0°;\ V_W = 10$ m/s; $v = 0°;\ \chi = 30°$ [DL-25]

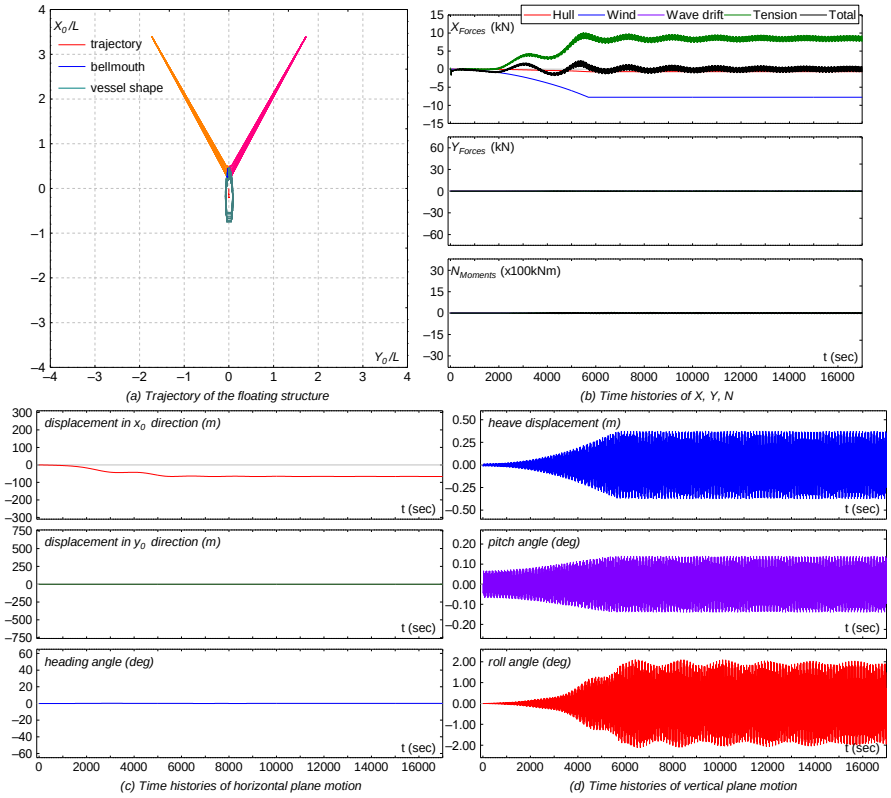

Fig. 3.24. $\lambda/L = 1.0;\ V_C = 1.0$ kn; $\alpha = 0°;\ V_W = 10$ m/s; $v = 0°;\ \chi = 60°$ [DL-29]

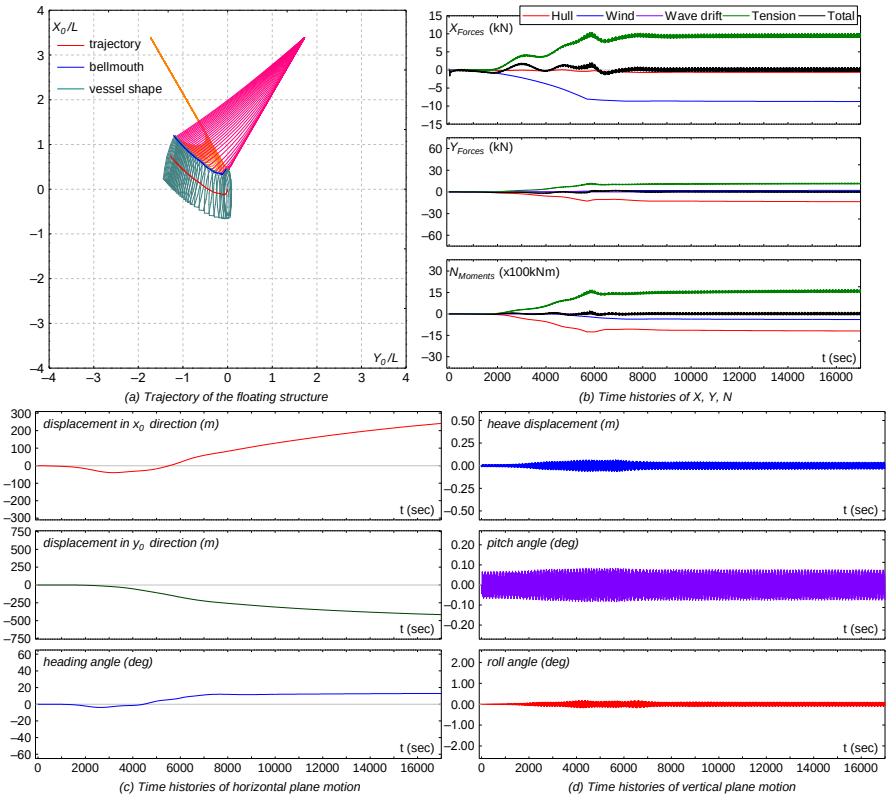

Fig. 3.25. $\lambda/L = 1.0$; $V_C = 1.0$ kn; $\alpha = 30°$; $V_W = 10$ m/s; $v = 0°$; $\chi = 30°$ [DL-26]

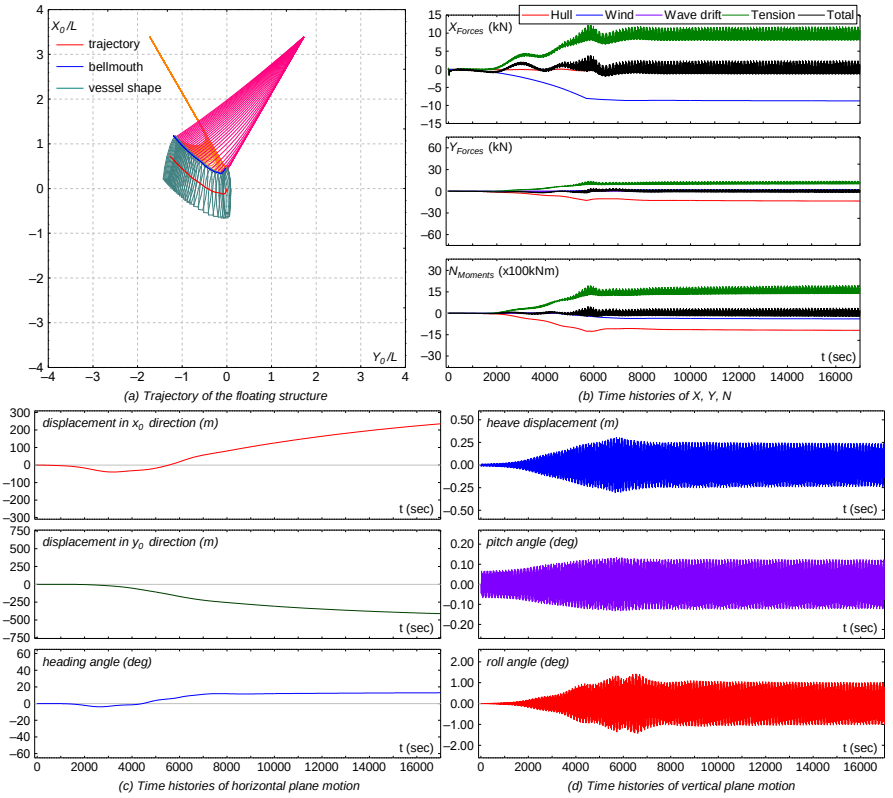

Fig. 3.26. $\lambda/L = 1.0$; $V_C = 1.0$ kn; $\alpha = 30°$; $V_W = 10$ m/s; $v = 0°$; $\chi = 60°$ [DL-30]

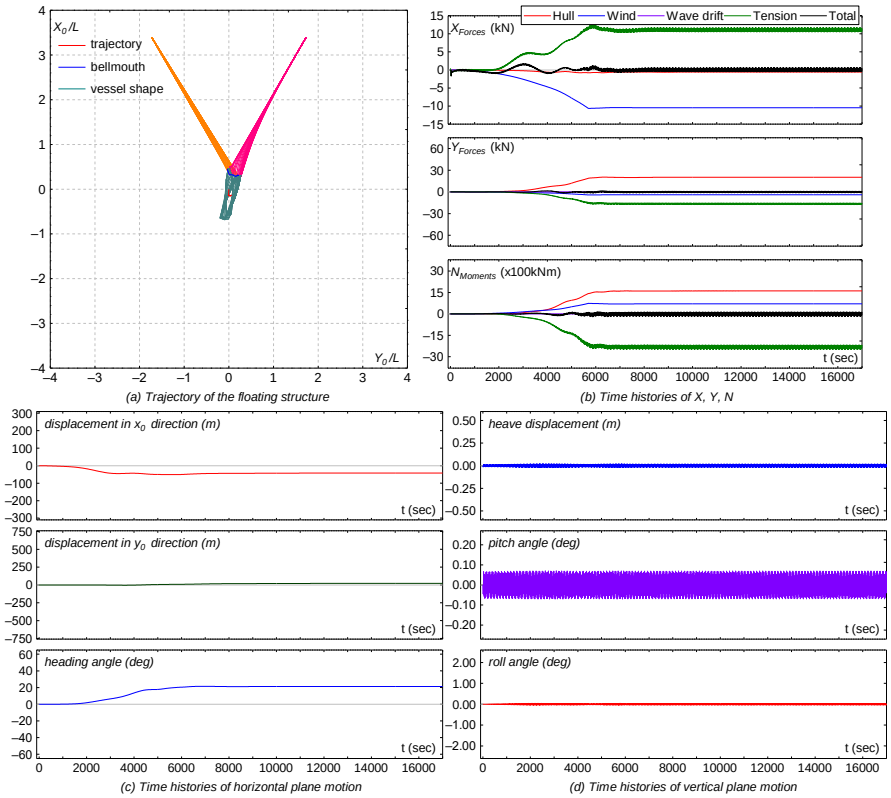

Fig. 3.27. $\lambda/L = 1.0$; $V_C = 1.0$ kn; $\alpha = 0°$; $V_W = 10$ m/s; $v = 45°$; $\chi = 30°$ [DL-27]

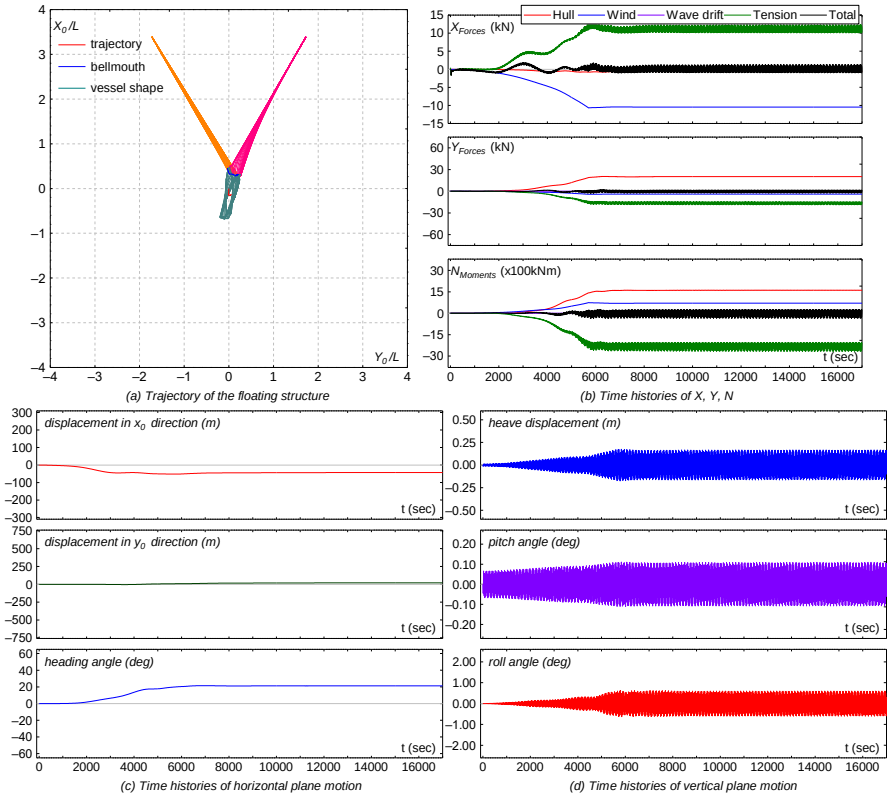

Fig. 3.28. $\lambda/L = 1.0$; $V_C = 1.0$ kn; $\alpha = 0°$; $V_W = 10$ m/s; $v = 45°$; $\chi = 60°$ [DL-31]

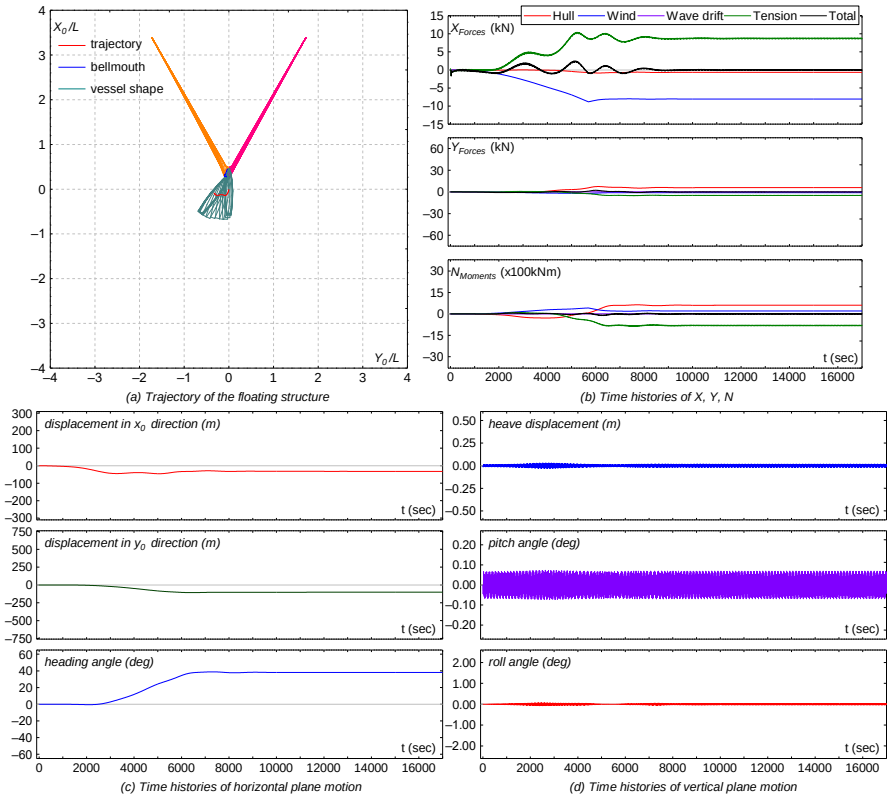

Fig. 3.29. $\lambda/L = 1.0$; $V_C = 1.0$ kn; $\alpha = 30°$; $V_W = 10$ m/s; $v = 45°$; $\chi = 30°$ [DL-28]

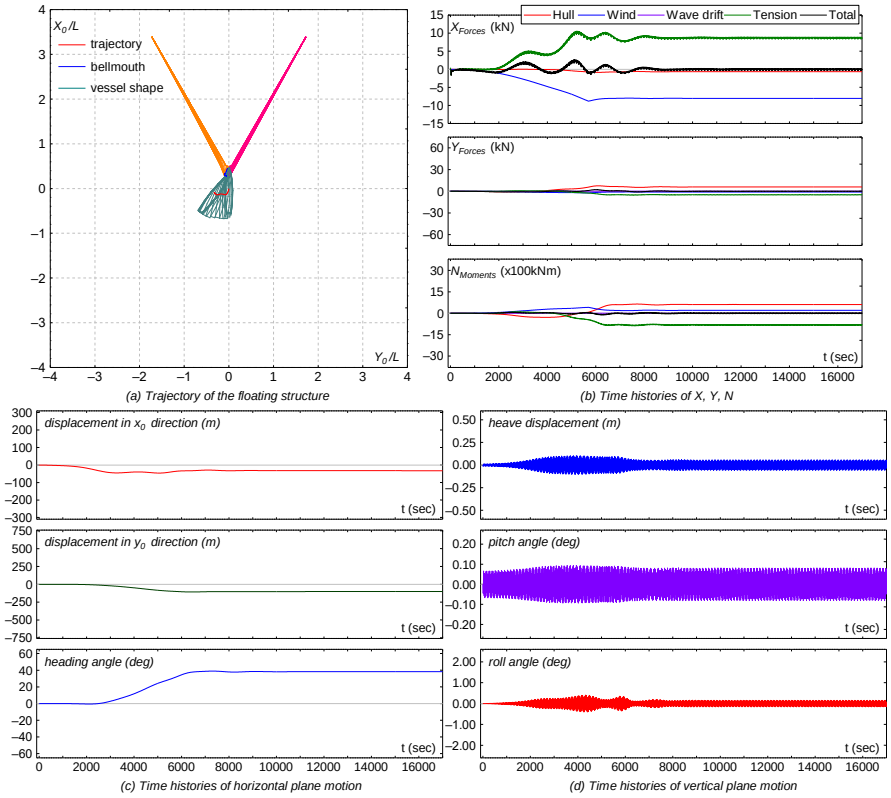

Fig. 3.30. $\lambda/L = 1.0$; $V_C = 1.0$ kn; $\alpha = 30°$; $V_W = 10$ m/s; $v = 45°$; $\chi = 60°$ [DL-32]

Again, in the condition where the wind force is considered, the larger wave direction also increase the vertical motions of the floating structure. It can be understood by comparing Figs. 3.24, 3.26, 3.28, and 3.30 with Figs. 3.23, 3.25, 3.27, and 3.29 respectively.

Moreover, for the case of the different directions of wind and current, the floating structure tends to experience rotational motion instead of translational drifting motion as shown in Fig. 3.27 to Fig. 3.30 due to the tension of both mooring lines. The rotational motion increases as the increases of the direction of external disturbances toward beam sea condition while the translational motion become larger when the magnitude of external forces enlarges

(3) Multi-leg Turret Mooring Line

In multi-leg turret mooring line system, the floating structure is moored by six mooring lines arranged as shown in Table 3.2 and Fig. 3.5. The connection point of the mooring lines are located at points $\left(x_{b_{1\sim6}}, y_{b_{1\sim6}}\right) = (160,0.0)$. It can be regarded that the floating structure can move freely following the direction of external forces. The simulation results for this mooring configuration type can be observed in Fig. 3.31 to Fig. 3.42. The discussions of those results are explained as follows.

According to the results, it can be confirmed that the proposed three-dimensional dynamics model of mooring line can reproduce the coupled motion between mooring lines and floating structure even for multi-leg turret mooring system. The results show that all mooring lines in the system move with the motion of the floating structure simultaneously. All mooring lines withstand the motion of the floating structure together and hence the floating structure doesn't move far away from her initial position. Moreover, the tendency associated with the relation of the external force conditions (the presence of wind, the effect of current and wave direction) are similarly noticed with the two previous mooring line configuration types. Current force coming from lateral direction is dominant comparing with those in longitudinal direction while the presence of wind increases the drift motion of the floating structure. Furthermore, the larger wave direction relative to bow direction also increases the vertical motion of the floating structure.

The other finding from this mooring line configuration type is described as follows. Since the floating structure is held by six mooring lines , the motion of the floating structure tends to be more stable comparing with that in double mooring lines type. As instance, it can be observed by comparing Figs. 3.37 and 3.38 with Figs. 3.25 and 3.26 respectively. Under the same conditions of external forces, only rotational motion occurs to the floating structure with multi-leg turret mooring while the floating structure with double mooring lines system

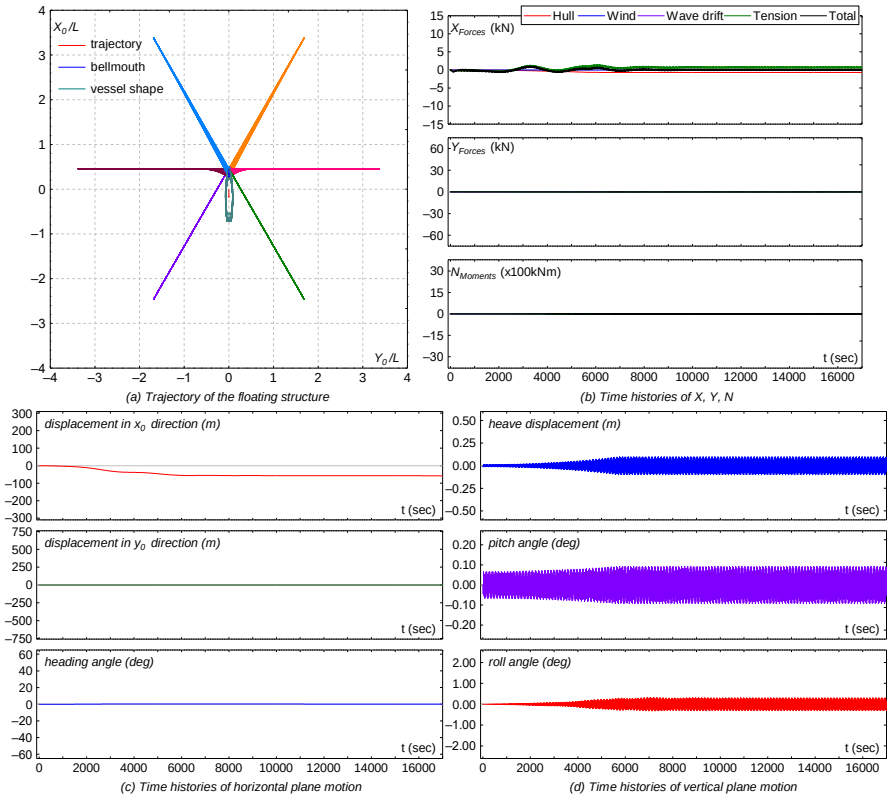

Fig. 3.31. $\lambda/L = 1.0$; $V_C = 1.0$ kn; $\alpha = 0°$; No wind; $\chi = 30°$ [SP-17]

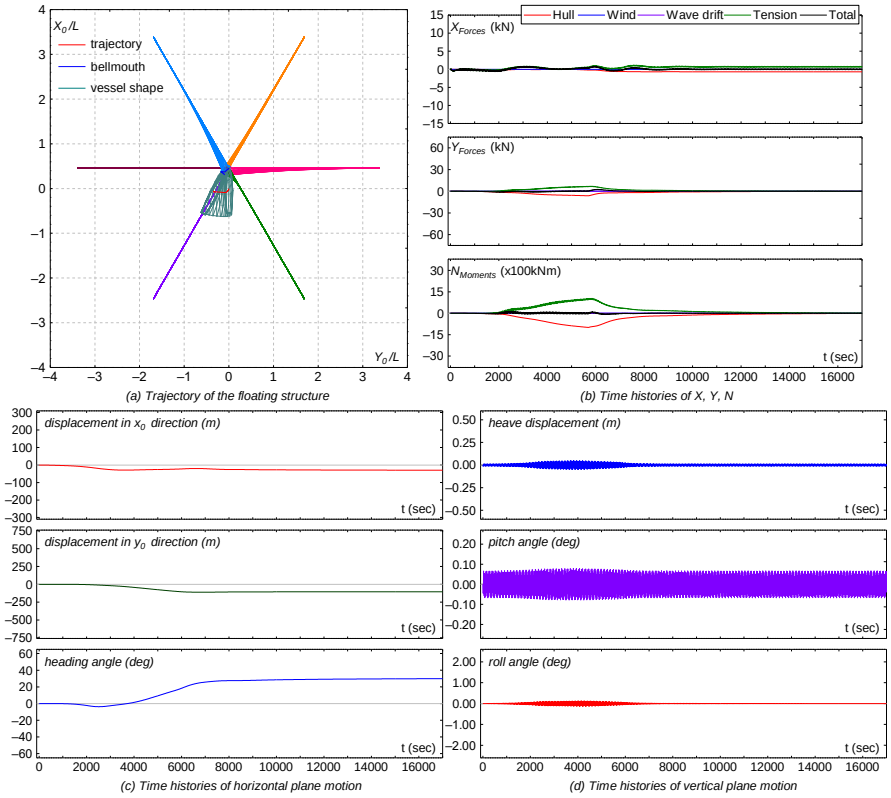

Fig. 3.32. $\lambda/L = 1.0$; $V_C = 1.0$ kn; $\alpha = 30°$; No wind; $\chi = 30°$ [SP-18]

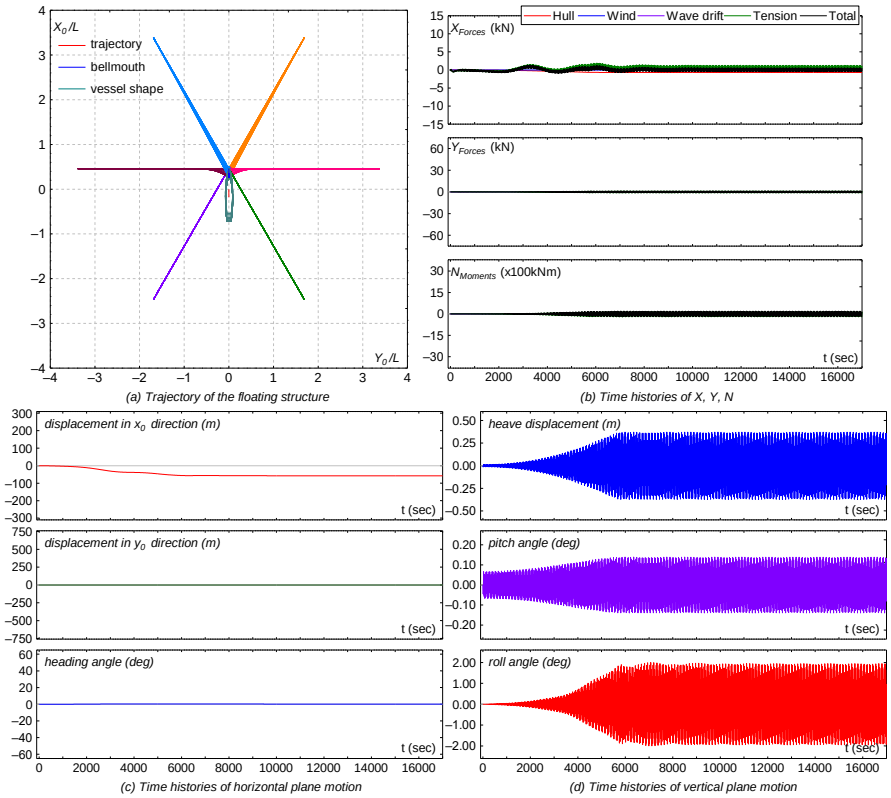

Fig. 3.33. $\lambda/L = 1.0$; $V_C = 1.0$ kn; $\alpha = 0°$; No wind; $\chi = 60°$ [SP-21]

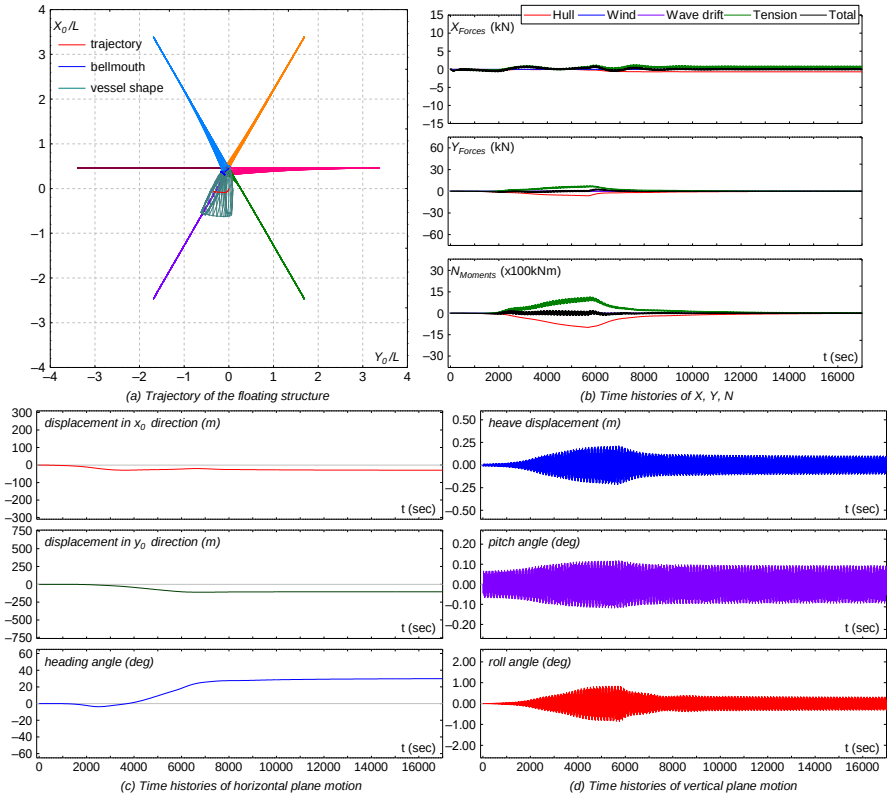

Fig. 3.34. $\lambda/L = 1.0$; $V_C = 1.0$ kn; $\alpha = 30°$; No wind; $\chi = 60°$ [SP-22]

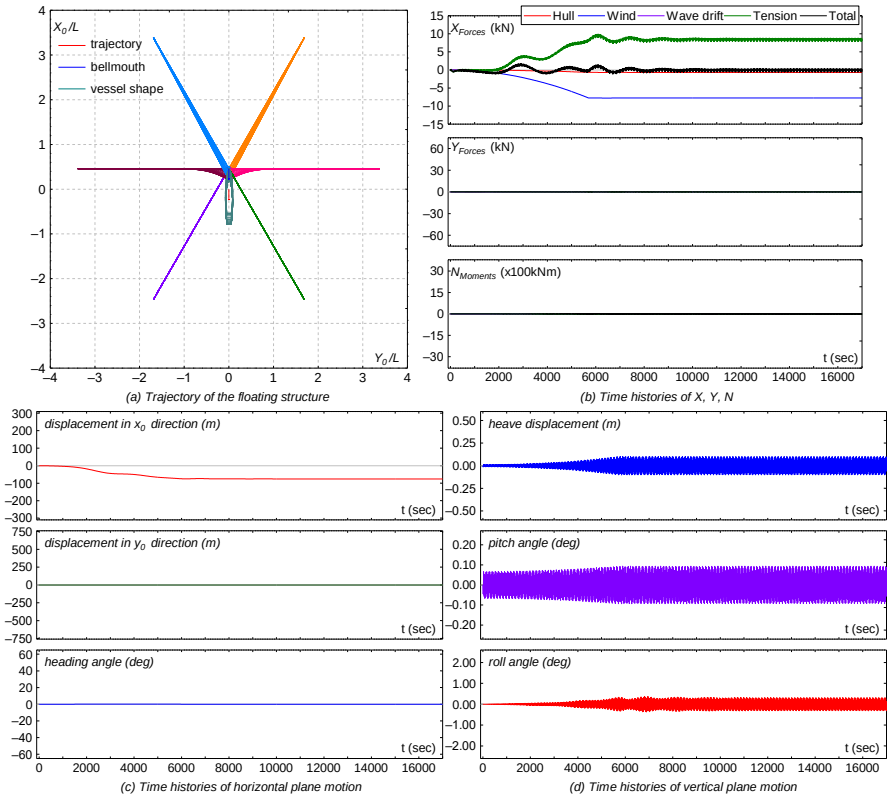

Fig. 3.35. $\lambda/L = 1.0$; $V_C = 1.0$ kn; $\alpha = 0°$; $V_W = 10$ m/s; $v = 0°$; $\chi = 30°$ [SP-25]

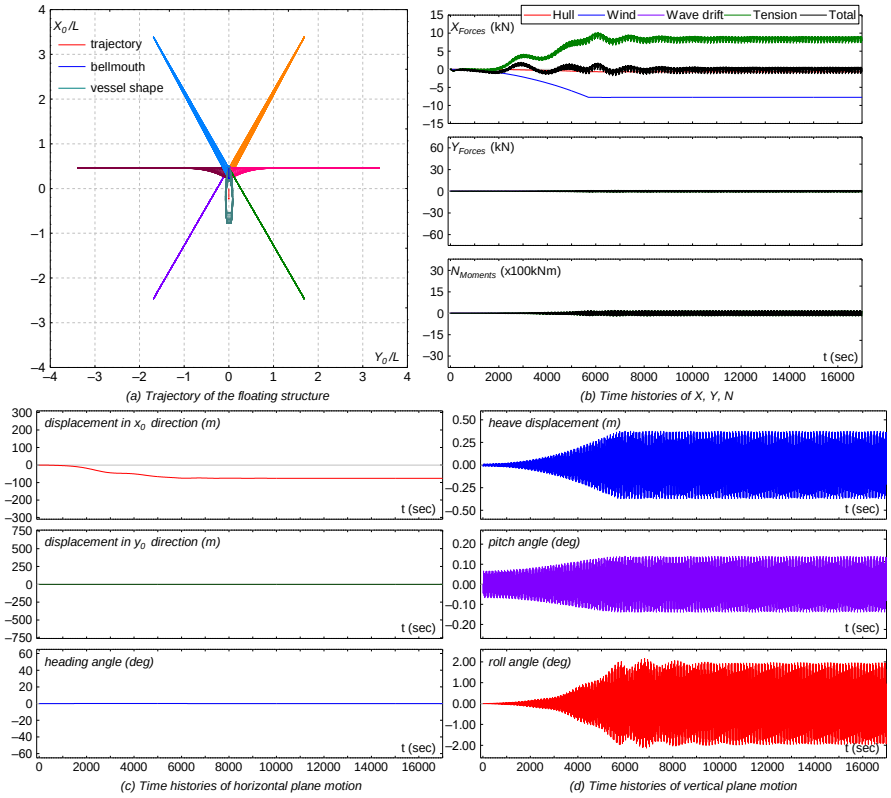

Fig. 3.36. $\lambda/L = 1.0$; $V_C = 1.0$ kn; $\alpha = 0°$; $V_W = 10$ m/s; $v = 0°$; $\chi = 60°$ [SP-29]

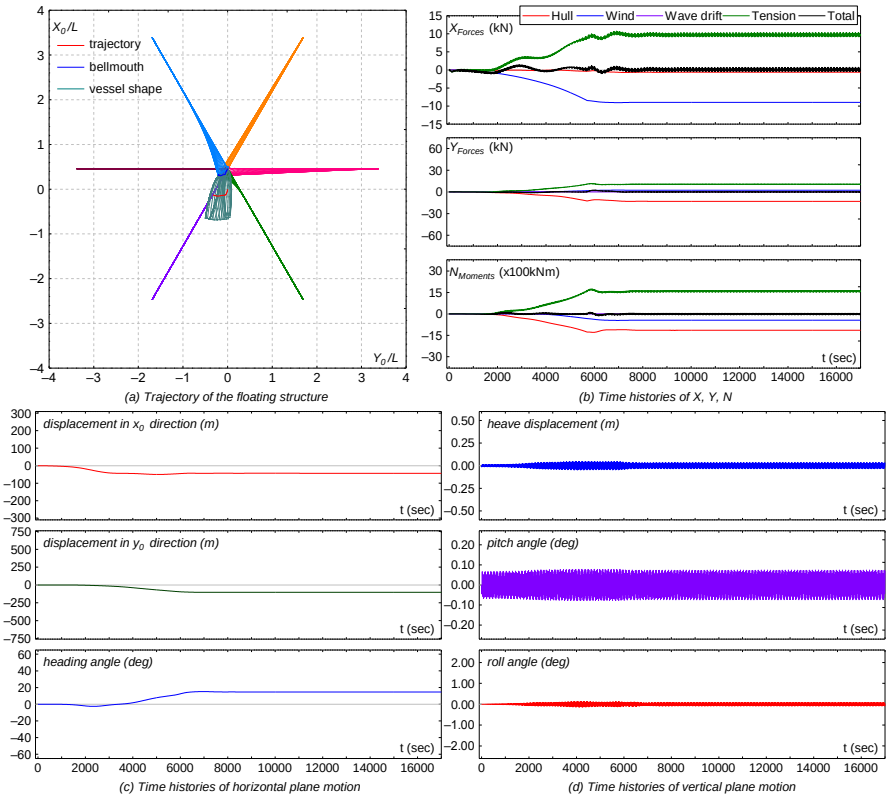

Fig. 3.37. $\lambda/L = 1.0$; $V_C = 1.0$ kn; $\alpha = 30°$; $V_W = 10$ m/s; $v = 0°$; $\chi = 30°$ [SP-26]

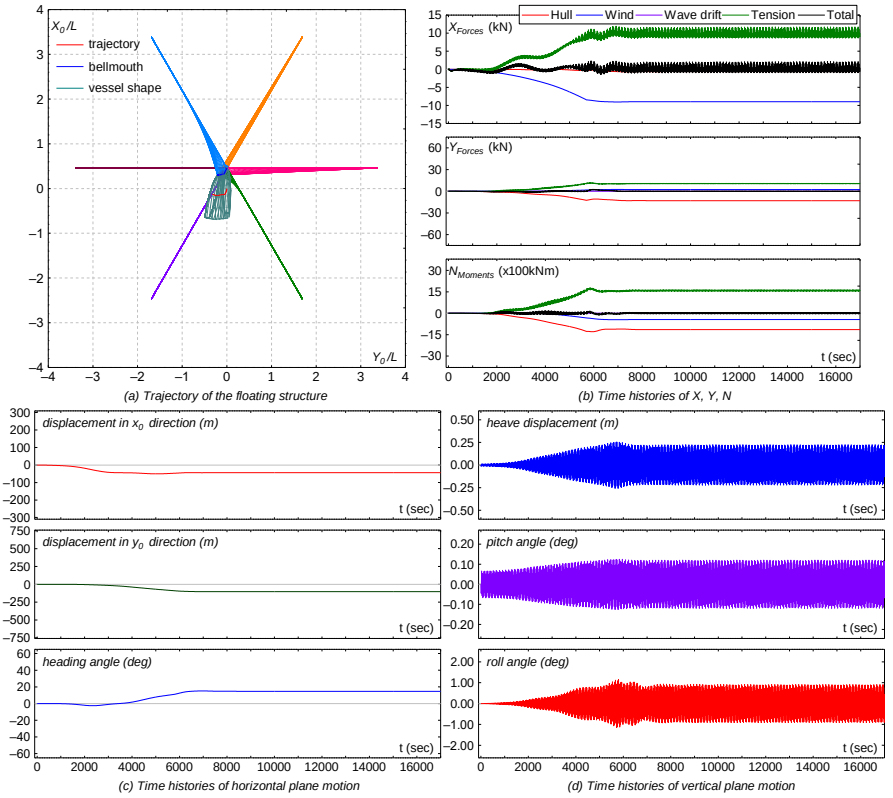

Fig. 3.38. $\lambda/L = 1.0$; $V_C = 1.0$ kn; $\alpha = 30°$; $V_W = 10$ m/s; $v = 0°$; $\chi = 60°$ [SP-30]

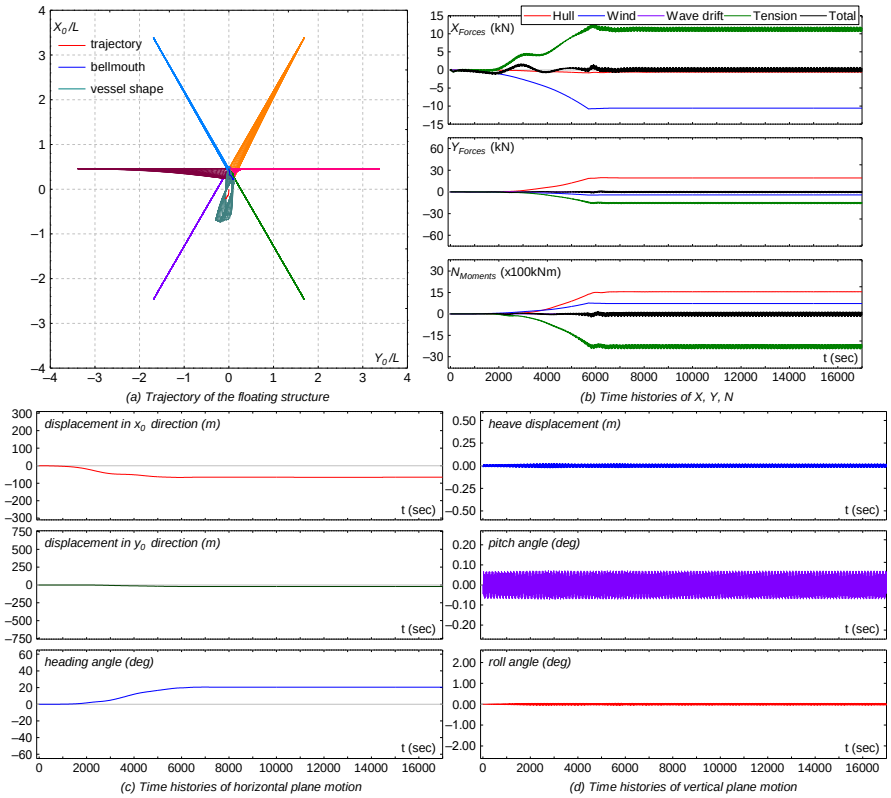

Fig. 3.39. $\lambda/L = 1.0;\ V_C = 1.0$ kn; $\alpha = 0°;\ V_W = 10$ m/s; $v = 45°;\ \chi = 30°$ [SP-27]

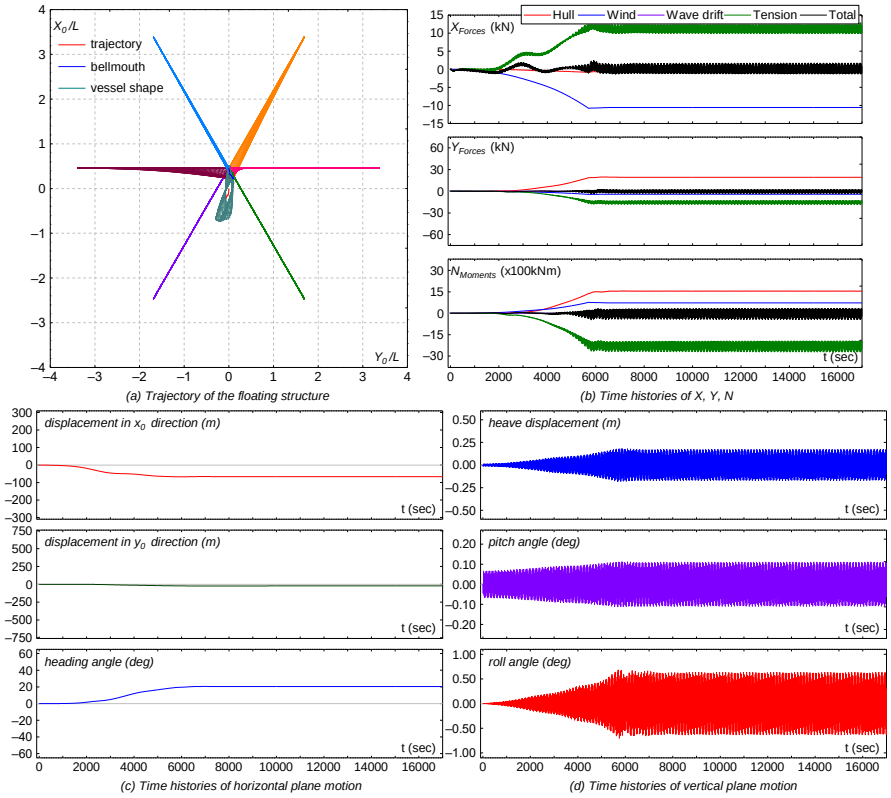

Fig. 3.40. $\lambda/L = 1.0;\ V_C = 1.0$ kn; $\alpha = 0°;\ V_W = 10$ m/s; $v = 45°;\ \chi = 60°$ [SP-31]

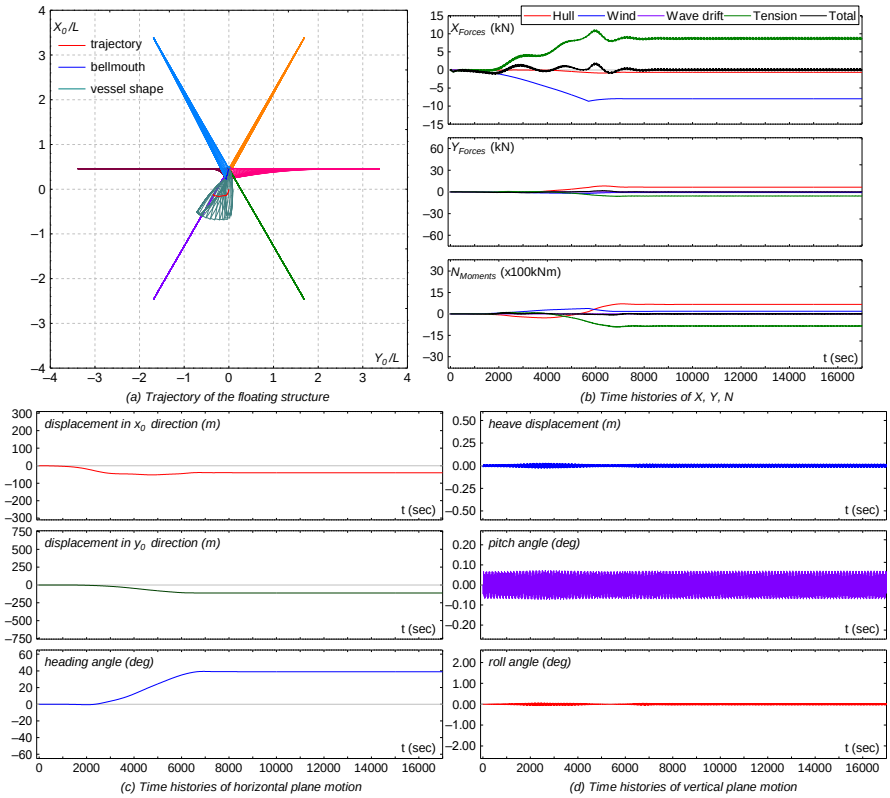

Fig. 3.41. $\lambda/L = 1.0$; $V_C = 1.0$ kn; $\alpha = 30°$; $V_W = 10$ m/s; $v = 45°$; $\chi = 30°$ [SP-28]

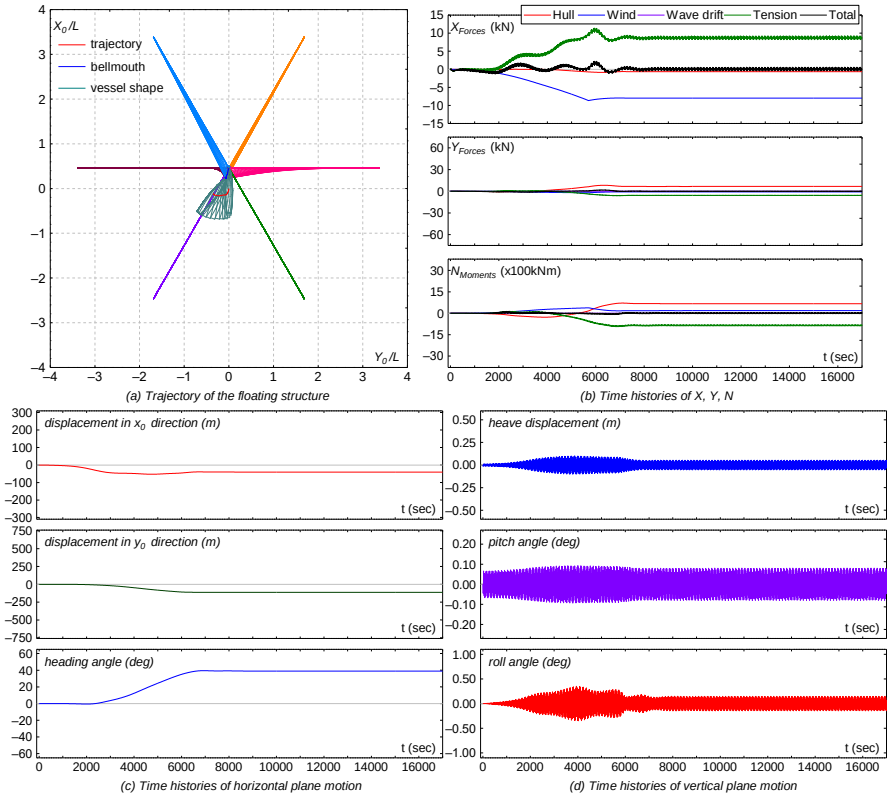

Fig. 3.42. $\lambda/L = 1.0$; $V_C = 1.0$ kn; $\alpha = 30°$; $V_W = 10$ m/s; $v = 45°$; $\chi = 60°$ [SP-32]

moves far away in lateral direction. Furthermore, it can be said that the proposed mooring line model is capable to reproduce the coupled motion between mooring lines and a floating structure.

(4) Multi-leg Spread Mooring Lines

In multi-leg spread mooring lines system, the floating structure is moored by six mooring lines arranged as shown in Table 3.2 and Fig. 3.5. The connection points of the mooring lines are located at multi points as follows; $(x_{b_1}, y_{b_1}) = (160\ \text{m}, 11\ \text{m})$, $(x_{b_2}, y_{b_2}) = (0.0\ \text{m}, 26.5\ \text{m})$, $(x_{b_3}, y_{b_3}) = (-160\ \text{m}, 20\ \text{m})$, $(x_{b_4}, y_{b_4}) = (-160\ \text{m}, -20\ \text{m})$, $(x_{b_5}, y_{b_5}) = (0.0\ \text{m}, -26.5\ \text{m})$, and $(x_{b_6}, y_{b_6}) = (160\ \text{m}, -11\ \text{m})$. It can be regarded that the floating structure can move freely to follow the direction of external force. The results of this mooring configuration type can be observed in Fig. 3.43 to Fig. 3.54. The discussions of those results are explained as follows.

Similar with multi-leg turret mooring system, the results of this configuration can also be confirmed that the proposed dynamics model of mooring line can reproduce the coupled motion between mooring lines and a floating structure for all mooring lines since all mooring line can move following the motion of the floating structure simultaneously. The mooring line tension generated by all mooring lines is capable to restrain the floating structure. The tendency related to the external forces shows the same tendency with the previous mooring line configuration. However, since the floating structure cannot move rotationally following the direction of external forces, lateral force and moment acting on the floating structure are larger comparing with the other mooring line configuration types. This condition can be found in Figs. 3.44, 3.46, 3.48, 3.50, 3.52, and 3.54. In these conditions, the tension force and moment in lateral direction (Y_T,N_T) become enlarge to compensate the large lateral force and moment generated by environmental forces.

Comparing the results of this configuration (Fig. 3.43 to Fig. 3.54) with the results of multi-leg turret mooring system (Fig. 3.31 to Fig. 3.42), it is understood that the acting external force can be minimized by introducing multi-leg turret mooring system since the floating structure in multi-leg turret mooring is free to rotate. Therefore, the tension of the mooring line of mutil-leg turret mooring system is also smaller than that of multi-leg spread mooring system. Although spread mooring system realizes small motion of the hull, the mooring line tension may increase if the floating structure received external forces from the lateral direction. Hence, the turret mooring system is considered to be more suitable for the area where external disturbances come from various directions while the spread mooring system is suitable if the directions of external disturbances are almost constant.

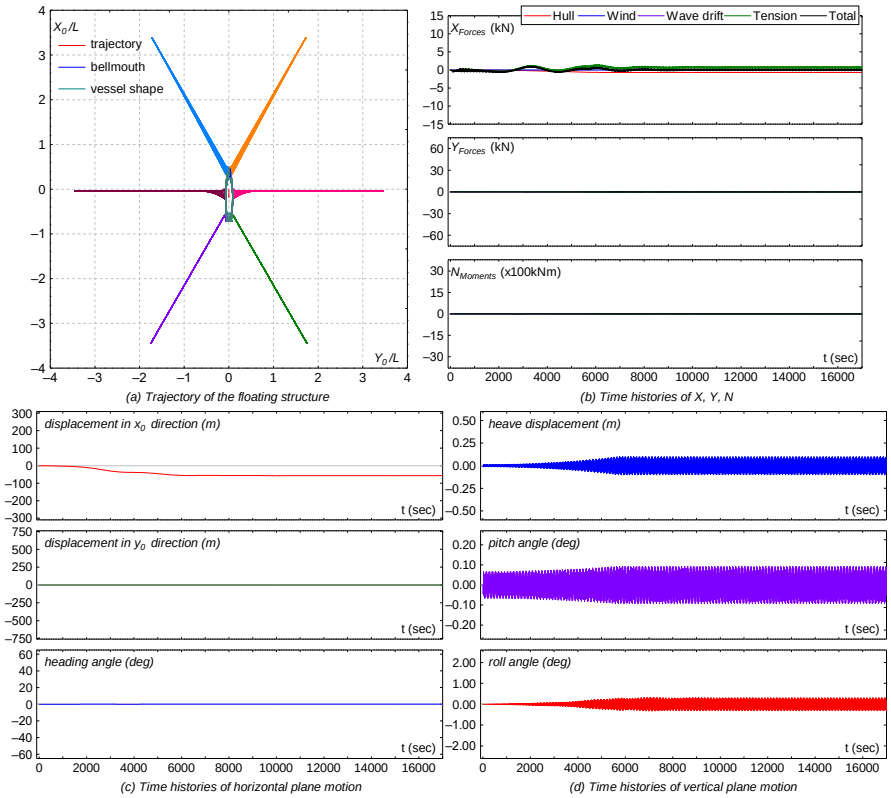

Fig. 3.43. $\lambda/L = 1.0$; $V_C = 1.0$ kn; $\alpha = 0°$; No wind; $\chi = 30°$ [SM-17]

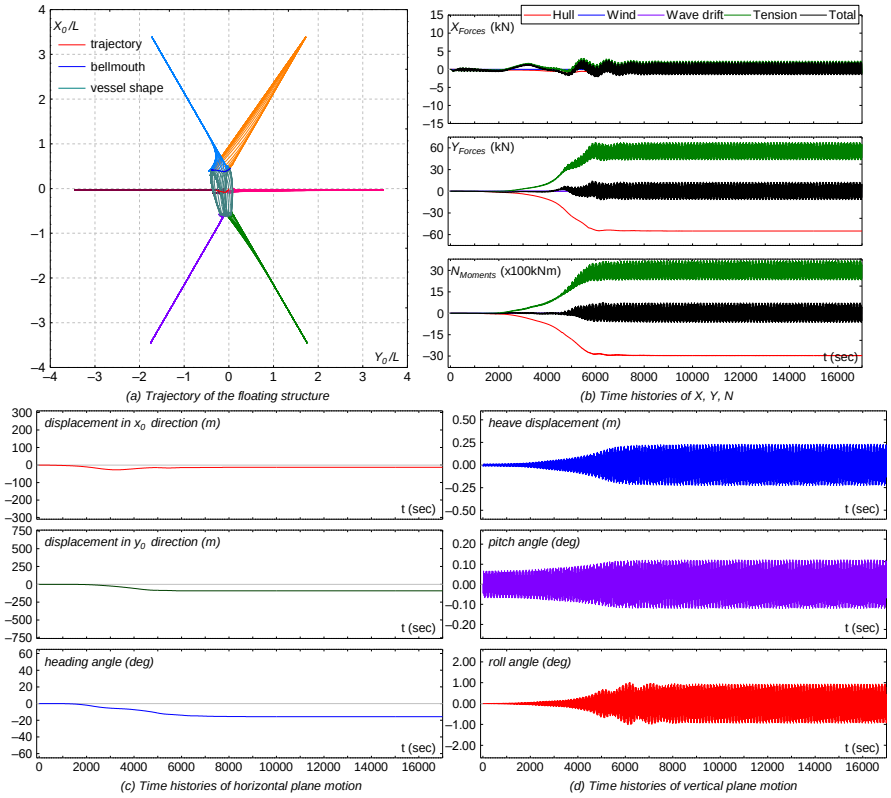

Fig. 3.44. $\lambda/L = 1.0$; $V_C = 1.0$ kn; $\alpha = 30°$; No wind; $\chi = 30°$ [SM-18]

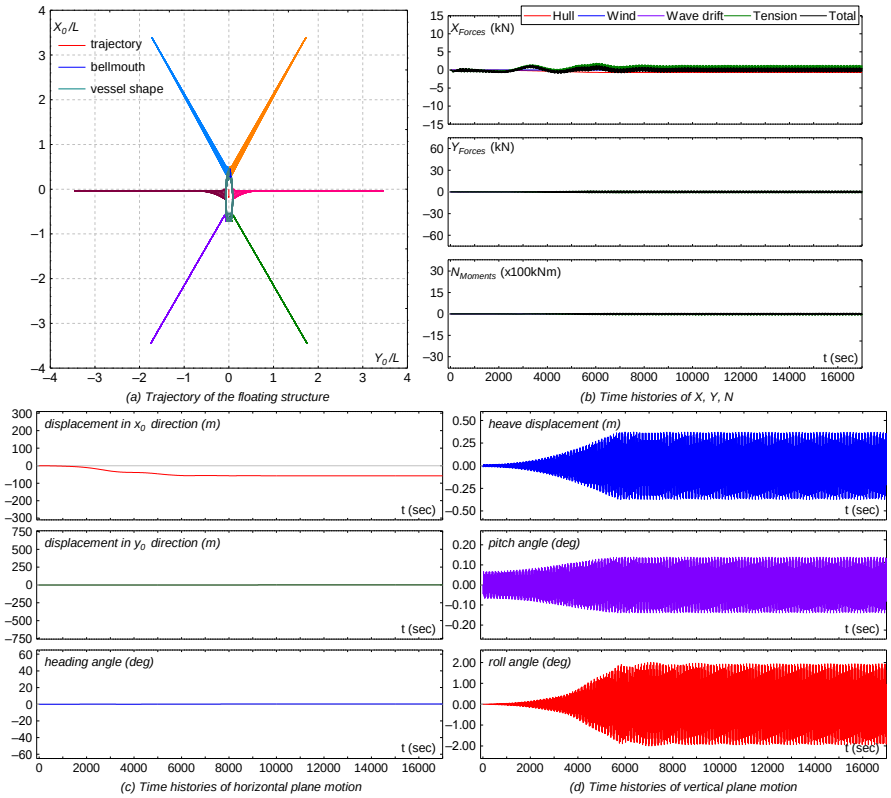

Fig. 3.45. $\lambda/L = 1.0$; $V_C = 1.0$ kn; $\alpha = 0°$; No wind; $\chi = 60°$ [SM-21]

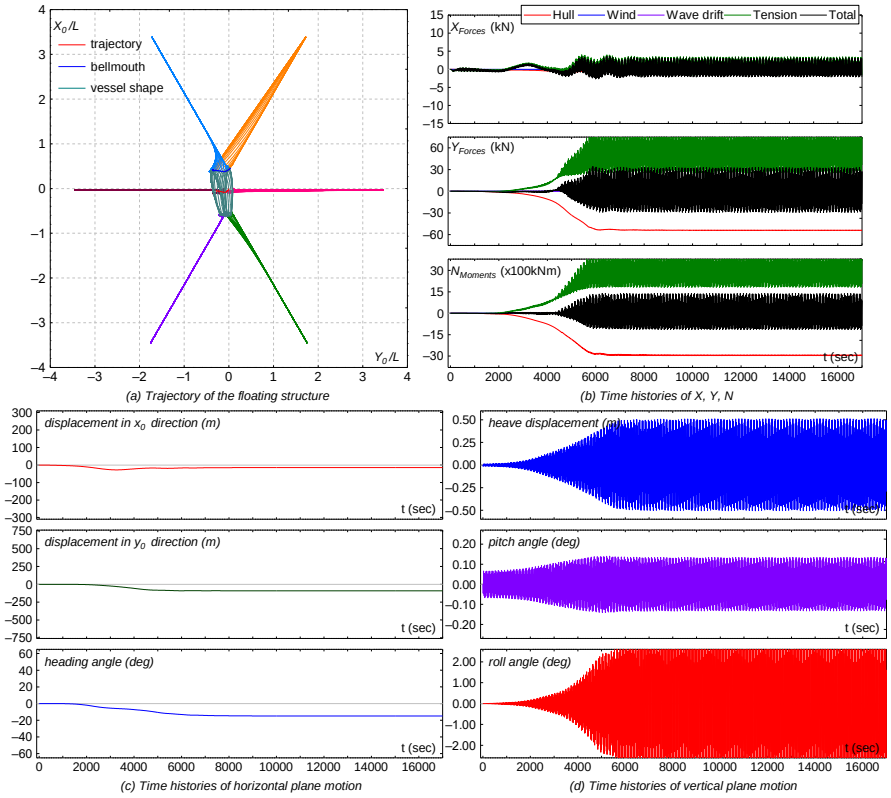

Fig. 3.46. $\lambda/L = 1.0$; $V_C = 1.0$ kn; $\alpha = 30°$; No wind; $\chi = 60°$ [SM-22]

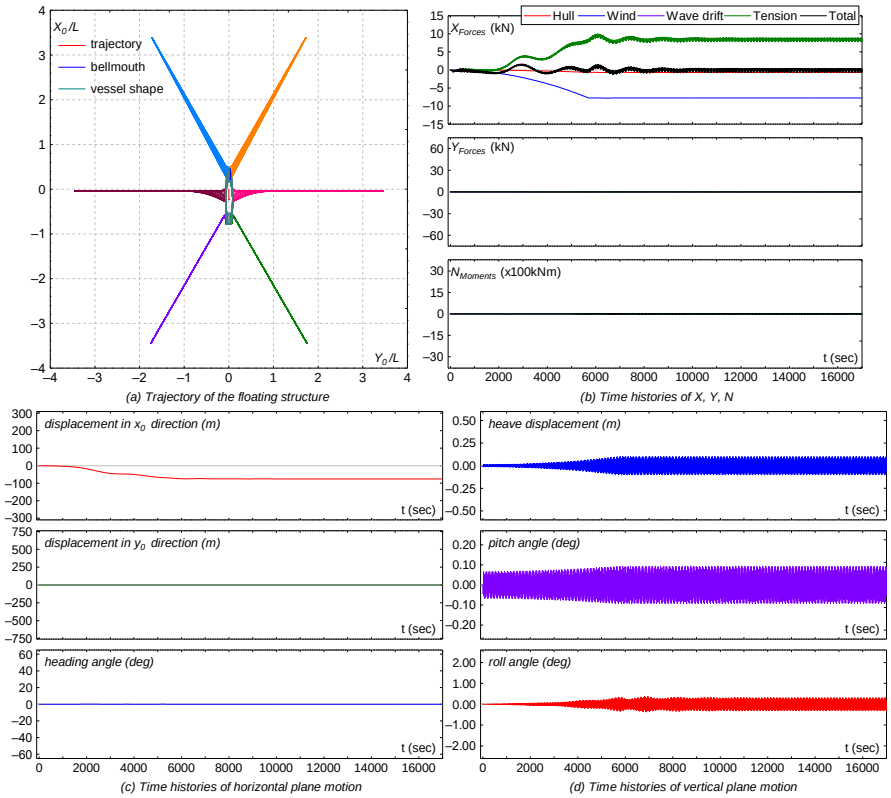

Fig. 3.47. $\lambda/L = 1.0;\ V_C = 1.0$ kn; $\alpha = 0°;\ V_W = 10$ m/s; $v = 0°;\ \chi = 30°$ [SM-25]

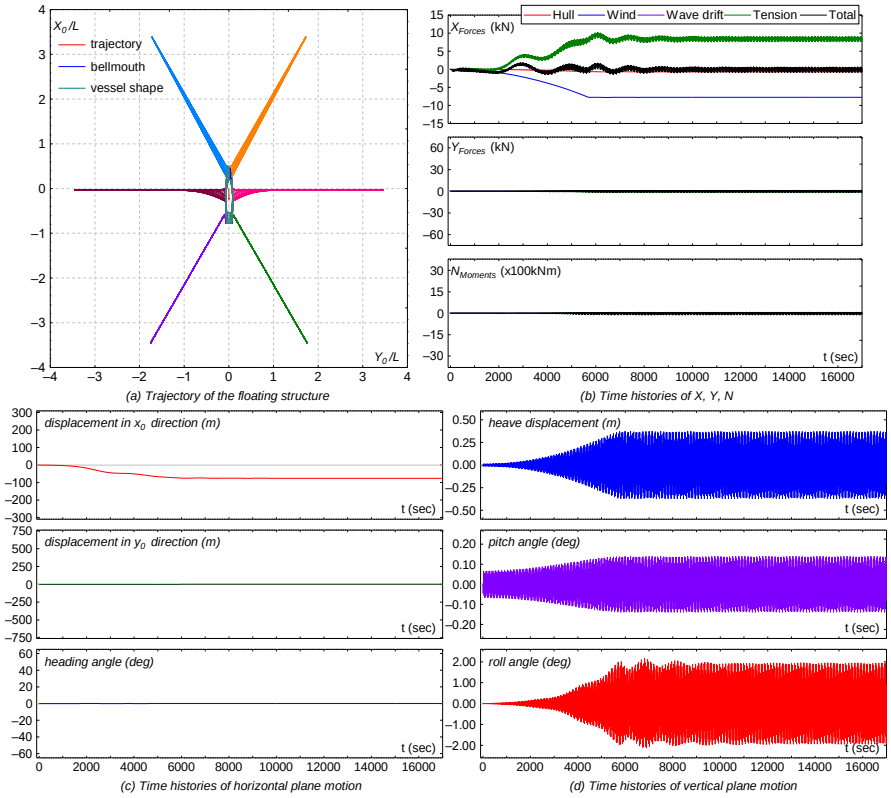

Fig. 3.48. $\lambda/L = 1.0;\ V_C = 1.0$ kn; $\alpha = 0°;\ V_W = 10$ m/s; $v = 0°;\ \chi = 60°$ [SM-29]

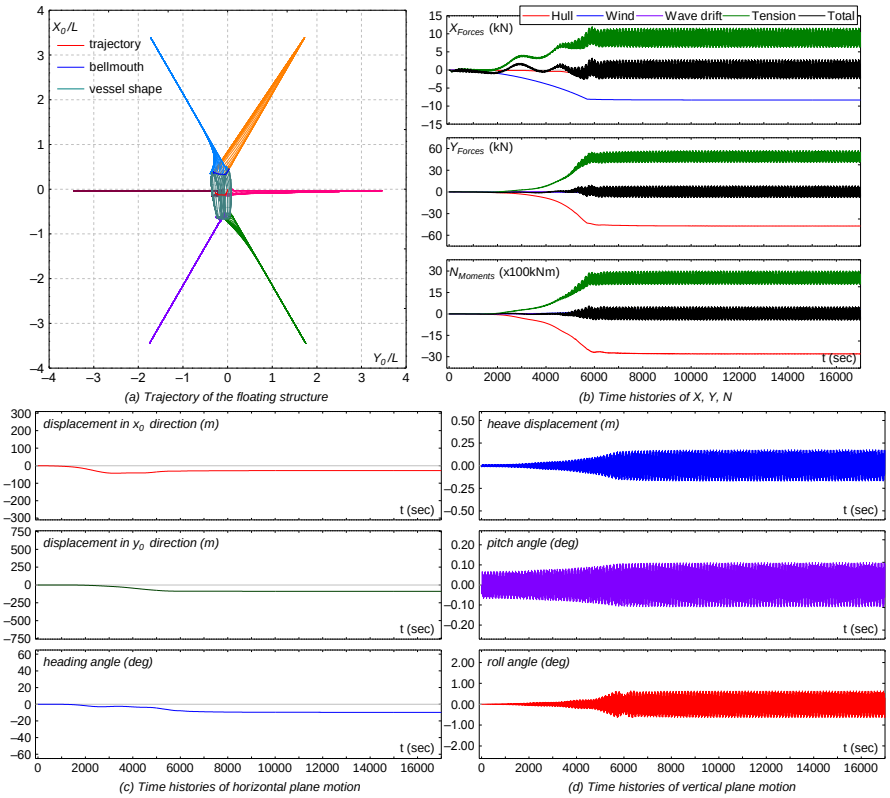

Fig. 3.49. $\lambda/L = 1.0;\ V_C = 1.0$ kn; $\alpha = 30°;\ V_W = 10$ m/s; $v = 0°;\ \chi = 30°$ [SM-26]

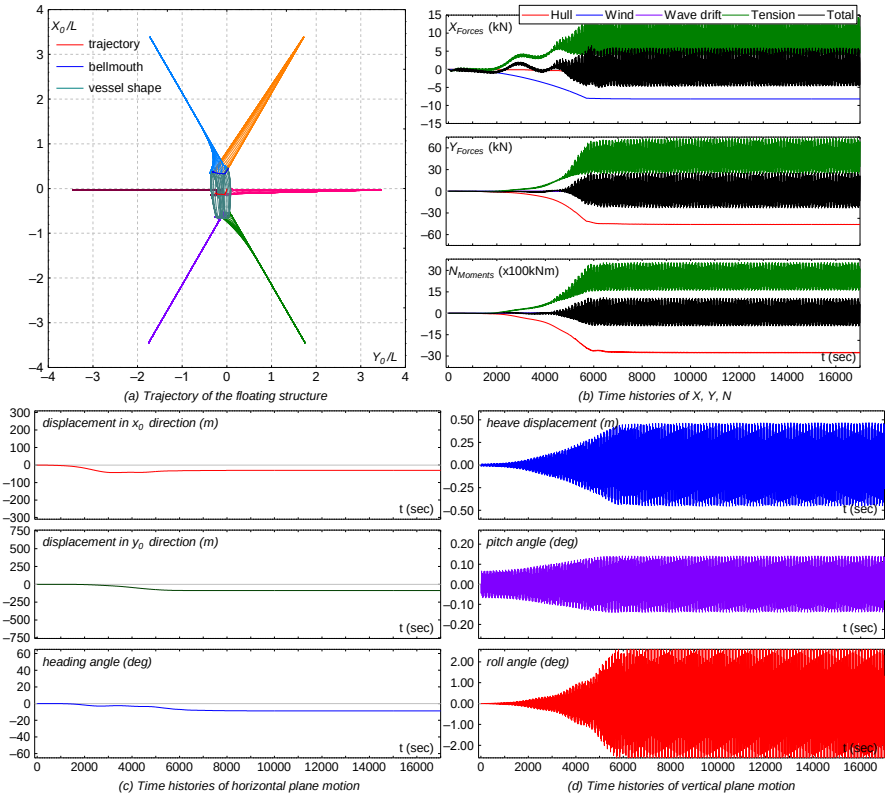

Fig. 3.50. $\lambda/L = 1.0;\ V_C = 1.0$ kn; $\alpha = 30°;\ V_W = 10$ m/s; $v = 0°;\ \chi = 60°$ [SM-30]

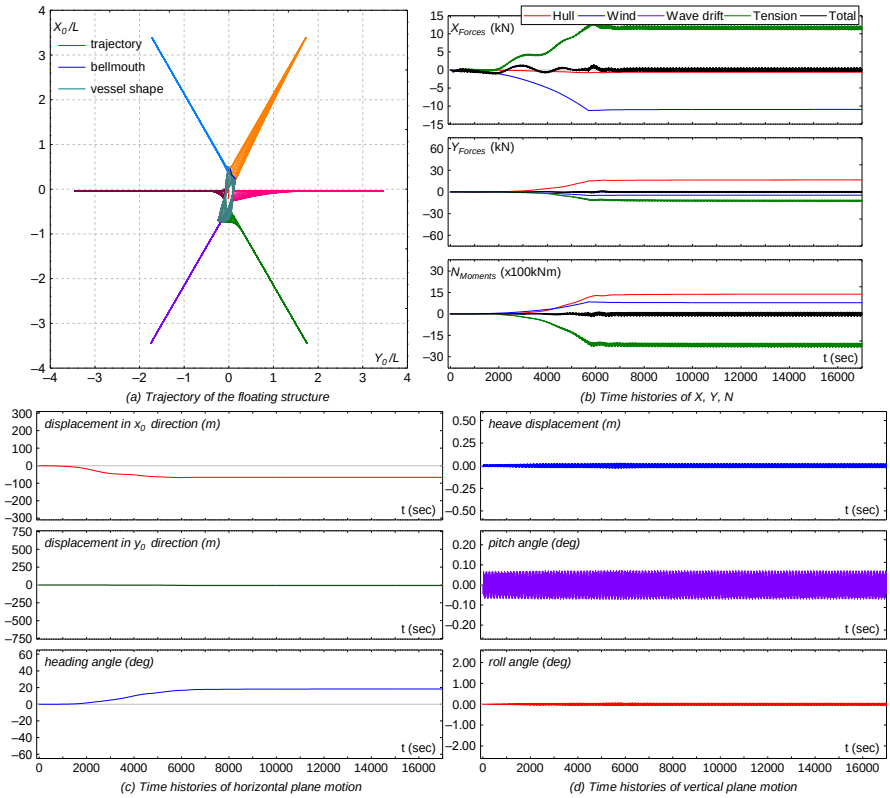

Fig. 3.51. $\lambda/L = 1.0$; $V_C = 1.0$ kn; $\alpha = 0°$; $V_W = 10$ m/s; $v = 45°$; $\chi = 30°$ [SM-27]

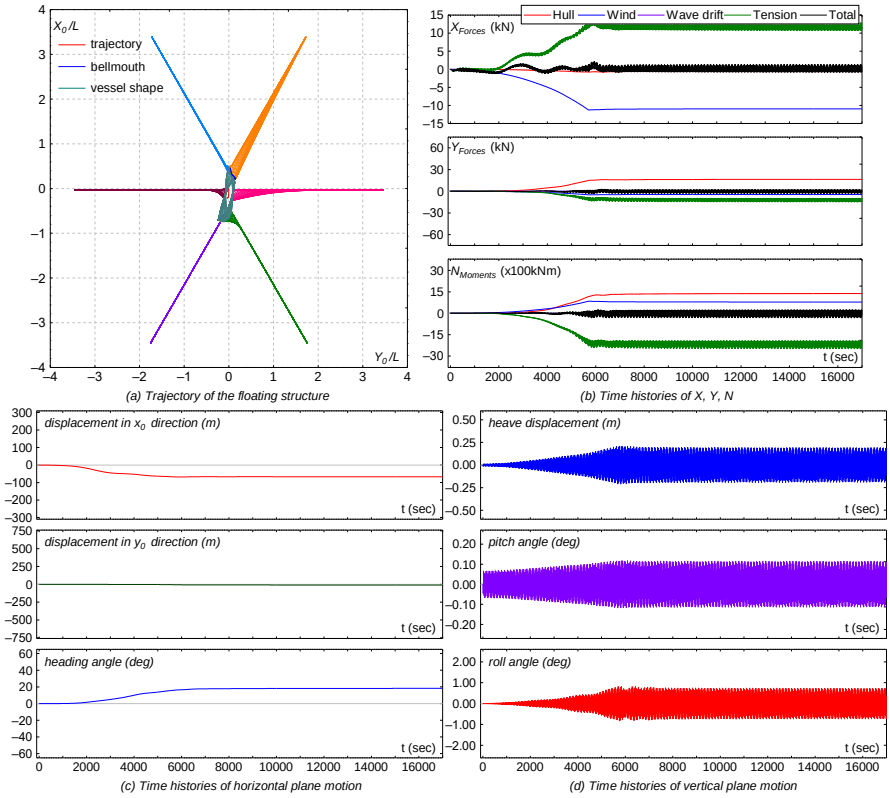

Fig. 3.52. $\lambda/L = 1.0$; $V_C = 1.0$ kn; $\alpha = 0°$; $V_W = 10$ m/s; $v = 45°$; $\chi = 60°$ [SM-31]

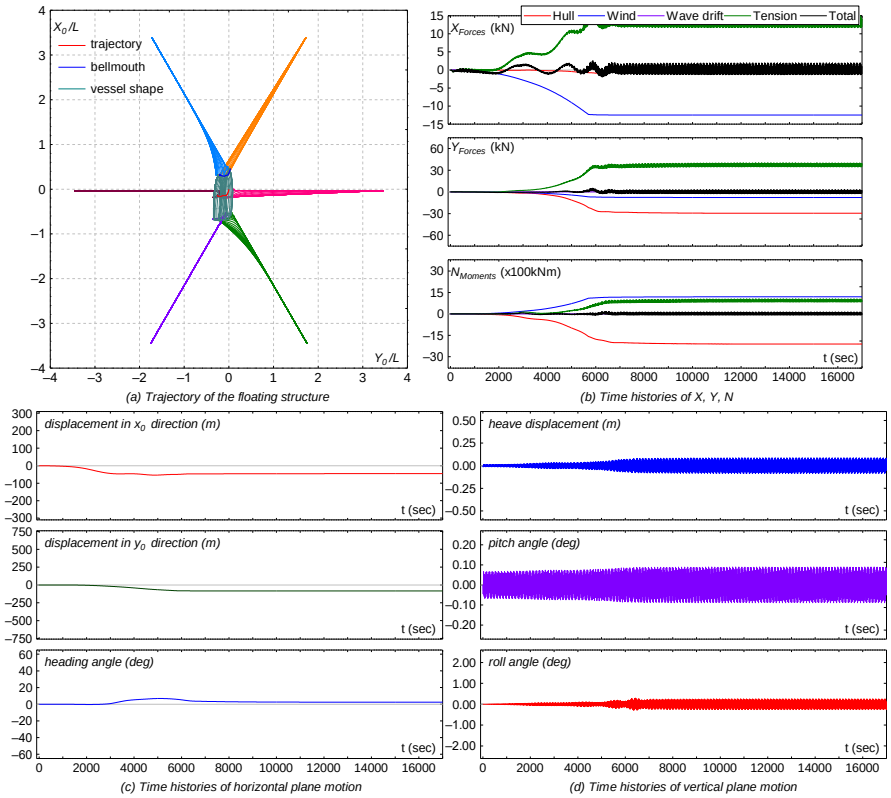

Fig. 3.53. $\lambda/L = 1.0$; $V_C = 1.0$ kn; $\alpha = 30°$; $V_W = 10$ m/s; $v = 45°$; $\chi = 30°$ [SM-28]

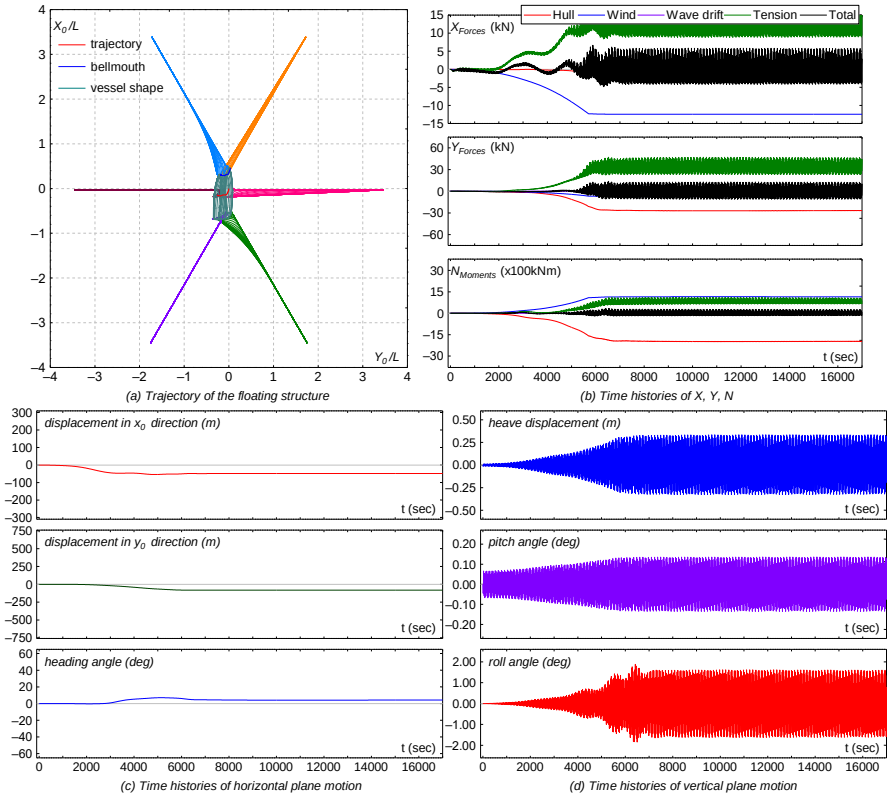

Fig. 3.54. $\lambda/L = 1.0$; $V_C = 1.0$ kn; $\alpha = 30°$; $V_W = 10$ m/s; $v = 45°$; $\chi = 60°$ [SM-32]

3.6. Concluding Remarks

Three-dimensional dynamics model for motion analysis of a floating offshore structure has been presented. Then three-dimensional mooring line dynamics model has been presented based on three-dimensional lumped mass method. The model is then coupled with the motion equations of a floating structure based on MMG model and conventional floating body motion to introduce the simultaneous motion between mooring lines and the 6 DOF motion of the floating structure. To verify the proposed model, dynamic coupled-motion between a ship-type floating structure and its mooring lines had been investigated by using developed simulation code.

In this chapter, four types of mooring line configuration system are investigated by using coupled equation model described in Chapter. 2 combining with the presented three-dimensional dynamics model of a mooring line. Each type of mooring configuration system is subjected to various environmental conditions mainly based on the difference of the ratio of wave length and ship length λ/L, the presence of wind force, the direction of current relative to bow direction, and the various directions of wave and wind. According to the results, the three-dimensional mooring line model can reproduce the tension as well as motion of mooring line even for multi-line conditions since the mooring line moves with the floating structure simultaneously. The tension of mooring line is also reasonable since the tendency of the total mooring line tension acting on the floating structure indicates reasonable results against the motion of the floating structure. The results, in general, come to the conclusion that by using the motion equations of a floating structure based on MMG model combined with the conventional floating body motion for vertical motion which are coupled with three-dimensional lumped mass method, the 6 DOF motions of the floating structure can be expressed simultaneously with the three-dimensional motions of the mooring lines including the effect of wind, wave, and current forces as well as the dynamic effects of the mooring lines. This model is capable to be applied even for various mooring line configuration types.

Furthermore, according to the motion analyses have been done for four mooring line configuration types, the following results are summarized,

- Since the current effect in longitudinal direction is smaller comparing with in lateral direction, the current force coming from lateral direction is more significant to affect the motion of the moored floating structure.
- The presence of wind force enlarges the drift horizontal plane motion of the floating structure.
- The vertical motion of the floating structure for all conditions especially for heave

and roll increase if wave direction relative to the heading of the floating structure increases.

- For the single line type, the floating structure can move freely (rotational and translation motion) following the direction of external disturbance. At the certain case, the floating structure moves far away depend on the combination of wave, wind, and current.
- Similar with the single line type, for double mooring line, the floating structure still can move freely, however the trajectory of the floating structure is less than single line condition since the restoring force generated by mooring line increases due to the increasing of the number of the mooring line.
- Unlike with single and double mooring line(s), the motion of the floating structure in the multi-leg turret mooring is more stable comparing both types. The tension generated by all mooring lines is sufficient to restrain the floating structure and thereby the floating structure doesn't move far away from her initial position. The floating structure tends to move rotationally following the direction of external forces.
- Though the motion of the floating structure in multi-leg spread mooring realizes small motion, the lateral force and moment acting to the floating structure becomes large if the external disturbances come from the lateral direction. Moreover, the tension of mooring line may become larger if the floating structure received external forces from the lateral direction.
- According to the simulation results, the multi-leg turret mooring is applicable for area where external disturbances come from various directions while multi-leg spread mooring is suitable for the area where the direction of external disturbances are almost constant.

Finally, the developed dynamics model including its application for various mooring line configuration types and environmental conditions shows feasible results and reasonable behavior of a moored floating structure can be investigated. Therefore, the motion of a floating structure can be analyzed properly using the proposed model, including the effects of wind, wave, and current forces and mooring line configuration types.

Chapter 4 Development of Three-Dimensional Dynamics Model for Multi-Component Mooring Line

4.1. Introduction

With increase of deep water oil and gas exploitation activities, floating offshore structures operated in deep water accrues. Therefore, mooring operation in deep water becomes one of the most important things to be considered. In the mooring operation in deep water, mooring line system becomes more complex and thereby several kinds of mooring line types and systems exist. Multi-component mooring line (MCML) system is widely used for deep water mooring operation since it has several advantages comparing with conventional mooring line (single-component mooring line). Ba, (2011) summarized the advantages of the multi-component mooring line based on two-component (polyester-chain) mooring line observed by Childers, (1974) as follows,

- It has lower pretension and lower operating mooring line tension, hence the life of the mooring line becomes longer comparing with that of chains which have uniform properties. From this, it can be noticed that appropriate variation of the properties of mooring line segment (even if all segment consist of chains) can decrease tension and increase the life of mooring line.
- It requires less manual operation of mooring line for reducing mooring line tension.
- It requires less anchor handling power for deploying mooring line.
- It has considerable capability for station keeping.

The illustration of multi-component mooring line including the relation with water depth can be seen in Fig. 4.1.

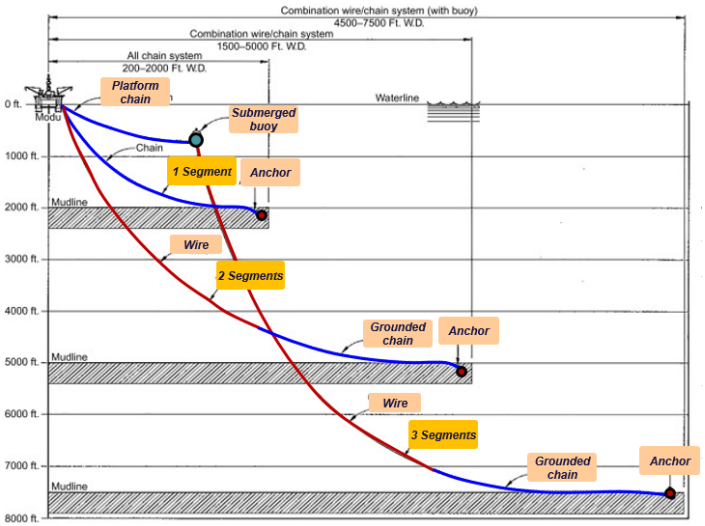

Fig. 4.1. Multi-component mooring line type (Aird,2019)

Since the multi-component mooring line is widely used for deep water mooring operation and it is expected to be escalated in the future, modelling of the multi-component mooring line involving the dynamic effects is required. Though the multi-component mooring line has been involved in many studies for investigating deep water floating structure (Vazquez-Hernandez et al., 2011; Qiao et al., 2013; Xie et al., 2015; Sanchez-Mondragon et al., 2018; Ghafari and Dardel, 2018; Zhao et al., 2013; and Lopez et al., 2017) and the multi-component mooring line itself was studied (Ansari, 1980; Nakajima et al., 1982; Van den Boom, 1985; Khan and Ansari, 1986; Ansari, 1991; and Chai et al., 2002), researches on modelling of multi-component mooring line including its dynamic effects were merely a few. Even if dynamic analysis method for multi-component mooring line exists, there are some limitations when incorporating the overall complexity of the dynamics of multi-component mooring line i.e. multi-segment properties, elasticity, anchor motion, etc. In addition, even though it can be introduced by using the FE method (Tahar and Kim, 2008), as described in the previous chapter, mathematical model based on the FE model is considered to be more complex, time consuming, and costly. Furthermore, the multi-component mooring line also needs to be modelled in three-dimensional manner because it naturally moves and is affected by external disturbance in three-dimensional space. Therefore, an adequate numerical method which can address the physical complexities and dynamic effects of the multi-component mooring line and also can take three-dimensional mooring line motion into consideration is absolutely demanded to provide accurate results for multi-component mooring line calculations.

This chapter provides three-dimensional dynamics model of a multi-component mooring line for motion analysis of a floating offshore structure including its verifications. This chapter is started by introducing the various configurations of multi-component mooring line in Section 4.2 which is mainly known for identifying the shape of a multi-component mooring line. Development of three-dimensional dynamics model is then proposed and presented in Section 4.3 while its verification both for a mooring line alone and a mooring line coupled with a ship-type floating offshore structure is presented in Section 4.4. Comparison between the developed three-dimensional dynamic model coupled with a ship-type floating offshore structure and two-dimensional model is presented and discussed in Section 4.5. Finally, the discussion of the proposed multi-component mooring line dynamics model is summarized in Section 4.6.

4.2. Multi-Component Mooring Line Configuration

Equations given for a multi-component mooring line is somewhat different from that for a single-component mooring line. The catenary equation for the single-component

mooring line cannot be applied for the multi-component mooring line which is made up by combination of segment line, clump weight or/and buoy, and anchor. Therefore, in order to investigate the behavior of a multi-component mooring line including its shape and tension, several kinds of geometric configurations are introduced to represent the condition/shape of the mooring line.

The geometric configuration of a multi-component mooring line is generally generated by inelastic catenary equations proposed by Ansari (1980) and summarized by Ba (2011) as follows,

$$\left.\begin{aligned} x_i &= a_i\left[\sinh^{-1}\left(\frac{s_i}{a_i}+\tan\theta_i\right)-\sinh^{-1}(\tan\theta_i)\right], \\ h_i &= a_i\left[\cosh\left(\frac{x_i}{a_i}+\sinh^{-1}(\tan\theta_i)\right)-\cosh(\sinh^{-1}(\tan\theta_i))\right], \\ s_i &= a_i\left[\sinh\left(\frac{x_i}{a_i}+\sinh^{-1}(\tan\theta_i)\right)-\tan\theta_i\right], \end{aligned}\right\} \tag{4.1}$$

where the following relations exist,

$$\left.\begin{aligned} \tan\theta_i &= \begin{cases} \tan\theta_{s_i} & ;\text{inactive or no } W_C \text{ at joint } i, \\ \tan\theta_{s_i}+\frac{W_{C_i}}{T_H} & ;W_C \text{ exists and active at joint } i, \end{cases} \\ \tan\theta_{i+1} &= \tan\theta_i+\frac{s_i}{a_i}, \\ a_i &= \frac{T_H}{w_{c_{l_i}}}, \\ \theta_i &= \tan^{-1}\left(\frac{T_{V_i}}{T_H}\right), \\ T_{V_i} &= \begin{cases} T_{V_{s_i}} & ;\text{inactive or no } W_C \text{ at joint } i, \\ T_{V_{s_i}}+W_{C_i} & ;W_C \text{ exists and active at joint } i. \end{cases} \end{aligned}\right\} \tag{4.2}$$

In which, x_i and h_i are the projected length of the i-th segment in horizontal and vertical directions respectively and s_i is the suspended length of the i-th segment. θ_i is an angle formed by horizontal plane and the line segment at i-th joint node, W_C is the weight of clump weight/buoy, $w_{c_{l_i}}$ is weight per unit length of segment line in water while T_H and T_V indicate the horizontal and vertical tension of the mooring line. Subscript i is segment line number.

Total horizontal distance between the top of mooring line (the attachment point) and the anchor point, denoted as X_{line}, is the summation of the part of mooring line laying on seabed x_{bot} and the horizontal projected direction of suspended segment line x_i. Similarly, total vertical elevation of suspended segment H_{line} can be obtained by summation of vertical projected direction of suspended segment line h_i. Here, the following relations exist,

$$\left.\begin{aligned} x_{bot} &= l_{tot} - \textstyle\sum_{i=1}^{n_i} s_i\,, \\ X_{line} &= l_{tot} - \textstyle\sum_{i=1}^{n_i} s_i + \textstyle\sum_{i=1}^{n_i} x_i\,, \\ H_{line} &= \textstyle\sum_{i=1}^{n_i} h_i\,, \end{aligned}\right\} \tag{4.3}$$

where l_{tot} is the total length of mooring line while n_i is number of segment line.

Due to the motion of the top point of a mooring line, several geometric configurations of multi-component mooring line occur. By using a multi-component mooring line consisting of three segment lines attached by a clump weight, five kinds of configurations of the multi-component mooring line were introduced by Ansari (1980) and Ba (2011). They are presented in the following subsection. In these mooring line configurations, the clump weight is attached at the connection point (joint) between segments 1 and 2. Segment 1 is the lowest segment of the mooring line which is connected by a pile anchor.

4.2.1. Multi-Component Mooring Line Configuration I

The mooring line shape representing the configuration I of a multi-component mooring line is shown in Fig. 4.2.

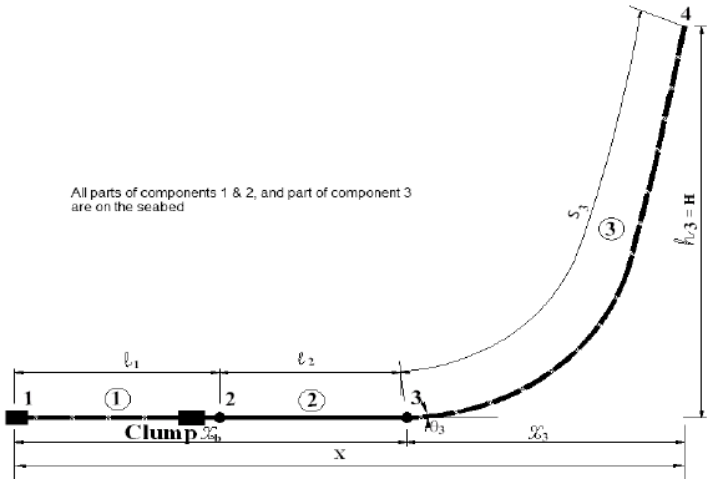

Fig. 4.2. Multi-component mooring line configuration I (Ba, 2011)

In this configuration, the following relation can be introduced,

$$\left.\begin{aligned} s_i &= 0 \quad \text{for} \quad i = 1{,}2, \\ \theta_i &= 0 \quad \text{for} \quad i = 1{\sim}3, \\ T_{V_i} &= 0 \quad \text{for} \quad i = 1{\sim}3, \\ x_{bot} &= \textstyle\sum_{i=1}^{2} l_i - s_3, \end{aligned}\right\} \tag{4.4}$$

in which l_i is segment line length. Thus, Eq. (4.1) becomes,

$$\left.\begin{aligned} x_3 &= a_3 \sinh^{-1}\left(\frac{s_3}{a_3}\right), \\ h_3 &= a_3\left[\cosh\left(\frac{x_3}{a_3}\right) - 1\right], \\ s_3 &= h_3\left[1 + \frac{2a_3}{h_3}\right]^{\frac{1}{2}}. \end{aligned}\right\} \tag{4.5}$$

Then, total horizontal projected length of the mooring line X_{line} and the vertical tension force at the mooring line top point T_{V_4} can be expressed as follows.

$$\left.\begin{aligned} X_{line} &= l_{tot} - s_3 + x_3, \\ T_{V_4} &= s_3 \cdot w_{c_{l_3}}. \end{aligned}\right\} \tag{4.6}$$

4.2.2. Multi-Component Mooring Line Configuration II

The configuration II for a multi-component mooring line shape is figured in Fig. 4.3.

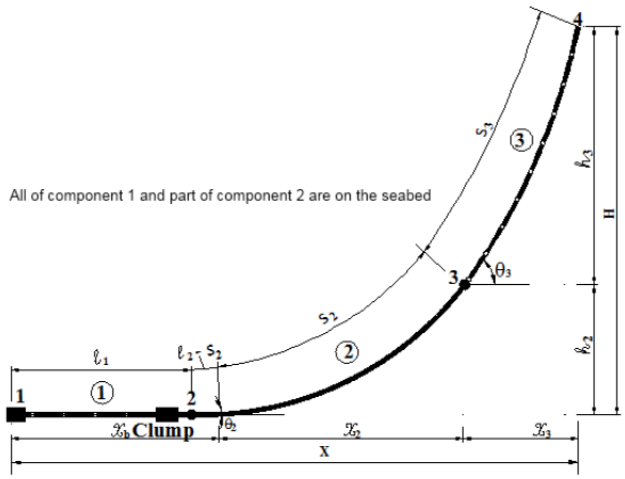

Fig. 4.3. Multi-component mooring line configuration II (Ba, 2011)

For the configuration II, the following relations exist,

$$\left.\begin{aligned} s_i &= 0 \quad \text{for} \quad i = 1, \\ \theta_i &= 0 \quad \text{for} \quad i = 1\sim2, \\ T_{V_i} &= 0 \quad \text{for} \quad i = 1\sim2, \\ s_2 &= \textstyle\sum_{i=1}^{2} l_i - x_{bot}, \\ s_3 &= l_3, \\ \tan\theta_3 &= \tan\theta_2 + \frac{s_2}{a_2}. \end{aligned}\right\} \tag{4.7}$$

Hence, Eq. (4.1) becomes,

$$
\left.
\begin{aligned}
x_2 &= a_2 \sinh^{-1}\left(\frac{s_2}{a_2}\right), \\
h_2 &= a_2\left[\cosh\left(\frac{x_2}{a_2}\right) - 1\right], \\
x_3 &= a_3\left[\sinh^{-1}\left(\frac{l_3}{a_3} + \frac{s_2}{a_2}\right) - \sinh^{-1}\left(\frac{s_2}{a_2}\right)\right], \\
h_3 &= a_3\left[\cosh\left(\frac{x_3}{a_3} + \sinh^{-1}\left(\frac{s_2}{a_2}\right)\right) - \cosh\left(\sinh^{-1}\left(\frac{s_2}{a_2}\right)\right)\right], \\
s_2 &= h_2\left[1 + \frac{2a_2}{h_2}\right]^{\frac{1}{2}}.
\end{aligned}
\right\} \tag{4.8}
$$

Then, the following relation can be expressed.

$$
\left.
\begin{aligned}
H_{line} &= \sum_{i=2}^{3} h_i\,, \\
X_{line} &= l_{tot} - l_3 - s_3 + \sum_{i=2}^{3} x_i\,, \\
T_{V_4} &= s_2 \cdot w_{c_{l_2}} + l_3 \cdot w_{c_{l_3}}.
\end{aligned}
\right\} \tag{4.9}
$$

4.2.3. Multi-Component Mooring Line Configuration III

Fig. 4.4 shows the configuration III of a multi-component mooring line shape.

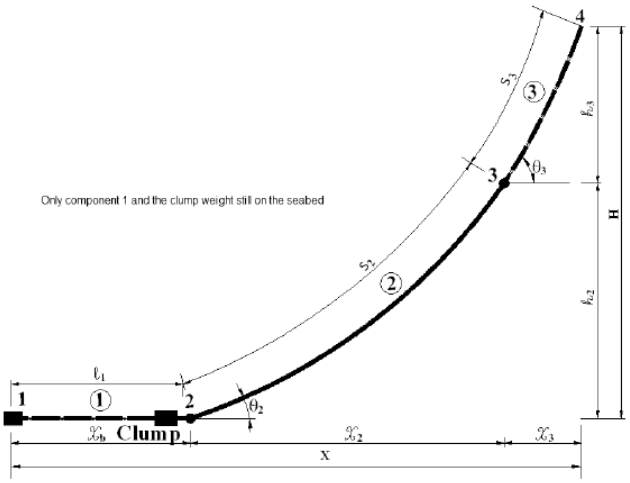

Fig. 4.4. Multi-component mooring line configuration III (Ba, 2011)

This configuration satisfies the following relations,

$$
\left.
\begin{aligned}
s_1 = \theta_1 &= T_{V_1} = 0, \\
s_i &= l_i \qquad \text{for} \qquad i = 2\sim3, \\
x_{bot} &= l_1, \\
T_{V_2} &= T_H \tan\theta_2\,.
\end{aligned}
\right\} \tag{4.10}
$$

Hence, Eq. (4.1) is reduced to,

$$\left.\begin{aligned} x_2 &= a_2\left[\sinh^{-1}\left(\frac{l_2}{a_2}+\tan\theta_2\right)-\sinh^{-1}(\tan\theta_2)\right],\\ h_2 &= a_2\left[\cosh\left(\frac{x_2}{a_2}+\sinh^{-1}(\tan\theta_2)\right)-\cosh(\sinh^{-1}(\tan\theta_2))\right],\\ x_3 &= a_3\left[\sinh^{-1}\left(\frac{l_3}{a_3}+\tan\theta_3\right)-\sinh^{-1}(\tan\theta_3)\right],\\ h_3 &= a_3\left[\cosh\left(\frac{x_3}{a_3}+\sinh^{-1}(\tan\theta_3)\right)-\cosh(\sinh^{-1}(\tan\theta_3))\right]. \end{aligned}\right\} \quad (4.11)$$

where, $\tan\theta_3 = \tan\theta_2 + \frac{l_2}{a_2}$. Finally, the following expression can be derived.

$$\left.\begin{aligned} H_{line} &= \sum_{i=2}^{3} h_i\,,\\ X_{line} &= l_1 + \sum_{i=2}^{3} x_i\,,\\ T_{V_4} &= T_H\tan\theta_2 + s_2\cdot w_{c_{l_2}} + l_3\cdot w_{c_{l_3}}. \end{aligned}\right\} \quad (4.12)$$

4.2.4. Multi-Component Mooring Line Configuration IV

The configuration IV of a multi-component mooring line shape illustrates in Fig. 4.5.

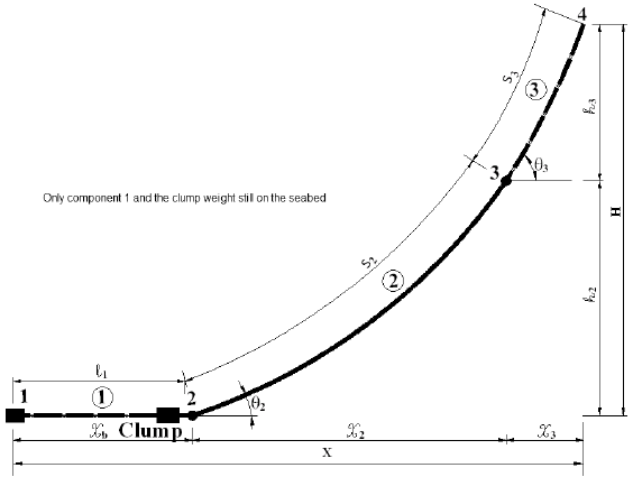

Fig. 4.5. Multi-component mooring line configuration IV (Ba, 2011)

In this configuration, the following relations exists.

$$\left.\begin{aligned} \theta_1 &= T_{V_1} = 0,\\ s_1 &= l_1 - x_{bot},\\ s_i &= l_i \qquad \text{for} \qquad i = 2\sim 3. \end{aligned}\right\} \quad (4.13)$$

Hence, Eq. (4.1) can be expressed as follows,

$$
\left.
\begin{aligned}
x_1 &= a_1 \sinh^{-1}\left(\frac{s_1}{a_1}\right), \\
h_1 &= a_1\left[\cosh\left(\frac{x_1}{a_1}\right) - 1\right], \\
x_2 &= a_2\left[\sinh^{-1}\left(\frac{l_2}{a_2} + \tan\theta_2\right) - \sinh^{-1}(\tan\theta_2)\right], \\
h_2 &= a_2\left[\cosh\left(\frac{x_2}{a_2} + \sinh^{-1}(\tan\theta_2)\right) - \cosh(\sinh^{-1}(\tan\theta_2))\right], \\
x_3 &= a_3\left[\sinh^{-1}\left(\frac{l_3}{a_3} + \tan\theta_3\right) - \sinh^{-1}(\tan\theta_3)\right], \\
h_3 &= a_3\left[\cosh\left(\frac{x_3}{a_3} + \sinh^{-1}(\tan\theta_3)\right) - \cosh(\sinh^{-1}(\tan\theta_3))\right],
\end{aligned}
\right\} \tag{4.14}
$$

where, $\tan\theta_2 = \frac{s_1}{a_1} + \frac{W_C}{T_H}$ and $\tan\theta_3 = \frac{s_1}{a_1} + \frac{W_C}{T_H} + \frac{l_2}{a_2}$. Thus, the following expressions can be obtained.

$$
\left.
\begin{aligned}
H_{line} &= \sum_{i=1}^{3} h_i\,, \\
X_{line} &= l_1 - s_1 + \sum_{i=1}^{3} x_i\,, \\
T_{V_4} &= s_1 \cdot w_{c_{l_1}} + W_C + \sum_{i=2}^{3} l_i \cdot w_{c_{l_i}}\,.
\end{aligned}
\right\} \tag{4.15}
$$

4.2.5. Multi-Component Mooring Line Configuration V

Finally, configuration V of a multi-component mooring line shape figured in Fig. 4.6.

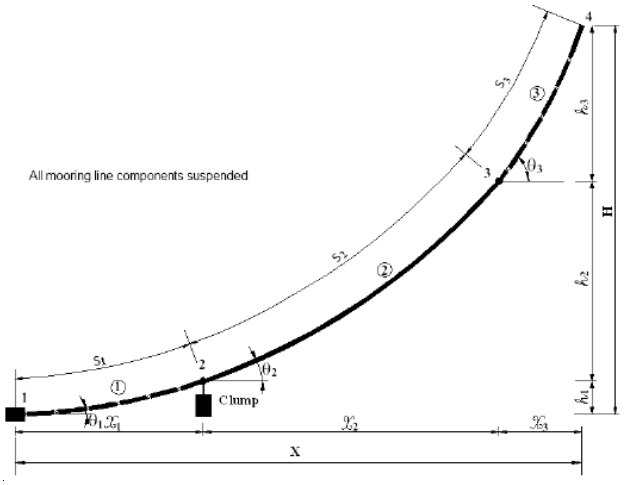

Fig. 4.6. Multi-component mooring line configuration V (Ba, 2011)

The following expressions represent this configuration,

$$
\left.
\begin{aligned}
x_{bot} &= 0, \\
s_i &= l_i \qquad \text{for} \qquad i = 1\sim3.
\end{aligned}
\right\} \tag{4.16}
$$

Hence, Eq. (4.1) can be rewritten as follows,

$$\left.\begin{aligned} x_1 &= a_1\left[\sinh^{-1}\left(\frac{l_1}{a_1}+\tan\theta_1\right)-\sinh^{-1}(\tan\theta_1)\right],\\ h_1 &= a_1\left[\cosh\left(\frac{x_1}{a_1}+\sinh^{-1}(\tan\theta_1)\right)-\cosh(\sinh^{-1}(\tan\theta_1))\right],\\ x_2 &= a_2\left[\sinh^{-1}\left(\frac{l_2}{a_2}+\tan\theta_2\right)-\sinh^{-1}(\tan\theta_2)\right],\\ h_2 &= a_2\left[\cosh\left(\frac{x_2}{a_2}+\sinh^{-1}(\tan\theta_2)\right)-\cosh(\sinh^{-1}(\tan\theta_2))\right],\\ x_3 &= a_3\left[\sinh^{-1}\left(\frac{l_3}{a_3}+\tan\theta_3\right)-\sinh^{-1}(\tan\theta_3)\right],\\ h_3 &= a_3\left[\cosh\left(\frac{x_3}{a_3}+\sinh^{-1}(\tan\theta_3)\right)-\cosh(\sinh^{-1}(\tan\theta_3))\right]. \end{aligned}\right\} \quad (4.17)$$

where, $\tan\theta_2=\tan\theta_1+\frac{W_C}{T_H}+\frac{l_1}{a_1}$ and $\tan\theta_3=\tan\theta_1+\frac{W_C}{T_H}+\sum_{i=i}^{2}\frac{l_i}{a_i}$. Thus, the following expressions can be given.

$$\left.\begin{aligned} H_{line} &= \sum_{i=1}^{3} h_i\,,\\ X_{line} &= \sum_{i=1}^{3} x_i\,,\\ T_{V_4} &= T_H\tan\theta_1+W_C+\sum_{i=i}^{3} l_i\cdot w_{c_{l_i}}\,. \end{aligned}\right\} \quad (4.18)$$

4.3. Development of Three-Dimensional Dynamics Model for Multi-Component Mooring Line

4.3.1. Problem Description of Multi-Component Mooring Line

A typical multi-component mooring line is shown in Fig. 4.7. The multi-component

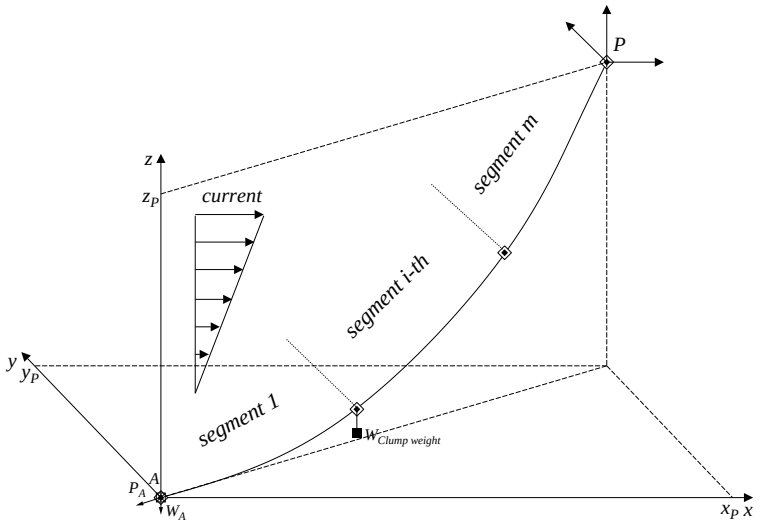

Fig. 4.7. Typical arrangement of multi-component mooring line

mooring line is composed of various mooring line components consisting of several identical or various segment lines, clump weight(s), and/or buoy(s). The clump weights and/or buoys are occasionally attached at the connection point between the segments. These components are used to increase anchor-holding capacity and to decrease mooring line tension respectively. The multi-component mooring line is subjected to the current force which directly acts on the mooring line depending on its vertical position. Wave, wind, and other external forces are enforced as the coupled forces acting on the top point of the mooring line. Meanwhile, bending and torsional stiffenesses of mooring line are neglected, since both stiffnesses do not influence mooring line tension too much as reported by Hall et al. (2014).

The dynamic behavior of each segment of a multi-component mooring line generally depends on its properties, water depth (current force), anchor-holding power, and external forces acting on the top point of the mooring line. However, since the segment lines are connected each other, their dynamic behavior is also affected by the weight and tension of other components connected to the segment. Similarly, the properties of an anchor, a clump-weight and a buoy which may be attached at the end of the segment also give significant effect to the segment line motions. Consequently, these items affect the dynamic behavior of entire multi-component mooring line.

Moreover, the diverse environmental loads which come from various directions drive the dynamic motions of a floating offshore structure in six degrees of freedom (6 DOF). These motions encourage the three-dimensional motion of the top point of the mooring line and hence these induce the three-dimensional dynamic motions of the mooring line. The diverse environmental loads also encourage the mooring line to move three-dimensionally. Therefore, a dynamics model for a multi-component mooring line must be constructed in three-dimensional manners. In addition, the features of an anchor must be expressed well including its motions and holding forces to satisfy the possibility of semi-taut mooring line conditions.

4.3.2. Technical Groundwork of Three-Dimensional Dynamics Model of Multi-Component Mooring Line

A dynamics model for a multi-component mooring line is constructed by applying a single-component mooring line dynamics model (Nakajima et al., 1983) to each segment line of a multi-component mooring line. This single-component mooring line model discretizes a mooring line equally dividing it into several massless spring elements based on three-dimensional lumped mass model described in Chapter 3. The elements are linked by a mass point which is regarded as a node. It is assumed that the weight of each element and external forces acting on each element are lumped to the node. Meanwhile, the motions of

uppermost and lowermost nodes are assumed to be given by arbitrary prescribed motion and to stay at a fixed point as a fixed anchor on the seabed respectively. This three-dimensional lumped mass model for a single-component mooring line is illustrated in Fig. 3.1.

The three-dimensional lumped mass model presented for a single-component mooring line is further adopted and modified to model a multi-component mooring line. Every segment of a multi-component mooring line is considered as a single-component line based on Nakajima's lumped mass model and then interconnected each other to build a lumped mass model for a multi-component mooring line. Each segment line is divided into N elements, which means the segment consists of $N-1$ nodes, while the external forces acting on the elements are congregated at these nodes. On the other hand, both ends of the segment need to be regarded as meaningless nodes which provide vacant nodes for attaching to an anchor, a sinker, or a buoy. Since the nodes for both ends of the segment are vacant, thereby the number of non-vacant nodes which is equal to $N-1$ is less than the number of element (N), boundary conditions for the ends of the segment are necessary to accommodate the redundant element. Thus, the mass of the element and inherent forces acting on the redundant element are equally distributed to the both adjacent nodes. Hence, the mass of the first lifted node δ_I and the previous node of the top node δ_N are 1.5 times greater than other nodes, whilst the nodes of both ends segments $(j = I-1;\ \ j = N+1)$ are considered as massless nodes $(\delta_j = 0)$.

Furthermore, connection points (joints) between adjacent segments are generated by bonding the top node of lower side segment with the bottom node of upper side segment. It means that the top node $(j = N+1)$ of i-th segment $\left(J_{i,(N+1)}\right)$ coincides to the bottom node $(j = 1)$ of $(i+1)$-th segment $\left(J_{(i+1),1}\right)$. In other words, both nodes can be regarded as identical node which can be merged into a joint node $(J_{i,(N+1)} = J_{(i+1),1})$. Since the joint node is generated by bonding two massless nodes, it also becomes a massless node. This condition does not satisfy the appropriate geometry of a multi-component mooring line, in which, a joint between segments should has mass even if there is no other attached component at the joint. Therefore, some additional constraints and improvements are established, especially for the joint node to comply with the conditions for the exact geometry and inherent features of a multi-component mooring line.

In static condition, the features of the joint node are modified to meet the basic physical meaning of a multi-component mooring line geometry as reported in Ansari (1980) described in Section 4.2. The lumped mass algorithms pertaining to the joint node are also improved when performing the dynamic motion analysis of a mooring line. The joint node must move freely and it can't be assumed as the prescribed motion or to stay at a fixed point likely in the single-component mooring line model. In other words, it can be said that the

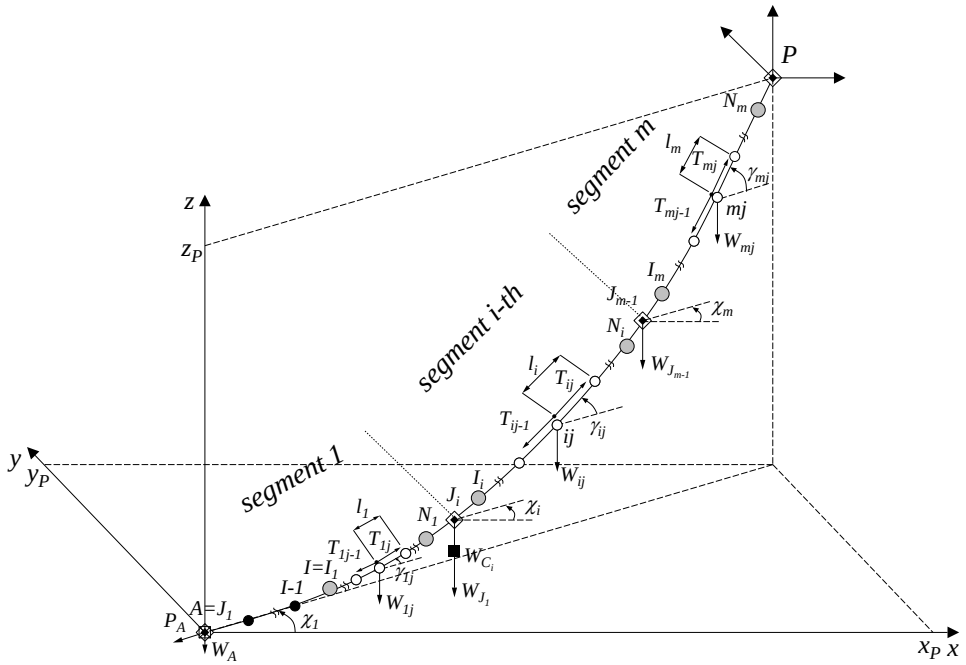

Fig. 4.8. Three-dimensional lumped mass model of multi-component mooring line

motion of the joint node is similar with the motion of common lumped mass nodes.

In order to express the dynamic motions of the joint node, the lumped mass algorithms used in common nodes are adopted and applied to the joint node. However, since the lumped mass algorithm in Nakajima's single-component line model excludes the dynamic motions of both end nodes, some modifications are established considering the dynamic effects from adjacent segment. Moreover, an appropriate anchor formulations are adopted to express the motion of bottom-end node of a mooring line (anchor point) whilst the motion of the top point of a mooring line is generated by 6 DOF motion of floating offshore structure. The dynamic lumped mass model for a three-dimensional multi-component mooring line can be constructed through these considerations.

4.3.3. Coordinate System of Mooring Line

The coordinate system for a multi-component mooring line developed in this study is shown in Fig. 4.8. As illustrated in the figure, a multi-component mooring line can be expressed by the three-dimensional lumped mass model. $A-xyz$ is a line coordinate system with the origin of z-axis on the seabed. The schematic diagram of the three-dimensional lumped mass model for a multi-component mooring line including their features is specifically displayed in the figure. As shown in the figure, a multi-component mooring line lumped mass model is considered as a continuum of several three-dimensional lumped mass models for segment lines, interconnecting each other and incorporated with an anchor

and clump weight/buoy. In the model, the top point of a uppermost segment line, which means the top point of a mooring line denoted by P, is the attached point of the mooring line on a floating offshore structure (bellmouth). Node A is the bottom-end of a lowermost segment regarded as an anchor point. Joints between the segments can be considered as joints with/without clump weight/buoy.

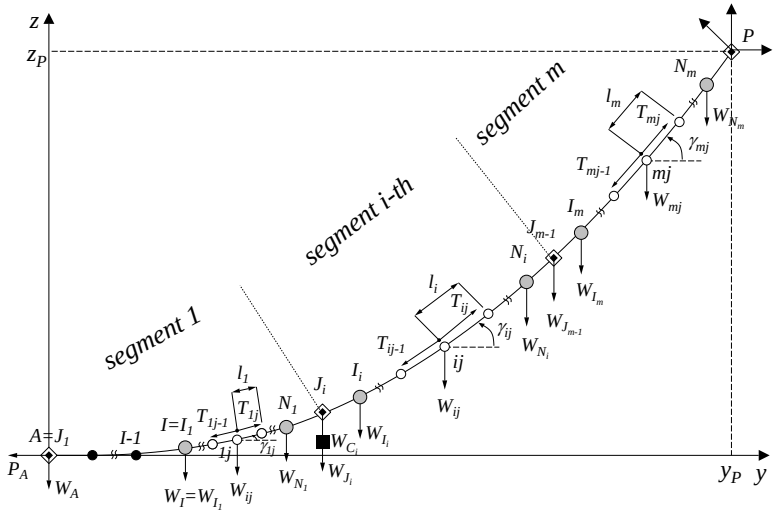

Fig. 4.9. Three-dimensional lumped mass geometry of multi-component mooring line (yz-plane)

The three-dimensional lumped mass model for a multi-component mooring line is referred to the line coordinate system $A - xyz$. The entire nodes can freely move in three-dimensional directions even for the anchor point, joints, and the top point and they provide three-dimensional mooring line motions. Whilst, the rotational motions of a line are disregarded since the effects of these motions on the dynamic behavior of a mooring line are not so considerable.

4.3.4. Multi-Component Mooring Line Features

The geometry of a multi-component mooring line model is detailed in Fig. 4.9. Here, a multi-component mooring line is composed by m segments and i-th segment is discretized into N_i elements while the mass of the segment is spread out into $N_i + 1$ nodes. An anchor point, a touchdown point, and the first lifted node are expressed by A, $I - 1$, and I respectively. J_i and P denote i-th joint node and the top point of the mooring line. In additions, W_{ij} is the weight of j-th node in i-th segment whilst segment length is denoted as l_i.

By adopting the fundamental of Nakajima's lumped mass model and integrating anchor feature at the anchor point node, node weights for a multi-component mooring line model

can be described as follows,

$$\left.\begin{array}{lll} W_A = W_{11} = \ w_A, & & \\ W_I = W_{rI} = 1.5 \ w_{l_r}, & & \\ W_{N_i} = W_{iN} = 1.5 \ w_{l_i} & ; \ i \ \geq r, & \\ W_{rj} = 1.0 w_{l_r} & ; \ I < j < N, & \\ W_{rj} = 0.0 & ; \ j < I, & \\ W_{ij} = 1.0 w_{l_i} & ; \ 1 < j < N \ , \ i \ \geq r, & \\ W_{ij} = 0.0 & ; \ i < r, & \end{array}\right\} \quad (4.19)$$

where r indicates the first lifted segment line number. In the meantime, the weight of the joint between segments is defined by characterizing the features of the multi-component line according to the basic insight of multi-component catenary method reported by Ansari (1980). Since this weight is pondered as the total weight of suspended part beneath the joint, including lifted clump weight/buoy, the weight of the joint can be written as,

$$W_{J_i} = \left.\begin{cases} \sum_{k=1}^{i} W_{S_k} + \sum_{k=2}^{i} W_{C_k} + W_A & ; W_{A_{act.}} \ \ and \ \ W_A \neq 0, \\ \sum_{k=1}^{i} W_{S_k} + \sum_{k=2}^{i} W_{C_k} & ; W_{A_{inact.}}, \\ \sum_{k=1}^{i} W_{S_k} & ; W_{A_{inact.}}, W_{C_{inact.}} or \ \ W_C = 0, \end{cases}\right\} \quad (4.20)$$

in which the component weights of the joint weights are given by,

$$\left.\begin{array}{ll} W_{S_k} = \sum_{i=1}^{k} \sum_{j=2}^{N} W_{ij}\,, & \\ W_{C_k} = w_{C_i} & ; W_{C_{act.}}, \\ W_{C_k} = 0 & ; W_{C_{inact.}}, \end{array}\right\} \quad (4.21)$$

In Eq. (4.20) and Eq. (4.21), subscripts $_{\cdot act.}$ and $_{\cdot inact.}$ represent the lifting condition (active or inactive) of joint node and anchor. The joint node is active when it is upraised from the seabed and vice versa. Active anchor occurs when there are no nodes lying on the seabed and hence the tension line pulls the anchor. Meanwhile, the weights of mooring line components are given as follows,

$$\left.\begin{array}{l} w_A = w_{c_A}, \\ w_{l_i} = w_{c_{l_i}} \ \times \ \bar{l}_i, \\ w_C = w_{c_{C_i}}, \end{array}\right\} \quad (4.22)$$

where w_{c_A}, $w_{c_{l_i}}$, and $w_{c_{C_i}}$ are the weight of an anchor, the weight of line segment per unit length, and the weight of clump weight/buoy in water respectively, while $\bar{l}_i$ indicates element length of the segment $(= l_i/N_i)$.

Furthermore, due to the considerations used to express the conditions of a joint node as aforedescribed, the joint node will become massless and weightless when the joint node is inactive (called as inactive-empty joint node J_{ie}). Accordingly, the dynamic lumped mass solutions become anomalous due to the conditions. Therefore, an adjustment for the nodes close to the joint must be carried out to tackle these problems.

The adjustment is carried out by distributing the mass of nodes which are adjacent to the inactive-empty joint node J_{ie} into the mass of inactive-empty joint node $\delta_{J_{ie}}$. The mass of the nodes around the inactive-empty joint node further become,

$$\left.\begin{aligned} \delta_{(ie-1,N)} &= 1.0 \;\; m_{l_{ie-1}}, \\ \delta_{J_{ie}} = \delta_{(ie-1,N+1)} = \delta_{(ie,1)} &= 0.5 \;\; (m_{l_{ie-1}} + \;\; m_{l_{ie}}), \\ \delta_{(ie,2)} &= 1.0 \;\; m_{l_{ie}}, \end{aligned}\right\} \tag{4.23}$$

where ie represents the number of inactive-empty joint node. By this manner, the adequate solutions for lumped mass matrix algorithm for a multi-component mooring line can be attained.

4.3.5. Static Analysis of Multi-Component Mooring Line

(1) Definition of Initial Line Geometric Configuration

In order to carry out static analysis by using the developed model, the initial geometric configuration of a mooring line is necessary to define the circumstance of each segment line at the initial condition such as fully laying on the seabed, partially suspended, or fully suspended segment. It encompasses the initial horizontal and vertical projected lengths as well as suspended length for each segment line. This initial state of a segment line is then used to introduce the initial status of a joint node (active/inactive) and thereby describes a constraint condition applied for the both ends of the segment. This constraint is required when calculating the initial shape of a multi-component mooring line by the present lumped mass model. The weight/mass of a joint node generated by its lower suspended segment must be known to obtain the initial shape of an upper segment.

Since the physical understanding of static condition for a mooring line in the lumped mass model is identical with the catenary method even for a multi-component line, the multi-component catenary line equations are used to express the initial line configuration. The typical types of line configurations and their equations (Eq. (4.1)) presented in Section 4.2 (Ansari, 1980; Ba, 2011) are used. Here, T_H for calculating a_i is replaced by initial tension T_{H0}. Furthermore, through the iteration process following the procedure in catenary method, the preliminary initial line configuration can be obtained and then used as the reference for static multi-component lumped mass calculation.

(2) Initial Shape of Multi-Component Mooring Line

The initial condition of a multi-component mooring line is obtained through the static analysis of each segment. The method proposed by Nakajima (1983) is adopted to introduce the initial condition of each segment. Since the method is literally described for a single-component line type that is slightly different from that for the segment of a multi-component line, it is applied to each segment considering multifarious treatments depending on the initial states of the segment. These multifarious treatments exist due to the various constraints that come from the various initial states of the segment.

To overcome the constraints, the initial states of segments are classified into three types, i.e. fully laying on the seabed, partially suspended, and fully suspended. The initial shape of each segment for the lumped mass model is then obtained by regarding the initial state of the segment as one of these three types and calculating the initial shape by using the constraint of the regarded type. Further, according to the constraint, the calculation summary for each type of initial shape can be described as follows.

The calculation of initial shape for a segment which is fully laying on the seabed or partially suspended is started by determining a touchdown point node, $j = I - 1$, since the touchdown point node may exist in these two types. The touchdown point node can be determined by iterating calculation using the following formula referring Eq. (3.5) to Eq. (3.6),

$$W_{i1} = \frac{z_{P_i}/\bar{l}_i - \sum_{j=1}^{N_i}\left[\left\{T_{ij}^{-1} + (A_i.E_i)^{-1}\right\}\sum_{k=2}^{j} W_{ik}\right]}{\sum_{j=1}^{N_i} T_{ij}^{-1} + N_i/(A_i.E_i)}, \tag{4.24}$$

where z_{P_i}, $\bar{l}_i$, A_i, and E_i are the vertical position of a top segment measured form its bottom end, original length, sectional area, and Young's modulus of the *i*-th segment, respectively. T_{ij} is calculated as follows,

$$T_{ij} = \sqrt{T_{i1}^2 - W_{i1}^2 + \left(\sum_{k=1}^{j} W_{ik}\right)^2}. \tag{4.25}$$

The iterative calculation is repeated until the weight of the touchdown point node, $W_{i(I-1)}$ $(I > 2)$, becomes greater than 0. In the iteration, W_{i1} is treated as 0 if the calculated value of W_{i1} is less than 0. Furthermore, by adopting Eq. (3.4) the initial segment shape can be calculated by the following equations,

$$\left.\begin{aligned} x_{i(j+1)} &= \sum_{i=1}^{k} l_{ik} \cos\gamma_{ik} \cos\chi_i, \\ y_{i(j+1)} &= \sum_{i=1}^{k} l_{ik} \cos\gamma_{ik} \sin\chi_i, \\ z_{i(j+1)} &= \sum_{i=1}^{k} l_{ik} \sin\gamma_{ik}, \end{aligned}\right\} \tag{4.26}$$

where x_{ij}, y_{ij}, z_{ij} γ_{ik}, and χ_i can be observed in Fig. 4.8.

Meanwhile, due to the absence of a node attached on the seabed, a fully suspended segment is introduced by calculating the initial shape of a segment based on Eq. (4.26) and omitting the calculation for the touchdown point node. In addition, weight correction for nodes close to the seabed given by Nakajima et al. (1983) is also applied.

4.3.6. Segment Line Consideration of Multi-Component Mooring Line

A lumped mass node matrix is adopted to introduce the flexibilities of both end nodes of a segment line. The flexibilities are aroused by extending the treatment of a segment to satisfy proper boundary condition at the nodes. Thus, additional nodes taken from upper or lower segment is appended to the considered segment to reproduce free motions of the end nodes.

In this improvement, each segment can be classified into three main conditions as shown in Fig. 4.10. In this figure, a segment can be regarded as the lowest segment $(i = 1)$, middle segment $(1 < i < m)$, or the top segment $(i = m)$ of a mooring line. The lowest and

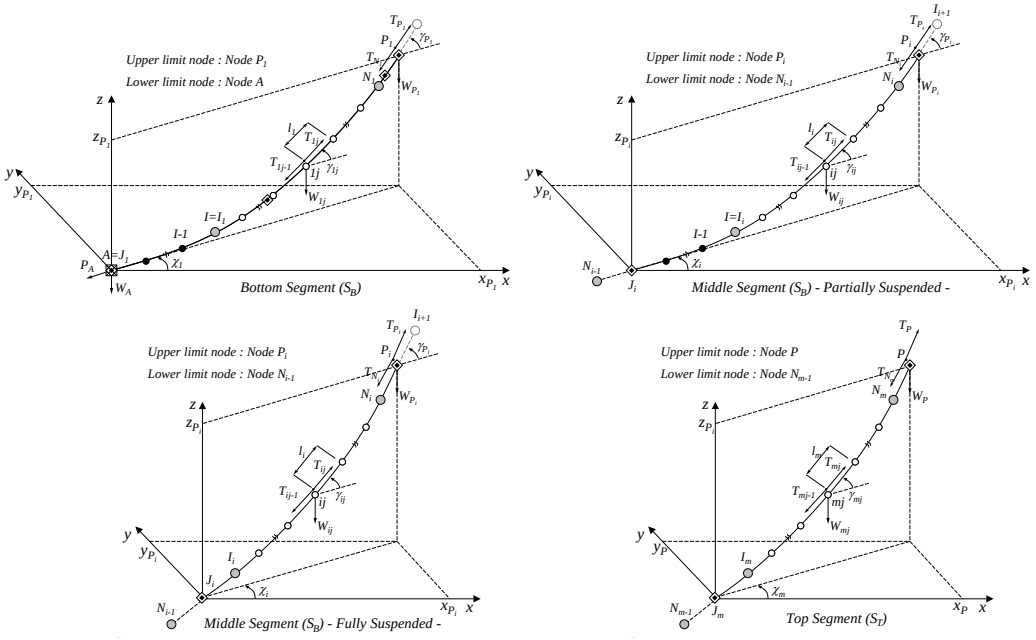

Fig. 4.10. Classification of segment conditions for three-dimensional lumped mass model of multi-component mooring line

middle segments then can be classified into partially suspended, fully laying on the seabed, and fully suspended segments while the top segment is classified into partially suspended and fully suspended segments. According to motion constraint for each end node of the segment, the boundary conditions for each segment type are as follows; bottom segment: the motion of bottom end is regarded as same as anchor motion while the top end moves flexibly, middle segment: the motion of both ends as regarded as flexible motion, and top segment: the motion of bottom end is regarded as flexible motion while the top end motion is prescribed. Furthermore, due to this improvement, the nodes which are regarded as flexible nodes in the lumped mass method are modified according to the types of segments, i.e. $(j = 2{\sim}N$ for $i = 1$, $j = 1{\sim}N+1$ for $1 < i < M$, and $j = 1{\sim}N$ for $i = m)$. Moreover, the coordinate system of mass point used for the equation of mooring line motion is considered by following the coordinate system for single-component lumped mass figured in Fig. 3.4.

4.3.7. Forces Acting on Mooring Line

Forces acting on the mooring line applied for the developed dynamics model for a multi-component mooring line are adopted from the formula used for the three-dimensional lumped mass model for a single-component mooring line presented in Section 3.2.3. Those forces can be summarized and rewritten as follows.

(1) Hydrodynamic Forces

Hydrodynamic forces acting on the node are expressed by the following equations,

$$\left.\begin{aligned} f_{dx_{ij}} &= -\left(\sin\bar{\beta}_{ij}\cdot\cos\bar{\theta}_{ij}\cdot\cos\phi_{ij} + \sin\bar{\theta}_{ij}\cdot\sin\phi_{ij}\right)f_{dn_{ij}} + \left(\cos\bar{\beta}_{ij}\cdot\cos\bar{\theta}_{ij}\right)f_{dt_{ij}},\\ f_{dy_{ij}} &= \left(\cos\bar{\beta}_{ij}\cdot\cos\phi_{ij}\right)f_{dn_{ij}} + \left(\sin\bar{\beta}_{ij}\right)f_{dt_{ij}},\\ f_{dz_{ij}} &= -\left(\sin\bar{\beta}_{ij}\cdot\cos\bar{\theta}_{ij}\cdot\cos\phi_{ij} - \cos\bar{\theta}_{ij}\cdot\sin\phi_{ij}\right)f_{dn_{ij}} + \left(\cos\bar{\beta}_{ij}\cdot\cos\bar{\theta}_{ij}\right)f_{dt_{ij}}, \end{aligned}\right\} \quad (4.27)$$

while hydrodynamic drag forces in normal and tangential directions are calculated by,

$$\left.\begin{aligned} f_{dn_{ij}} &= -\tfrac{1}{2}\rho C_{dn_i} D_{c_i}\bar{l}_i\left|u_{n_{ij}}\right|u_{n_{ij}},\\ f_{dt_{ij}} &= -\tfrac{1}{2}\rho C_{dt_i} D_{c_i}\bar{l}_i\left|u_{t_{ij}}\right|u_{t_{ij}}, \end{aligned}\right\} \quad (4.28)$$

where,

$$\begin{aligned} u_{t_{ij}} &= u_{\xi_{ij}},\\ u_{n_{ij}} &= \sqrt{u_{v_{ij}}^2 + u_{\eta_{ij}}^2},\\ \emptyset_{ij} &= \tan^{-1}\left(\frac{u_{\eta_{ij}}}{u_{v_{ij}}}\right), \end{aligned} \quad (4.29)$$

in which $u_{\xi_{ij}}$, $u_{v_{ij}}$, and $u_{\eta_{ij}}$ are obtained by the following matrix,

$$\begin{bmatrix} u_{\xi_{ij}} \\ u_{v_{ij}} \\ u_{\eta_{ij}} \end{bmatrix} = \begin{bmatrix} \cos\bar{\beta}_{ij}\cos\bar{\theta}_{ij} & \sin\bar{\beta}_{ij} & \sin\bar{\theta}_{ij}\cos\bar{\beta}_{ij} \\ -\sin\bar{\beta}_{ij}\cos\bar{\theta}_{ij} & \cos\bar{\beta}_{ij} & -\sin\bar{\beta}_{ij}\sin\bar{\theta}_{ij} \\ -\sin\bar{\theta}_{ij} & 0 & -\cos\bar{\theta}_{ij} \end{bmatrix} \times \begin{bmatrix} \dot{x}_{ij} - v_{x_{ij}} \\ \dot{y}_{ij} - v_{y_{ij}} \\ \dot{z}_{ij} - v_{z_{ij}} \end{bmatrix}. \tag{4.30}$$

The components of the above formulations are considered to be same as those used in a single-component mooring line.

(2) Current Velocities

Current velocities acting on the mooring line can be rewritten as follow,

$$\left.\begin{aligned} v_{x_{ij}} &= v_{c_{ij}}\cos\alpha_c\,, \\ v_{y_{ij}} &= v_{c_{ij}}\sin\alpha_c\,, \\ v_{z_{ij}} &= 0. \end{aligned}\right\} \tag{4.31}$$

where the current distribution in vertical direction given by Eq. (3.7) is used.

(3) Line-Seabed Interaction Forces

Again, by adopting Eq. (3.12), the friction force generated by the interaction between mooring line and the seabed can be given as,

$$\begin{bmatrix} f_{g_{x_{ij}}} \\ f_{g_{y_{ij}}} \\ f_{g_{z_{ij}}} \end{bmatrix} = -w_{c_{l_i}}\lambda_{c_{l_i}} l_{laying_i} \begin{bmatrix} \dot{x}_{ij} \\ \dot{y}_{ij} \\ \dot{z}_{ij} \end{bmatrix}. \tag{4.32}$$

Furthermore, the holding anchor power given by Eq. (3.48) becomes the following equation for the multi-component mooring line,

$$P_A = \; w_a\lambda_a e^{-0.05\kappa} + w_{c_{l_i}}\lambda_{c_{l_i}} l_{laying_i}, \tag{3.48}$$

in which, $\lambda_{c_{l_i}}$ and l_{laying_i} are the friction coefficient of mooring line at the seabed and the length of the laying part of the segment.

4.3.8. Governing Equations and Solution

Similar with three-dimensional lumped mass method for a single-component mooring line, the method that considers the elongation of mooring line is applied for deriving the solutions for three-dimensional lumped mass model of multi-component mooring line. By considering the elasticity of a mooring line, the governing equations of three-dimensional motion of a mass point j for each segment i can be solved by difference formulas using

Houbolt method expressed in Eq. (3.36). Thus, the following equation can be introduced,

$$\left.\begin{aligned} x_{ij}^{n+1} &= \tfrac{5}{2}x_{ij}^{n} - 2x_{ij}^{n-1} + \tfrac{1}{2}x_{ij}^{n-2} + \left(R_{ij}^{n+1}\cdot T_{ij}^{n+1} - P_{ij}^{n+1}\cdot T_{ij-1}^{n+1} + U_{j}^{n+1}\right)/2, \\ y_{ij}^{n+1} &= \tfrac{5}{2}y_{ij}^{n} - 2y_{ij}^{n-1} + \tfrac{1}{2}y_{ij}^{n-2} + \left(O_{ij}^{n+1}\cdot T_{ij}^{n+1} - H_{ij}^{n+1}\cdot T_{ij-1}^{n+1} + V_{ij}^{n+1}\right)/2, \\ z_{ij}^{n+1} &= \tfrac{5}{2}z_{ij}^{n} - 2z_{ij}^{n-1} + \tfrac{1}{2}z_{ij}^{n-2} + \left(S_{ij}^{n+1}\cdot T_{ij}^{n+1} - Q_{ij}^{n+1}\cdot T_{ij-1}^{n+1} + W_{ij}^{n+1}\right)/2, \\ &\left(j = 2\sim N, j\in S_B;\ \ j = 1\sim N+1, j\in S_M;\ \ j = 1\sim N, j\in S_T\right), \end{aligned}\right\} \tag{4.49}$$

where R_j, P_j, O_j, H_j, S_j, and Q_j; U_j, V_j, and W_j; and f_{dxj}, f_{dyj}, f_{dzj} can be expressed by adopting same formula for single-component mooring line. S_B, S_M and S_T represent the bottom, middle, and top segment, respectively. T_{ij} is given as follows,

$$T_{ij}^{n+1} = \tilde{T}_{ij}^{n+1} + \Delta T_{ij}^{n+1}. \tag{4.50}$$

Furthermore, simultaneous equations to determine the unknown parameter ΔT_{ij} are derived as follows,

$$\begin{bmatrix} -\tilde{F}_{i2}^{n+1} & \tilde{G}_{i2}^{n+1} & 0 & 0 & \cdots & 0 & 0 & 0 \\ \tilde{E}_{i3}^{n+1} & -\tilde{F}_{i3}^{n+1} & \tilde{G}_{i3}^{n+1} & 0 & \cdots & 0 & 0 & 0 \\ 0 & \tilde{E}_{i4}^{n+1} & -\tilde{F}_{i4}^{n+1} & \tilde{G}_{i4}^{n+1} & \cdots & 0 & 0 & 0 \\ \vdots & \vdots & \vdots & \vdots & \ddots & \vdots & \vdots & \vdots \\ 0 & 0 & 0 & \cdots & \cdots & \tilde{G}_{iN_i-1}^{n+1} & 0 & 0 \\ 0 & 0 & 0 & \cdots & \cdots & -\tilde{F}_{iN_i}^{n+1} & \tilde{G}_{iN_i}^{n+1} & 0 \\ 0 & 0 & 0 & \cdots & \cdots & \mathrm{E}_{iN_i+1}^{n+1} & -\tilde{F}_{iN_i+1}^{n+1} & \tilde{G}_{iN_i+1}^{n+1} \end{bmatrix} \begin{bmatrix} \Delta T_{i1}^{n+1} \\ \Delta T_{i2}^{n+1} \\ \Delta T_{i3}^{n+1} \\ \Delta T_{i4}^{n+1} \\ \vdots \\ \Delta T_{iN_i-2}^{n+1} \\ \Delta T_{iN_i-1}^{n+1} \\ \Delta T_{iN_i}^{n+1} \end{bmatrix} = \begin{bmatrix} -\tilde{\Psi}_{i2}^{n+1} \\ -\tilde{\Psi}_{i3}^{n+1} \\ -\tilde{\Psi}_{i4}^{n+1} \\ -\tilde{\Psi}_{i5}^{n+1} \\ \vdots \\ -\tilde{\Psi}_{iN_i-1}^{n+1} \\ -\tilde{\Psi}_{iN_i}^{n+1} \\ -\tilde{\Psi}_{iN_i+1}^{n+1} \end{bmatrix}, \tag{4.51}$$

in which the respective coefficients can be seen in Eq. (3.41). Then, to solve Eq. (4.51), the values of the following function must be zero to satisfy the constraint conditions.

$$\tilde{\Psi}_{ij}^{n+1} = \left(\tilde{x}_{ij}^{n+1} - \tilde{x}_{ij-1}^{n+1}\right)^2 + \left(\tilde{y}_{ij}^{n+1} - \tilde{y}_{ij-1}^{n+1}\right)^2 + \left(\tilde{z}_{ij}^{n+1} - \tilde{z}_{ij-1}^{n+1}\right)^2 - \bar{l}_i^2\left(1 + \tilde{T}_{ij-1}^{n+1}/E_i\cdot A_i\right)^2. \tag{4.52}$$

Finally, by solving the Eq. (4.51) iteratively until ΔT_{ij} converges, the segment line tension and its motion can be obtained. Then, through the calculation of each segment continuously, the motion of a mooring line can be obtained. Here, the properties of a bottom-end node of the i-th segment is regarded as the top node of the $(i-1)$-th segment, $(j_{i,1} = j_{(i-1),(N+1)})$.

4.4. Verification of Developed Multi-Component Mooring Line

In order to verify the capability of the proposed model for a multi-component mooring line, numerical simulations were carried out through two steps. First, the simulations were established for individual multi-component mooring line only excluding the coupling with a

floating structure while the second one took the coupling with a floating structure into consideration. It means the motion of the top point of the mooring line was given by prescribed motion in the first step simulation while the top point moves with the floating structure in the second step.

4.4.1. Verification of Multi-Component Mooring Line Alone

In the simulations, prescribed harmonic motion was adopted to introduce the top point motion of a mooring line while anchor motion was introduced by Eq. (3.47). In these simulations, various conditions of multi-component mooring line were evaluated to ensure the effectiveness of the proposed method. The variation consists of three conditions such as uniform segment line without clump weight, uniform segment line with clump weight, and non-uniform segment line with clump weight representing realistic conditions. In these simulations, the uniform segment line means the segment lines have identical properties.

Table 4.1. The properties of uniform multi-component mooring line without clump weight

Notation	Single-comp. mooring line	Muti-comp. mooring line
$l_{line.}$ (m)	1595.00	1595.00
$l_{seg.}$ (m)	-	1st : 400.00 2nd : 600.00 3rd : 595.00
w_c (kg)	299.80	299.80
D_c (mm)	117.00	117.00
E (kgf/m^2)	2.15×10^9	2.15×10^9
D_w (m)	500.00	500.00

(1) Uniform Multi-Component Mooring Line without Clump Weight

A multi-component mooring line consisting of three segment lines which have identical properties was examined and compared with a single-component mooring line having the identical property with the segment lines. This simulation is necessary to examine the ability of the present model in terms of representing a single-component mooring line. In the simulation, the segment properties of both mooring lines are same and the line length of the single-component line is equal to the total line length of the multi-component line. In other words, the multi-component mooring line is equivalent with the single-component mooring line. Those properties of both single- and multi-component mooring lines are shown in Table 4.1. The water depth denoted as D_w is taken as 500 m in this simulation.

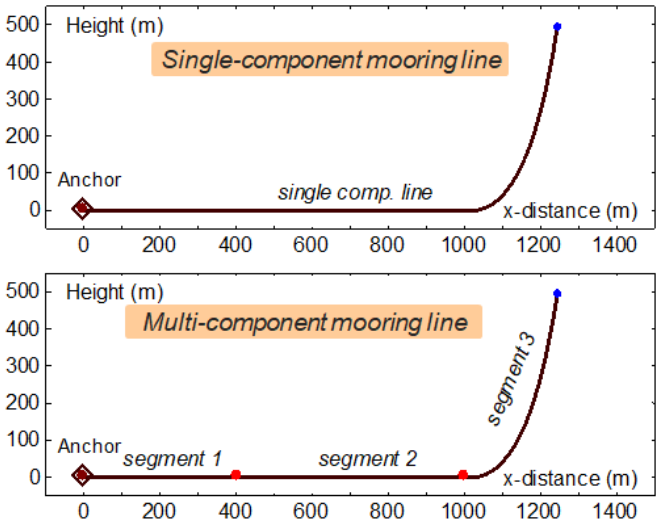

Fig. 4.11. Illustration of single and multi-component mooring line for the simulation of uniform multi-component mooring line without clump weight

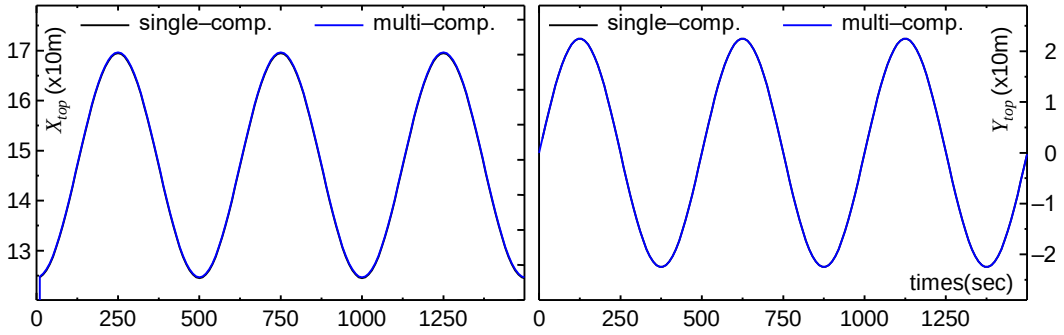

Fig. 4.12. Top point motions for uniform segment line without clump weight

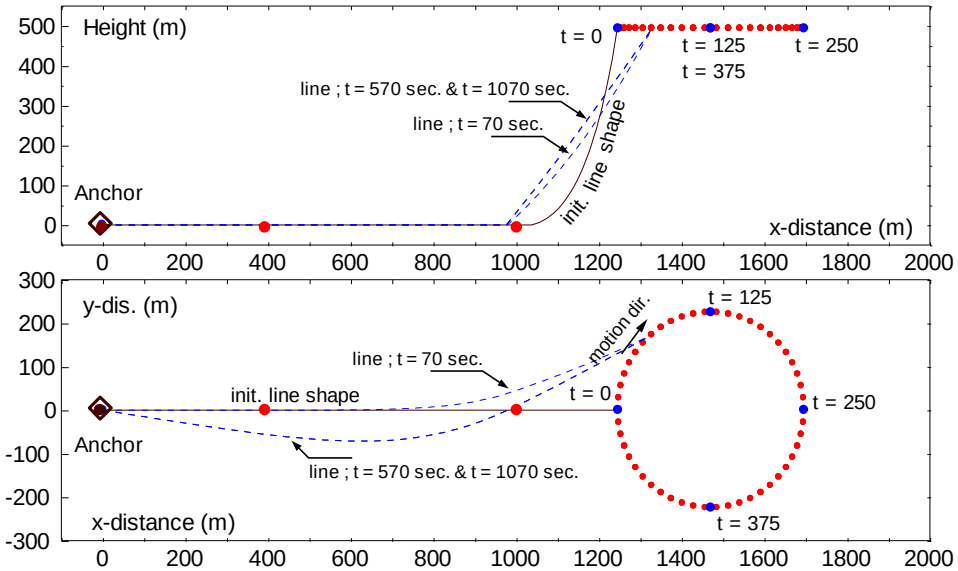

Fig. 4.13. Top point trajectory for uniform segment line without clump weight

The simulated result of the multi-component mooring line using the proposed method is compared with the result of the single-component line calculated by using single-component line lumped mass method described in Chapter 3. Numerical simulation code for single-component line based on Chapter 3 was built to examine the results of the present method. The total number of elements and the value of calculation time step were considered to be same with those used in the present method. Moreover, the initial line conditions such as prescribed motion of the top point and anchor condition are also same for both calculations. The illustration of both models is shown in Fig. 4.11.

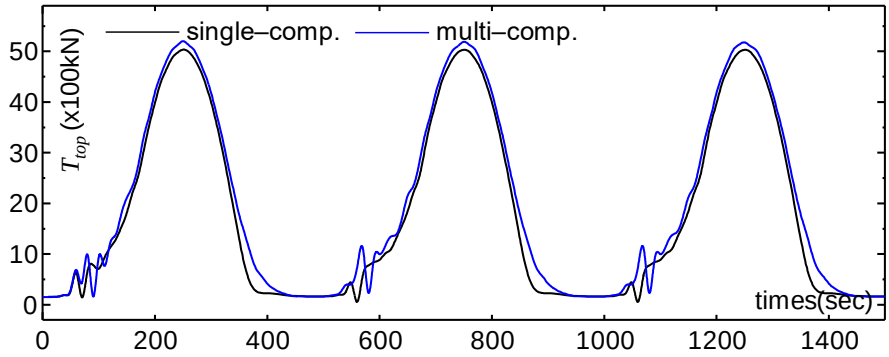

Fig. 4.14. Tension result for uniform segment line without clump weight

In the numerical simulation, the following assumptions were made. An anchor is fixed on the seabed with suitable holding power. The seabed is flat and friction force exists between mooring line and the seabed. Current velocity is regarded as zero and initial tension of mooring line $T_{Preten.}$ is 23 kN. Meanwhile, prescribed circular motion of 450 m in diameter in a horizontal plane is given to the top point of mooring line. Since the motion of the top point in vertical direction is usually smaller comparing with motions in the horizontal plane, the motion in z-axis direction can be neglected. The displacements of the top point of mooring line of both calculations are shown in Fig. 4.12. and Fig. 4.13.

Figure 4.14 shows the tension of the multi-component mooring line which consists of uniform segments. It was calculated by the present method. The tension of the single-component mooring line calculated by single line lumped mass method is also shown in the figure. The figure represents that both tensions have good agreement each other during the prescribed circular motion of the top end. At the peaks of tensions, a little difference is observed. It is considered that is was caused by the dynamic effect of mooring line motion due to the multi-component line conditions. When a mooring lines is treated as a single-component line, it is divided into some elements. They are treated as lumped masses and their masses are assumed to be equal to 1.0 δ_j except for the top and bottom end points. Meanwhile, when a mooring line is treated as a multi-component line, there are some joint

nodes between components next to each other. The mass of a lumped mass corresponds to the joint node is calculated as the summation of the lower suspended segments. It means the joint node is regarded as a cluster of mass, while the joint nodes are not considered in the single-component line. These differences cause the dynamic effect of multi-component line. The increase of dynamic effect in multi-component line provides the greater tension comparing with that of the single-component line.

Meanwhile, the irregularity appeared around the trough of the tension curve. It is expected that the drastic change of the direction of node velocity due to the circular motion of the top end point caused the irregularity. It can be observed in Fig. 4.13 especially for t = 70 sec., t = 570 sec., and t = 1070 sec. On these time, lifting up of mooring line occurs and the irregularity is induced. It causes the transient motion of the mooring line that increases the dynamic effect of the mooring line. Since the dynamic effect in multi-component line is greater than that in single-component line, the irregularity becomes greater in multi-component line as shown in the figure.

According to the results, it can be noted that the present method can delineate a single-component mooring line if it is considered as a multi-component mooring line which consists of segments having identical properties. The dynamic behavior of a multi-component mooring line can be also recognized well. The simulation results of both models show a similar tendency. Therefore, it can be confirmed that the present method is proper to apply for the prediction of the motions of uniform segment multi-component mooring line.

(2) Uniform Multi-Component Mooring Line with Clump Weight

To investigate the applicability of the present method for the exact multi-component mooring line, a uniform segment multi-component mooring line including a clump weight was examined. In this simulation, a multi-component mooring line properties presented by Nakajima et al. (1982) are used. The mooring line consists of two uniform segments and they are connected by a clump weight at the joint between them. Prescribed harmonic

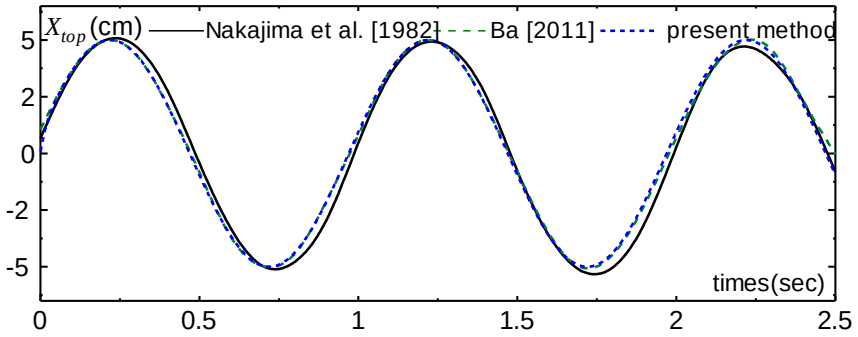

Fig. 4.15. Reproduced prescribed horizontal oscillation motion given for uniform multi-component line with clump weight

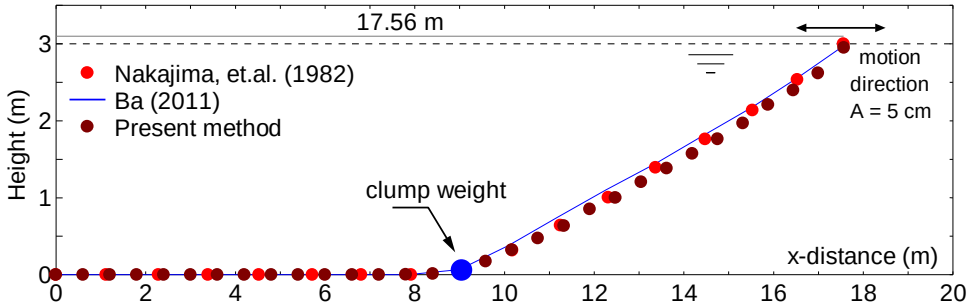

Fig. 4.16. Initial condition of uniform multi-component mooring line with clump weight

oscillation motion in horizontal direction with maximum amplitude of 5 cm has been used for describing the top point motions of the mooring line. The prescribed motion is shown in Fig. 4.15. In this case, both segments have 9.0 m length and the water depth is 3.0 m. The horizontal distance between the initial position of the top point and an anchor is 17.56 m.

The initial shapes of the uniform mooring line with a clump weight which is in static equilibrium condition are presented in Fig. 4.16. The figure shows the static condition obtained by the present method comparing with the static conditions given by Nakajima et al. (1982) and Ba (2011). Based on the figure, the static condition of the three methods shows reasonable agreement. Thus, it can be confirmed that the static calculation method given by the current method can reproduce the static multi-component mooring line well.

Time domain simulation results of the mooring line due to the prescribed motion of top point shown in Fig. 4.15 are presented in Fig. 4.17. In this figure, the tensions obtained by

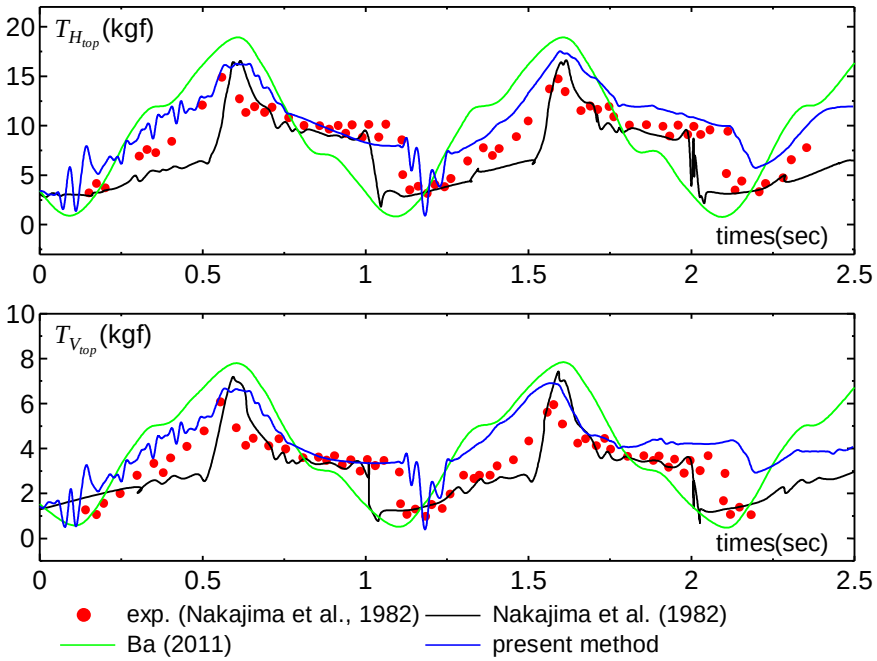

Fig. 4.17. Tension result of uniform multi-component mooring line with clump weight

the present method are compared with experimental and simulation results presented by Nakajima et al. (1982) and simulation results by Ba (2011). According to the figure, agreement among the results simulated by using the proposed method and the other three results can be observed. Though there are some differences between the result of the presented method and the others' results, the tendency of the tension curve is almost similar. The maximum tension obtained by the presented method is close to the others although it is not exactly the same. Comparing with the simulation results by Ba (2011), the differences can be denoted due to the fact that his results are obtained by the modified Lagrange's equation which doesn't allow the inclusion of line elasticity. Meanwhile, comparing with experimental and simulation results by Nakajima et al. (1982), the differences is occurred during the processes of lifting up and laying down of the clump that causes the irregular effect. Moreover, the differences are also caused by the adequate number of node and time increment Δt. The number of node and time increment must be determined properly.

In order to achieve better accuracy, a sufficient number of nodes must be considered further, since it strongly affects to the dynamics of mooring line particularly when dealing with small oscillation motion of the top point. This motion leads a low frequency motion of mooring line which increase nonlinear manner of each segment and hence it may decrease the accuracy of the results when the nonlinearity of mooring line increases due to certain condition such as lifting up/laying down of clump weight. As instance, the convergence of calculation for this calculation case depending on the number of nodes and time increment

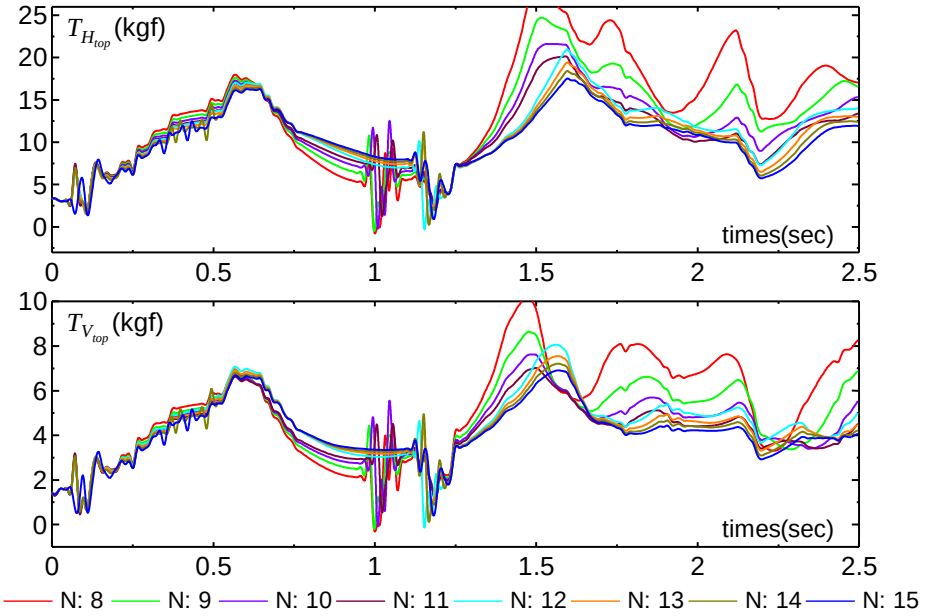

Fig. 4.18. Calculation convergence due to the different of the number of node (Δt=0.012 sec.)

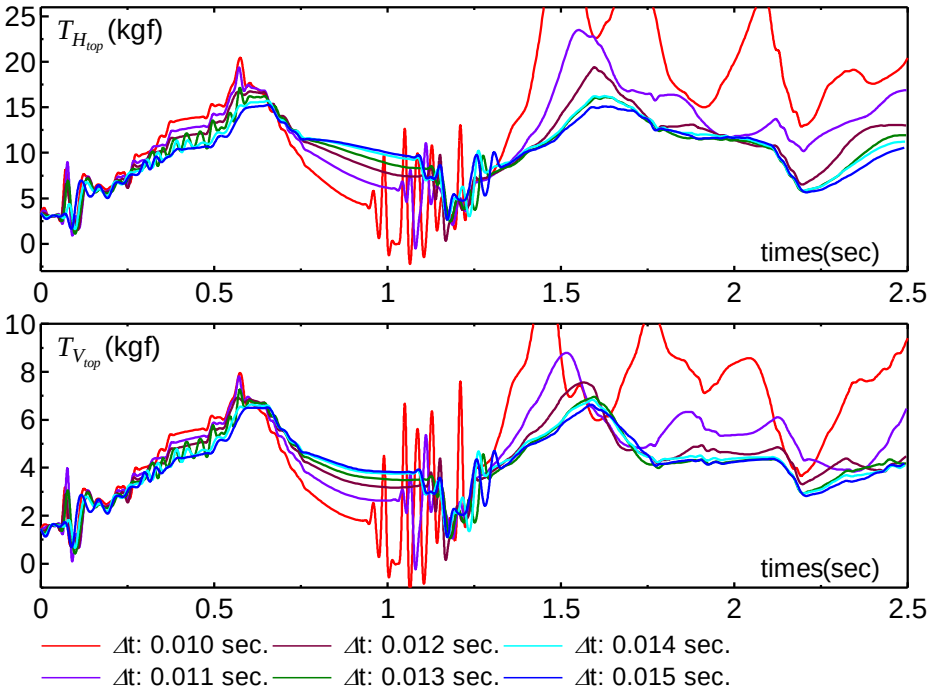

Fig. 4.19. Calculation convergence due to the different of increment time (N = 13)

are shown in Fig. 4.18 and Fig. 4.19 respectively. According to those results, when the numbers of node increases, calculation results are stabilized. Even so, the time increment also affects to the convergence of calculation as shown in Fig. 4.19. This condition can be noticed as negative values of tension appeared in Fig. 4.19 when the clump weight is lifted up/laid down while the time increment is not sufficient ($\Delta t = 0.010$ sec.). Thus, an analysis of integration stability and its convergence must be numerically investigated involving an appropriate combination of the number of node and time increment. Thereby, according to the investigation of the convergence of calculation, the number of nodes and time increment used for this case were set as 15 nodes and 0.012 sec. The calculation results are shown in Fig. 4.17.

According to Fig. 4.17, it is understood that transient motion exists when clump weight is lifted up and lays down back to the bottom. The weight of the clump weight affects to the drastic change of tension load on the mooring line. The impact load on mooring line tension occurs when the clump weight is lifted up from the seabed while the tension will change drastically when the clump weight lays on the seabed again. These loads can cause the sustainable effect that provides the irregular tension. The effects of these transient loads can be observed at the trough of tension curve that indicates the tension when clump weight is lifted up or lays down. In that part, the significant tension which can be recognized by small irregular tension still exists due to the sustainable effect of the transient loads. Moreover, the

irregular tensions are also affected by the small prescribed top point motion that may cause the oscillation effect of mooring line. It increases the oscillation of mooring line motions. In addition, discrepancies exist due to the differences of the number of element and the time interval used in the simulation.

Furthermore, based on the results, the present method can be introduced for the prediction of the dynamic behavior of multi-component mooring line with uniform segments including a clump weight. Even though the time series of tension doesn't exactly agree with the experimental and simulation results provided by other presented papers, the tendency of the tension as well as the maximum tension are close to the others. The differences of present method against the others can be described reasonably. Despite that, the trend of the tension is in good agreement, the present method can be considered to be applicable. Therefore, the present lumped mass method can be used to investigate the uniform multi-component line with the attached clump weight.

(3) Non-Uniform Multi-Component Mooring Line with Clump Weight

To guarantee the application of the technique presented in this paper, a realistic multi-component mooring line is used for examining the validity of the method. The multi-component mooring line consists of three segments which have different properties respectively. An anchor and a clump weight are also included in the mooring line system to represent a realistic condition of a mooring line. The clump weight is connected at the joint

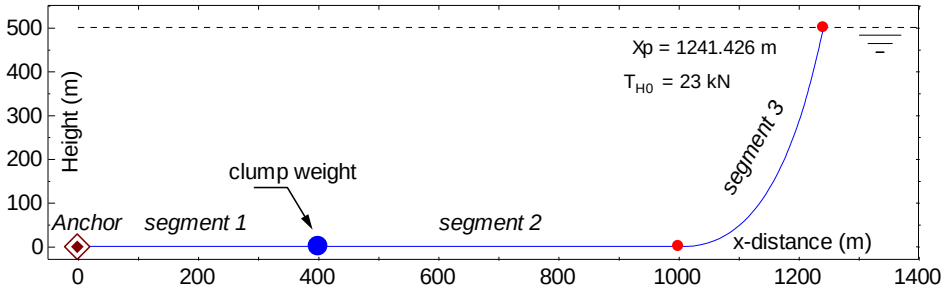

Fig. 4.20. Non-uniform multi-component mooring line with clump weight

Table 4.2. The properties of non-uniform multi-component mooring line with clump weight

Notation	Segment 1	Segment 2	Segment 3
$l_{seg.}$ (m)	400.00	600.00	595.00
w_c (kg)	99.80	59.80	299.80
D_c (mm)	109.00	87.00	117.00
E (kgf/m^2)	1.21×10^9	1.03×10^9	2.15×10^9
W_a (kg)	17250.00	T_{Preten} (N)	23000.00
W_C (kg)	2897.52	D_w (m)	500.00

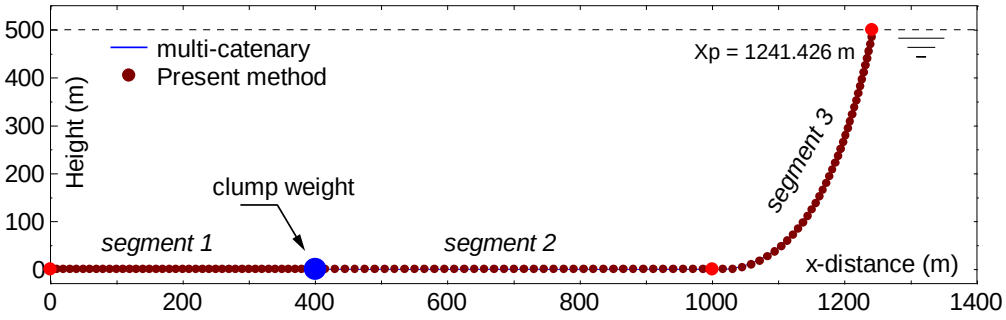

Fig. 4.21. Initial condition non-uniform multi-component mooring line with clump weight

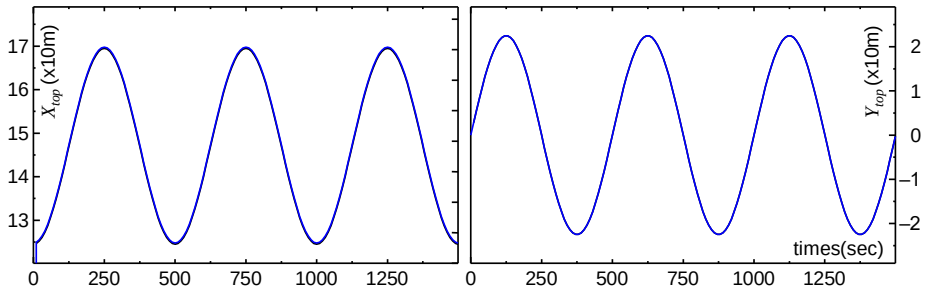

Fig. 4.22. Non-uniform multi-component mooring line with clump weight

of the first and the second segments while the other joint is left without a clump weight. The illustration of the mooring line condition is figured in Fig. 4.20 while the characteristics of each component of mooring line can be seen in Table 4.2. Furthermore, the initial conditions of the mooring line calculated by this method comparing with the multi-catenary method are shown in Fig. 4.21.

The simulation of dynamic motions for this mooring line is conducted through the prescribed circular motion of the top point that is similarly used for the uniform multi-component line without a clump weight. The simulation conditions are same with that, however, the anchor motion is introduced by Eq. (3.47). The displacement of the top point is presented in Fig. 4.22. In this simulation, to investigate the effect of a clump weight and anchor holding power, the whole segments are endeavored to be suspended due to the

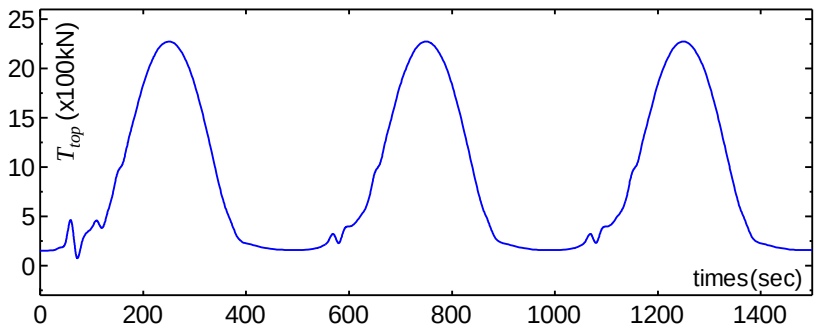

Fig. 4.23. Tension for non-uniform multi-component mooring line with clump weight

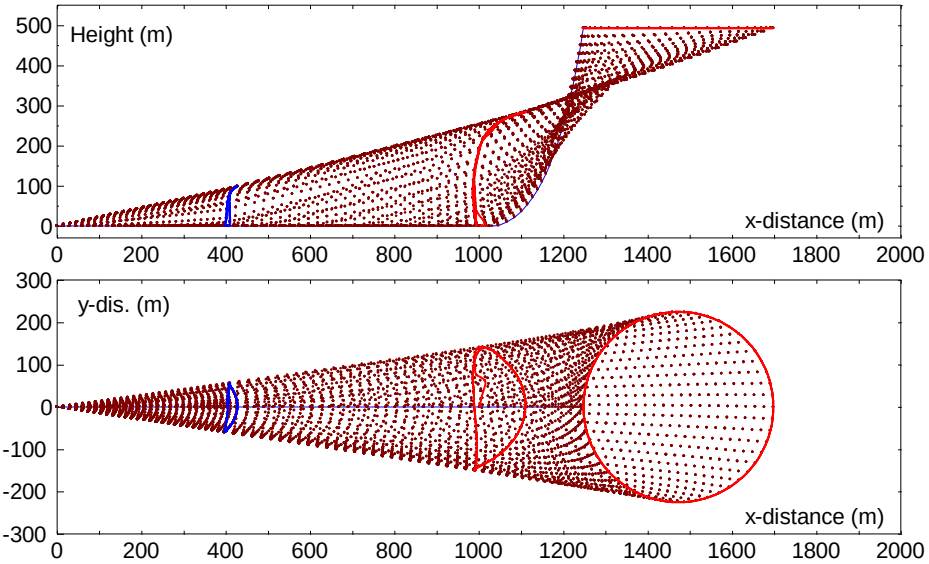

Fig. 4.24. Shape of dynamic motion of the non-uniform multi-component mooring line

prescribed motion by the top end point. Once the whole segments are suspended, the overall dynamic motions of multi-component line part including the clump weight can be presented. Thus, the capability of the present method for non-segment multi-component mooring line can be assessed.

The results of the tension for this simulation are depicted in Fig. 4.23. Based on the figure, time domain simulation results of tension show a reasonable condition because the tension has proper tendency corresponding the motion of the top point. Here, the tension firstly increases as the displacement of the top point increases. After it reaches the maximum value, the tension decreases due to the motion of the top point which moves toward the initial position. It is repeated for three times. In this result, similarly as shown in Fig. 4.8, a little irregular tension of mooring line is also observed when the top point moves with the maximum velocity. This irregularity is caused by the transient motion of the top point. In this condition, the upper part of the mooring line is forced to move with sudden change of acceleration and it causes the sudden little impact load to mooring lines.

Meanwhile, the motion of the mooring line can be observed by the locus of mooring line shown in Fig. 4.24. According to this figure, it can be denoted that the motion of the mooring line shows complicated trajectory, while the top point moves with circular motions. Moreover, the motion of clump weight also can be recognized through the figure. The clump weight moves in three-dimensional space while the anchor is remained to stay at the initial position because of its holding power. Based on these results, it can be confirmed that the proposed method can be useful to investigate the three-dimensional multi-component mooring line motion even for non-uniform segment and with attached clump weight.

4.4.2. Verification of Multi-Component Mooring Line Coupled with Floating Offshore Structure

(1) Conditions of Verification

Because the research which treats a multi-component mooring line in three-dimensional manner is limited, the proposed multi-component mooring line model is verified against three-dimensional single-component mooring line model which has been validated by experiments (Nakajima et al., 1983). In order to represent identical single-component mooring line models in both models, a multi-component mooring line composed of three segments having identical properties is used in the developed model. The properties and main particulars of mooring lines used in both models are completely same. The properties of an anchor connected to the both mooring lines are also equal. The properties of single- and multi-component mooring lines presented in Table 4.1 are used for both single- and multi-component mooring lines respectively in this verification.

Both single- and multi-component mooring lines are then coupled with a ship-type floating structure subjected to wave, wind, and current loads to verify the effectiveness of the proposed multi-component mooring line model. The coupled-motion between the mooring line and the floating structure is calculated by using the coupled model presented in Chapter 2 (Eqs. (2.134)-(2.135)). In this coupled model, the floating structure is considered to be moored by single point mooring line system at the sea having 500 m depth. A mooring line is connected to the vessel at bow and deployed toward the bow direction. The mooring line angle ξ_1 is $0°$ while an anchor is attached on the bottom-end of the mooring line.

Furthermore, in order to consider the effect of the directions of external disturbances, two cases are investigated in this verifications works. In the first case, noted as case A, all external disturbances come from the same directions. On the other hand, the direction of wind is different from those of wave and current in the second case (case B). Wave height, wind speed, and current velocity are assumed to be 2 m, 10 m/s, and 1 knot respectively.

(2) Verification Results

A ship-type floating offshore structure adopted from ESSO OSAKA which has principal dimensions shown in Table 3.3 is used to be coupled with a single- and multi-component mooring lines described above. Both coupled models are then examined and compared each other in terms of mooring line tension, the motions and the trajectory of the floating structure for the two environmental loads cases. In the case A, wave, wind, and current come from the same direction which is in $30°$ relative to the bow, while the directions of wave, wind, and current in the case B are assumed to be $30°$, $0°$, and $30°$ respectively.

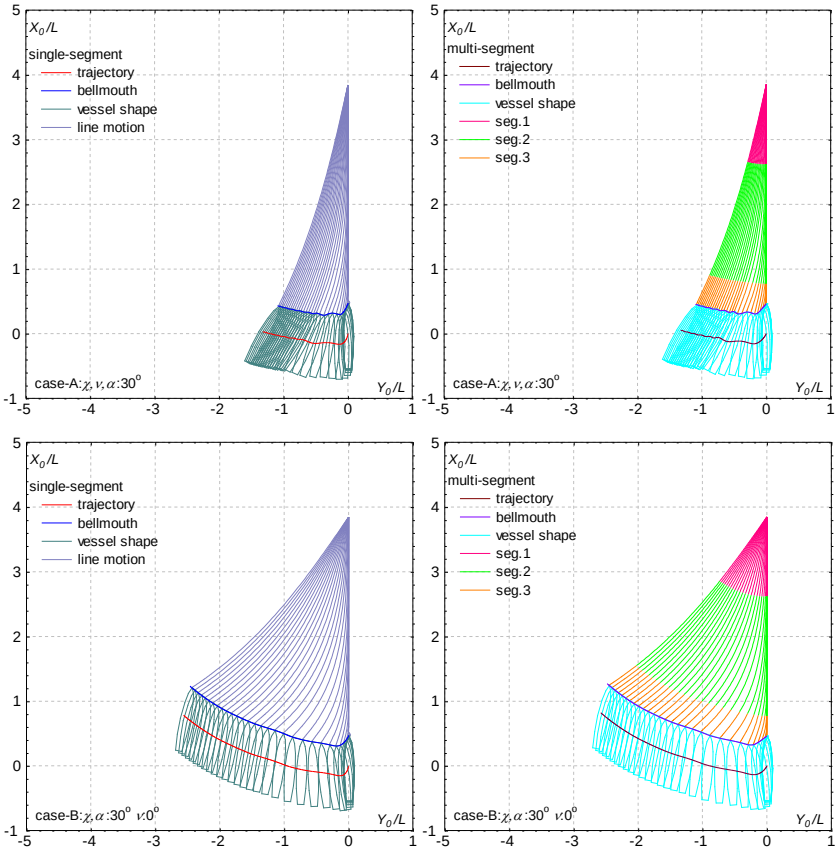

Fig. 4.25. Trajectories in verification of multi-component mooring line

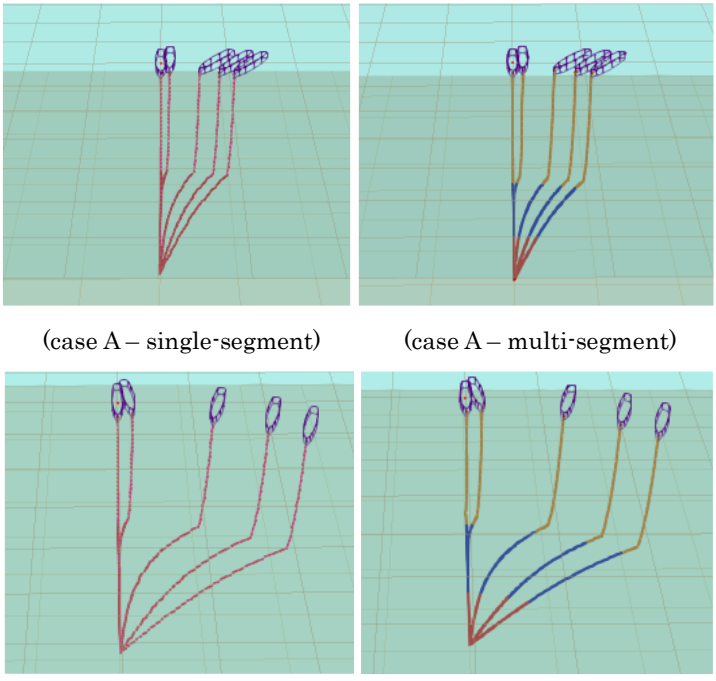

(case A – single-segment) (case A – multi-segment)

(case B – single-segment) (case B – multi-segment)

Fig. 4.26. Three-dimensional motions of mooring line for verification case (every 4000 sec.)

The trajectories of the floating structure with single- or multi-component mooring line for both cases are depicted in Fig. 4.25. According to the figure, since all external disturbances dominantly come from $30°$ for the case A, the heading angle of the ship-type floating offshore structure changes toward the direction of the disturbances. On the other hand, the ship-type floating offshore structure moves farther away in lateral direction comparing with the case A due to the increase of lateral force and yawing moment by the external disturbances. The figure also shows that the trajectories and mooring line motions for single- and multi-component mooring lines are quite similar. This similarity is portrayed in detail in Fig. 4.26 showing the three-dimensional motions of the mooring lines. It is observed that the proposed multi-component mooring line model can reproduce the motion of single-component mooring line calculated by using the three-dimensional single-component mooring line model proposed by Nakajima et al. (1983).

Mooring line tension and 6 DOF motion of the vessel with single- or multi-component mooring line in the two cases are presented in Fig. 4.27 and Fig. 4.28. According to these figures, line tension and vessel motions for both mooring line models indicate good agreement, though there is slight discrepancy at the beginning of the simulation. It is considered that the discrepancy caused by the transient environmental loads acting on the floating structure which cause instability in the calculation of transient tension at the beginning of the simulation. Then, this discrepancy can be neglected. Even further, this discrepancy does not affect too much to the trajectories and the motions of the vessel as shown in Fig. 4.28. In the figure, although the motions are not exactly same, the tendency and magnitude of the motions calculated by the two mooring line models have good congruence. This congruence is even denoted for all motion modes in the both cases. Accordingly, the developed multi-component mooring line dynamics model can be used to

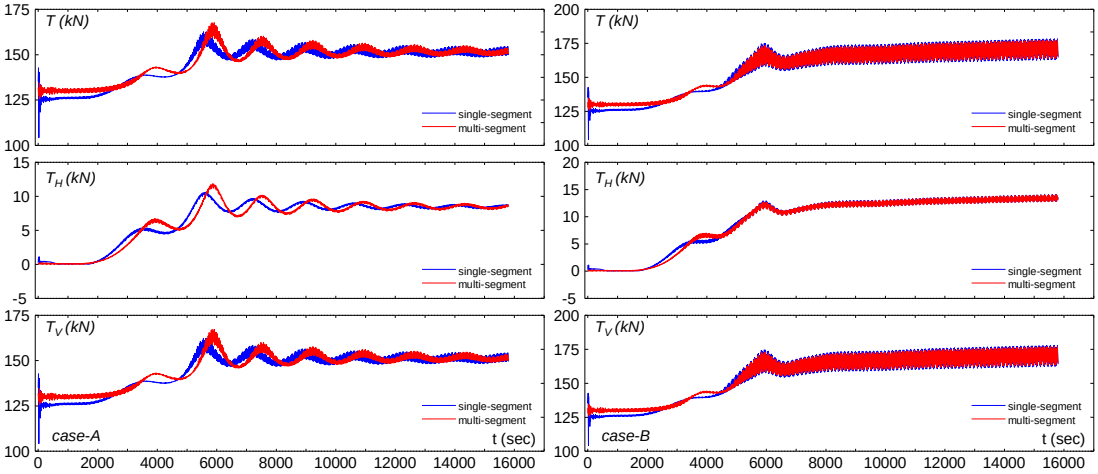

Fig. 4.27. Mooring line tension of single- and multi-component mooring lines

investigate the influence of multi-component mooring line on coupling motion of a floating offshore structure.

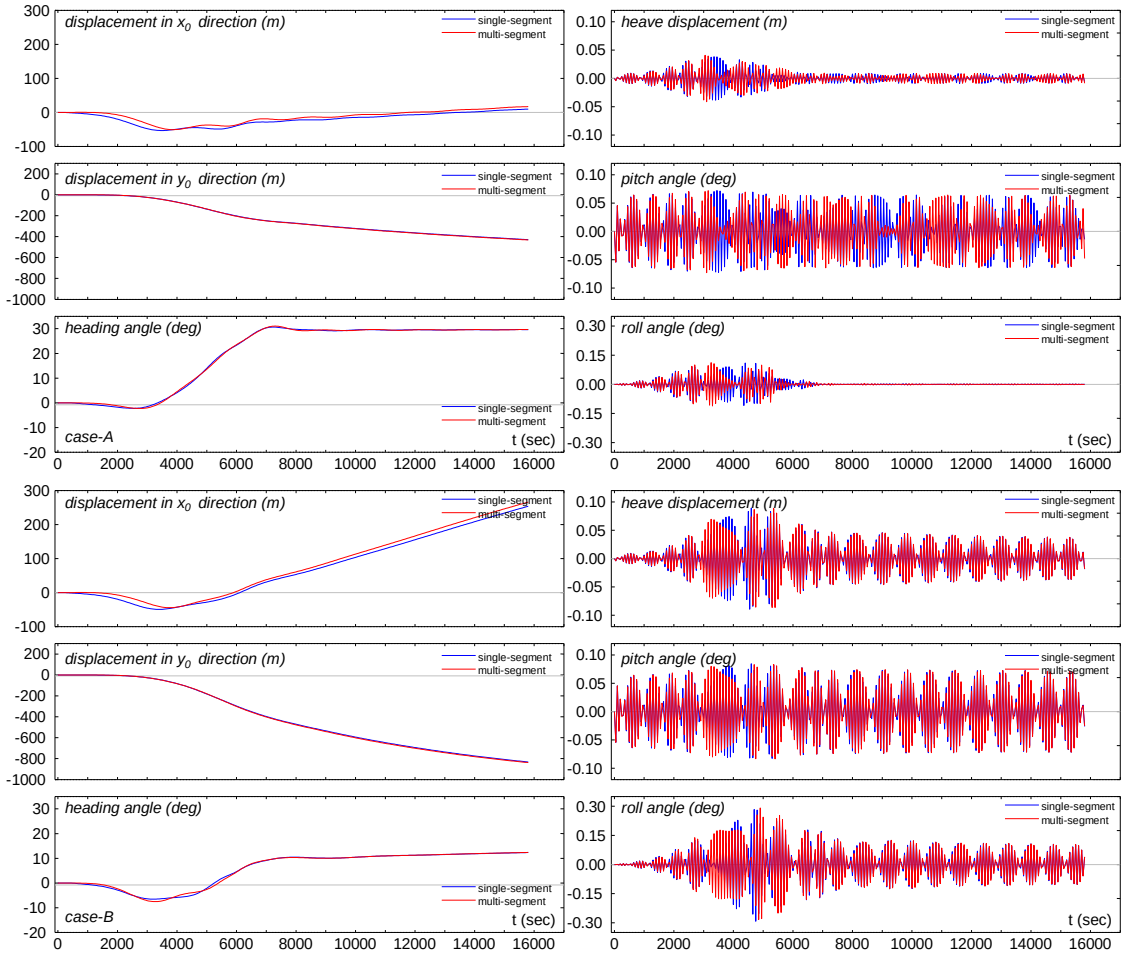

Fig. 4.28. The motion of floating structure with single- and multi-component mooring lines

4.5. Comparison Against Two-Dimensional Model Results

4.5.1. Conditions of the Comparison

To investigate the effect of three-dimensional manner of a mooring line in the analysis of mooring line dynamics, the developed three-dimensional dynamics model is compared with two-dimensional mooring line model. Both two- and three-dimensional models are implemented to simulate the motion of a mooring line with a ship-type floating structure used in Section 3. The mooring line is regarded as a multi-component mooring line consisting of various segment line properties while the mooring line configuration and water depth are same with those used in Section 4.4.2. The properties of each line segment presented in Table 4.2 are used excluding the clump weight while pretension is given as 4500 N.

Two-dimensional dynamics model used for the comparison is literally similar with the developed three-dimensional model, however, the lateral motion of a mooring line (y-axis direction) is neglected. It means that all force components coming from the lateral direction of the mooring line and their effects are omitted to only reflect the two-dimensional manner of a mooring line. Generally speaking, only longitudinal and vertical forces are affected to the mooring line tension.

In this comparison work, three different cases are investigated to observe the effect of three-dimensional manner under the various directions of the environmental loads. The first case, denoted as Case I, is conducted with $5°$ of wave, wind, and current directions to represent the environmental loads coming from the direction close to the longitudinal direction of the mooring line as well as the heading of the floating structure. $30°$ of all external disturbances is applied for considering the effect of lateral environmental loads and it is presented in Case II. Finally, the directions of wave, wind, and current are assumed as $0°$, $15°$, and $30°$ respectively for Case III to verify the effect of three-dimensional model under the various combinations of the external loads. Wave height, wind speed, and current velocity are assumed to be 4 m, 20 m/s, and 2 knot respectively.

4.5.2. Comparison Results

The comparison results of two- and three-dimensional models are presented in Fig. 4.29 to Fig. 4.31. The results of mooring line tension for both models can be observed in Fig. 4.29. According to the figure, the tension of both models for Case I is not too much different. Forces acting on the three-dimensional mooring line model are dominantly generated by longitudinal forces since all external forces come from the longitudinal direction of the mooring line. Consequently, forces coming from the lateral direction of mooring line are measly and not affected to the tension of the three-dimensional mooring line model significantly. This condition is alike with the condition of two-dimensional calculation which does not take the lateral force into account. Therefore, the trajectory of the floating structure and the mooring line motions for Case I shown in Fig. 4.30 and Fig. 4.31 are almost similar.

However, as the increasing of the lateral forces acting on the mooring line, the mooring line tension increases as depicted in Fig. 4.29 for Case II. The lateral forces enlarge the dynamic motions of the mooring line and hence these forces induce the mooring line tension. Both horizontal and vertical components of tension are also different between the two models since the mooring line motion is different as noted in Fig. 4.29-Case II. The trajectories of the floating structure for both models which can be discerned in Fig. 4.30-Case II are slightly different due to the difference of the mooring line tension. Based on the

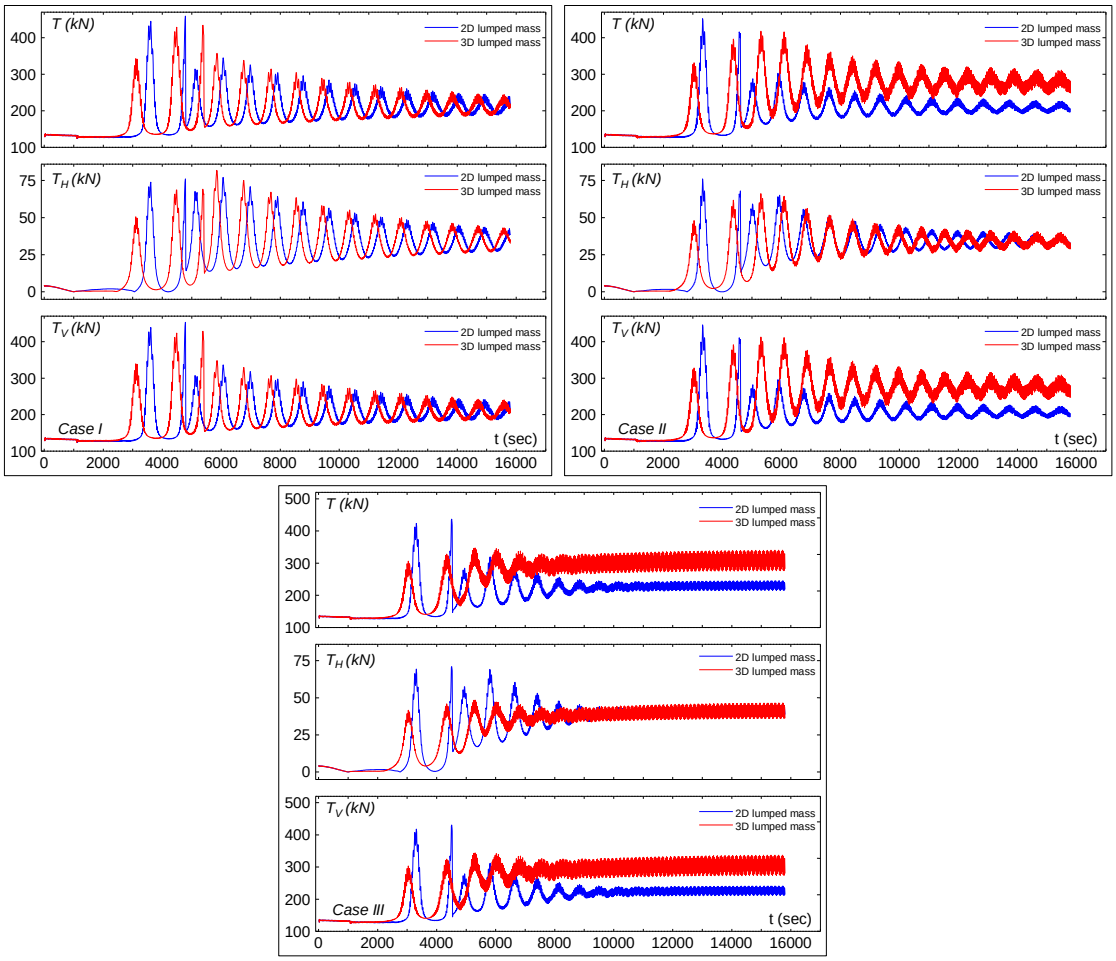

Fig. 4.29. Comparison of mooring line tension for two- and three-dimensional models

figure, the floating structure with the three-dimensional lumped mass model is a little bit more pulled by the mooring line since the mooring line tension of the three-dimensional model is greater than that with the two-dimensional model. It can be confirmed by the trajectory of a bellmouth position with the three-dimensional model which is somewhat close to the anchor position comparing with that with the two-dimensional model. More detail, the three-dimensional motion of the floating structure and the mooring line are portrayed in Fig. 4.31-Case *II*.

Meanwhile, a tendency similar to the results for Case *II* appears for Case *III* in which the various directions of the environmental loads are considered. They are presented in Fig. 4.29 and Fig. 4.30 for Case *III* and can be verified in detail in Fig. 4.31-Case *III*. According to the figures, the floating structure with the three-dimensional model in this case is also slightly more pulled by the mooring line than that with two-dimensional model. The mooring line tension generated by the three-dimensional model is greater than that for two-dimensional model. The mooring line tension increases due to the effect of lateral force

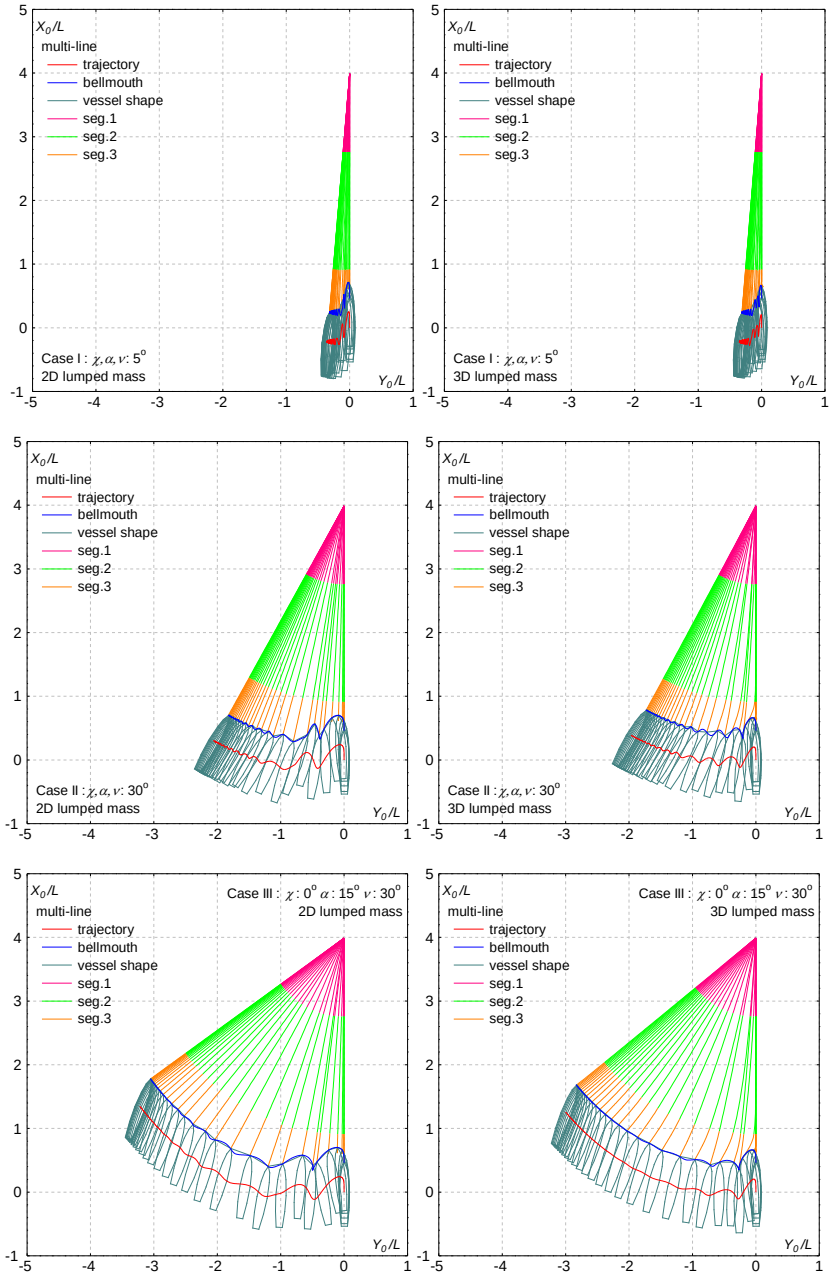

Fig. 4.30. Comparison of the trajectories for two- and three-dimensional models

components induced by the environmental loads coming from various directions.

Based on these three comparison results, even the trajectory of the floating structure with two- and three-dimensional models are similar, some peculiarities occur in the implementation of a two-dimensional model, especially for the mooring line tension. These peculiarities increase when considering the complicated directions of environmental loads. This situation can affect to the accuracy of the prediction of structural reliability for the mooring line and hence the safety of the floating structure. Therefore, the results of dynamic

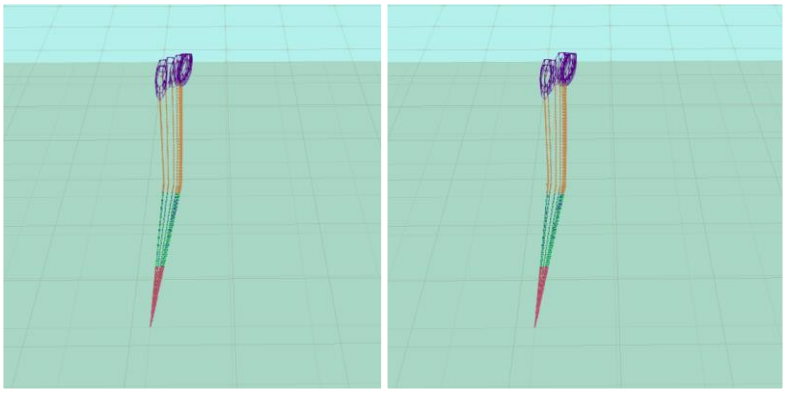

(case I – 2D model) (case I – 3D model)

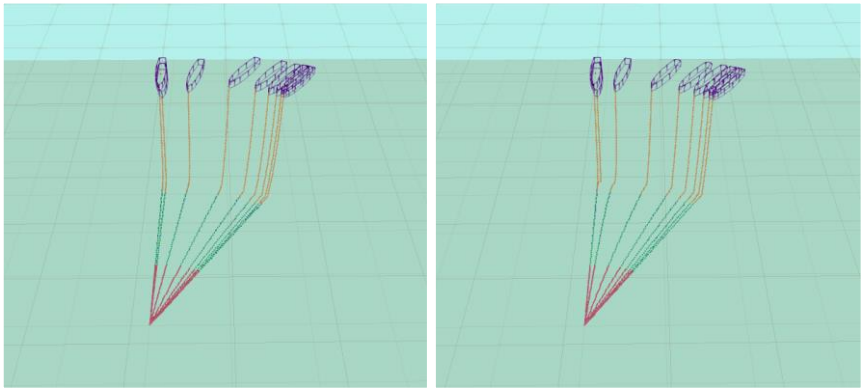

(case II – 2D model) (case II – 3D model)

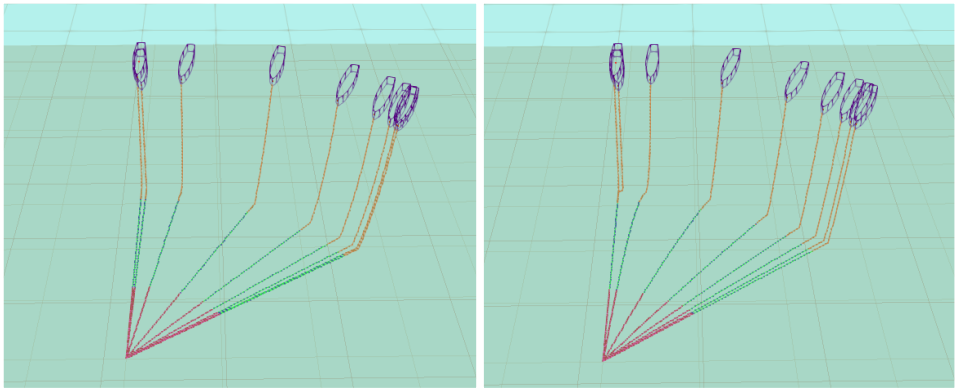

(case III – 2D model) (case III – 3D model)

Fig. 4.31. Comparison of three-dimensional motion of mooring line for two- and three-dimensional models

performance of a mooring line based on a two-dimensional model may inflict the lack of calculation accuracy and thereby the three-dimensional treatment of mooring line is necessary.

4.6. Concluding Remarks

Three-dimensional multi-component mooring line dynamics model has been developed in this chapter based on three-dimensional lumped mass method. The dynamics model of multi-component mooring line motions was developed by extending the single-component mooring line lumped mass method. The model takes the complexity which may inherent to a multi-component mooring line including segments having different properties, line-seabed interaction, elasticity, and anchoring problem into consideration. The motions of a multi-component mooring line are obtained through the individual motions of its segments allowing the motion of the joint.

To examine the capability of proposed method, various conditions of mooring line were investigated. A uniform segment multi-component mooring line without a clump weight is firstly calculated and compared with single-component mooring line lumped mass method. The comparison results indicate a good agreement. A multi-component mooring line consists of uniform segment with a clump weight was investigated and compared with the other numerical and experimental results presented in published papers. These results also show reasonable agreement with both numerical and experimental results. Finally, a multi-component mooring line made of the combination of non-uniform segments and a clump weight as well as an anchor was evaluated. The dynamic motion of the multi-component mooring line can be investigated by using the present method. Therefore, confirming the results, the three-dimensional dynamic analysis of multi-component mooring lines can be investigated by the proposed method even for the mooring line consists of non-uniform segment properties, a clump weight and an anchor. The inclusion of line-seabed friction forces and the motion of an anchor are also included in the proposed dynamics model.

Furthermore, to verify the implementation of proposed model to be coupled with a floating offshore structure, the developed dynamics model is then coupled with a ship-type floating offshore structure and firstly verified against the motion of a single-component mooring line simulated by validated numerical method. The verification is carried out by comparing the simulated motion of a multi-component mooring line consists of identical segment with the motion of an equivalent single-component mooring line. Good agreements are gained between the results of both mooring lines in the coupled analysis under wave, wind, and current.

The developed model is then compared with two-dimensional dynamics model to investigate the effect of three-dimensional motions in calculating mooring line dynamics. The comparison results note that the similar results are gained when the external disturbances dominantly come from the longitudinal direction of the mooring line. However, the mooring

line tension significantly increases when the external forces coming from the lateral direction of mooring line increase. Moreover, the comparison results also conclude that the dynamic performance of mooring line needs to be conducted in three-dimensional manner since the implementation of two-dimensional model may give the deficiency of pertinence, especially in complicated external loads condition.

According to these results, the three-dimensional dynamics model of a multi-component mooring line can be considered to be applied for performing the coupled-motion analysis of a floating offshore structure moored by multi-component mooring line system. Even further, this developed dynamics model can be implemented for investigating the motion of moored floating offshore structure considering realistic conditions including the realistic properties of the multi-component mooring line as well as realistic environmental conditions.

Chapter 5 Coupled Analysis of Three-Dimensional Multi-Component Mooring Line and Floating Offshore Structure

5.1. Introduction

In Chapter 4, three-dimensional dynamics model for a multi-component mooring line is proposed and it is successfully implemented for coupled-motion analysis of a floating offshore structure under environmental loads. Since the combination of environmental forces and water depth as well as mooring line properties may affect the performance of mooring line and hence the coupled-motion of the floating structure, the implementation of the proposed dynamics model needs to be investigated by considering possible environmental conditions.

Moreover, according to literature studies, the investigation of dynamic motions of a floating offshore structure taking account of possible environmental conditions at target location is considerably important (Fontaine et al., 2013). The motions are sensitive to the directions of environmental loads (Lopez et al., 2017) and even vulnerable to the both in-line and in-between line conditions (Svalastog, 2013). Thus, possible environmental loads including collinear (all external disturbances come from same direction) / non-collinear (each external disturbance comes from different direction individually) and in-line / in-between line conditions must be considered when performing the coupled motion analysis of a floating offshore structure with mooring lines.

This chapter performs numerical simulations of a ship-type floating offshore structure moored by using the three-dimensional dynamics model of multi-component mooring line under environmental conditions based on measured data at target location. The multi-component mooring line model is developed by extending three-dimensional lumped mass method presented in Chapter 4. Actual meteorological and oceanographic (metocean) data and multi-leg mooring line system consisting of multi-component mooring line type are implemented in the simulations. The simulations representing the coupled model of the mooring line and the floating structure is then used for investigating the impact of the present dynamics model of mooring line on the response of the floating structure and the tension of the mooring line itself. Various cases involving collinear and non-collinear environmental loads combining with inline and in-between line conditions are investigated.

In this chapter, the conditions of the numerical simulations are described in Section 5.2 while the overview of metocean data at target location used in these simulations are presented in Section 5.3. Furthermore, the results of the simulations are discussed in Section

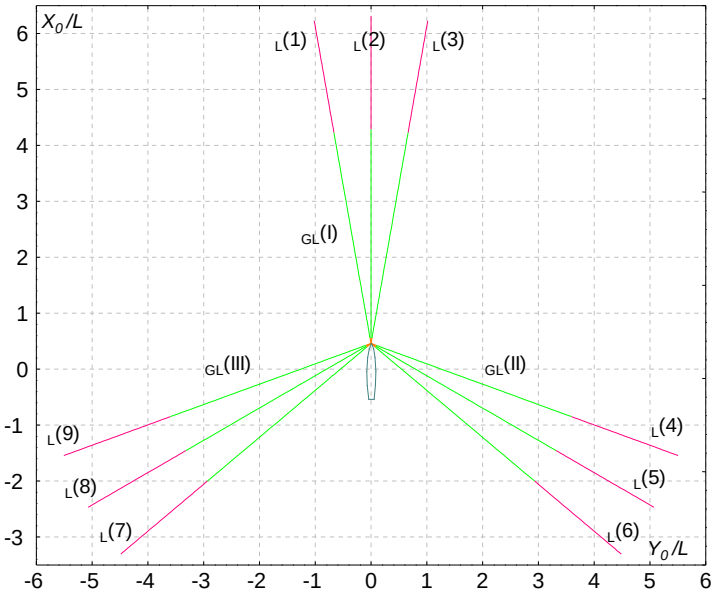

Fig. 5.1. Mooring line arrangement of the ship-type floating offshore structure

5.4. At the end, this chapter is concluded by Section 5.5, to summarize the implementation of the coupled dynamics model applied for the possible environmental conditions based on measured metocean data at the target location.

5.2. Simulation Conditions

In order to verify the capability of the proposed three-dimensional dynamics model of a multi-component mooring line, analyses of coupled motions of multi-component mooring lines and a ship-type floating offshore structure are conducted. In these analyses, the floating structure is moored by single point multi-leg mooring system whereby the mooring lines are collected to three groups. Each group contains three multi-component mooring lines and they are deployed by $10°$ each other. Meanwhile, the groups of the mooring lines are spread off by $120°$. The schematic view of the multi-component mooring lines coupled to the ship-type floating offshore structure is shown in Fig. 5.1.

Fig. 5.2. Location of Masela field used in the numerical simulation analyses

The moored floating structure is assumed to be subjected to environmental loads representing operations at sea. The environmental loads are generated based on measured metocean data at target location. The newest gas field discovered in Indonesia known as Masela field is adopted as the target location used in the analyses. The principle dimensions of the ship-type floating offshore structure are assumed referring those of a VLCC (ESSO OSAKA) which has equivalent capacity complying with the required dimensions at the offshore field. The location of the Masela field is presented in Fig. 5.2 while the principle dimensions of the floating structure are presented in Table 3.3.

Additionally, the properties of a multi-component mooring line are defined based on conventional mooring line properties used in Indonesian sea. The combination of R3 studless chains having different material properties and length are used in order to attain the sufficient tension and cost efficiency of the mooring line. In the combination, the strongest segment with enough length is placed at the bottom of the mooring line to increase holding power. The middle segment has the weakest properties, but is the longest segment, to accommodate the flexible motions of the mooring line. The uppermost segment is composed by material

Table 5.1. Mooring line properties for numerical simulation analyses

Notation	Segment 1	Segment 2	Segment 3
$l_{seg.}$ (m)	660.00	1595.00	220.00
w_c (kg)	322.93	210.16	299.80
D_c (mm)	127.00	102.00	117.00
E (kgf/m^2)	4.89×10^9	1.03×10^9	2.15×10^9
W_a (kg)	17250.00	T_{Preten} (N)	23000.00
$Type$	Chain	Chain	Chain

having sufficient strength and enough length to restrain tension acting on the connection point of the floating structure without giving excessive weight. The properties of these segments are presented in Table 5.1.

Moreover, appropriate simulation cases must be considered to verify the proposed mooring line model. In present analyses, simulation cases for collinear (wave, wind, and current come from same direction) and non-collinear (wave, wind, and current come from different directions) conditions given by the DNV-OS-E301 rule are firstly applied. However, since the consideration of other combinations of external disturbances must be important in the analyses, three other combinations are also investigated. The directions of external disturbances in these three combinations are the actual direction of wave based on the measured data (Case 2), a direction between two groups of the mooring lines (Case 3), and a direction in-line with one of the mooring line groups (Case 4). Simulations for these three

Table 5.2. Various cases used for numerical simulation analyses

Conditions	Case No.	System	External disturbance directions (deg.)		
			Wave	Wind	Current
Rules	Case 1A	Collinear	15		
	Case 1B	Non-collinear	0	30	45
Measured data	Case 2A	Collinear	22.3675		
	Case 2B	Non-collinear	22.3675	52.3675	67.3675
In between line	Case 3A	Collinear	60 (between line group I & II)		
	Case 3B	Non-collinear	60	90	105
In-line	Case 4A	Collinear	120 (in-line line group II)		
	Case 4B	Non-collinear	120	150	165

cases both in collinear and non-collinear conditions are carried out. The wave direction in these non-collinear conditions is defined referring to the collinear condition. Meanwhile, the directions of the other disturbances are defined against the wave direction by following configuration given in the rule. It means that the wind and current direction are defined as $30°$ and $45°$ against wave direction. In these simulations, the collinear condition is denoted as subcase A while the non-collinear condition is subcase B against the main cases (Case 1-4). The entire variation of cases applied in the analyses including their notation name are presented in Table 5.2.

5.3. Metocean Data

When environmental data representing certain location are considered, metocean data at the considered location are required. In these simulations, a set of metocean data at the Masela field must be applied to calculate environmental loads acting on the ship-type floating offshore structure and its mooring lines. The metocean data including wave height, wave period, wind speed, and their directions are taken from the global database presented in the ftp site of National Oceanic and Atmospheric Administration (NOAA). The metocean

Table 5.3. Summary of metocean data characteristic provided by NOAA

Characteristic	Information
Latitude range	$-77.5° \sim 77.5°$
Longitude range	$0° \sim 359.5°$
Mesh size	$0.5° \times 0.5°$ (55.56 km $\times$ 55.56 km)
Time (1 day)	00.00 ; 03.00 ; 06.00 ; 09.00 ; 12.00 ; 15.00 ; 18.00 ; 21.00
Weather data	wave height, wave period, wave direction, wind speed (north-south, east-west)

Table 5.4. Mooring line properties for numerical simulation analyses

Parameter	Value
Water depth	783 m
Wave height (100-years)	4.9612 m (H_s)
Wave period (100-years)	17.1268 sec. (T_p)
Wind speed (100-years)	21.2426 m/sec.
	(10 m above sea level in 1-hour mean wind)
Wave & wind directions (100-years)	22.3675 deg. (relative to North)
Current speed (10-years)	1.10 m/s = 2.1382 knots

data contain wind and wave information for the worldwide every 3 hours in a mesh unit (based on latitude and longitude coordinate). The summary of metocean data provided by NOAA is shown in Table 5.3. The metocean data at (-09.0;130.50) representing the closest latitude and longitude coordinate of Masela field which are taken for these simulations.

Furthermore, water depth is taken from NOAA National Center for Environmental Information while current velocity is defined from DNV-OS-E301 rules due to the limitation of available data. These metocean data are further processed to provide long-term environmental data required by the rules/regulations. In this study, DNV-OS-E301 rule is adopted. According to the rule, significant wave of wave height H_s and wave period T_p, wind data for100-years return period, and current data for 10-years return period are generated as presented in Table 5.4.

5.4. Simulation Results Analysis

5.4.1. Simulation Based on Applied Rule – Case 1

In this simulation, case variations for collinear (Case 1A) and non-collinear (Case 2B) conditions are taken according to DNV-OS-E301 rule. All external disturbances for the collinear condition come from $15°$ relative to the bow, while wave, wind, and current come from $0°$, $30°$, and $45°$ respectively for the non-collinear condition. The trajectory of the ship-type floating offshore structure and horizontal forces acting on the floating structure both in the collinear and non-collinear conditions are presented in Fig. 5.3.

According to the figure, it can be found that the mooring lines can move simultaneously interrelating each other following the external disturbances. The final heading of the floating structure in both collinear and non-collinear conditions correspond to the directions of the external disturbances. Moreover, it can be understood from vessel shapes drawn every 500 seconds on the trajectories that the vessel experiences larger lateral motion in the non-collinear condition comparing with the collinear condition. The lateral motion is caused by

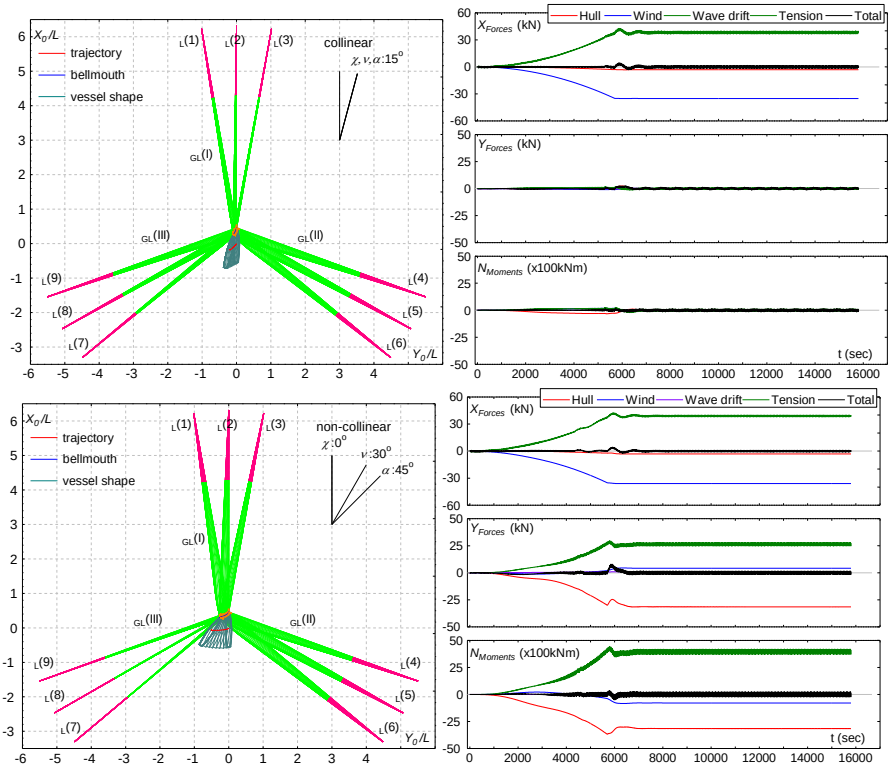

Fig. 5.3. Trajectories and horizontal forces – Case 1 (collinear and con-collinear)

the increase of lateral force and yawing moment due to the spread of the directions of external disturbances.

The 6 DOF motion of the ship-type floating offshore structure is presented in Fig. 5.4. Based on the figure, motion in x_0-direction in the collinear condition is slightly greater than that in the non-collinear condition while motion in y_0-direction and yaw motion in the non-collinear condition are much greater than those in the collinear condition. External disturbances applied for the collinear condition have the same direction which is close to the heading of the floating structure. They tend to force the floating structure to move toward

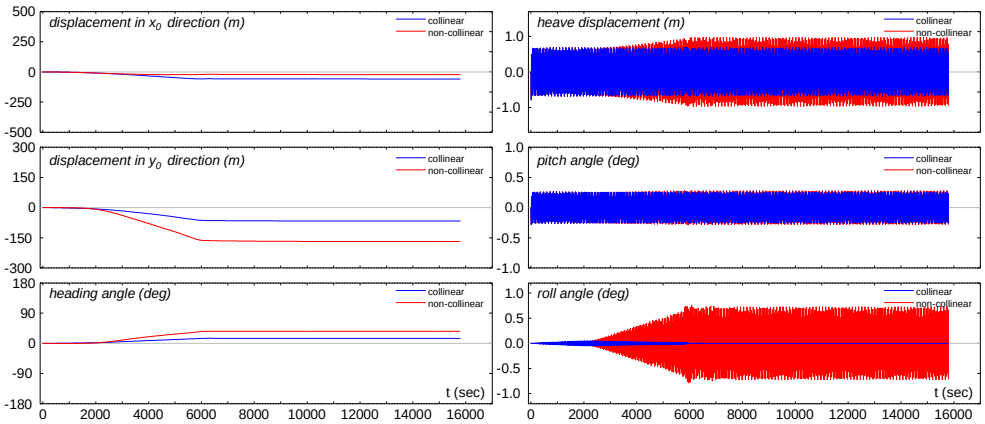

Fig. 5.4. 6 DOF motion for Case 1 (collinear and con-collinear)

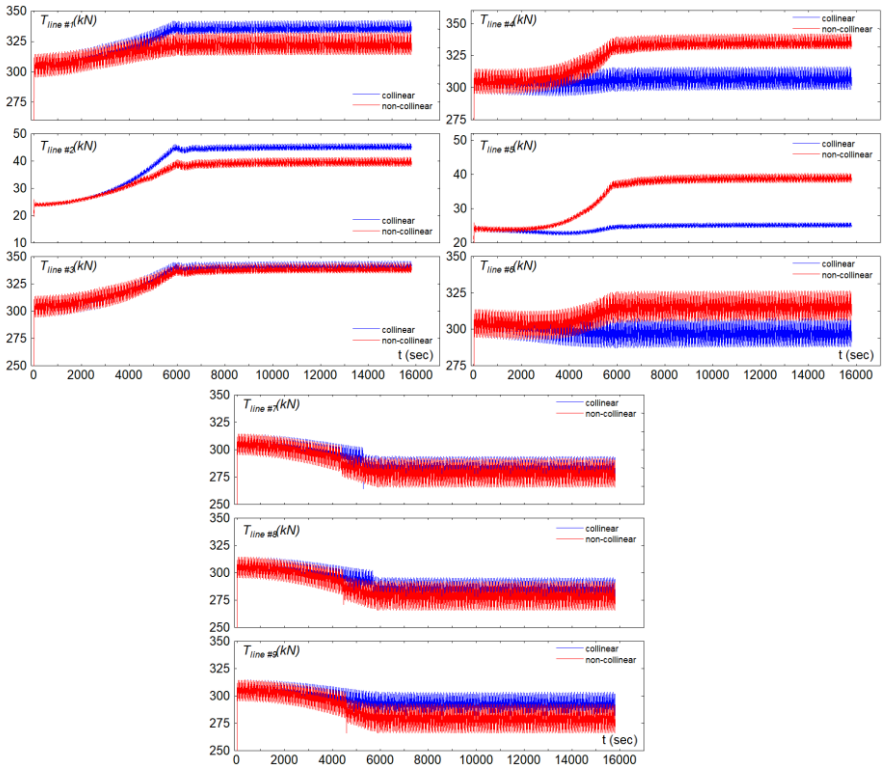

Fig. 5.5. Tension of each mooring line for Case 1 (collinear and con-collinear)

longitudinal direction, then motion in x_0-direction is relatively greater than the rest of motions in horizontal plane. On the other hand, greater lateral motions (motion in y_0-direction and yaw) can be observed in the non-collinear condition and heave motion is slightly greater than that in the collinear condition. It means that the effect of the environmental loads in lateral direction increases the heave motions. In additions, while pitch motion for both conditions show the identical results, the roll motion for the non-collinear condition is considerably greater than that for the collinear condition due to the increase of lateral force. It also enlarges the roll motion for the non-collinear condition whilst longitudinal force which is dominant in the collinear condition leads minuscule roll motion.

Furthermore, dynamic coupling between mooring line tension and the motion of the floating structure can be observed in Fig. 5.5. The tendency of the tension of each mooring line for both collinear and non-collinear conditions is completely different. It strongly relates to the motions of the floating structure and the position of a bellmouth on the vessel during the simulation. According to the figure, the following description may be able to figure the relations between the motions of the floating structure and the tension of its mooring line. Since the floating structure moves away from the anchor point of the line 3 in both collinear and non-collinear conditions, the maximum tension occur in the line 3. Even so, the floating structure moves backward which is almost negative direction of the x_0-axis in the collinear

condition. This motion is almost vertical to line group GL II and hence the mean tension of lines in GL II (line 4-6) is almost constant. On the other hand, in the non-collinear condition, the floating structure tends to move away from GL II. Thus, the tension of mooring lines 4-6 increases. These conditions can be also confirmed by the tension of the line 1 which is greater than that for the non-collinear condition. In addition, as the result that the floating structure moves toward the GL III for both collinear and non collinear conditions, three lines associated with GL III (lines 7-9) experience slack condition. It means that the tension of these three mooring lines decrease during the simulation as pictured in Fig. 5.5. Finally, it can be said that the proposed dynamics model for a multi-component mooring line can simulate mooring line tension well in coupling with the motion of a ship-type floating offshore structure under the rule requirement conditions.

5.4.2. Simulation Based on Possible Directions of External Disturbances – Case 2

In this case, the measured direction of external disturbances (wave and wind directions) denoted in Table 5.1 are used as the collinear condition (Case 2A). Wave direction shown in Table 5.1 is further used for the non-collinear condition while wind and current directions

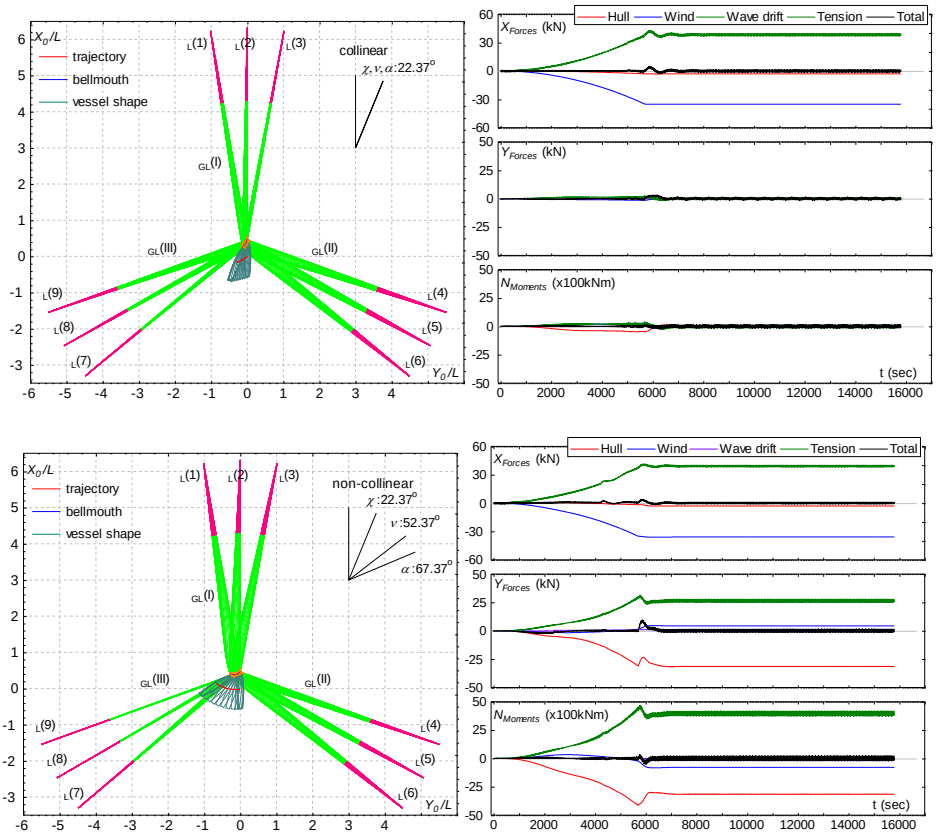

Fig. 5.6. Trajectories and horizontal forces – Case 2 (collinear and con-collinear)

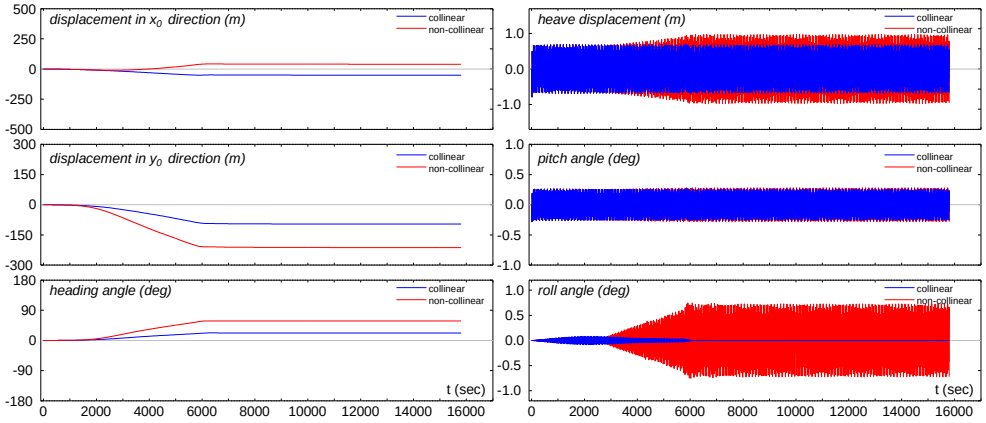

Fig. 5.7. 6 DOF motions for Case 2 (collinear and con-collinear)

are defined referring the rule, namely wave, wind, and current directions are 22.3675°, 52.3675°, and 67.3675° respectively (Case 2B).

The trajectories of the ship-type floating offshore structure and its mooring lines as well as horizontal forces acting on the vessel are depicted in Fig. 5.6. Both results for the collinear and non-collinear conditions are similar with the results of Case 1 because the actual directions of external disturbances are not different too much from those used in Case 1. In Case 2A, longitudinal motion affected by the environmental loads is dominant. It can be confirmed from the figure in which lateral force and yawing moment are almost equal to

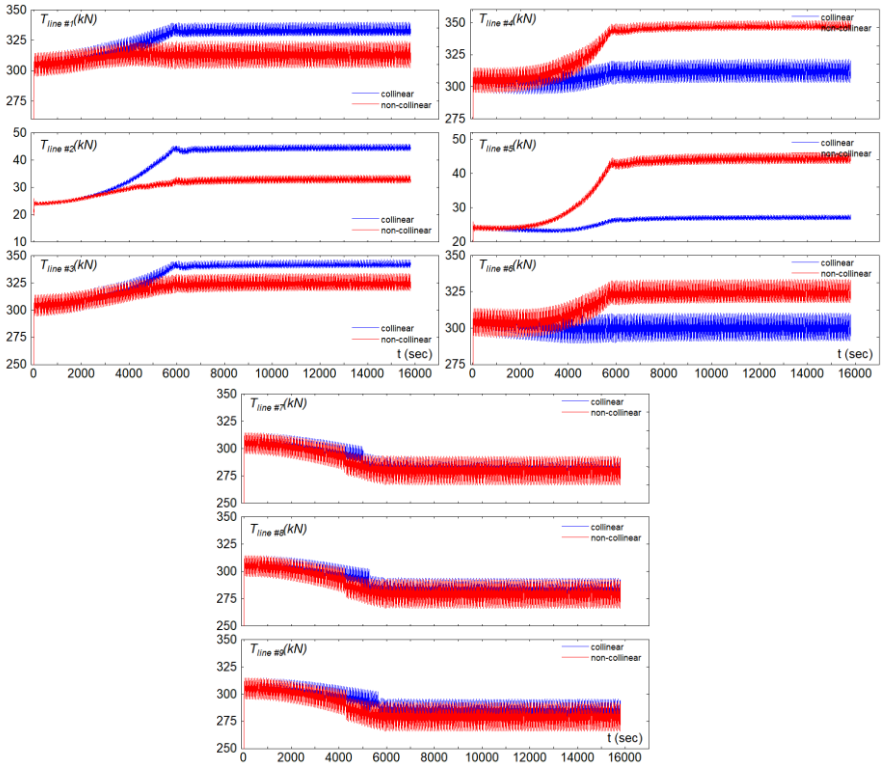

Fig. 5.8. Tension of each mooring line for Case 2 (collinear and con-collinear)

zero whilst longitudinal force is considerably significant.

Similar tendency also appears in Case 2B for the non-collinear condition. Due to the difference among wind, current, and wave directions, lateral force acting on the vessel increases and it force the floating structure to move toward lateral direction. It can be observed by the shapes of the floating structure drawn every 500 seconds and the time histories of horizontal forces shown in Fig. 5.6. They are similar to the results for Case 1B.

The motions of the floating structure for Case 2 are shown in Fig. 5.7. Similar with the results for Case 1, sway and yaw motions for both collinear and non-collinear conditions have identical tendency with Case 1. However, in this case, surge motion in backward direction is observed for the collinear condition while the floating structure tends to move forward for the non-collinear condition. Other motions such as heave, pitch, and roll show similar tendency with those of Case 1.

The effect of the motion of the floating structure on mooring line tension can be investigated through Fig. 5.8. Because the motions of the floating structure have similar tendency with those of Case 1, the tension for each mooring line generally show resembling result comparing with that in Case 1. However, the mooring line which has the maximum tension among all lines is different with that in Case 1. In this case, the maximum tension occurs in the line 3 for the collinear condition and the line 4 for the non-collinear condition while it occurs in the line 3 for both conditions in Case 1. The greater angle of wave directions as well as wind and current for this case increases the lateral force acting on the floating structure. Consequently, the floating offshore structure moves in lateral direction farther away comparing with that in Case 1 and hence the motion increases the tension of the line 4. These entire elucidations give comprehension that the coupled motions of a floating structure and mooring lines can be investigated by the dynamics model for mooring line proposed in present study.

5.4.3. Simulation for In-between Line Condition – Case 3

To investigate the effect of direction of external disturbances relative to the arrangement of mooring lines, external disturbances coming from the direction between two line groups are considered in present case. Here, external disturbances which come from the direction between GL I and GL II are applied for the collinear (Case 3A) and non-collinear (Case 3B) conditions. In Case 3A, all external disturbances come from $60°$ relative to the bow. On the other hand, wave comes from the same direction as Case 3A whilst the directions of wind and current are $30°$ and $45°$ relative to wave direction respectively in Case 3B.

Fig. 5.9 shows the trajectory of the ship-type floating offshore structure during the simulations with the time histories of horizontal forces for both collinear and non-collinear

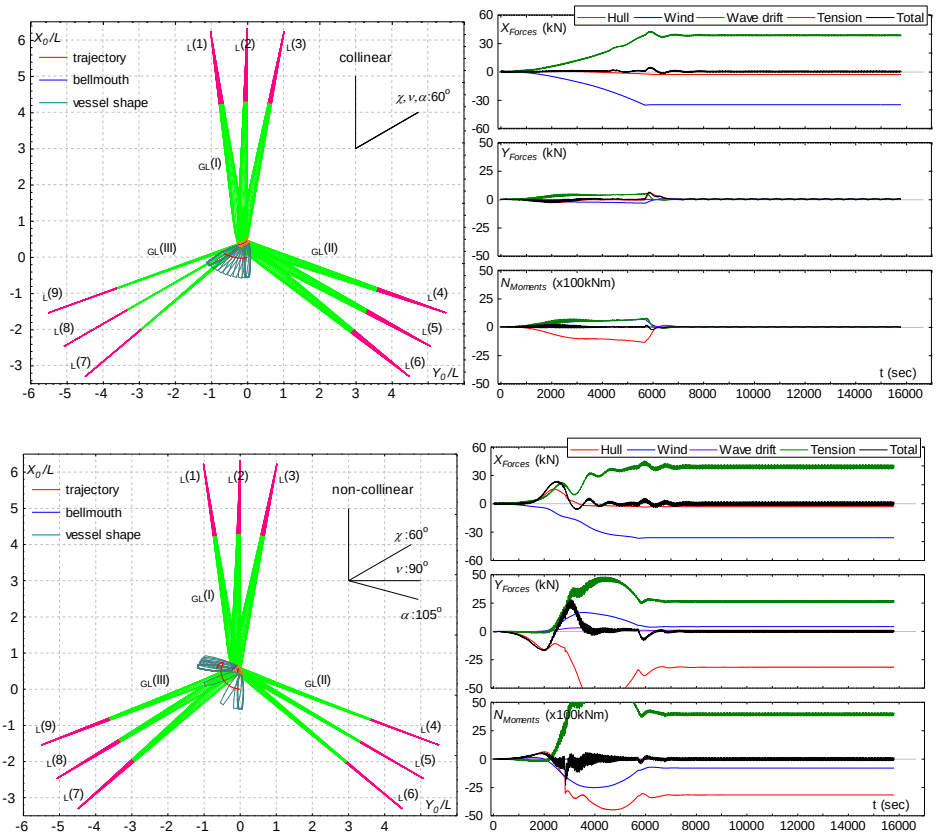

Fig. 5.9. Trajectories and horizontal forces – Case 3 (collinear and con-collinear)

conditions. In the collinear condition, the motions of the floating offshore structure are not so different from Cases 1A and 2B. However, lateral force and yawing moment are observed at the beginning of the simulation since the external disturbances force the floating structure to turn around its bow position. Then, the floating structure will be placed in beam sea or bow sea condition at the beginning of the simulation. The lateral force and yawing moment vanish when the heading of the floating structure is in-line with the direction of external disturbances. Finally, external disturbances come from the direction between GL I and GL II, in other words, the direction is exactly in-line with GL III. The tension of GL I and GL II become bigger whilst that of GL III hardly change. Meanwhile, lateral force and yawing moment are observed in the non-collinear condition (Case 2B) and the amplitudes of them are much greater at the beginning of the simulation because the directions of external disturbances spread around beam sea condition. Thus, the floating structure as well as its mooring line moves following the combined environmental loads until it reaches the equilibrium position. These descriptions can be noticed in Fig. 5.9.

The motions of the ship-type floating offshore structure coupled with multi-component mooring lines in this case can be evaluated by Fig. 5.10. It can be found that the tendency of

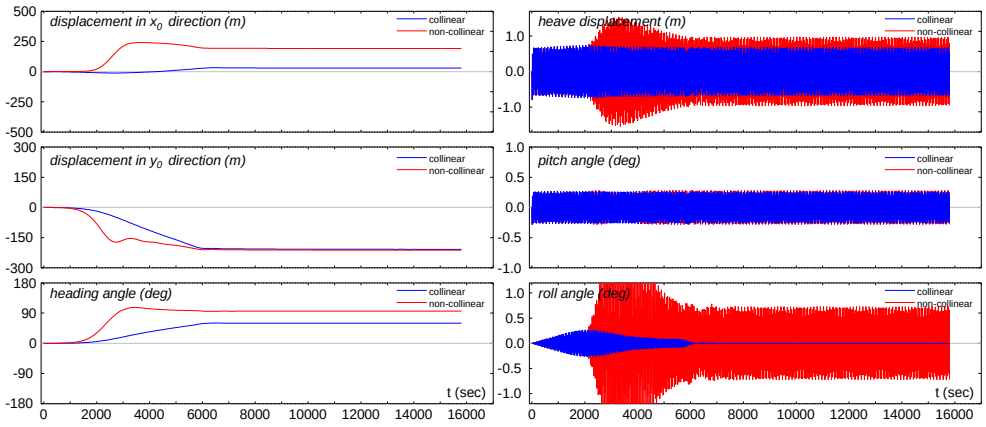

Fig. 5.10. 6 DOF motions for Case 3 (collinear and con-collinear)

the motions in the non-collinear condition comparing with those in the collinear condition is alike with those for Cases 1 and 2. Even so, the obvious differences can be characterized at the beginning of the simulations for the non-collinear condition in which the motions increase temporarily due to large lateral force and yawing moment acting on the floating structure. The temporary increase of motion almost happens for all motion modes and it becomes greater for surge, yaw, heave, and roll motions.

Mooring line tension affected by the coupled motions is presented in Fig. 5.11. From the figure, because all external disturbances in the collinear condition come from the

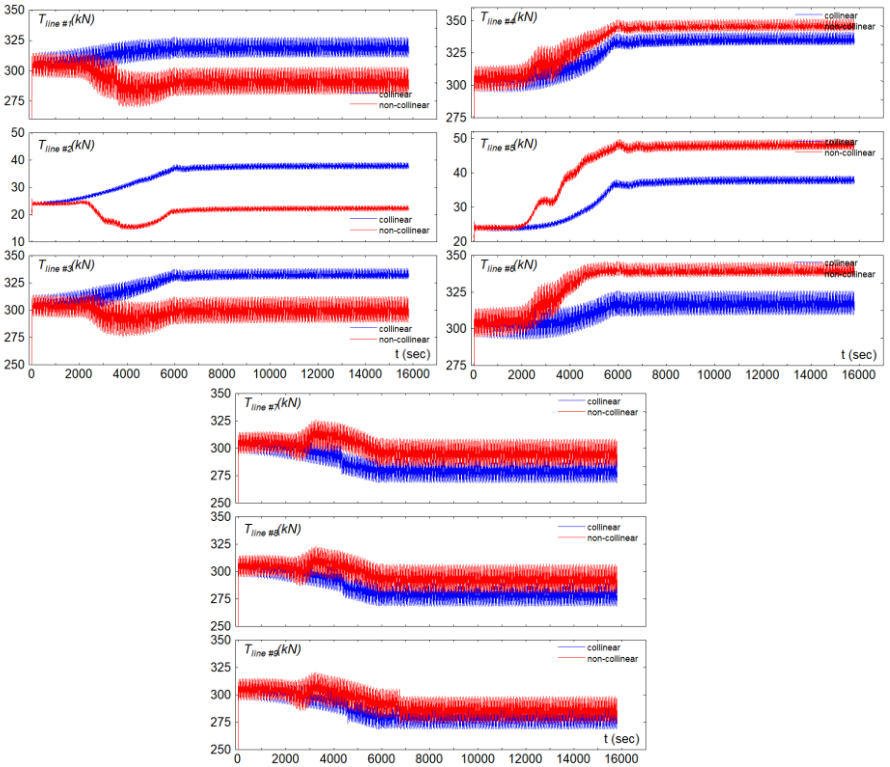

Fig. 5.11. Tension of each mooring line for Case 3 (collinear and con-collinear)

direction between GL I and GL II, environmental loads which are restrained by mooring lines are distributed to the both line groups. In conforms to the tension shown in the figure where the maximum tension in the collinear condition occurs in both of GL I and GL II (lines 1, 3, 4, and 6). On the other hand, since the resultant directions of the total environmental loads for the non-collinear condition comes from the in-line direction against the line 3 as observed by the final heading of the floating structure, the maximum tension occurs in the line 3. This description can be noticed by the tension of the line 3 and the final heading of the floating structure pictured in Fig. 5.11 and Fig. 5.9 for the non-collinear condition respectively.

5.4.4. Simulation for In-line Condition – Case 4

To consider the other condition of external disturbances, analysis of the floating structure coupled with mooring lines under in-line condition is investigated. In this condition, all external disturbances in the collinear condition (Case 4A) and wave in the non-collinear condition (Case 4B) come from the direction which is in-line with GL II (120°), meanwhile wind and current direction in the non-collinear condition are defined based on the wave direction. The trajectories of the ship-type floating offshore structure for both collinear and

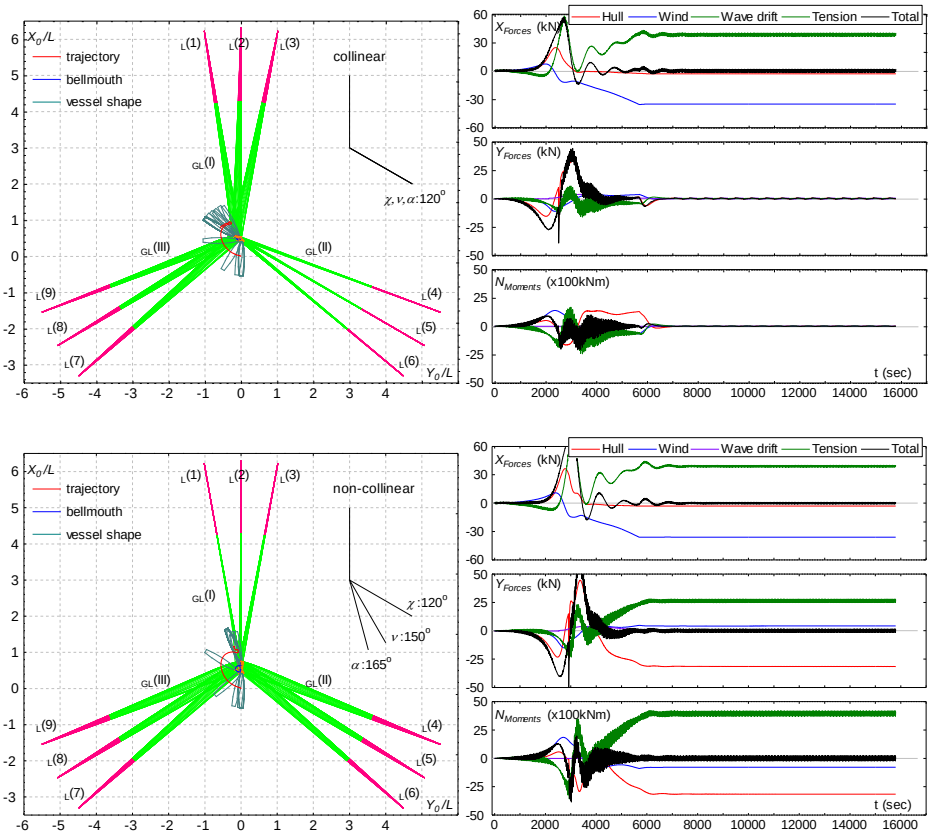

Fig. 5.12. Trajectories and horizontal forces – Case 4 (collinear and con-collinear)

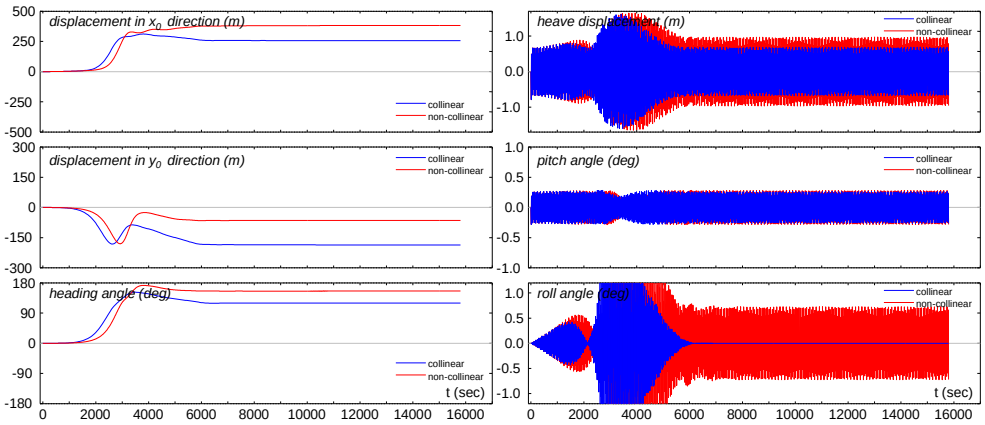

Fig. 5.13. 6 DOF motion for Case 4 (collinear and con-collinear)

non-collinear conditions are presented in Fig. 5.12.

According to the figure, the shapes of the floating structure drawn every 500 minutes and its trajectory in both collinear and non-collinear conditions show similar results concerning to the directions of external disturbances. In the collinear condition, the floating structure moves following the direction of external disturbances which is in-line with GL II. In consequences, the mooring lines in GL II tend to move to the same direction with external disturbances while the mooring lines in GL I and GL III tend to move toward negative direction of y_0 axis. This condition is different from that in the non-linear condition in

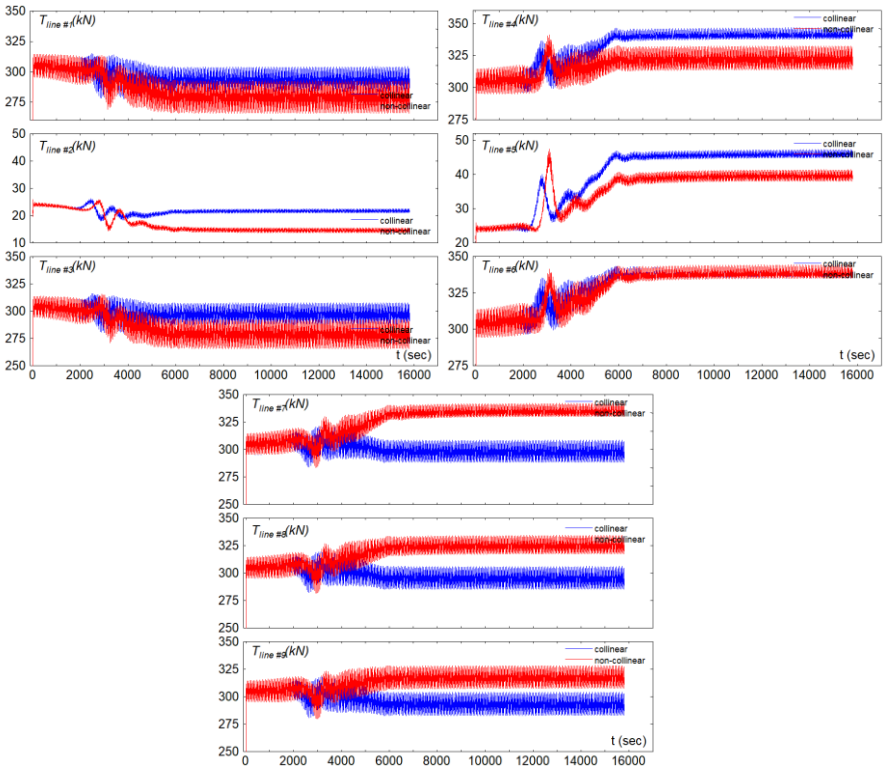

Fig. 5.14. Tension of each mooring line for Case 4 (collinear and con-collinear)

which the total environmental loads force the floating structure to move toward GL I. Thus, the floating structure rotate around its bow until its heading angle reaches the opposite direction. As shown in the figure for the non-collinear condition, mooring lines in GL II and GL III move toward positive direction of x_0 axis and hence the mooring lines in GL I experience slack condition. The horizontal forces portrayed in the figure prove this condition.

The motions of the floating structure delineated in Fig. 5.13 indicate the same tendency for other cases concerning to the relation between collinear and non-collinear conditions. Beside the floating structure experiences larger vertical motions when dealing with the non-collinear condition, different direction of external disturbances in this conditions cause unpredictable horizontal motions. These motions are extremely affected by the configuration of the directions of external disturbances. It's easy to say that the horizontal motions of the floating structure are much more sensitive against the direction of external disturbances. Furthermore, as shown in Fig. 5.14, the maximum tension for Case 4A occurs in mooring lines in GL II. Because GL II is in-line with the all of external disturbances and environmental loads concentrated on the GL, GL II should withstand these loads. In consequence, the mooring line in GL II must withstand environmental loads almost singly. Moreover, the maximum tension is distributed to lines in GL II and GL III for Case 4B since the resultant direction of environmental loads comes from nearly in-between those two line groups.

5.4.5. Three-Dimensional Coupled-Motions

Three-dimensional multi-component mooring line motions incorporating a ship-type floating offshore structure are presented in Fig. 5.15. Form the figure, it can be recognized that the proposed model successfully reproduce the dynamic behavior of a multi-component mooring line coupled with the motion of the floating structure. According to the figure, a multi leg mooring line system composed of nine multi-component mooring lines can simultaneously move with the ship-type floating offshore structure and the shapes of mooring lines change continuously following the motion of the floating structure. The figure also indicates that all segment members of the mooring lines move simultaneously interconnecting each other alike a continuum of a mooring line. Therefore, confirming to the results, the proposed model for a multi-component mooring line dynamics, beside it gives the conformity pertaining to the mooring line tension, is also effective to visualize the three-dimensional motions of the mooring lines. Thereby, the analyses of the motion of the floating structure involving the motions and mooring line tension can be properly involving in this proposed model including the visualization of their motions.

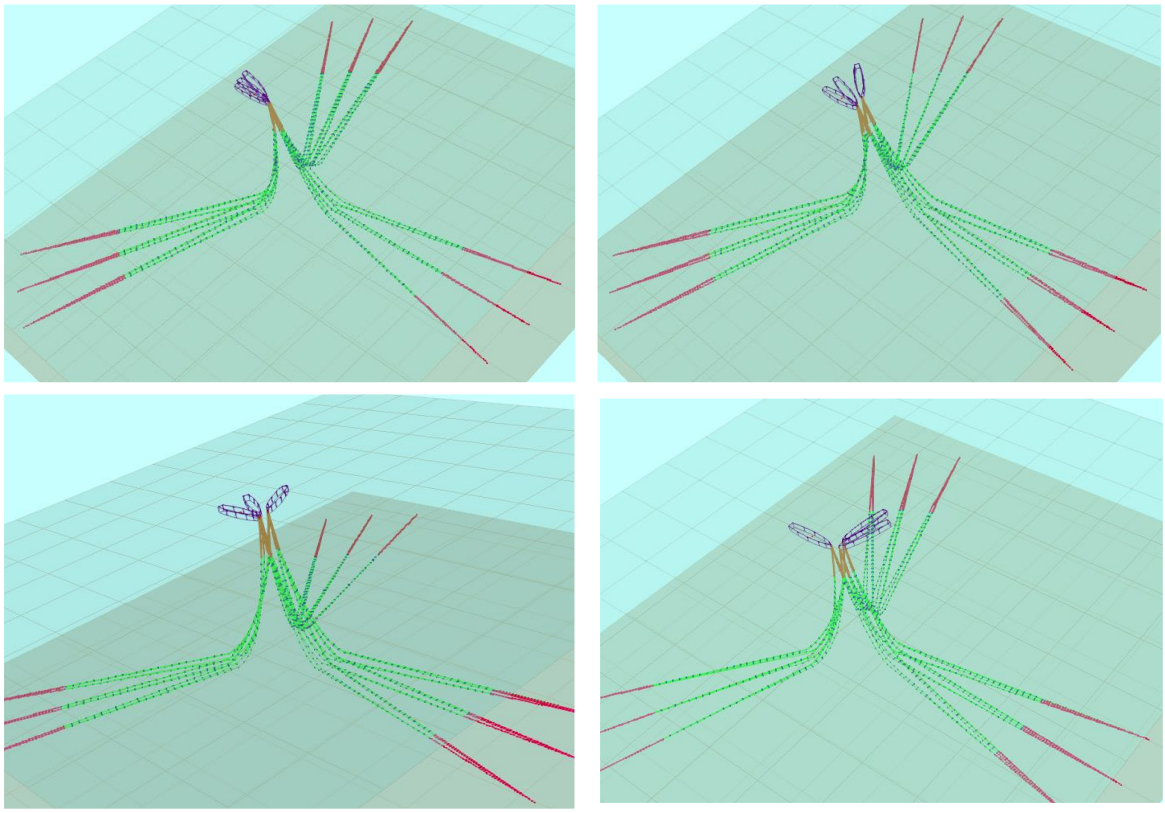

Fig. 5.15. Typical of three-dimensional coupled- motion
for simulation cases by considering measured metocean data (every 4000 sec.)

5.5. Concluding Remarks

The proposed three-dimensional dynamics model of multi-component mooring line is applied for the analysis of a moored ship-type floating offshore structure subjected to actual environmental conditions representing realistic operations. The analyses are conducted under collinear and non-collinear conditions of external disturbances for four main cases i.e. based on a rule defined in DNV-OS-E301, actual environmental conditions, in-between and in-line conditions of external disturbances. According to the analyses, external disturbances in the collinear condition force the floating structure to move in longitudinal direction rather than lateral direction whilst those in the non-collinear conditions increase lateral force and yawing moment as well as associated motions due to the various directions of external disturbances. In the non-collinear condition, motion in y_0-direction, roll, heave, and yaw motions are relatively greater than those in the collinear condition while a slight diversity is observed on motion in x_0-direction and pitch motion. Moreover, the direction of external disturbances related to in-line and in-between against mooring line considerably affect to the mooring line tension itself. For the in-between conditions, environmental loads will be

shared by two associated mooring lines which are close to the direction of external disturbances meanwhile the in-line conditions, the maximum tension will be occur in associated the in-line with mooring line.

In addition, the results generally show that the proposed dynamics model is considered to be an adequate model for representing dynamic behavior of a multi-component mooring line since the coupling of the model with the floating structure provides appropriate relations between them as well as against the environmental conditions. Therefore, confirming the results, the proposed coupled dynamics model of a multi-component mooring line is capable to be applied for the analyses of the motion of a floating structure, to investigate the coupled dynamic motions and mooring line tension, even for dealing with the measured metocean data at a certain target location. It also can provide the motion of a multi-component mooring line in three-dimensional manner.

Further study is expected to be performed to validate the present model using commercial software for mooring line analysis or experimental work in the coupled motion analysis. The model will also be applied for solving other problems related to mooring line to study the ability of the model against the existing mooring line problems. More detailed consideration will be included to improve the accuracy of the model.

Chapter 6 Conclusions

In this research, three-dimensional dynamics model of mooring lines for coupled analysis of floating offshore structure in deep water was proposed. The three-dimensional dynamics model has been presented based on three-dimensional lumped mass model. The dynamics model is applied for a single-component mooring line and extended for a multi-component mooring line. Verifications of the developed dynamics model has also been carried out and those results showed good agreements. Numerical simulations established by using both single- and multi-component mooring line models conclude that the dynamics model can be applied for coupled motion analysis of floating offshore structure properly. The coupled model is even capable to be applied for coupled motion analysis of the floating structure considering realistic multi-component mooring lines and environmental conditions. The summary of this research is described as follows.

Chapter 1 introduced a general overview of this study including the recent situation of deep water operation, offshore structure, and deep water mooring line system. A summarized literature review was presented associated with the review of mooring line dynamics, multi-component mooring line, and approaches for mooring line analysis The objectives and expected outcome of this research as well as a brief layout of this thesis were also presented. The necessities of three-dimensional dynamics model applied for coupled analysis of floating offshore structure in deep water were described in this chapter.

The numerical model used for simulating simultaneous motion of a ship-type floating offshore structure and mooring lines considering wave, wind, and current was presented in Chapter 2. A method to calculate the motion of a floating body in waves based on New Strip Method (NSM) has been presented. The comparison of simulated results using the calculation method against experimental results has been presented and it showed a good agreement between both results. Furthermore, the coupling motion equations of a floating body established by the combination of horizontal plane motion based on MMG model and vertical motion based on conventional model for a floating body motions were presented. The coupling motion equations of a floating body can cover wave (1^{st} and 2^{nd} order forces), wind, and current as well as mooring line tension simultaneously. By using the coupling motion equations, the 6 DOF motion of a moored floating offshore structure can be reproduced for analyzing coupled motion between the floating structure and its mooring lines in deep water.

In Chapter 3, the three-dimensional dynamics model for single-component mooring line has been presented by integrating interaction between the mooring line and the seabed as well as the consideration of anchor force and its motion. The numerical simulations of

dynamic-coupled motion between the mooring line and a floating structure have been carried out for four types of mooring line configurations under various environmental conditions. The simulated motion showed feasible results and hence the reasonable behavior of a moored floating structure can be investigated. Therefore, the motion of a floating structure considering the effects of wind, wave, and current forces and mooring line configuration types can be expressed and analyzed by using the proposed model.

The three-dimensional dynamics model of multi-component mooring line has been proposed in Chapter 4. The dynamics model was developed by extending single-component mooring line lumped mass method taking the complexity of the multi-component mooring line i.e. hydrodynamic forces, different properties of segment line, line-seabed interaction, elasticity, and anchoring problem. The verifications of the developed model were carried out both for the motion of the multi-component mooring line alone and the coupled motion of such mooring line and a floating structure. The verifications were also conducted for a multi-component line consisting of uniform segments without/with a clump weight and a multi-component line consisting of non-uniform segments with a clump weight. On the other hand, in order to verify the coupling of such mooring line and a floating structure, the simulated coupling motion of a multi-component mooring line consisting of identical segment and a floating structure were compared with coupling motion with equivalent single-component mooring line. As the result, excellent agreements were gained from the verified cases. Moreover, from the comparison between simulated results with three-dimensional and two-dimensional models could conclude that the evaluation of the dynamic performance of mooring line needed to be conducted in three-dimensional manner since the implementation of two-dimensional model may give the deficiency of pertinence, especially in complicated external loads condition.

Finally, the proposed three-dimensional dynamics model of a multi-component mooring line were applied for the numerical analyses of a moored ship-type floating offshore structure subjected to possible environmental conditions at a particular target location. The results of numerical analyses were presented in Chapter 5. Possible operation conditions including target floating offshore structure, mooring line and its configurations, and the environmental conditions based on measured metocean data were applied for the analyses. Four cases of environmental conditions i.e. based on a rule, based on measured data, in-between conditions, and in-line conditions were investigated under collinear and non-collinear conditions. According to the results, external disturbances in the collinear condition force the floating structure to move in longitudinal direction rather than lateral direction whilst those in the non-collinear conditions increase lateral force and yawing moment. In the non-collinear condition, motion in y_0-direction, roll, heave, and yaw motions are relatively greater than

those in the collinear condition while a slight diversity is observed on motion in x_0-direction and pitch motion. Moreover, the direction of external disturbances related to in-line and in-between against mooring line considerably affect to the mooring line tension itself. Therefore, the proposed coupled dynamics model is capable to be applied for the analyses of the motion of a floating structure, even for dealing with the measured metocean data at a certain target location. It also can provide the motion of a multi-component mooring line in three-dimensional manner.

From the above results, it can be said that practical calculation method for the coupled motion analysis of a floating offshore structure and a mooring line was established properly in this research. Even further, for the sake of the achievement of more accurate results, the comparison of coupled motion analysis performed by using this proposed method with the results obtained by commercial softwares and/or experimental works will be valuable for the further study. Moreover, since the time domain motions of a floating body in waves are usually introduced as the impulse response functions, the inclusion of memory effect functions in the coupling motion equations can be deliberated in the further research. In addition, to enhance the ability of the method to be applied for solving the advanced problems related to mooring lines, the implementation of models for particular problems such as the simulations consideration of extreme/tsunami loads, damaged mooring lines, other materials of mooring line (polyester, nylon, etc.), irregular seabed, etc., will be interesting research theme in the future. The consideration of the limit of mooring lines as well as floating offshore operability required by classifications rules/regulations such as safety factor related to mooring line tension, floating structure excursion limit, etc., can be included to complement this research.

Acknowledgement

Firstly, I am very gratefully acknowledging to my supervisor, Professor Yoshitaka Furukawa, for his invaluable and great guidance, supports, and encouragement throughout the period of my study in Kyushu University. He not only supervised my study, but also provided great supports and helps for my daily life in Japan. I could not complete my study and my research successfully without his great supports. I am greatly indebted to my supervisor.

I am grateful to Professor Tomoaki Utsunomiya, Department of Marine Systems Engineering, Faculty of Engineering, Kyushu University, and Professor Changhong Hu, Division of Renewable Energy Dynamics, Research Institute for Applied Mechanics (RIAM), Kyushu University who proofread the entire thesis. I am very thankful for great comments for my research.

I am thankful to Mr. Yasuaki Nakiri for his advice for a year during my first year and Mr. Hiroshi Ibaragi for his support for carrying experiment and provided great knowledge related experimental works. Thanks also for Mr. Takafumi Shiiba for his discussion.

Many thanks for former master students Taku Sasaki and Taiga Suzuki for great discussion to study and solve the problem of floating body motions in wave. Thank you for together developing the numerical program related to floating body motions in wave and for all supports in daily life in campus.

I would like to thank to all members of Marine Dynamics and Control Laboratory during my study including Bora Choe (my same level mates for struggling together), Fakhri Akbar Ayub, Kazunori Kajikuri, Yusuke Sato, Daichi Ohta, Ippei Sakai, Keisuke Tajima, Ryuga Kusaka, Yuki Takahara, Kenshi Yamashita, Ryuto Miyajima, Kento Yamauchi, Yukari Hosoi, Chinami Morikawa, Heejin Lee and all fourth grade undergraduate students for their support during my study.

Finally, I would like to express gratitude for my parents, my brother and sister, and my wife, Iin Ika Yeni for their supports and encouragements. This thesis is dedicated to my little family.

References

Aamo, O.M., Fossen, T.I., 2000. Finite element modelling of mooring lines. Mathematics and Computers in Simulation. 53, 415-422.

Ahn, Y.K., 2003. On the dynamic positioning system of FPSO. Doctoral Thesis, Graduate School of Engineering, Department of Maritime Engineering, Kyushu University.

Ansari, K.A., 1980. Mooring with multicomponent cable systems. J E. Res. Tech. 102, 62-69.

Ansari, K.A., 1991. On the design of multi-component cable system for moored offshore vessels. Energy Convers. Mgmt. 31, 295-307.

Ansari, K.A., 1999. Development in offshore engineering. Gulf Professional Publishing. Houston, Texas, USA. Ch.5, 195-224.

Antonutti, R., Peyrard, C., Incecik, A., Ingram, D., 2018. Dynamic mooring simulation with Code_Aster with application to a floating wind turbine. Ocean Eng. 151, 366-377.

Azcona, J., Munduate, X., Gonzalez, L., Nygaard, T.A., 2017. Experimental validation of a dynamic mooring lines code with the tension and motion measurement of a submersed chain. Ocean Eng. 129, 415-427.

Ba, U.M., 2011. Analysis of mooring and steel catenary risers system in ultra deepwater. Doctoral Thesis, School of Marine Science and Technology, Faculty of Science, Agriculture and Engineering, Newcastle University.

Bauduin, C., Naciri, M., 2000. A contribution on quasi-static mooring line damping. J. of Offshore Mech. and Arctic Eng. 122, 125-133.

Bhattacharjee, S., Majhi, S., Smith, D., Garrity, R., 2014. Serpentina FPSO mooring integrity issues and system replacement: unique fast track approach. Proc. of Offshore Technology Conference, pp. 1-29.

Bucham, B., Driscoll, F.R., Nahon, M., 2004. Development of a finite element cable model for use in low-tension dynamics simulation. J. of Applied Mechanics. 71, 476-485.

Bureau Veritas NI 461 DTO, 1998. Quasi-dynamic analysis of mooring systems, Recommended practice, Tentative issue, May 1998.

Bureau Veritas NI 493 DTM, 2004. Classification of mooring system for permanent offshore units, Guidance note, June 2004.

BP p.l.c., 2019. BP Energy Outlook 2019 edition. [online]. Available at: www.bp.com.

Cerviera, F, Fonseca, N, Pascoal, R., 2013. Mooring system influence on the efficiency of wave energy converters. Int. J. of Marine Energy, 3-4, 65-81.

Chai, Y.T., Varyani, K.S., 2006. An absolute coordinate formulation for three-dimensional flexible pipe analysis. Ocean Eng. 33, 23-58.

Chai, Y.T., Varyani, K.S., Barltrop, N.D.P., 2002a. Semi-analytical quasi-static formulation for three-dimensional partially grounded mooring system problems. Ocean Eng. 29, 627-649.

Chai, Y.T., Varyani, K.S., Barltrop, N.D.P., 2002b. Three-dimensional lump-mass formulation of a catenary riser with bending, torsion and irregular seabed interaction effect. Ocean Eng. 29, 1503-1525.

Chen, X.B., 2004. Hydrodynamics in offshore and naval applications-part I. Proc. of 6th International Conference on Hydrodynamics, The University of Western Australia, Perth.

Chen, X.B., 2005. Hydrodynamic analysis for offshore LNG terminals. Proc. of 2nd International Workshop on Applied Offshore Hydrodynamics, Rio de Janeiro, Brazil.

Chen, X.B., 2006. Middle-field formulation for the computation of wave-drift loads. J. Eng. Math. 59.61-82.

Chen, X.B., Rezende, F. 2009. Efficient computations of second-order low-frequency wave load. Proc. of the 28th International Conference on Ocean, Offshore and Arctic Engineering, Honolulu, Hawaii.

Chen, L., Basu, B., Nielsen, S.R.K., 2018. A coupled finite difference mooring dynamics model for floating offshore wind turbine analysis. Ocean Eng. 162, 304-315.

Childers, M.A., 1973. Mooring systems for hostile waters. Petroleum engineer 45(5):58-70.

Childers, M.A. 1974. Deep water mooring - part II: The ultradeep water spread mooring system. Petroleum engineer 2, 108-118.

Chiou, R.B., 1990. Nonlinear hydrodynamic response of curved singly-connected cables. Ph.D. Thesis. Oregon State University.

Escalante, M.R., Sampaio, R., Rosales, M.B., Ritto, T., 2011. A reduced order model of a 3d cable using proper orthogonal decomposition. Mecanica Computacional. 30, 1143-1158.

Det Norske Veritas, 1996, Part 6 Chapter 2, Position Mooring (POSMOOR), Rules for Classification of Mobile Offshore Units, Det Norske Veritas.

Det Norske Veritas, 2008, Part 6 Chapter 2, Position Mooring (POSMOOR), Rules for Classification of Mobile Offshore Units, Det Norske Veritas.

Det Norske Veritas, 2013. DNV-OS-E301: Position Mooring, October 2013.

Figuiredo, P.A., Brojo, F.M., 2017. Parametric study of multicomponent mooring lines at catenary form in terms of anchoring cost. Energy Procedia. 136, 456-462.

Fontaine, E., Orsero, P., Ledoux, A., Nerzic, R., Prevosto, M., Quiniou, V., 2013. Reliability analysis and response based design of a moored FPSO in West Africa. Structural Safety. 41, 482-96.

Fujiwara, T., Ueno, M., Nimura, T., 1998. Estimation of wind force on the hull. J. of SNAJ, Vol. 183

Ganesan T.S., Sem, D., 2015. Direct time domain analysis of floating structures with linear and nonlinear mooring stiffness in a 3d numerical wave tank. Applied Ocean Research, 51, 153-170.

Garret, D.L., 1982. Dynamic analysis of slender rods. J. Energy Resour. Tech. 104(4), 302-306.

Garret, D.L., 2005. Coupled analysis of floating production system. Ocean Engineering. 32, 802-816.

Ghafari, H., Dardel, M., 2018. Parametric study of catenary mooring system on the dynamic response of the semi-submersible platform. Ocean Eng. 153, 319-332.

Ha, T.P, 2011. Frequency and time domain motion and mooring analysis for FPSO operating in deep water. Doctoral Thesis, School of Marine Science and Technology, Faculty of Science, Agriculture and Engineering, Newcastle University.

Hall, M., Bucham, B., Crawford, C., 2014. Evaluating the importance of mooring line model fidelity in floating offshore wind turbine simulations. Wind Energy. 17, 1835-1853.

Hall, M., Goupee, A., 2015. Validation of a lumped-mass mooring line model with DeepCwind semisubmersible model test data. Ocean Eng. 104, 590-603.

Haraguchi, T., Ohmatsu, S., 1983. On an improved solution of the oscillation problem on non-wall sided floating bodies and a new method for eliminating the irregular frequencies. 66th meeting of the western shipbuilding association.

Heurtier, J.M., Buhan, P.L., Fontaine, E., Cunff, C.L., Biolley, F., Berhault, C., 2001. Coupled dynamic response of moored FPSO with risers. Proc. of the Eleventh International Offshore and Polar Engineering Conference. Stavanger, Norway, 2001.

Honda, K., 1992. Outline of ship handling. Seizando-shoten. (written in Japanese).

Huang, S., 1994. Dynamic analysis of three-dimensional marine cables. Ocean Eng. 21, 587-605.

Inoue, K., Usui, H., 1993. Design guidelines for anchorage viewed from an anchor danger index. Proc. of the Japan Navigation Association, No. 90.

Isherwood, R.M., 1972. Wind resistance of merchant ships. The Royal Institution of Naval Architects.115, 327-338.

Jacob, B.P., Bahiense, R.d.A., Correa, F.N., Jacovazzo, B.M., 2012a. Parallel

implementations of coupled formulations for the analysis of floating production system, part I: Coupling formulations. Ocean Engineering. 55, 206-218.

Jacob, B.P., Franco, L.D., Rodriguez, M.V., Correa, F.N., Jacovazzo, B.M., 2012b. Parallel implementations of coupled formulations for the analysis of floating production system, part II: Domain decomposition strategies. Ocean Engineering. 55, 209-234.

Ji, C., Cheng, Y., Yan, Q., Wang, G., 2016. Fully coupled dynamic analysis of a FPSO and its MWA system with mooring lines and risers. Applied Ocean Research. 58, 71-82.

Ji, C.Y., Yuan, Z.M., Chen, M.L., 2011. Study on a new mooring system integrating catenary with taut mooring. China Ocean Eng. 25(3), 427-440.

Johanning, L., Smith, G.H., Wolfram, J., 2005. Toward design standards for WEC moorings. Proc. of the Sixth European Wave and Tidal Energy Conference. Glasgow, UK, 2005.

Johanning, L., Smith, G.H., Wolfram, J., 2007. Measurements of static and dynamic mooring line damping and their importance for floating WEC devices. Ocean Eng. 34, 1918-1934.

Jonkman, J.K., 2007. Dynamics modelling and loads analysis of an offshore floating wind turbine. Technical Report National Renewable Energy Laboratory. Midwest Research Institute.

Journee, J.M.J., Massie, W.W., 2001. Offshore Hydromechanics. Delft University of Technology.

Katifeoglou, S.A., Chatjigeorgiou, I.K., 2012. Dynamic interaction of catenary risers with the seafloor. Applied Ocean Research. 38, 1-15.

Kashiwagi, M., 1995. Prediction of surge and its effects on added resistance by means of the enhanced unified theory. Transactions of West-Japan Society of Naval Architects. 89. 77-89.

Kashiwagi, M., Iwashita, H., 2012. Ship and ocean engineering series No.4: Hull motion-seaworthiness performance edition. The Japan Society of Naval Architects and Ocean Engineering (JASNAOE). (written in Japanese).

Kashiwagi, M., Ohkusu, M., 1991. Second-order steady force and yaw moment on a ship advancing in waves. Research Institute for Applied Mechanics, Kyushu University.

Kashiwagi, M., Ohkusu, M., 1993. Study on the wave-induced steady force and moment. J. of the Society of Naval Architects of Japan. 185-193.

Kashiwagi, M., Kawazoe, K., Inada, M., 2000. Calculation of Ship Sway and Drag in Wave. J. of the Kansai Society of Naval Architects, Japan. 85-94. (written in Japanese).

Khan, N.A., Ansari, K.A., 1986. On the dynamics of a multicomponent mooring line. Comput. Struct. 22(3), 311-334.

Kijima, K., Nakiri, Y., Katsuno, T., Furukawa, Y., 1990. On the manoeuvring performance of a ship with the parameter of loading condition. J. of the Society of Naval Architects of Japan, Vol. 168.

Kinoshita, T., 2003. Practical hydrodynamics on floating body: part I - Numerical calculation method of motion. Seizando-shoten.

Kreuzer, E., Wilke, U., 2003. Dynamic of mooring systems in ocean engineering. Applied Mechanics. 73, 270-281.

Lee, J.F., Tu, L.F., 2018. Finite element modeling of a single-point multi-segment mooring in water waves. Ocean Eng. 160, 461-470.

Lo, A., 1982. Nonlinear dynamic analysis of cable and membrane structure. Ph.D. Thesis. Oregon State University.

Lopez, J.T., Tao, L., Xiao, L., Hu, Z., 2017. Experimental study on the hydrodynamic behavior of an FPSO in a deepwater region of the Gulf of Mexico. Ocean Eng. 129, 549-566.

Low, Y.M., Langley, R.S., 2006. Time and frequency domain coupled analysis of deepwater floating production systems. Applied Ocean Research. 28, 371-385.

Low, Y.M., Langley, R.S., 2008. A hybrid time/frequency domain approach for efficient coupled analysis of vessel/mooring/riser dynamics. Ocean Engineering. 35, 433-446.

Maeda, H., 1959. Wave excitation forces on two dimensional ships of arbitrary sections. J. of the Society of Naval Architects of Japan, Vol.126. 55-83. (written in Japanese).

Manabe, D., 1960. Ship's yawing in waves. Memories of the Faculty of Engineering, Kyushu University. 20, 1-34.

Maruo, H., 1960. The drift of a body floating on waves. J. of Ship Research. 4, 336-373.

Masciola, M., Robertson, A., Jonkman, J., Coulling, A., Goupee, A., 2013a. Assessment of the importance of mooring line dynamics on the global response of the DeepCwind floating semisubmersible offshore wind turbine. Proc. of the Twenty-third International Offshore and Polar Engineering Conference. Anchorage, AK, USA, 2013.

Masciola, M., Robertson, A., Jonkman, J., Robertson, A., 2013b. Implementation of a multisegmented, quasi-static cable model. Proc. of the Twenty-third International Offshore and Polar Engineering Conference. Anchorage, AK, USA, 2013.

Matha, D., Schlipft, M., Pereira, R., Jonkman, J., 2011. Challenges in simulation of aerodynamics, hydrodynamics, and mooring-line dynamics of floating offshore wind turbines. Proc. of the Twenty First International Offshore and Polar Engineering Conference. Hawaii USA, 2011.

Mavrakos, S.A., Papazoglou, V.J., Triantafyllou, M.S., Hatjigeorgiou, J., 1996. Deep water

mooring dynamics. Ocean Eng. 9, 181-209.

Montano, A., Restelli, M., Sacco, R., 2007. Numerical simulation of tethered buoy dynamics using mixed finite elements. Comp. Method in Applied Mech. and Eng. 196, 4117-4126.

Motora, S., 1959a. On the measurement of added mass and added moment of inertia for ship motions. J. of the Society of Naval Architects of Japan. 105, 83-92.

Motora, S., 1959b. On the measurement of added mass and added moment of inertia for ship motions, Part 2: Added mass abstract for the longitudinal motions. J. of the Society of Naval Architects of Japan. 106, 59-62.

Motora, S., 1959c. On the measurement of added mass and added moment of inertia for ship motions, Part 3: Added mass for the transverse motions. J. of the Society of Naval Architects of Japan. 106, 63-68.

Motora, S., 1960a. On the measurement of added mass and added moment of inertia for ship motions, Part 4: Pitching motion. J. of the Society of Naval Architects of Japan. 107, 83-89.

Motora, S., 1960b. On the measurement of added mass and added moment of inertia for ship motions, Part 5: Heaving motion. J. of the Society of Naval Architects of Japan. 107, 91-95.

Muto, H., Furukawa, Y., Ibaragi, H., Koyanagi, Y., Aramaki, S., 2010. Mathematical model for hydrodynamic force acting on a ship hull with large drift angle. Proc. of AMEC 2010.

Nakajima, T., Motora, S., Fujino, M., 1982. On the dynamic analysis of multi-component mooring lines. Proc. of the Fourteenth Offshore Technology Conference. 105-121.

Nakajima, T., 1983. Static and dynamic analyses of mooring line by using the lumped mass method. Sumitomo Heavy Industries Technical Report.

Nakajima, T., Motora, S., Fujino, M., 1983. A three-dimensional lumped mass method for the dynamic analysis of mooring lines. J. of the Society of Naval Architects of Japan. 154, 192-202. (written in Japanese)

Newman, J.N., 1967. The drift force and moment of ship in waves. J. of Ship Research. 11, 51-60.

Newman, J.N., Sclavounos, P., 1980. The unified theory of ship motions. Proc. of 13th Symposium on Naval Hydrodynamics, Tokyo, Japan.

OCIMF, 1997. Mooring equipment guidelines, second edition. Oil Companies International Marine Forume. 23-31.

OCIMF, 2010. Estimating the environmental loads on anchoring systems. Oil Companies

International Marine Forume. 9.

Ogawa, Y., Oyama, T., Kijima, K. 1977. MMG Report I: Mathematical model of maneouvring motions. Bulletin of the Society of Naval Architects of Japan. 575. (written in Japanese).

Ormberg, H., Larsen, K., 1998. Coupled analysis of floater motion and mooring dynamics for a turret-moored ship. Applied Ocean Research. 20, 55-67.

Palm, J., Paredes, G.M., Eskilsson, C., Pinto, F.T., Bergdahl, L., 2013. Simulation of mooring cable dynamics using a discontinuous Galerkin method. Proc. of the Fifth Computaional Methods in Marine Engineering Conference. Hamburg, Germany, 2013.

Qiao D., Li, B., Ou, J., 2013. Comparative analysis on coupling effects between an innovative deep draft platform and different mooring models. Brodogradnja: Teorija i praksa brodogradnje i pomorske tehnike. 63(2012)4, 318-328.

Roussel, P., 1976. Numerical solution of static and dynamic equations of cables. Comp. Method in App. Mech. And Eng. 9, 65-74.

Samadi, M., Hassanabad, M.G., 2017. Hydrodynamic response simulation of catenary mooring in the spar truss floating platform under Caspian Sea condition," Ocean Engineering, 137, 241-246.

Sanchez-Mondragon, J., Vazquez-Hernandez, A.O., Cho, S.K., Sung, H.G., 2018. Yaw motion analysis of a FPSO turret mooring system under wave drift force. Applied Ocean Research. 74, 170-187.

Sasa, K., Incecik, A., 2012. Numerical simulation of anchored ship motions due to wave and wind forces for enhanced safety in offshore harbor refuge. Ocean Eng. 44, 68-78.

Shanying, L., Liping, S., Shinguang, Z., Heming, J., Yunlong, G., 2013. The comparison and analysis between catenary mooring system and taut mooring system in FPSO. Advances in Information Sciences and Service Sciences (AISS). 5:4.

Svalastog, A.K.D, 2017. Analysis and design of mooring and turret systems for ship-shaped floating production systems (FPSOs). Master thesis. Department of Marine Technology, Norwegian University of Science and Technology (NTNU).

Tahar, A., Kim, M. H., 2008. Coupled-dynamic analysis of floating structures with polyester mooring lines. Ocean Eng. 35, 1676-1685.

Takahashi, T., 1987. A practical prediction method of added resistance of a ship in waves and the direction of its application to hull form design. Transaction of The West-Japan Society of Naval Architects. 75, 75-95. (written in Japanese).

Takaishi, K., Kuroi, M., 1977. A practical method of calculation of ship motion in waves. Second Symposium on Seaworthiness, The Society of Naval Architects of Japan. 109-

134. (written in Japanese).

Tjavaras, A.A., 1996. The dynamics of highly extensible cables. Ph.D. thesis. Massachusetts Institute of Technology.

Triantafyllou, M.S., Bliek, A., Shin, H., 1985. Dynamic analysis as a tool for open-sea mooring system design. Trans. SNAME. 93, 303-304.

Van den Boom, H.J.J., 1985. Dynamic behaviour of mooring lines. Proc. of BOSS Conference. Bureau Veritas NR 493 R02 E.

Vazquez-Hernandez, A.O., Ellwanger, G.B., Sagrilo, L.V.S., 2011. Long-term response analysis of FPSO mooring systems. Applied Ocean Research. 33, 375-383.

Vryhof Anchors, 2010. Anchor Manual 2010. Vryhof Anchors. http://www.vryhof.com/pdf/anchor_manual.pdf.

Wang, C.M., Watanabe, E., Utsunomiya, T., 2008. Very Large Floating Structures. Taylor & Francis. London and New York.

Walton, T.S., Polachek, H., 1960. Calculation of transient motions of submerged cables. J. Mathematics of Computation. 14, 27-46.

Watanabe, I., Toki, N., Ito, A., 1994. Strip method. 11th Marine Dynamics Symposium on Applications of Ship Motion Theory to Design. The Society of Naval Architects of Japan.167-187. (written in Japanese)

Xie, Z.T., Yang, J.M., Hu, Z.Q., Zhao, W.H., Zhao J.R., 2015. The horizontal stability of an FLNG with different turret locations. Int. J. Naval Architecture and Ocean Eng. 7, 244-258.

Xiong, L., Yang, J., Zhao, W., 2016. Dynamics of taut mooring line accounting for the embedded anchor chains. Ocean Eng. 121, 403-413.

Xu S., Ji, C., Soare, C.G., 2018. Experimental and numerical investigation a semi-submersible moored by hybrid mooring systems. Ocean Eng. 163, 641-678.

Yamano, T., Saito, Y., 1997. An estimation method of wind forces acting on ships. J. of the Kansai Society of Naval Architects. 228, 91-100.

Yasukawa, H., Yoshimura, Y., 2015. Introduction of MMG standard method for ship maneuvering predictions. J. of Marine Science and Technology. 20, 37-52.

Yoneta, K., Januma, S., Karasuno, K., 1992. Analysis vessel's wind forces through the utilization of a physical-mathematical model-II. J. of Japan Institute of Navigation. 86, 169-177.

Yuan, Z.M., Incecik, A., Ji, C.Y., 2014. Numerical study on a hybrid mooring system with clump weights and buoys. Ocean. Eng. 88, 1-11.

Zhao W., Yang, J., Hu, Z., Xie, B., 2013. Hydrodynamics of an FLNG system in tandem

offloading operation. Ocean Eng. 57, 150-162.
Zhao, D., Hu, Z., Zhou, K., Chen, G., Chen, X., Feng, X., 2018. Coupled analysis of integrated responses of side-by-side offloading FLNG system. Ocean Engineering. 168, 60-82.